



**HAL**  
open science

# Controlled organolithium chemistry in flow microreactors: micromixer effect, synthesis and end-functionalization of polymyrcene

Katia Maria Pérez Aneliz

► **To cite this version:**

Katia Maria Pérez Aneliz. Controlled organolithium chemistry in flow microreactors: micromixer effect, synthesis and end-functionalization of polymyrcene. Chemical and Process Engineering. Normandie Université, 2022. English. NNT: 2022NORMIR34 . tel-04416357

**HAL Id: tel-04416357**

**<https://theses.hal.science/tel-04416357>**

Submitted on 25 Jan 2024

**HAL** is a multi-disciplinary open access archive for the deposit and dissemination of scientific research documents, whether they are published or not. The documents may come from teaching and research institutions in France or abroad, or from public or private research centers.

L'archive ouverte pluridisciplinaire **HAL**, est destinée au dépôt et à la diffusion de documents scientifiques de niveau recherche, publiés ou non, émanant des établissements d'enseignement et de recherche français ou étrangers, des laboratoires publics ou privés.



Normandie Université

**THESE**

**Pour obtenir le diplôme de doctorat**

**Spécialité Chimie**

**Préparée au sein de l'INSA ROUEN NORMANDIE**

**Controlled organolithium chemistry in flow microreactors: micromixer effect, synthesis and end-functionalization of polymyrcene**

**Présentée et soutenue par  
Katia Maria PEREZ ANDELIZ**

**Thèse soutenue publiquement le 13/12/2022  
devant le jury composé de**

Pr. Christophe SERRA	Professeur des universités, Institut Charles Sadron, Strasbourg	Rapporteur
Dr. Stéphanie OGNIER	Maître de conférences, Institut de Recherche de Chimie Paris, Chimie ParisTech – PSL	Rapporteuse
Pr. Valérie LANGLOIS	Professeur des Universités, Institut de Chimie et des Matériaux Paris-Est, Université Paris Est Créteil	Examinatrice
Pr. Fabrice BUREL	Professeur des universités, PBS, Institut National des Sciences Appliquées de Rouen	Directeur de thèse
Dr. Julien LEGROS	Directeur de recherche CNRS, COBRA, Université de Rouen Normandie	Co-directeur de thèse
Dr. Daniela VULUGA	Maitre de conférences, PBS, Institut National des Sciences Appliquées de Rouen	Co-encadrante de thèse

**Thèse dirigée par Pr. Fabrice Burel (PBS), Dr. Julien Legros (COBRA) et Dr. Daniela Vuluga (PBS), laboratoire PBS/COBRA**



## Acknowledgements

I would like to express my sincere gratitude to the members of my PhD jury, Dr. Stéphanie Ognier, Prof. Christophe Serra, and Prof. Valerie Langlois, who agreed to review this thesis manuscript. Thanks should also be addressed to Dr. Louise Hespel for reviewing my work over these years and for her advices.

I sincerely thank my thesis director Prof. Fabrice Burel for introducing me this vast world of polymers. Words cannot express my gratitude to my thesis co-director Dr. Julien Legros, and my supervisor Dr. Daniela Vuluga because more than supervisors I consider you as my chemist parents.

This endeavor would not have been possible without the support of the institutions MESCyT-INSA-UASD-Embassy of France, who gave me the opportunity of being part of CALIOPE program.

I am also grateful to my professors, Dr. Sebastien Leveneur and Dr. Corine Lacour. I have learned very much from you, thanks. I also want to thank Joan Jimenez and Elsa Acosta for encouraging me in this life project.

This project would not have been possible without the help of Catherine Legrand (PBS), Denis, Françoise, Camille, and Laurent Croguennoc at IRCOF many thanks.

I cannot begin to express my thanks to Batoul Rkein and Baptiste Picard, who, are more than colleagues but also considered my friends. Both of you guys are excellent chemists.

I would also want to pay my special regards to my friends and coworkers at PBS and COBRA laboratories: Vincent, Klara, Aurélie, Monica, Camille, Sandra, Ahmad, Mahmoud, Rita, Jana, Hadi, Serguey, Mathias, Seydou, Margot, Gaspard, Sandra, Melissa, Clément DSJ, Amaury and Aël. The famous “labo 232” has been my home, thanks also to Maxime, Fanny, Philippe, Marian, Youssou, and Valmir for all the special moments. Special thanks to Alan, because he was part of this project. I cannot forget to thank “Les sportifs du Dimanche” Mélanie, Cyril and Titouan, for their support as friends and for giving me cherished advices in all aspects of life.

Thanks to my friends from Dominican Republic, Lady and Azael, Elly, Jorge Junior and Katty, Johanna Abel, Dino and Sally, Nelson and Denisse, Ariel, Sory, Argenis and Ingar, Felipe and Fanny Romero, Claudine, Jalissi, Nelsy, Jose Luis, Tony and the butterflies Diana, Maribel, and Bilkys.

Also, I want to thank my pastors, Lizardo Martinez, Ezequiel Estrella, Ezequiel Molina, Francis and Myriam Burette, Jude, and my church's friends (les filles de rive droite). Claudine merci pour tes prières. Antoine, merci de m'encourager pour la soutenance.

I would like to acknowledge my friends and second family from Caliope II: Jose, Rosy, Anibal, Oscar, Sarita, Balkydia, Yessica, Clara, Leandro, Pahola and Sophie. You guys are the best, I love you so much! Also, I want to thank other friends in the different Caliope groups.

If I am here, is because of my God and my lovely family, thanks to my dad, my mom/friend Francisca, Silvio, Felipin, Pablin, Elias, Peter, Karina, Freed, Elkys, Ismael, Karla, Kelly, Rosa Ramirez, David, my uncles, aunts, and cousins. I especially want to thank Alfonsina, Anna, Fernando, and Annemarie; because this time in Europe near you have been amazing. Fer, Marie gracias por las correcciones, un abrazo.



*In the memory of my grandmother,  
Para mi abuelita con amor.*

## Table of contents

<b>Acknowledgements</b> .....	<b>2</b>
<b>Table of contents</b> .....	<b>5</b>
<b>List of tables</b> .....	<b>8</b>
<b>List of figures</b> .....	<b>10</b>
<b>Abbreviation list</b> .....	<b>14</b>
<b>Abstract</b> .....	<b>17</b>
<b>Résumé</b> .....	<b>18</b>
<b>General introduction</b> .....	<b>19</b>
<b>1. State of the art</b> .....	<b>23</b>
<b>1.1 Introduction</b> .....	<b>24</b>
<b>1.2 An alternative: continuous flow chemistry</b> .....	<b>24</b>
1.2.1 General features	25
1.2.2 Devices in continuous flow systems	35
1.2.3 Analysis tools online /inline	40
1.2.4 Flash Chemistry	43
<b>1.3 An interesting terpene: myrcene</b> .....	<b>45</b>
<b>1.4 Synthesis of polymyrcene</b> .....	<b>48</b>
1.4.1 Radical polymerization of myrcene	49
1.4.2 Coordinative polymerization of myrcene	50
1.4.3 Cationic polymerization of myrcene	51
1.4.4 Anionic polymerization	52
1.4.5 Polymer analysis	55
<b>1.5 Conclusions</b> .....	<b>59</b>
<b>1.6 Bibliography</b> .....	<b>60</b>
<b>2. Controlled organolithium chemistry in flow microreactors: comparative performance of micromixers</b> .....	<b>66</b>
<b>2.1 Introduction</b> .....	<b>67</b>
<b>2.2 Flash chemistry</b> .....	<b>69</b>
<b>2.3 Results and discussion</b> .....	<b>71</b>
<b>2.4 Micromixers</b> .....	<b>74</b>
<b>2.5 Influence of the design and sizing of the flow micromixer</b> .....	<b>75</b>
<b>2.6 Effect of micromixers with an angle ranging from 135 to 30°</b> .....	<b>77</b>
<b>2.7 Computational fluid dynamics study (CFD) of 45° micromixer</b> .....	<b>83</b>
<b>2.8 Conclusion</b> .....	<b>85</b>
<b>2.9 Bibliography</b> .....	<b>86</b>
<b>3. Anionic polymerization of myrcene under batch and flow conditions</b> .....	<b>89</b>
<b>3.1 Introduction</b> .....	<b>90</b>
<b>3.2 General reaction parameters</b> .....	<b>90</b>
3.2.1 Myrcene as monomer	90

3.2.2	Anionic polymerization	90
3.2.3	Initiator	92
3.2.4	Solvents	93
3.2.5	Temperature	93
3.2.6	Scale	94
3.2.7	Temperature	96
3.2.8	Microstructure	98
<b>3.3</b>	<b>Continuous flow reactors</b>	<b>99</b>
3.3.1	Setup	99
3.3.2	Mixers and mixing	100
3.3.3	Flow rate	101
3.3.4	Reactor size and flow rate	101
3.3.5	Influence of temperature	104
3.3.6	Microstructure	105
3.3.7	Space-time yield and parallelization	106
3.3.8	Kinetic modeling of myrcene polymerization in continuous flow	107
<b>3.4</b>	<b>Conclusions</b>	<b>112</b>
<b>3.5</b>	<b>Bibliography</b>	<b>113</b>
<b>4.</b>	<b>Chapter 4:End-functionalization and Telechelic polymyrcene in a continuous flow system</b>	<b>117</b>
<b>4.1</b>	<b>Introduction</b>	<b>118</b>
<b>4.2</b>	<b>Living polymerization</b>	<b>121</b>
4.2.1.	Synthesis of polymyrcene TMS end-functionalized in flow conditions	122
<b>4.3</b>	<b>Telescoped anionic polymerization of myrcene/functionalization with CO<sub>2</sub> in a flow system</b>	<b>123</b>
<b>4.4</b>	<b>Telechelic polymyrcene</b>	<b>128</b>
4.4.1	Initiator synthesis	129
4.4.2	Results for bifunctionalized polymyrcene with TMS ending under batch	130
4.4.3	Effects of different variables on the polymer	131
4.4.4	Results for bifunctionalized polymyrcene with TMS ending under flow conditions	131
4.4.5	Results for the synthesis of bifunctionalized polymyrcene with CO <sub>2</sub> H ending under microflow conditions	132
<b>4.5</b>	<b>Conclusions</b>	<b>134</b>
<b>4.6</b>	<b>Bibliography</b>	<b>135</b>
<b>5</b>	<b>General conclusions and perspectives</b>	<b>139</b>
	<b>General conclusions</b>	<b>139</b>
	<b>Perspectives</b>	<b>140</b>
	Green solvents	140

<b>6</b>	<b>Résumé general.....</b>	<b>141</b>
	<b>Experimental Section.....</b>	<b>178</b>

## List of tables

<i>Table 1.1: Different ways of inducing the mixture in microfluidics devices.</i> .....	36
<i>Table 1.2: W/W % of Myrcene in different plants (excerpt from Behr and Johnen, 2009).<sup>50</sup></i> .	46
<i>Table 1.3: Approximate prices per mol of butadiene and some common terpenes (Sigma Aldrich, 2022).<sup>40</sup></i> .....	48
<i>Table 1.4: Summary table of Polymyrcene synthesis.</i> .....	52
<i>Table 1.5: pKa of conjugate acid in DMSO (Bordwell, F. G. Acc. Chem. Res. 1988, 21, 456).<sup>64</sup></i> .	53
<i>Table 2.1: Effect of T-shaped (90°) and W-shaped (45°) micromixers and flow rates on the conversion of 2.1 into 2.2.<sup>a</sup></i> .....	75
<i>Table 2.2: Effect of micromixers with an angle ranging from 135 to 30° at moderate flow rate (3.5 mL/min) on the conversion of 1 into 2.2.<sup>a</sup></i> .....	78
<i>Table 2.3: Effect of micromixers with angle ranging from 135 to 30° at high flow rate (8.4 mL/min) on the conversion of 2.1 into 2.2.<sup>a</sup></i> .....	79
<i>Table 2.4: Yields of 2.2 using different micromixers ID 0.25 and 0.5 mm, Q 3.5 and 8.4 mL/min.<sup>a</sup></i> .....	79
<i>Table 3.1: Polymerization reaction using 0.11 g of myrcene.</i> .....	95
<i>Table 3.2: Polymerization reaction using 1 g of myrcene.<sup>a</sup></i> .....	95
<i>Table 3.3: Polymerization reaction using 17 g of myrcene.<sup>a</sup></i> .....	96
<i>Table 3.4: Batch polymerization of myrcene at different scales after 1 min reaction (filled up to 60%).</i> .....	96
<i>Table 3.5: Microstructure of polymyrcene under batch conditions at 10 °C.</i> .....	99
<i>Table 3.6: Results after polymerization using W and T micromixers (R<sub>1</sub>=1 m, T=10 °C).</i> .....	100
<i>Table 3.7: Different experiments with 0.25/0.1 myrcene/n-BuLi (mL/min) flow rate at 10°C.</i> .....	102
<i>Table 3.8: Experiments using 0.5, 1 and 8 m reactor with various flow rates (t<sup>R</sup> fixed at 75 s).</i> .....	102
<i>Table 3.9: Experiments using 8 m reactor at 10°C with different flow rates.</i> .....	103

<i>Table 3.10: Experiments with the same flow rate, myrcene /n-BuLi (mL / min): 0.25 / 0.1, different length of reactors at 20 °C.</i>	104
<i>Table 3.11: Polymerization of myrcene in microflow conditions at different temperatures. <math>t_R=75s</math></i>	105
<i>Table 3.12: Microstructure batch vs flow.</i>	106
<i>Table 3.13: Comparison of kinetic values found for different polymers.</i>	107
<i>Table 3.14: Estimated kinetic constants and statistical data.</i>	109
<i>Table 3.15: Parameter correlation matrix.</i>	110
<i>Table 3.16 Comparison between kinetics values of myrcene's polymerization at different conditions.</i>	112
<i>Table 4.1: Stereoselective polymerization and functionalization of polymyrcene and isoprene at 50 °C by Visseaux et al.<sup>33</sup></i>	120
<i>Table 4.3: Experiments for the end-functionalization of PMYR with CO<sub>2</sub> at 10 °C.<sup>a</sup></i>	126
<i>Table 4.4: Molar concentration and number of equivalents of reagents for anionic polymerization of myrcene in batch.</i>	131
<i>Table 4.5: Temperature effect on the polymerization of myrcene in batch. (1 g Myrcene).</i>	131
<i>Table 4.7: Results for anionic polymerization of myrcene with TMS endings in a continuous flow reactor.</i>	132
<i>Table 4.8: Molar concentration and volumetric flows of reagents used in microflow conditions.</i>	133
<i>Table 4.9: Dimensions and residence time of reactors used in microflow conditions.</i>	133
<i>Table 4.10: Results for anionic polymerization of myrcene with CO<sub>2</sub>H endings in a continuous flow reactor.</i>	134

## List of figures

Figure 1.1: Representation of nano-, micro-, mili- and meso- scale. ....	24
Figure 1.2: Scheme of a continuous flow system.....	25
Figure 1.3: Temperature profile in a round-bottom flask (right) and in a microfluidic reactor (left).....	27
Figure 1.4: Specific exchange area in batch and continuous flow. ....	29
Figure 1.5: Laminar and turbulent flow.....	30
Figure 1.6: Evolution of mixing. ....	31
Figure 1.7: Parallelization of the reactors in flow. ....	33
Figure 1.8: Scale-out and parallelization (excerpt from Monbaliu, J.-C. M.; Legros, J. Will the next Generation of Chemical Plants Be in Miniaturized Flow Reactors? Lab on a Chip <b>2022</b> ). <sup>30</sup> .....	34
Figure 1.9: Phosgenation Reactions in a Continuous Flow Reactor (Yasukouchi, H.; Nishiyama, A.; Mitsuda, M. <b>2018</b> , 22 (2), 247–251.). <sup>33</sup> .....	35
Figure 1.10: Pictograms used for continuous flow reactors. ....	36
Figure 1.11: Passive mixers such as Y-shape T-shape and W-shape and symbols.....	37
Figure 1.12: Valves used in microfluidics systems.....	38
Figure 1.13: Photos of a peristaltic pump (middle), syringe-pump (right) and its symbol (below).....	38
Figure 1.14: BPR symbol (left), image (middle), heated back pressure regulator assembly (right).....	39
Figure 1.15: Mass flow controller, symbol (left), and real photo (right).....	39
Figure 1.16: Integrated systems in continuous flow: Vapourtec® (left) and Corning® (right) .....	40
Figure 1.17: Liquid-Liquid Separator (Zaiput®).....	40
Figure 1.18: Scheme of online/inline system. ....	41
Figure 1.19: Real photo of NMR inline (excerpt from Picard et al. 2017). <sup>32</sup> .....	42
Figure 1.20: Infrared symbol in MF.....	42
Figure 1.21: Hellma® Flow-through cells. ....	43
Figure 1.22: Generation and trapping of microfluidic o-bromophenyllithium (excerpt from Yoshida et, al. 2007). <sup>46</sup> .....	43
Figure 1.23: Anionic polymerization of styrene in continuous flow (excerpt from Nagaki et al., 2019). <sup>49</sup> .....	44
Figure 1.24: Some typical terpenes.....	45
Figure 1.25: Alpha and beta-Myrcene structure and chemical properties.....	46

Figure 1.26: $\beta$ -pinene pyrolysis into $\beta$ -Myrcene.....	47
Figure 1.27. Structure similarities between butadiene; isoprene and myrcene.....	47
Figure 1.28: Polymerization of Myrcene and its different microstructures.....	49
Figure 1.29: Free radical polymerization of myrcene with emulsion technique. ....	50
Figure 1.30: Coordinative polymerization of Myrcene with neodymium borohydride as the catalyst.....	51
Figure 1.31: Cationic Myrcene polymerization with a natural catalyst Maghnite (Mag-H+).	51
Figure 1.32: Alkylolithiums, n-butyllithium, sec-butyllithium and tert-butyllithium.....	53
Figure 1.33: Steps in anionic polymerization of Myrcene (for sake of clarity, only 1,4-addition is shown). ....	54
Figure 1.34: Representation of a GPC column.....	56
Figure 1.35: THF-SEC-derived molar mass distributions of Polymyrcene for various polymerization degree values (10, 25, 50, 100, and 200) synthesized by anionic polymerization in THF. (excerpt from Zhang, et al ACS Sustainable Chem. Eng. <b>2022</b> , 10 (29), 9654–9664. <a href="https://doi.org/10.1021/acssuschemeng.2c03755">https://doi.org/10.1021/acssuschemeng.2c03755</a> . <a href="https://creativecommons.org/licenses/by/4.0/">https://creativecommons.org/licenses/by/4.0/</a> ) .....	56
Figure 1.36: <sup>1</sup> H NMR spectrum of polymyrcene with its attributions.....	58
Figure 1.37: Infrared spectrum of Polymyrcene (excerpt from Preetom Sarkar and Anil K. Bhowmick. RSC Adv. 4, no. 106 (2014): 61343–54). ....	58
Figure 2.1 Multilamellar mixer (excerpt from “Microfluidic mixers : a short review,” Elveflow. [Online]. Available: <a href="https://www.elveflow.com/microfluidic-tutorials/microfluidic-reviews-and-tutorials/microfluidic-mixers-short-review/">https://www.elveflow.com/microfluidic-tutorials/microfluidic-reviews-and-tutorials/microfluidic-mixers-short-review/</a> . [Accessed: 07-Nov-2022]). <sup>4</sup> .....	68
Figure 2.2 : Organolithium chemistry with unprotected alkyl iodophenones a) Setup of fluidic assembly b) Photo of the assembly with the M2 and M3 T-shape mixers and the R2 reactor (Excerpt from Kim, H., Nagaki, A., & Yoshida, J. I. (2011). Nature communications, 2(1), 1-6). <sup>11</sup> .....	70
Figure 2.3 Reactivity of halogenated nitrobenzenes with microfluidic organolithies: switching between kinetic and thermodynamic products (excerpt from Nagaki, A., Kim, H., & Yoshida, J. I. (2009). Angewandte Chemie, 121(43), 8207-8209). <sup>12</sup> .....	70
Figure 2.4: Synthesis and reactivity of vinylcarbenoids 2 from gem-dibromoalkenes 1. ....	73
Figure 2.5: Generation and trapping of a carbenoid A from gem-dibromoalkene (2.1) under batch and continuous flow conditions.....	73
Figure 2.6 : Reactor tubing ID = 500 $\mu$ m, L = 3 cm.....	74
Figure 2.7: Proposed path for the synthesis of Panomifene from a vinyl carbenoid. ....	74
Figure 2.8: Set up of Lithium-halogen exchange on gem-dibromoalkene.....	75
Figure 2.9 : Micromixers angles design.....	77
Figure 2.10 : Micromixers angles. ....	77
Figure 2.11 : Yield of 2.2 according to the angle of the micromixer.....	80



Figure 2.12: Lithium aggregates, (1) Hexamer, (2) Tetramer (3) Dimer, (excerpt from McGarrity and Ogle, 1985). <sup>14</sup> .....	81
Figure 2.13 Evolution of E/Z ratio of 2.2 according to time in a flow set up.....	82
Figure 2.14 : Reaction in MF with methylbenzoylformate. ....	82
Figure 2.15: Synthesis of compound (E)-2.3 under microflow conditions (see Supporting information for details). ....	83
Figure 2.16 CFD of a V-shaped micromixer, with an angle of 45°; ID 0.25mm. ....	83
Figure 2.17: Velocity temporal variations at two points, micromixer 45°, ID 0.25 mm .....	84
Figure 3.1: Anionic polymerization of myrcene with an alkyl-lithium (for sake of clarity, the scheme was drawn starting with a 1,4-addition).....	91
Figure 3.2: Study of degradation of n-BuLi at 30 °C in a THF/hexane solution.....	94
Figure 3.3: Decomposition of THF with organolithium. ....	94
Figure 3.4: Experimental setup for batch polymerization of myrcene with temperature control. ....	97
Figure 3.5: Temperature inside the reactor (17 g myrcene, bath 10 °C) .....	97
Figure 3.6: <sup>1</sup> H NMR (300 MHz, CDCl <sub>3</sub> ) spectrum of polymyrcene in batch at 10 °C in THF/hexane. Microstructure calculations: b=1.13(1H); c=(14.57-1.13)/2=6.72(1H); a=(15.70-6.72-1.13)/2=3.92(1H); a=3.92/11.77=33%, b=1.13/11.77=10%, c=6.72/11.77=57% .....	98
Figure 3.7: Diagram of the setup used in microflow conditions for the synthesis of polymyrcene. Flow rate of myrcene/n-BuLi/ MeOH (mL/min): 0.25/0.1/0.1 respectively, 1 min reaction. Reactor geometry: 0.75 mm ID, 1-meter length.....	99
Figure 3.8: T- and W-shaped micromixers. ....	100
Figure 3.9: Stainless steel microreactors .....	101
Figure 3.10: Microflow Setup. ....	101
Figure 3.11 Comparison between different length reactors at 10°C.....	104
Figure 3.12: Simulation vs experimental trend of concentration vs residence time at 10 ° C. ....	110
Figure 3.13 Simulation vs experimental trend of concentration vs residence time at 20 ° C. ....	111
Figure 3.14: Experimental concentration vs simulation concentration of myrcene (10 and 20 °C).....	111
Figure 4.1: Synthesis of hydroxyl-terminated polyisoprene. <sup>24,25</sup> .....	118
Figure 4.2: Poly hydroxyl-terminated polystyrene (excerpt from Takahashi, Y.; Nagaki, A. Anionic Polymerization Using Flow Microreactors. <i>Molecules</i> <b>2019</b> , 24 (8), 1532. <a href="https://doi.org/10.3390/molecules24081532">https://doi.org/10.3390/molecules24081532</a> ). <sup>27</sup> .....	118
Figure 4.3: Functionalization of dienes with α-halo-ω-aminoalkanes .....	119
Figure 4.4: Synthesis of Sulfonate end-capped polymers. <sup>29</sup> .....	119

<i>Figure 4.5: Addition of a carboxylic acid group to polymers with CO<sub>2</sub>.....</i>	<i>119</i>
<i>Figure 4.6: Protected functionalized initiator. ....</i>	<i>119</i>
<i>Figure 4.7: End-functionalization of polymyrcene by trapping benzophenone.....</i>	<i>120</i>
<i>Figure 4.8: Results obtained in the anionic polymerization in flow conditions at 10 °C.....</i>	<i>121</i>
<i>Figure 4.9: Functionalization of polymyrcene TMS-end group.....</i>	<i>122</i>
<i>Figure 4.10: Experimental set up for TMS end-functionalization with mix THF/TMScI. ....</i>	<i>122</i>
<i>Figure 4.11: Reaction of phenyl-lithium with carbon dioxide.....</i>	<i>123</i>
<i>Figure 4.12: Interphase in batch (left) vs continuous flow (right). ....</i>	<i>124</i>
<i>Figure 4.13: Set up of telescoped anionic polymerization of myrcene/functionalization with CO<sub>2</sub> in a flow system (MFC = mass flow controller). ....</i>	<i>125</i>
<i>Figure 4.14: Synthesis of polymyrcene acid end-functionalized with CO<sub>2</sub> in flow conditions. ....</i>	<i>125</i>
<i>Figure 4.15: <sup>13</sup>C NMR (300 MHz, CDCl<sub>3</sub>) of polymyrcene ketone in batch at 10°C.....</i>	<i>126</i>
<i>Figure 4.16: <sup>13</sup>C NMR of polymyrcene end-group acid, MF conditions: flow rate myrcene/n-BuLi/CO<sub>2</sub> 0.25:0.1:1.36 mL/min respectively at 10°C.....</i>	<i>127</i>
<i>Figure 4.17: End-functionalization of PMYR: reactivity according to batch or flow conditions. ....</i>	<i>127</i>
<i>Figure 4.18: 1,4 dilithiumbutane.....</i>	<i>128</i>
<i>Figure 4.19: Transformation reaction of 1,4-diiodobutane into 1,4-dilithiumbutane by treatment with tert-butyllithium .....</i>	<i>129</i>
<i>Figure 4.20: Degradation of tert-butyllithium and concentration of 1,4-dilithiumbutane over time at 20°C. ....</i>	<i>130</i>
<i>Figure 4.21: Anionic polymerization of polymyrcene bifunctionalized with TMS (for sake of clarity, the scheme was drawn starting with a 1,4-addition). ....</i>	<i>130</i>
<i>Figure 4.22: Setup for bifunctionalization of polymyrcene TMS end-group.....</i>	<i>132</i>
<i>Figure 4.23 : Setup for bifunctionalization of polymyrcene CO<sub>2</sub>H end-group.....</i>	<i>133</i>

## Abbreviation list

### A

**APS** Ammonium persulphate

### B

**BPR** Back pressure regulator

### C

**CHCl<sub>3</sub>** Chloroform

**conv.** Conversion

### D

**DB-5** Non polar and low bleed column

**DBA** 1,1 dibromo-3,3,3-trifluoroprop-1-en-2-yl)benzene

**DBN** 2-(2,2-dibromovinyl)naphthalene

**DCM** Dichloromethane

**DiLi** Dilithiumbutane

**DMA** Dynamic Mechanical Analysis

**DSC** Differential scanning calorimetry

### E

**equiv. or eq** equivalents

### F

**FBW** Fritsch-Buttemberg-Wiechell

**FEP** Fluorinated Ethylene Propylene

### G

**GC-MS** Gas chromatography coupled to mass spectrometry

**GPC or SEC** Gel permeation chromatography or Size Exclusion Chromatography

### H

**HCl** Hydrogen Chloride

**HPLC** High Performance Liquid Chromatography

### I

**inox** Stainless steel

***i*-PrOH** 2-propanol

**IR** Infrared spectroscopy

### L

**LiBr** Lithium bromide

### M

**MALDI-TOF** Matrix-assisted laser desorption/ionization- time of flight

**MeOH** Methanol

<b>MesLi</b>	Mesityllithium
<b>MF</b>	Microfluidics
<b>MFC</b>	Mass flow controller
$\overline{Mn}$	Molar mass
<b>MYR</b>	Myrcene
<b>N</b>	
<b><i>n</i>-Bu</b>	<i>n</i> -butyl
<b><i>n</i>-BuLi</b>	<i>n</i> -butyl lithium
<b>NMR</b>	Nuclear Magnetic Resonance
<b>O</b>	
<b>ODEs</b>	Ordinary differential equations
<b>P</b>	
<b>PEEK</b>	Polyetheretherketone
<b>PFA</b>	Perfluoroalkoxy alkane
<b>pKa</b>	Acid dissociation constant (Ka) of a solution
<b>PMYR</b>	Polymyrcene
<b>R</b>	
<b>Ref.</b>	Reference
<b>RT</b>	Room temperature
<b>Rdt.</b>	Yield (Rendement)
<b>S</b>	
<b><i>s</i>-BuLi</b>	<i>sec</i> -butyllithium
<b>STY</b>	Space-time yield
<b>T</b>	
<b>T%</b>	Transmittance
<b><i>t</i>-BuLi</b>	<i>tert</i> -butyllithium
<b>Tg</b>	Glass-transition temperature
<b>TGA</b>	Thermogravimetric analysis
<b>THF</b>	Tetrahydrofuran
<b>TMEDA</b>	N,N,N,'N"tetramethylethylenediamine
<b>TMS</b>	Trimethylsilyl
<b>TMSCI</b>	chlorotrimethylsilane

<b>Symbol</b>	<b>Meaning</b>	<b>Usual unit</b>
<b>t<sup>R</sup></b>	Residence time	(s or min)
<b>ID</b>	Internal diameter	(mm)
<b>P</b>	Pressure	(bar)
<b>Q</b>	Volume flow rate	(mL/min)
<b>A</b>	Transversal surface	(mm <sup>2</sup> )
<b>Re</b>	Reynolds number	(dimensionless)
<b>ρ</b>	Fluid density	(mg/mL)
<b>v</b>	Fluid velocity	(mm/min or mm/s)
<b>μ</b>	Fluid viscosity	(Pa·s)
<b>L</b>	Length or diameter	(mm or μm)
<b>k</b>	Velocity constant (1st order reaction)	(s <sup>-1</sup> )
<b>eq</b>	Number of equivalents	(mol)
<b>C<sub>A</sub></b>	Compound A concentration	M (mmol/mL)
<b>Δ<sub>r</sub> H</b>	Enthalpy	(joules)
<b>V</b>	Volume	(mL)
<b>d<sub>t</sub></b>	Internal diameter of the tubular reactor	(mm)
<b>U</b>	Overall heat transfer coefficient	(W·m <sup>2</sup> /°C)
<b>T</b>	Temperature	(°C)
<b>T<sub>ex</sub></b>	External temperature	(°C)
<b>D</b>	Diameter	(mm or μm)
<b>Đ</b>	Dispersity	(dimensionless)
<b>FD</b>	Functionalization degree	(%)
<b>r</b>	radius	(mm or μm)
<b>S</b>	Surface	(m)
<b>M<sub>n</sub></b>	Molar mass	(g/mol)
<b>M<sub>n</sub><sub>th</sub></b>	Theoretical molar mass	(g/mol)
<b>STY</b>	Space time yield	(kg/L/h)

## Abstract

The reactions studied herein rely on the chemistry of organolithium compounds in miniaturized flow reactors: regioselective bromine-lithium exchange reaction on a vinyl compound by mean of micro-mixers with various shapes, and controlled polymerization of myrcene, a bio-based analogue of isoprene.

Thus, sixteen passive mixers with different angles and diameters were assessed on Li-Br exchange on a *gem*-dibromo vinyl compound with *n*-BuLi at various flow rates: highest flow rates in a fine mixer ( $\theta = 45^\circ$ , ID = 0.25 mm) allows a Z/E selectivity exceeding 90%, simply at 20 °C.

Moreover, the flow polymerization of myrcene with *n*-BuLi was developed to reach low  $\overline{M}_n$ . Thus, reproducible living polymerization with finely controlled oligomerization was achieved. In addition, a further inlet feeding the flow system with CO<sub>2</sub> allowed the selective end-functionalization of polymyrcene with a carboxyl group. This work opens the door to a new sustainable process to obtain controlled and functionalized oligomers.

**Keywords:** organolithium, microfluidics, micromixers, selectivity, myrcene, polymerization, end-functionalization, carbon dioxide

## Résumé

Les réactions étudiées ici reposent sur la chimie des composés organolithiés dans des réacteurs miniaturisés à flux continu : réaction régiosélective d'échange Br-Li sur un composé vinylique au moyen de micro-mélangeurs de formes variées, et polymérisation contrôlée du Myrcène, un analogue biosourcé de l'isoprène.

Ainsi, seize mélangeurs passifs avec différents angles et diamètres ont été évalués sur l'échange Li-Br d'un composé vinylique *gem*-dibromé avec le *n*-BuLi à différents débits : les débits les plus élevés dans un mélangeur fin ( $\theta = 45^\circ$ , DI = 0.25 mm) permettent une sélectivité Z/E dépassant 90%, simplement à 20 °C.

De plus, la polymérisation en flux continu du myrcène avec le *n*-BuLi a été développée pour atteindre de faibles  $\overline{M}_n$ . Ainsi, une polymérisation vivante reproductible avec une oligomérisation finement contrôlée a été réalisée. De plus, une autre entrée alimentant le système en flux avec du CO<sub>2</sub> a permis la fonctionnalisation terminale sélective du polymyrcène avec un groupe carboxylique. Ce travail ouvre la porte à un nouveau procédé durable pour obtenir des oligomères contrôlés et fonctionnalisés.

**Mots-clés :** Organolithiens, microfluidique, micromélangeurs, sélectivité, myrcène, polymérisation et fonctionnalisation, dioxyde de carbone

## General introduction

Over the years, the problem of direct dependence on petroleum products has not been solved. It is well known that petroleum sources are not everlasting. So, what are we going to do to solve this problem? There are various valuable chemical products from non-renewable sources, among which polymers represent an essential part. For example, in 2000 the production of plastics in the world was estimated as 193 million metrics ton, further in 2020, it was estimated as 367 million metrics ton and it is continuing increasing (Fig 1).<sup>1,2,3</sup>

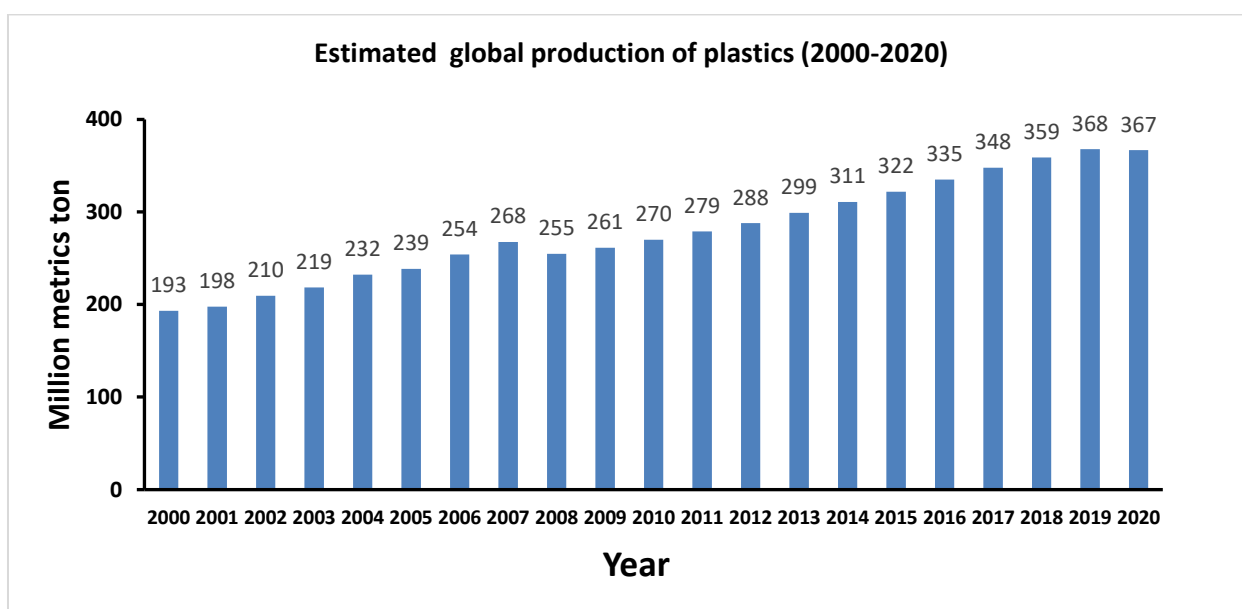


Fig 1: Estimated global production of plastics (2000-2020).

So basically, if we do not have petroleum, we will not have polymer products. This justifies the fact that researchers have been working to alternative resources to reduce this dependence.

An important step is to develop polymers in an ecological way using monomers from natural sources. Polymers from renewable resources, such as polymyrcene, are an alternative solution that could replace those from non-renewable resources (*e.g.*, polybutadiene in this case). In this line,  $\beta$ -myrcene is found as product of the pyrolysis of  $\beta$ -pinene, but this monoterpene is also present in fruits and different plants.<sup>4,5</sup>  $\beta$ -Myrcene has been polymerized by various pathways: cationic,<sup>6</sup> anionic,<sup>7</sup> coordinative,<sup>8</sup> and free and



controlled radical polymerization.<sup>9,10</sup> However, there are some difficulties in the current polymer production methods (macrobatch). One difficulty is the effectiveness of the system to control the internal temperature within the reactor. Another problem is that, even if it is possible to control the polymer's molecular mass and the dispersity index ( $\bar{M}_w/\bar{M}_n$ ) during the polymerization reaction, it may require a catalyst and/or high temperatures, according to method chosen.<sup>11</sup>

For these reasons, many researchers are working on transitioning discontinuous batch to continuous flow reactors. The use of modern technologies, such as microfluidics, seems to generate better results in the control of dispersity and would allow further development into industrialization.<sup>12,13</sup>

Flow chemistry makes it possible to carry out chemical reactions more controlled manner than chemistry in batch mode. Among the reasons for choosing continuous flow chemistry, transfer capacity of heat/temperature control of the reaction medium, process intensification and fine reaction control (residence time within the flow reactor) are prominent features.

Since promising pioneering results,<sup>14</sup> research in continuous flow chemistry has been expanding internationally. It is used in several fields, such as: organic chemistry, pharmaceutical industry, health (medical equipment), with microfluidic devices for sample analysis and diagnosis, biology (micro-biological research), cell culture assisted by 3D printing, the cosmetics industry, energy (plasma containment models), etc., even the NASA is concerned because coffee's machines in the spacecraft are made with the bases of microfluidics systems. In France, chemical industries such as Oril, Novalix, Minakem and Solvay companies regularly advertise on the benefits of flow chemistry.

Therefore, the changes to continuous flow are coming gradually, because there is a vast family of molecules to develop, and it requires time for research, and optimization. For example, based on the continuous flow concept, controlled polymerization has already been developed for various compounds, such as: styrene,<sup>15</sup> alkyl methacrylate,<sup>16</sup> and Isobutyl vinyl ether,<sup>17</sup> and others. Nevertheless, it is observed that the handling of polymers and polymerization in micro-channels is challenging at high flow rates and at high-pressure

drop (this is due to the viscosity of the polymer solutions; the viscosity increases during polymerization).

However, even if there are still some difficulties for the polymerization processes, the field is open to opportunities of improvement. For this reason, **this PhD project is based on the use of microflow systems (developed in COBRA laboratories) for the anionic polymerization of bio-based myrcene (domain of the PBS laboratory, to develop macromolecular chemistry strategies).**

In view of this, **chapter 1's** primary goal is to present the idea of continuous flow chemistry and its key components. The controlled polymerization of myrcene using continuous flow reactors is suggested in the second section. The myrcene's primary attributes and features are introduced. Different pathways to obtain polymyrcene are presented. Various methods for characterizing and analyzing polymers are also drawn in order to better understand the myrcene polymerization.

**Chapter 2** the influence of sixteen passive mixers with ID = 0.5- and 0.25 mm internal diameters and eight various angles of 135°, 120°, 105° (Y mixers), 90° (T mixer), 75°, 60°, 45°, and 30° (W mixers) will be investigated. The most effective micromixer for the process in terms of chemical selectivity (one of several possible products) and geometric selectivity will then be determined by varying several parameters.

Once the mixing effect studied, numerous aspects of the continuous flow of myrcene will be investigated in **chapter 3** including residence time, flow rate, the impact of temperature, and the microstructure of polymyrcene, among others. Before highlighting the major accomplishments of this work, a kinetic model of myrcene polymerization in continuous flow will be presented in the final section.

In **Chapter 4** the goal is to demonstrate how polymyrcene can be end-functionalized in continuous flow reactors principally with CO<sub>2</sub> gas. Further using a bifunctional initiator telechelic polymyrcene will be synthesized to finally have access to reactive oligomers that can be incorporated into materials.

The results obtained are summarized in a general conclusion, to finish with some perspectives regarding this work.

# Chapter 1

**State of the art**

## 1.1 Introduction

First, the purpose of this chapter is to introduce the concept of continuous flow chemistry and its main parameters. As continuous flow chemistry makes it possible to carry out chemical reactions more controlled manner than chemistry in batch mode. In a second part, controlled polymerization of myrcene using continuous flow reactors is proposed. The main features and properties of the myrcene are introduced. As the myrcene polymerization has only been performed under batch conditions, different pathways to obtain polymyrcene are described. Finally, to better understand the myrcene polymerization, various techniques used to analyze properties and characterize polymers are also drawn.

## 1.2 An alternative: continuous flow chemistry

Continuous flow consists in passing one or more different fluids (liquid, gas) through tubes, a single microreactor or a microfluidic system. Different scales can be used to describe a continuous flow reactor such as nano-, micro-, milli- or meso- according to the reactor diameter (Figure 1.1)

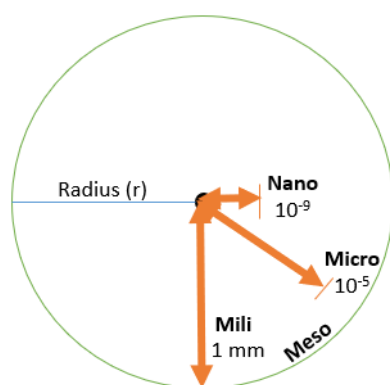


Figure 1.1:Representation of nano-, micro-, mili- and meso- scale.

However, these designations are not subject to strict rules because the complexity of continuous flow systems can lead to the use of devices of different sizes in the same assembly, which makes a strict nomenclature irrelevant. This concept of microfluidics is

based on the use of small volumes of fluids and one or more devices of less than 1 millimeter of internal diameter (ID). There is no restriction on the use of units, so in this manuscript we will speak indistinctly of mm or  $\mu\text{m}$  of ID.

Continuous flow chemistry is an alternative to substitute batch reactors. Since, it allows to carry out chemical reactions in a more controlled manner than chemistry in batch mode. Figure 1.2 shows a typical continuous flow system.

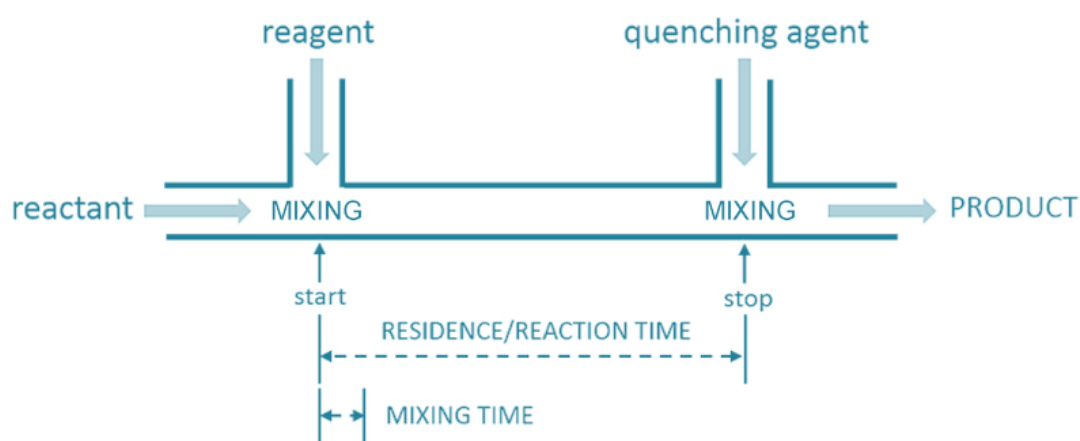


Figure 1.2: Scheme of a continuous flow system.

Among the advantages of using continuous flow in chemistry are:

- To synthesize products in a more secure and fast way (small volumes, efficiency in heat and mass transfer).<sup>19</sup>
- To perform effective reactions (efficiency and selectivity).<sup>20</sup>
- Limiting the energy consumption of installations (cooling/heating).<sup>21</sup>

### 1.2.1 General features

As long as continuous flow is a part of chemistry, different parameters can be used to optimize reaction conditions. Thereby, through this part, the main changeable parameters will be described. Also, in microflow chemistry, specific equipment can be used and will be presenting in this section.

## **Flow rate (Q)**

The flow rate is an essential parameter for characterizing the reaction in the micro-reactor. According to the literature,<sup>22</sup> by changing the flow rate only, different conversion, yield and selectivity results can be obtained. If we stay with the same concentration, just changing the relative flow rate, we can have different molar relationships between reagents.

## **Concentration (C)**

In continuous flow reactors, the concentration of the reagents is another crucial parameter for characterizing chemical reactions since it will influence the miscibility of the fluids, and the reaction speed rate.<sup>23</sup> In the first instance, for the implementation of a continuous flow system, the concentrations are fixed according to the stoichiometric quantities of the reaction. The concentration can also change the productivity of the reaction because the concentration of the limiting reagent will induce a certain mass of the final product obtained for a given timing of sample collection.

## **Volume (V)**

The low volume of continuous flow reactors also reduces explosion damage, as the volume is directly related to the production capacity or heat consumption of the reaction. In addition, it makes it possible to consider reactions at tiny molecular scales.<sup>24</sup>

The volume in a microflow reactor as cylinder is calculated as a function of the internal diameter (ID) and the length of the tubing (Equation 1.1).

$$V = \frac{\pi d_t^2 L}{4} \quad \text{Equation 1.1}$$

Where:

$d_t$ , is the internal diameter of the tubular reactor (m).

$L$ , length of the tubular reactor (m).

## **Temperature (T)**

Microfluidics systems are more efficient in heat transfer than batch systems because the transfer of energy is linked to the reactor geometry. The use of micro-reactors allows the

faster evacuation of heat, and maintains conditions closer to the isotherm, thanks to the ability of micro-reactors to exchange heat with its environment.

It may be noted that there are differences between the temperature distribution profile in a flask (batch) in comparison with the continuous flow reactor, see Figure 1.3.

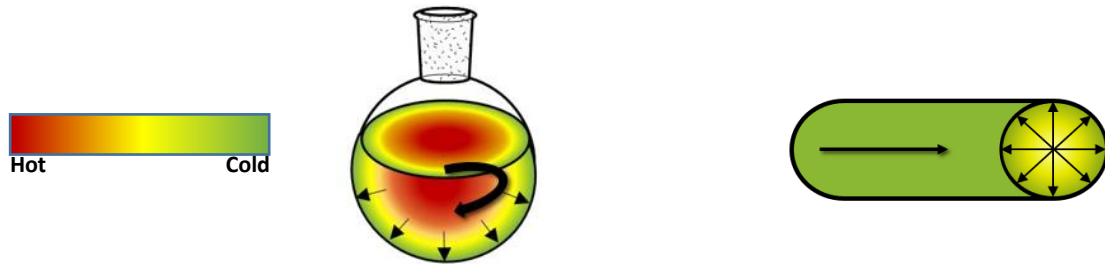


Figure 1.3: Temperature profile in a round-bottom flask (right) and in a microfluidic reactor (left).

To assess the difference between the heat release of a reactor in batch and continuous flow first we must consider the case of an exothermic reaction.<sup>25</sup> In an exothermic reaction of order 1, the ratio between the heat flux released by the reaction and the heat flux evacuated by exchange is the following:

$$\frac{\text{heat flux released by the reaction}}{\text{heat flux removed by exchange}} = \frac{kC_A(-\Delta_r H)V}{US(T - T_{ex})} \quad \text{Equation 1.2}$$

Where:

$k$  is the specific rate constant for a 1<sup>st</sup> order reaction in s<sup>-1</sup>.

$C_A$  is concentration of compound A in mol.L<sup>-1</sup>.

$\Delta_r H$  is the enthalpy of the reaction in Joules (J).

$U$  is the Overall exchange coefficient in W.m<sup>2</sup>K<sup>-1</sup>.

$S$  is the surface (m)

$(T - T_{ex})$  is the temperature difference between the reaction medium and the cooling medium in K.

This equation is used to describe the heat transfer ratio between the reaction medium and the cooling medium. If the heat flow released by the reaction is bigger than the heat flow



removed by exchange, the temperature inside the reactor will increase, being a deficiency in the system.

On a general standpoint, to control the temperature in the reactor, two parameters have to be considered, the overall exchange coefficient and the specific area of exchange.

The exchange coefficient  $U$  describes the efficiency with which heat can pass through the reactor's wall and the cooling medium. This coefficient depends on hydrodynamic conditions, the thermal conduction performance of the wall material between the coolant and the reaction medium.  $U$  is also inversely proportional to the size of the reactor.

The specific area of exchange has to be calculated, because it depends on the design of the reactor. This specific area of exchange is expressed by the ratio  $\frac{S}{V}$  where the surface of transfer ( $S$ ) has an inverse relation with the reactor's diameter.<sup>25</sup> For example, for a cylindrical continuous flow reactor, the specific area of exchange is according to Equation 1.3:

$$\frac{S}{V} = \frac{2\pi hr}{\pi hr^2} = \frac{2}{r} = \frac{4}{d} \quad \text{Equation 1.3}$$

Where:  $V$ : volume (m<sup>3</sup>),  $S$ : area or surface (m<sup>2</sup>),  $r$ : radius (m),  $h$ : height (m)  $d$ : diameter (m)

However, in batch reactors like a round-bottom flask; the specific exchange area is totally different and is calculated by using this Equation 1.4:

$$\frac{S}{V} = \frac{6\pi rh}{\pi h^2(3r - h)} \quad \text{Equation 1.4}$$

Where:  $V$ : volume (m<sup>3</sup>),  $S$ : area or surface (m<sup>2</sup>),  $r$ : radius (m),  $h$ : height (m)  $d$ : diameter (m)

This shows that, the specific exchange area of the reactor influences the evacuation of heat and consequently the temperature control of the reaction. Figure 1.4 presents the specific exchange area for a 10 mL batch reactor and also for a microfluidic reactor of 0.1 cm and 0.025 cm. This example shows how the geometry of the reactor can affect the specific exchange area and consequently the heat transfer.

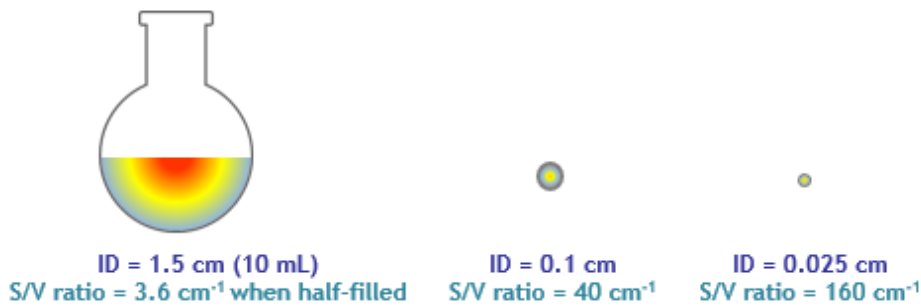


Figure 1.4: Specific exchange area in batch and continuous flow.

This explains why the temperature control in microfluidics is better than batch, and why the scale is very important to make a good comparison between the efficiency of continuous flow and batch reactors.

### Viscosity ( $\mu$ )

The fact that the two fluids have different viscosities gives rise to velocity profiles not symmetrical to the channel inlet and consequently in the center of the mixer.<sup>26</sup> In other words, it could influence the mixing.

Besides, in polymerizations reactions, the viscosity can increase due to the increasing molar mass of polymers and also, is directly linked to the temperature. It could be an issue in polymerization reactions in continuous flow and it has to be considered.

### Mixing

In several reactions, principally those are very fast, mixing represents a challenge in batch conditions. Ideally, the mixing time has to be shorter than reaction time and sometimes is not the case.

- **Mixing time**

Different from the *mixing time* in a batch reaction, where the phenomenon is controlled by the convective transfer in a turbulent flow, in continuous flow the *mixing time* is ruled by Fick's Law (Equation 1.5).<sup>25</sup>

$$t_{mixing} = \frac{d_t^2}{4D}$$

Equation 1.5

Where:

$d_t$  is the internal diameter of the tubular reactor (m).

$D$  is the diffusion coefficient of Fick's Law ( $m^2.s^{-1}$ ).

The mixing time in a micromixer can be estimated by the following Equation 1.6:

$$t_m = 100 \left( \frac{\mu}{\varepsilon} \right)^{0.5} \quad \text{Equation 1.6}$$

Where:  $\mu$ : dynamic viscosity of the fluid (Pa.s),  $\varepsilon$ : specific power dissipated ( $W.m^{-3}$ ) calculated by  $\varepsilon = \Delta P \cdot \frac{Q_v}{V}$ , where,  $\Delta P$  the pressure drop across the mixer of volume  $V$  and  $Q_v$  is the volumetric flow rate.

Another advantage of microflow conditions is that energy of fluids can be dissipated, resulting in mixing times of milliseconds.

### Types of flow and mixing

In most of microfluidic devices the fluids never change their laminar flow conditions due to 'low values' of Reynolds number (Re), reason why the mixture could be considered to rest only on molecular inter-diffusion in a tubular microreactor. Re is described as the relationship between the inertial forces and the viscous forces within a fluid subject to relative internal motion due to the various velocities of the fluid.

Regimes are classified according to the calculation of the Re:

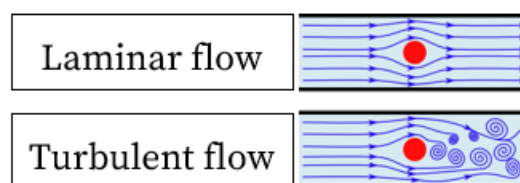


Figure 1.5: Laminar and turbulent flow.

- If  $Re < 2000$ , the flow is called laminar.
- If  $2000 < Re < 4000$ , the flow is called transitional.
- If  $Re > 4000$ , the flow is called turbulent.

The type of flow is based on the value of Re:  $Re = \frac{\rho v L}{\mu}$

Where,  $\rho$  = fluid density ( $g.m^{-3}$ ),  $v$  = fluid velocity ( $m.s^{-1}$ ),  $\mu$  = fluid viscosity ( $g.m^{-1}.s^{-1}$ ),  $L$  = length or diameter of the tube (m)

In microflow conditions, the flow is considered to be laminar, since there is no turbulence and recirculation eddies in microreactors mean that radial mixing is strictly due to diffusion.

For example, Figure 1.6 shows how mixing can be developed in a microfluidic reactor.<sup>24</sup> If we consider the case of a reaction like:

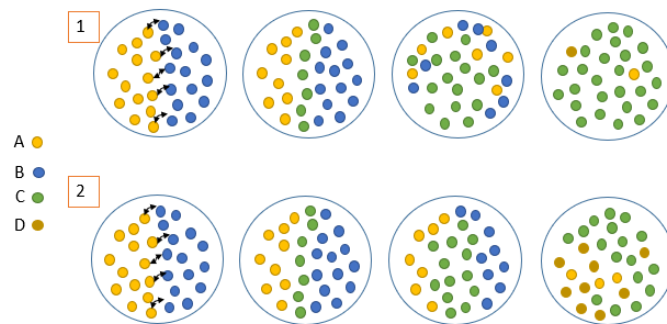


Figure 1.6: Evolution of mixing.

This phenomenon can be explained by the kinetics of the reaction. If there is a good mixing, kinetic rules that apply under homogeneous conditions are respected. Thus, the reaction 1 (with  $r_1=k_1[A][B]$ ), could take place selectively without reaction 2, ( $r_2=k_2[A][C]$ ) if  $k_1>k_2$ . In contrary, if the mixing is not good the reaction 2 can occur, resulting in the formation of D even if  $k_1>k_2$ . However, the reality is often not so simple with multiple possibilities of reactions.

There are two types of mixing depending on the energy source: active mixing and passive mixing. If external energy is used, it is called active mixing. If we use the inner energy of the flow, it is called passive mixing. Passive mixing uses the energy of the flow-through pumping action or hydrostatic potential.<sup>27</sup>

### Pressure (P)

One parameter that could more influence mixing is the pressure. As the pressure drop is related to the energy input expended in the mixing process. Therefore, better mixing

performance can generally be achieved by applying higher pressure drops. However, the highest mixing efficiency is achieved with this type of static mixers which provide some mixing performance with the lowest pressure drop.

Another fact is that the pressure drop can reduce the efficiency of pumping the fluids through the reactor, especially in a long microfluidic reactor where the pressure drops seem to be higher.

### Residence time ( $t^R$ )

The reaction time is controlled by the *residence time* inside the continuous flow reactors. Residence time is the average time required to pass a fluid or solution through the micro-reactor. The residence time is calculated following Equation 1.7:

- Reaction time = Residence time =  $t^R = f(V_{reactor}, Q_1 + Q_2)$

$$t^R = \frac{V}{Q} \quad \text{Equation 1.7}$$

$V$ : volume (mL)

$Q$ : volumetric flow rate (mL.min<sup>-1</sup>)

As the *residence time* depends on the reactor volume, this increases with the length of the channel and decreases with the flow rate.

The short residence time characteristic is extremely useful in control reactions involving an unstable reagent of intermediate short duration.

### Space-time yield (STY)

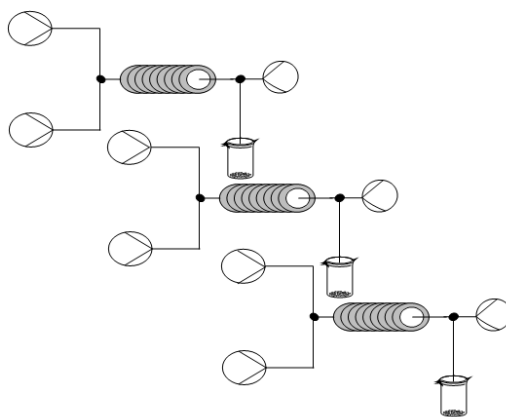
This term was proposed by Haber, Greenwood, Rideal and Taylor in 1915-1919. Space-time yield is defined as the quantity of product per unit of volume per unit of time.<sup>28</sup> The calculation corresponds to the following Equation 1.8:

$$\text{Space - time yield} = \frac{\text{Productivity} \left(\frac{\text{kg}}{\text{h}}\right)}{\text{Volume of reactor (L)}} \quad \text{Equation 1.8}$$

Space-time yield can be used as a criterion for estimating relative activities of chemical reactants or catalyst surfaces and reaction order.

### Numbering up (parallelization) and scale-out

In microflow conditions it is possible to increase the productivity by increasing the numbers of reactors in parallel, this is called “numbering up”.<sup>29</sup> Therefore, once the space-time yield of a microreactor is calculated, it is only necessary to multiply it by the number of reactors in parallel (Figure 1.7).



*Figure 1.7: Parallelization of the reactors in flow.*

Among the advantages of the numbering up of micro devices are: if there is a problem in any reactor, the production is not stopped completely, and another is the easy control of the system once the parameters are settled.

Another method in continuous flow to increase production is the ‘scale out’ or increasing of the channel’s internal diameter (Figure 1.8). This strategy is often favored by chemical companies that allow reach larger quantities of product with few optimization.

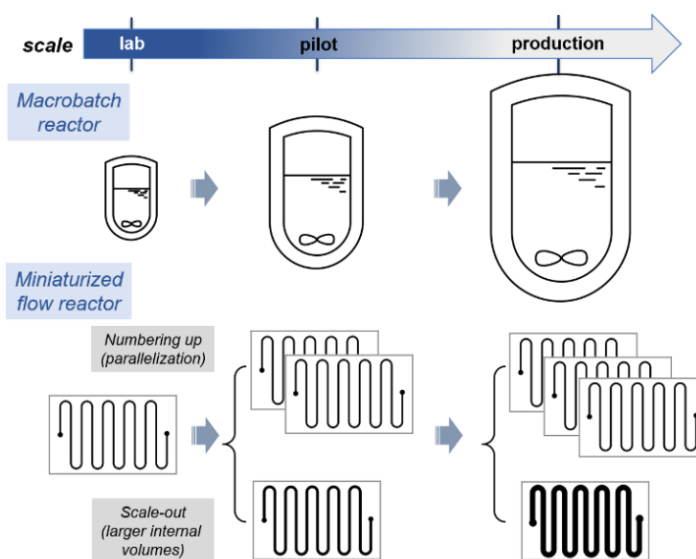


Figure 1.8: Scale-out and parallelization (excerpt from Monbaliu, J.-C. M.; Legros, J. *Will the next Generation of Chemical Plants Be in Miniaturized Flow Reactors? Lab on a Chip* 2022).<sup>30</sup>

## Process safety

Continuous flow reactors allow improvements in safety process: such devices make possible to handle and process large quantities of dangerous chemicals without exposing the operator. Microstructured reactors are not inherently safe, but because the explosion region is smaller, the range of acceptable operating conditions for microreactors is increased.<sup>31</sup> There are many examples of synthesis and utilization of very hazardous compounds in continuous flow. For example, the oxidative neutralization of a chemical warfare agent has been reported by Picard et al. in a continuous flow system.<sup>32</sup> Another example, it is the use of triphosgene to generate phosgene in continuous flow, since triphosgene is less toxic than phosgene. Phosgene is a very poisonous gas at room temperature, member of the chemical and war gases family of suffocating agents, and is frequently used in organic synthesis due to its strong reactivity, utility, and cost-effectiveness. Due to its toxicity, using phosgene in batch procedures on an industrial scale is difficult. Using an assembly as present below (Figure 1.9) Mitsuda *et al.* show that is possible to generate this hazardous compound in the synthesis of pharmaceutical intermediates in continuous flow.<sup>33</sup>

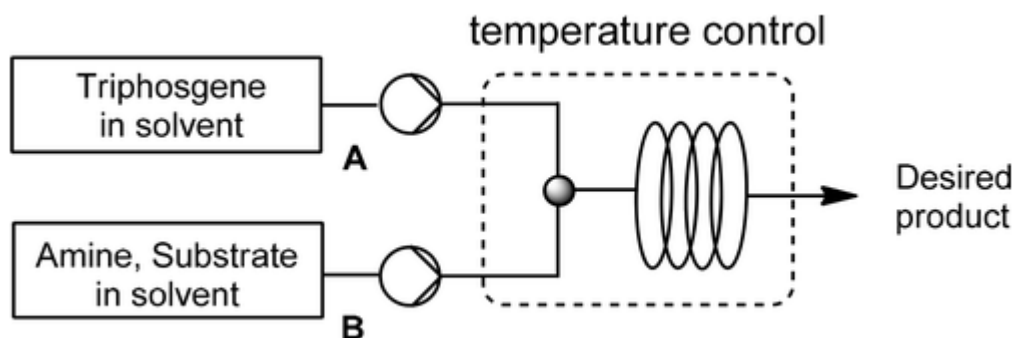
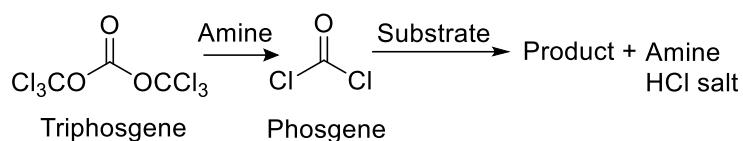


Figure 1.9: Phosgenation Reactions in a Continuous Flow Reactor (Yasukouchi, H.; Nishiyama, A.; Mitsuda, M. 2018, 22 (2), 247–251.).<sup>33</sup>

The system is composed of two inlets, one with triphosgene in toluene (A) and another with the substrate (B), alcohols, in this case, *eg*, menthol, mixed with tributylamine in toluene. It generates the phosgene that reacts with the substrate, giving the desired product. In batch this reaction is extremely dangerous but in flow is possible to perform it.

### 1.2.2 Devices in continuous flow systems

There are different types of devices in continuous flow systems. Its conception and design depend on their use and application. In order to keep a consistent definition, we will define microfluidics any fluidic device, which as at least one of the flow zones with a section diameter less than 1 millimeter.



## Microflow reactors

In microfluidic systems, the microreactor is the microchannel where the reaction takes place. A continuous flow reactor can have different shapes depending on the use. It can also be made from various materials like glass, stainless steel, perfluoroalkoxy alkane (PFA), Polyether ether ketone (PEEK). Pictogram used in literature to describe a continuous flow reactor is represented here (Figure 1.10).

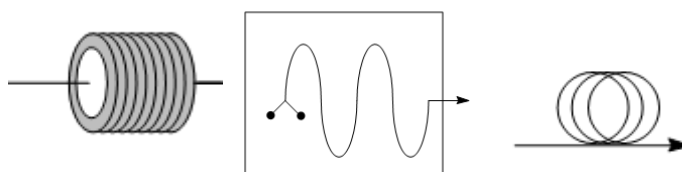


Figure 1.10: Pictograms used for continuous flow reactors.

## Mixers

There are two types of mixers depending on the energy source: active mixers and passive mixers. In an active micromixer, the mixing is accelerated by using disruption from an external field. Passive or static mixer uses the energy of the flow.<sup>27</sup>

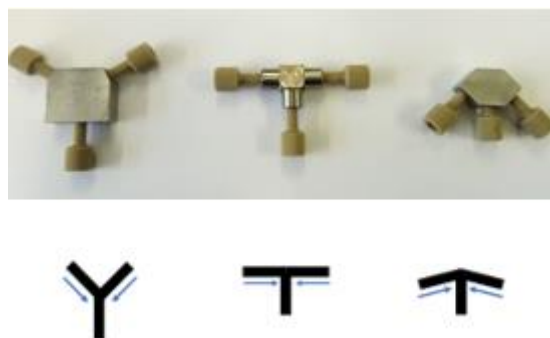
Due to the need to have a good mixing to get an effective reaction, there are several designs of micromixers. As each one has different characteristics, several authors have studied different types of micromixers. Table 1.1 lists two different types of micromixers with different ways of inducing the mixture.

Table 1.1: Different ways of inducing the mixture in microfluidics devices.

Type	Mixing means for inducing mixing
Active	Ultra-sonic <sup>34</sup>
	Acoustically induced vibrations <sup>35</sup>
	Small turbines <sup>36</sup>
	Integrated micro valves / pumps <sup>37</sup>
	Periodic flow rate variation <sup>38</sup>
Passive/ static	Feeding devices, called interdigital <sup>39</sup>
	Flow guidance in split and recombine <sup>40</sup>
	Chaotic mixing creates eddy-based flow patterns <sup>41</sup>

Figure 1.11 shows typical passive mixers, such as T-shape, W-shape, Y-shape. The difference between these mixers lies in the angle between the channels,  $\theta = 90^\circ$  for T-shaped and for W-shaped (also known as V or anchor-shaped) and Y-shape the angle is variable.<sup>42</sup>

Figure 1.11: Passive mixers such as Y-shape T-shape and W-shape and symbols.



### Internal diameter and geometry of micromixers

A small change in the micromixer diameter can significantly affect the reaction.<sup>43</sup> The fluid speed decreases as the diameter of the micromixer increases and vice versa. The flow rate (Q) of fluid directly depends on the linear velocity (v) of the fluid and the cross-section of the pipe (A) (Equation 1.9):

$$v = \frac{Q}{A}$$

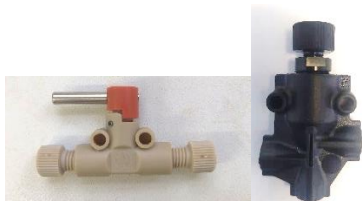
Equation 1.9

This equation implies that if a change in the internal diameter is produced, consequently, the flow rate will be affected, and also the molar relationship between the reagents. However, the micromixer diameter is not the only characteristic to be considered. The shape of the device is also important.

According to Kolbl *et al.* mixing times cannot be deduced from reactions of chemical tests by applying simple mixing models which do not consider the specific geometry of the micromixers. In a simulation of T and Y micro-mixers, Gobby *et al.*,<sup>26</sup> show that the angle seems to have a slight effect on the mixture and in the drop pressure. Yoshida also observed a significant difference in organolithium reactivity (very fast reactions) between T-shaped and W-shaped micromixers.

## Valves

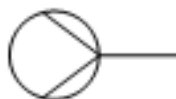
A valve is a mechanical element with which the flow of liquids or gases can be started, stopped, or regulated by employing moving parts that open or close, partially or entirely, the passage of the fluid. In continuous flow systems, valves are necessary to control the passage of fluid through the different channels (Figure 1.12).



*Figure 1.12: Valves used in microfluidics systems.*

## Continuous flow injection systems

In order to shift fluids into the system, it is necessary to use mechanical devices called pumps. Pressure-driven pumps are largely used in continuous flow. There are various kinds of pumps, such as peristaltic pumps, syringe pumps, HPLC pumps, and others as electro-osmotic pumps that use an electric field to generate flow or pressure. The Figure 1.13 shows two examples of pumps frequently used in the laboratory, a peristaltic and a syringe pump, also a symbol commonly used to do the schema of continuous flow systems.



*Figure 1.13: Photos of a peristaltic pump (middle), syringe-pump (right) and its symbol (below).*

## Back pressure regulators (BPR)

Some devices allow the control of the pressure in a microfluidics system. There is a device called back pressure regulator that allows regulation of pressure due to a size reduction within device (Figure 1.14, middle). There is also a version with an integrated heater sold by Vapourtec (Figure 1.14, right).



Figure 1.14: BPR symbol (left), image (middle), heated back pressure regulator assembly (right).

## Mass flow controller

Widely used in gas-liquid reactions the mass flow controller, as the name suggests, allows the control of the quantity gas volume, or mass, sent inside the flow system. By connection with a computer, it is possible to send a signal to the device to close or open more its inner valve. Figure 1.15 shows the symbol commonly used and a representation of the device.



Figure 1.15: Mass flow controller, symbol (left), and real photo (right).

## Integrated systems

Some companies are developing from the simplest to the most complex continuous flow reactor system. Integrated systems have pumps, connectors, valves, lamps, mixers, reactors in the same cage. For example, Vapourtec and Corning are two companies (among others) that provide integrated systems where it is possible to perform reactions from small to large volumes of solution (Figure 1.16).



Figure 1.16: Integrated systems in continuous flow: Vapourtec® (left) and Corning® (right)

### Purification in continuous flow: Liquid-Liquid or Gas-Liquid Separators

Some devices like membranes for Liquid-Liquid or Gas-Liquid Separators or commonly called “Zaiput®” (due to the name of the company that commercialize most of them) allow an effect separation of the aqueous and organic phases. Its operating principle is simple, a membrane inside the apparatus allows the passage of the organic fluid (yellow), allowing the separation of the aqueous part, in blue (Figure 1.17).



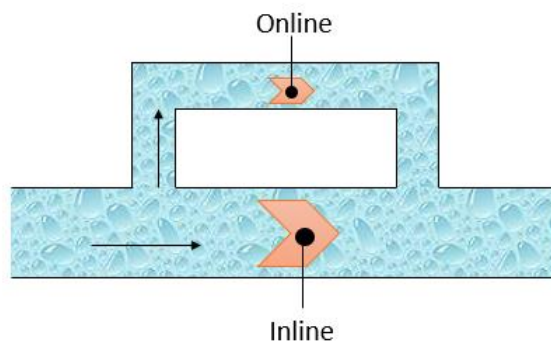
Figure 1.17: Liquid-Liquid Separator (Zaiput®)

#### 1.2.3 Analysis tools online /inline

A big advantage of continuous flow system is the analysis online/inline because it becomes possible to analyze reactions in real time, which is harder to perform in batch reactors.

The online analysis process is based on the use of a kind of bypass that allows to analyze the flow and return the sample to its original source. The inline analysis allows to directly

analyze the flow without disturbing the system, generally consists of sensors that help the detection of characteristic signals of the system (Figure 1.18).



*Figure 1.18: Scheme of online/inline system.*

Currently there are two famous techniques for the analysis online/inline in continuous flow, NMR and IR spectroscopy.

## **NMR**

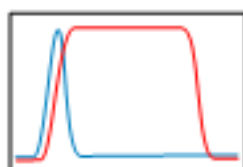
Characterization of polymers by nuclear magnetic resonance spectroscopy (NMR) gives detailed structural information for product development and quality control. NMR seems to be a good online analysis technique. Although there are still many improvements to be made, notably related to the use of non-deuterated solvents and the magnetic field capacity or power of the apparatus. The fact that an NMR at the bench already exists opens the possibilities of automatization of the entire flow system.<sup>44</sup> Figure 1.19 shows a NMR at the bench for a continuous flow system.



Figure 1.19: Real photo of NMR inline (excerpt from Picard et al. 2017).<sup>32</sup>

### **Infrared spectroscopy**

Infrared spectroscopy is another technique largely used to online analysis. This technique allows to follow the apparition of different functional groups in the molecules. Figure 1.20 is a symbol commonly used in schemes for continuous flow processes.



**FlowIR**

Figure 1.20: Infrared symbol in MF.

### **Spectroscopy ultraviolet-visible**

The spectroscopy technique involving photons with wavelengths in the field of ultraviolet.<sup>45</sup> For example, Hellma® a specialized German manufacturer sells flow-through cells that allow the analysis inline of the compounds in the flow (Figure 1.21).



Figure 1.21: Hellma® Flow-through cells.

With this technique it is possible to analyze the samples inline using an UV-visible spectrophotometer by connecting the continuous flow system to this type of cells.

A spectrophotometer is a device that detects a quantity of photons (light's energy) absorbed after they have passed through a sample solution. By measuring the intensity of light detected, the spectrophotometer may also estimate the concentration of a known chemical compound.

#### 1.2.4 Flash Chemistry

Microfluidic systems are a powerful tool for reactions involving highly unstable intermediates. For example, in a pioneering work, Yoshida *et al.* showed that *o*-bromophenyllithium, which is known to decompose into benzyne very quickly under batch conditions, could be generated in 0.8 s using continuous flow reactors, and trapped before decomposition (Figure 1.22).<sup>46</sup>

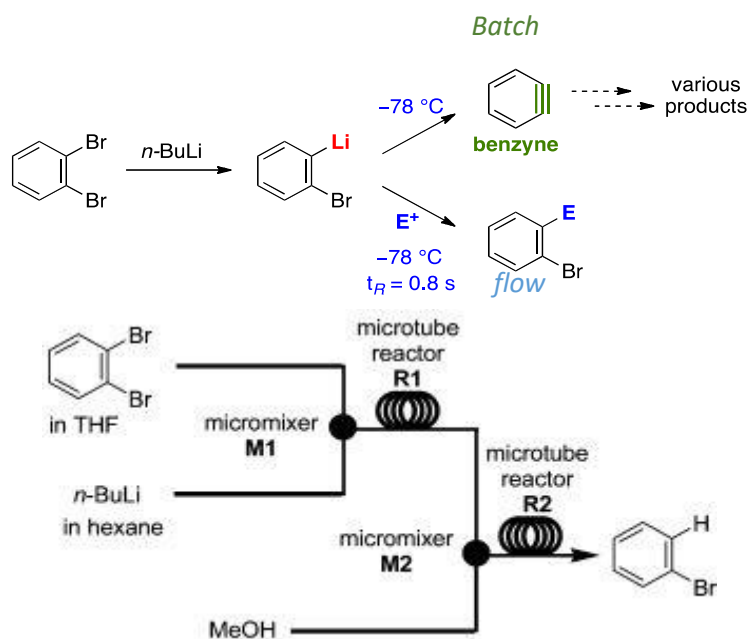


Figure 1.22: Generation and trapping of microfluidic *o*-bromophenyllithium (excerpt from Yoshida *et al.* 2007).<sup>46</sup>



The reaction of *o*-bromophenyllithium with *n*-BuLi, followed by reaction with a good electrophile, yields between 69-81% of desired products in microflow conditions.

### Anionic polymerization in continuous flow reactors

Devices like microreactors can be used for organic synthesis, medicine production, and as a way to control polymer structures in the reaction. For the synthesis of polymers, it is essential to precisely control the molar mass and its distribution, using a highly controlled block polymerization.

Based on the continuous flow micro-reactor concept, anionic polymerization has been developed for various compounds, such as: styrene, alkyl methacrylates, Isobutyl vinyl ether.<sup>47-16</sup> For example Nagaki et al. have been working in the anionic polymerization of styrene, using homemade microreactors and simple T-shape micromixers.<sup>48</sup> They use a system with an inlet with styrene in THF and sec-Butyllithium in cyclohexane (Figure 1.23). The reaction neutralization is stopped by collecting the reactor outlet in methanol. This system allows to make polystyrene with molar masses between 1200 and 20000 g/mol with a dispersity between 1.09-1.13.

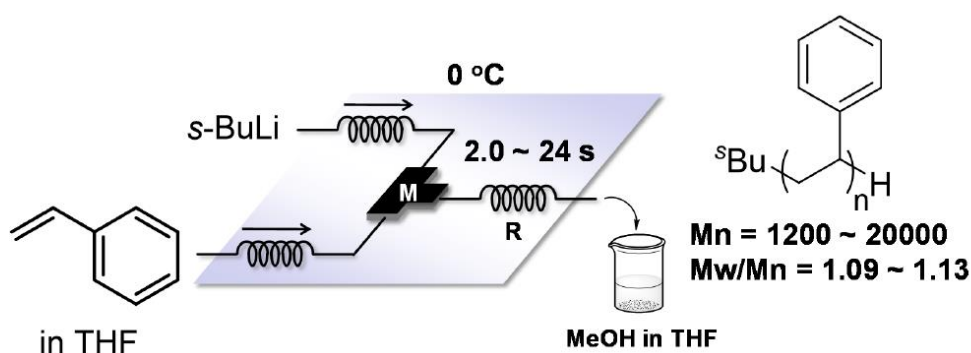


Figure 1.23: Anionic polymerization of styrene in continuous flow (excerpt from Nagaki et al., 2019).<sup>49</sup>

These results show that it is possible to carry out anionic polymerization in continuous flow and that is easy to control from large to small molar masses ( $\overline{M}_n$ ) of polymer.

As modern technologies such as microfluidics allow the control of polymerization, and nowadays, the tendency is to synthesize polymers from renewable resources is proposed the polymerization of myrcene, a bio-based analog of isoprene.

### 1.3 An interesting terpene: myrcene

Natural terpenes or terpenoids, are interesting molecules that can be found widely in different plants, mostly conifers trees.<sup>50</sup> It was also found that terpenes are produced in other living organisms, such an endophytic fungus<sup>51</sup> and swallowtail butterflies.<sup>52</sup>

Terpenes are compounds with the formula  $(C_5H_8)_n$ . Their classification is linked to the number of carbons:  $n=1$ , hemiterpene *e.g.* isoprene ( $C_5$ );  $n=2$ , monoterpenes ( $C_{10}$ );  $n=3$ , sesquiterpenes ( $C_{15}$ );  $n=4$ , diterpenes ( $C_{20}$ );  $n=5$ , sesterterpenes ( $C_{25}$ );  $n=6$ , triterpene ( $C_{30}$ );  $n=8$ , tetraterpene ( $C_{40}$ ); and polyterpene when  $n>8$ . In addition, they follow the “isoprene rule” which means that terpenes are composed of two or more isoprene units. Generally, terpenes can be of three different types: acyclic (*e.g.*, myrcene), monocyclic (limonene) and bicyclic (pinene). Figure 1.24 shows some typical terpenes found in the nature.

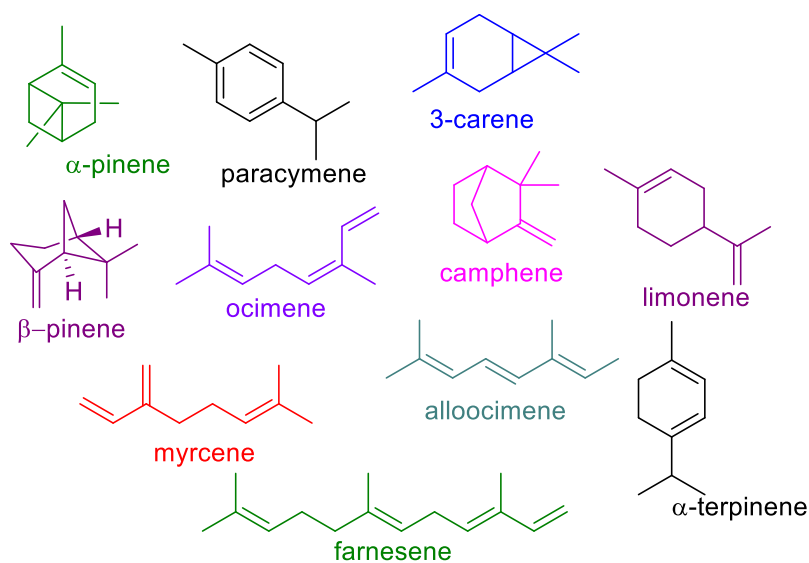
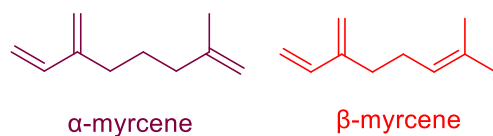


Figure 1.24: Some typical terpenes.

Myrcene belongs to monoterpenes family, and it exists under two forms,  $\alpha$ -myrcene (2-methyl-6-methylideneocta-1,7-diene) and  $\beta$ -myrcene (7-methyl-3-methylideneocta-1,6-diene), (Figure 1.25).



Chemical Formula: C<sub>10</sub>H<sub>16</sub>  
 Exact Mass: 136.13  
 Molecular Weight: 136.24

*Figure 1.25: Alpha and beta-Myrcene structure and chemical properties.*

Both forms are found in nature, but  $\alpha$ -myrcene is not abundant, and because of this,  $\beta$ -myrcene is often simply called myrcene in literature.<sup>53-54</sup> ***So, in this work  $\beta$ -myrcene is also mentioned as just myrcene in most cases.***

$\beta$ -Myrcene is known for its role in flavoring and aroma agent. Due to its characteristics it is used for different applications in food industries such as beverages and food manufacturing.<sup>53</sup> As show in Table 1.2, this monoterpene is present in fruits and in different plants such as cannabis, wild thyme, celery, ginger root, rosemary, ylang ylang, bay, parsley, nutmeg, etc.<sup>50</sup>

*Table 1.2: W/W % of Myrcene in different plants (excerpt from Behr and Johnen, 2009).<sup>50</sup>*

Origin	w/w (%)
Field wormwood	11.2
Bay leaf. type "anise"	12.8
Ylang ylang fruit	24.7
Wild thyme	39.1
Jambu flower	11.8
Juniper berry	11.0
Leaf oil from zanthoxylum ovalifolium	19.8

For example,  $\beta$ -myrcene is present in wild thyme in a mass quantity of 39.1%, 24.7% for Ylang Ylang fruit, and 19.8% in leaf oil from zanthoxylum ovalifolium, which are percentages that are not negligible. Unfortunately, nowadays, the process of extraction is still expensive, and it has to be developed more.

Fortunately, many terpenes can be found from a variety of turpentine, obtained by distillation of resin, harvested from live trees. Turpentine also can be recovered from the waste streams of paper mills.<sup>55</sup>

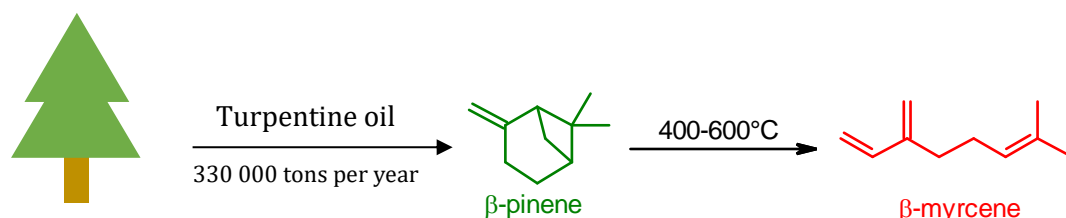


Figure 1.26:  $\beta$ -pinene pyrolysis into  $\beta$ -Myrcene.

$\beta$ -Pinene is the most common component in turpentine and can be distilled from it.<sup>56</sup>  $\beta$ -Myrcene can also be obtained as a product of  $\beta$ -pinene pyrolysis (Figure 1.26).<sup>55</sup> With this pyrolysis, it is possible to achieve high selectivity (86-95%) and good yields (85%), reasons for which, this is the method most used industrially.<sup>53</sup> There are many Myrcene-producing companies in the world, the main players being DRT, Bordas, Florida Chemical, Florachem, Yasuhara Chemical, Natural Aroma Products, Xinghua Natural Spice and Sky Dragon, Fine-Chem. The global production of  $\beta$ -Myrcene was estimated to 23,182 million tons in 2019.<sup>2</sup> Currently,  $\beta$ -Myrcene is commercially available in two forms: an untreated technical quality  $\sim$ 75% and in a high-purity  $>$ 90%.

$\beta$ -Myrcene is an attractive material for the production of alternative polymers. Due to its structure, it can easily be considered as a monomer substitute of polybutadiene and polyisoprene, obtaining polymyrcene with similar characteristic (Figure 1.27).

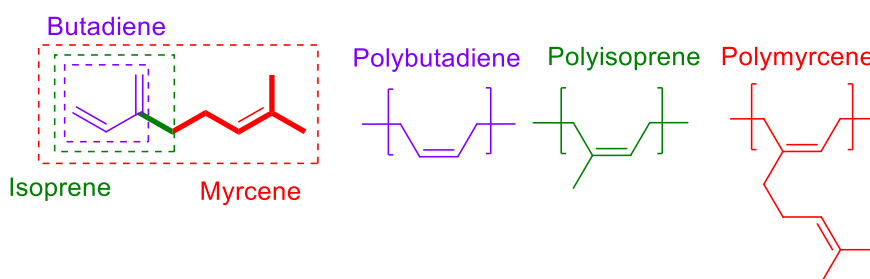


Figure 1.27. Structure similarities between butadiene; isoprene and myrcene.

In the search for a good substituent for butadiene the price of different monomers including myrcene, was considered (Table 1.3)<sup>57</sup>

Table 1.3: Approximate prices per mol of butadiene and some common terpenes (Sigma Aldrich, 2022).<sup>40</sup>

Monomer	Purity (%)	CAS Number	Molecular weight (g/mol)	Price per kg (€)	Price per mol (€)
<b>2,3-Dimethyl-1,3-butadiene</b>	>97	513-81-5	82.14	891	75.45
<b>β-Myrcene</b>	>90	123-35-3	136.23	110	16.65
<b>Ocimene (Mixture of isomers)</b>	>90	13877-91-3	136.24	740	112.02
<b>Farnesene (Mixture of isomers)</b>	-	18794-84-8	204.36	310	63.35
<b>Alloocimene (Mixture of isomers)</b>	> 80	673-84-7	136.23	205	34.91

Comparing *β-myrcene*'s prices with other similar monomers, myrcene has the lowest cost per mole, even butadiene from non-renewable resources is more expensive.

Studies reveal that myrcene exhibits lower toxicity compared with other monomers such as styrene,  $LC50_{Myrcene} > 163 \text{ mg/L}$  comparing to  $LC50_{styrene} \leq 20 \text{ mg/L}$ .<sup>58,59</sup>

To sum up, myrcene exhibits low toxicity,<sup>58</sup> which makes its use easy. Myrcene can be polymerized in different pathways (anionic, cationic, *etc*) and additionally, as a starting material, it is inexpensive. All these features make this interesting terpene *β-myrcene*, the object of much research and including this work.

#### 1.4 Synthesis of polymyrcene

Polymyrcene has been synthesized using different pathways such as free or controlled radical polymerization, and coordinative, cationic, and anionic polymerization The

Polymyrcene microstructure is composed of different isomers (four in total). These isomers are 1,4 *cis* and *trans*, 3,4 structure and 1,2 vinyl (Figure 1.28).

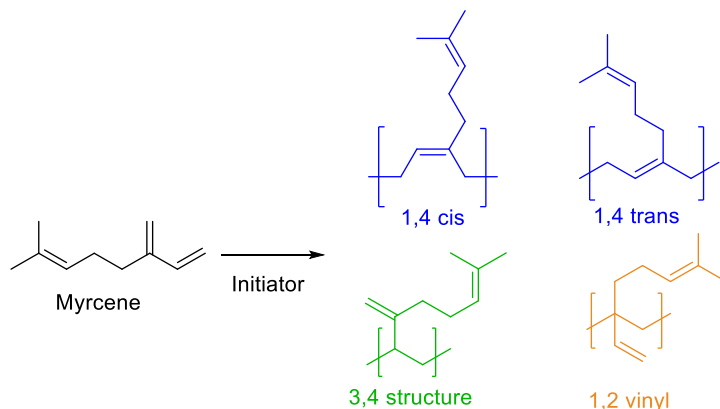


Figure 1.28: Polymerization of Myrcene and its different microstructures.

#### 1.4.1 Radical polymerization of myrcene

Radical polymerization is the most used type of polymerization industrially; more than 35% of the polymers produced each year in the United States of America are made with this technique. It is highly used because of its simplicity and tolerance to humidity. It allows obtaining polymers with high molar mass and long structures. Because of the high reactivity of the radicals, there is always a termination phase, with random and permanent ending groups in the polymer chains created. In previous works, Polymyrcene has been synthesized by free and controlled radical polymerization using a variety of initiators. In addition, for environmental reasons, radical polymerization can be achieved in bulk (solvent free).<sup>9</sup>

**Free radical polymerization** of myrcene was achieved using the emulsion polymerization technique, using ammonium persulfate (APS) as an initiator and *tert*-butyl hydroperoxide (TBHP) as free radical generator (Figure 1.29), as reported by Sarkar *et al.*<sup>60</sup>

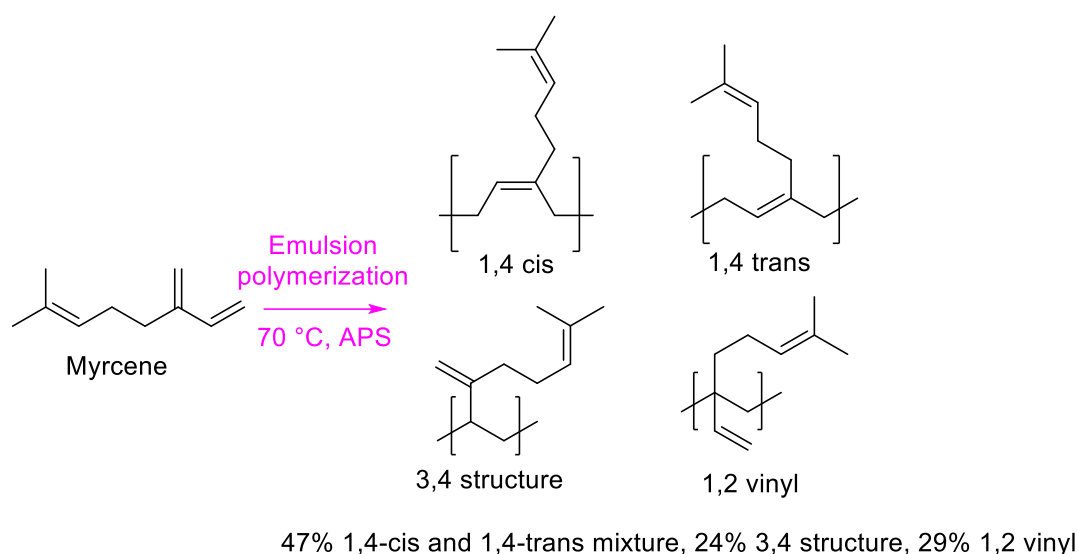


Figure 1.29: Free radical polymerization of myrcene with emulsion technique.

Likewise, Trumbo *et al.* reported the copolymerization of Myrcene with styrene, methyl methacrylate or *p*-fluorostyrene, and as initiator azobis isobutyronitrile (AIBN).<sup>10</sup> Unfortunately, high dispersity of polymyrcene have been observed in this kind of polymerization ( $D > 2.2$ ).

Bauer *et al.* reported a **controlled radical copolymerization** of Myrcene and styrene in bulk, using AIBN and dibenzoyl peroxide (DBPO) as an initiator of the reaction.<sup>9</sup> Low dispersity values have been observed in this kind of polymerization ( $D = 1.3-1.6$ ).

An advantage of this kind of polymerization is high molar mass of polymyrcene. However, it is not possible to synthesize block polymers or star polymers in radical polymerization.

#### 1.4.2 Coordinative polymerization of myrcene

Loughmari *et al.* reported coordinative polymerization of myrcene with neodymium borohydride as the catalyst (Figure 1.30), leading to polymyrcene (PMYR) high molar mass (20000-60000) with low dispersity ( $D = 1.27-2.02$ ).<sup>61</sup>

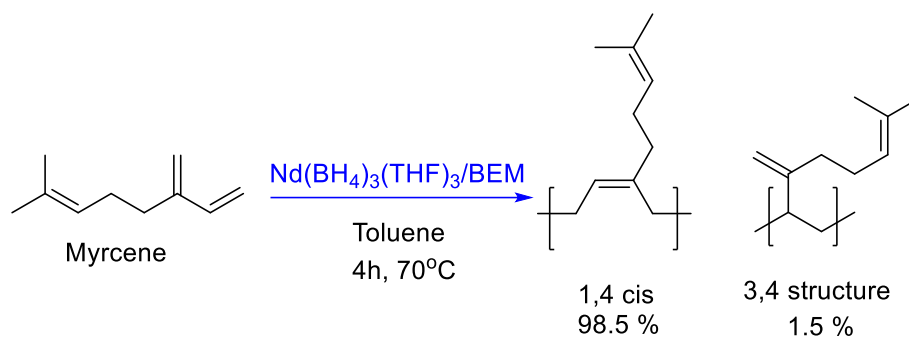


Figure 1.30: Coordinative polymerization of Myrcene with neodymium borohydride as the catalyst.

Also, by using a neodymium-based catalytic system Banda-Villanueva, *et al.* 2022, showed that the polymers obtained after the via coordination polymerization of Myrcene at 70 °C had a disposition predominantly at 1,4 of the diene unit in the chain polymer using cyclohexane.<sup>62</sup> Nevertheless, a polymerization's issue is that it requires a catalyst that is not easy to order from suppliers.

#### 1.4.3 Cationic polymerization of myrcene

**Cationic copolymerization and homopolymerization** of myrcene and styrene were achieved by Hulnik *et al.* using a water-dispersible Lewis acid surfactant.

Otmane *et al.* also performed cationic myrcene polymerization with a natural catalyst Maghnite (Mag-H<sup>+</sup>)(Figure 1.31).<sup>63</sup>

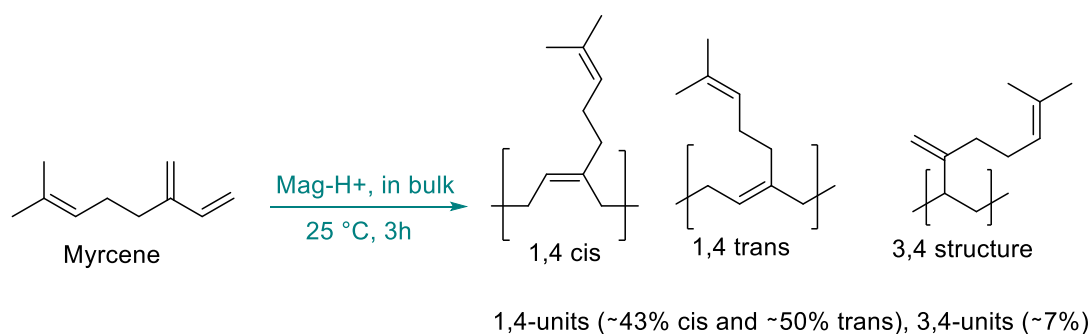


Figure 1.31: Cationic Myrcene polymerization with a natural catalyst Maghnite (Mag-H<sup>+</sup>).

One advantage of this type of polymerization is high molar mass.

Various disadvantages of this type of polymerization include:

- The need of use of catalyst that are not very commercial.
- Anhydrous conditions are a must due to the high sensitivity of the metal complexes involved.



- The partial conversion of the monomer.

*Table 1.4: Summary table of Polymyrcene synthesis.*

<b>Polymerization</b>	<b><math>\overline{M}_n</math> (g/mol)</b>	<b><math>\overline{D}</math></b>	<b>Conversion (%)</b>	<b>Ref.</b>
<b>Free radical</b>	33970-1009780	1.77-3.13	66-98	60
<b>Controlled radical</b>	9000-40000	1.3-1.6	30-65	9
<b>Coordinative</b>	20000-60000	1.27-2.02	50-92	61
<b>Cationic</b>	934	1.15	57	63

#### 1.4.4 Anionic polymerization

##### **General considerations**

Pure monomers and solvents, as well as dry conditions are mandatory in anionic polymerization to prevent any undesired consumption of the active center. The active center being the site on a chain carrier where reaction takes place.

##### **Monomers**

Apart from heterocyclic molecules, monomers susceptible to anionic polymerization usually have substituents that stabilize the electronegative charge (electronegative withdrawing groups) of the active center. These include non-polar monomers such as styrene, butadiene, isoprene or others 1,3 dienes and polar monomers<sup>12</sup> such as vinylpyridine, acrylates or vinyl ketones.

The reactivity of the active center is related to the pKa of the corresponding conjugate acid. Highest pKa values meaning least reactive monomers or highest reactive center. Thus, in copolymerization reactions, an order of monomer introduction is needed for a successful

reaction since only monomers with higher pKa can initiate polymerization of other monomers (lower pKa) (Table 1.5).<sup>64</sup>

Table 1.5: pKa of conjugate acid in DMSO (Bordwell, F. G. Acc. Chem. Res. 1988, 21, 456).<sup>64</sup>

Monomer	pKa of conjugate acid in DMSO*
Dienes	43-44
Styrene	43-43
Alkyl methacrylates	30-31
Oxiranes	29-32

## Initiator

Organolithiums are very good molecules to react as good nucleophiles and strong bases. This is linked to the covalent carbon-lithium bonds which is polar because of a huge difference of electronegativity between carbon (2.55) and lithium (0.98).<sup>65</sup> For example, *n*-butyllithium, *sec*-butyllithium and *tert*-butyllithium (Figure 1.32) have a pKa of approximately 50, 51, and 53, values in H<sub>2</sub>O.<sup>66,67</sup> Although pyrophoric, these compounds may be used as initiators in anionic polymerization reactions.

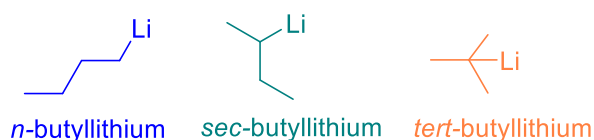


Figure 1.32: Alkylolithiums, *n*-butyllithium, *sec*-butyllithium and *tert*-butyllithium.

## Solvents

Solvents used are essentially hydrocarbons and ethers which will not interfere with the active center contrary to alcohols, esters or halogenated solvents. However, their solvation power can influence the final microstructure of the polymer as well as the polymerization kinetic.

In particular, alkylolithium compounds are aggregated in hydrocarbon solution and the degree of aggregation depends on the structure of the initiator. Oppositely, a very low

degree of aggregation is observed in a more polar solvent such as THF, and the rate of initiation and propagation are increased.<sup>68</sup>

Moreover, for dienes, ex: isoprene, it was demonstrated that 1,4 structures are predominant in apolar solvents, while 1,2 or 3,4 microstructure are predominant in THF.<sup>69</sup>

The living nature of anionic polymerization denoting the absence of termination and chain transfer reactions during chain-growth polymerization is of interest.

It is possible to control the degree of polymerization of the final polymer according to:

$$Xn = \frac{[M]_0}{I_0} \quad \text{Equation 1.10}$$

$Xn$  = polymerization degree

$[M]_0$  = initial concentration monomer

$I_0$  = initial concentration initiator

A narrow molecular weight distribution polymer ( $\mathcal{D} \leq 1.1$ ) can be obtained given a comparable or faster rate of initiation ( $R_i$ ) relative to propagation ( $R_p$ ). The molecular weight distribution is then related to the degree of polymerization according to:

$$\mathcal{D} = 1 + \frac{1}{Xn} \quad \text{Equation 1.11}$$

In anionic polymerization, the **initiation step** is achieved when electronic transfer takes place. The **propagation** step begins with the addition of the monomers, and then to finish with the **deactivation or termination** of the reaction (Figure 1.33).

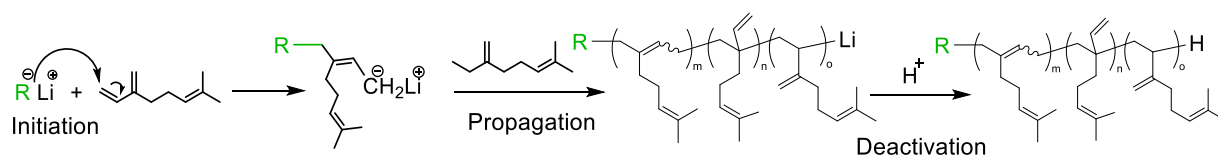


Figure 1.33: Steps in anionic polymerization of Myrcene (for sake of clarity, only 1,4-addition is shown).

This type of polymerization is interesting due to its low dispersity and because it produces good elastomers. These elastomers are polymers, manufactured or natural, with elastic characteristics. Rubber is an example of a natural or manmade polymer with elastic characteristics.

## **Anionic polymerization of terpene/myrcene in batch**

Biobased 1,3-diene monomers such as  $\beta$ -myrcene and  $\beta$ -farnesene have been anionically polymerized. In 1988, Newmark and Majumdar synthesized anionically *cis*-polymyrcene and *cis*-polyfarnesene using *sec*-butyllithium in hexane.  $^{13}\text{C}$  NMR analysis revealed predominant 1,4-microstructures.<sup>70</sup> In the same way, Ávila-Ortega *et al.* reported the anionic synthesis of amine  $\omega$ -terminated  $\beta$ -myrcene polymers, using *sec*-butyllithium as initiator <sup>71</sup>.

## **Polymyrcene Applications**

In numerous patents, Polymyrcene is mentioned as being used, for instance, in coatings, paints, drying oils, emulsifiers,<sup>72</sup> phenolic resins, adhesives,<sup>73</sup> and vulcanizable elastomers.<sup>74</sup>

Copolymerization is a common procedure to modify the characteristics of polymers. There is currently a patent that describes the procedure for obtaining a copolymer based on myrcene and styrene.<sup>73</sup> In the patent, it is shown that the copolymer has a remarkably low hot melt viscosity in comparison to other copolymer based on Styrene-Isoprene with the same molar mass.

### **1.4.5 Polymer analysis**

There are different analytical methods for the characterization of polymers. Depending on the properties to analyze, techniques exist such as: Gel permeation chromatography (GPC), Differential scanning calorimetry (DSC), Thermogravimetric analysis (TGA), Nuclear magnetic resonance (NMR), Infrared spectroscopy (IR), and many other.

## **Gel permeation chromatography (GPC)**

Gel permeation chromatography or Size Exclusion Chromatography (GPC or SEC) is the general name for separating molecules according to their size by letting the solution flow through a packed bed with a porous medium.<sup>75</sup> The mobile phase is normally a common organic solvent, and the stationary phase is a porous material that allows the passage of polymer molecules. Normally, the largest molecules pass through the stationary phase without entering in the pores unlike the smaller ones. This leads to molecules of different

sizes having different travel times through the column, thus allowing the characterization of the molecules depending on the retention time in the column (Figure 1.34).

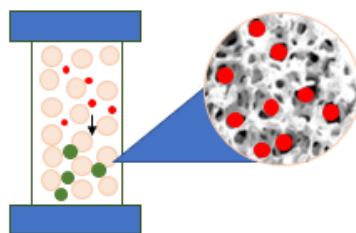


Figure 1.34: Representation of a GPC column.

For example, Figure 1.35 represents a typical chromatogram of Polymyrcene with different polymerization degrees.<sup>76</sup>

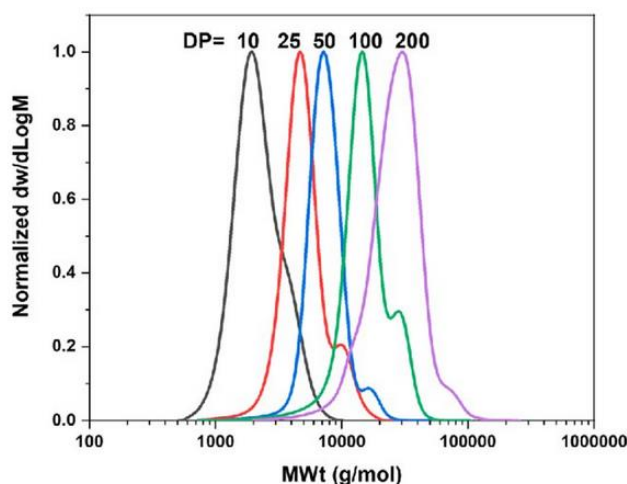


Figure 1.35: THF-SEC-derived molar mass distributions of Polymyrcene for various polymerization degree values (10, 25, 50, 100, and 200) synthesized by anionic polymerization in THF. (excerpt from Zhang, et al ACS Sustainable Chem. Eng. **2022**, 10 (29), 9654–9664. <https://doi.org/10.1021/acssuschemeng.2c03755>. <https://creativecommons.org/licenses/by/4.0/>)

With this GPC technique it is possible to know dispersity values ( $\mathfrak{D}$ ) and molar mass of polymers.

### Differential scanning calorimetry (DSC)

Differential Scanning Calorimetry (DSC) is a technique for detecting endothermic and exothermic transitions. With the DSC technique, it is possible to determine transformation temperatures and enthalpy of solids and liquids as a function of temperature. The sample and reference are kept at almost the same temperature throughout the experiment, and the heat flow can be measured.<sup>77</sup>

Glass transition temperature is one of the interesting values obtained by this technique. The glass transition is the reversible change to an amorphous polymer or amorphous regions of a semi-crystalline polymer from (or to) a viscous or elastic to (or of) a rigid and relatively fragile material. The glass transition temperature provides invaluable information about the polymer. When heating a polymer from the glassy state, it transitions from hard and fragile material to a softer material with more viscous properties. It makes it possible to predict product performance, informing processing conditions, and is often used for quality control. This transition occurs at a temperature called glass transition point or temperature or  $T_g$ .<sup>78</sup>

### **Thermogravimetric analysis (TGA)**

Thermogravimetric analysis is the technique that measures the change in mass of a sample during a controlled temperature program in a specified atmosphere. This technique is used to study those thermal processes that carry associated changes in mass, such as decomposition, sublimation, vaporization, oxidation, desorption, etc.

The most critical applications of the TGA include the study of oxidative stability of materials, study of polymer degradation profiles, the study of thermal stability of materials, analysis of the composition of a sample such as moisture content, volatility, etc., and determination of the temperature of the transformations.

### **Nuclear magnetic resonance (NMR)**

Nuclear magnetic resonance (NMR) is a physical phenomenon that relies on the quantum mechanical properties of atomic nuclei. The NMR for polymers does not refer to a single methodology because synthetic and natural polymers have a wide range of dynamic and structural features.<sup>79</sup> Using NMR, it is possible to determine the structure of the polymers, their molar mass, purity, conversion, yield and many other characteristics.

For example, Figure 1.36 shows the characterization of polymyrcene, presenting the proton attribution for each isomer (1,4 cis/trans, 3,4 structure, 1,2 vinyl), according to the literature.<sup>80</sup>

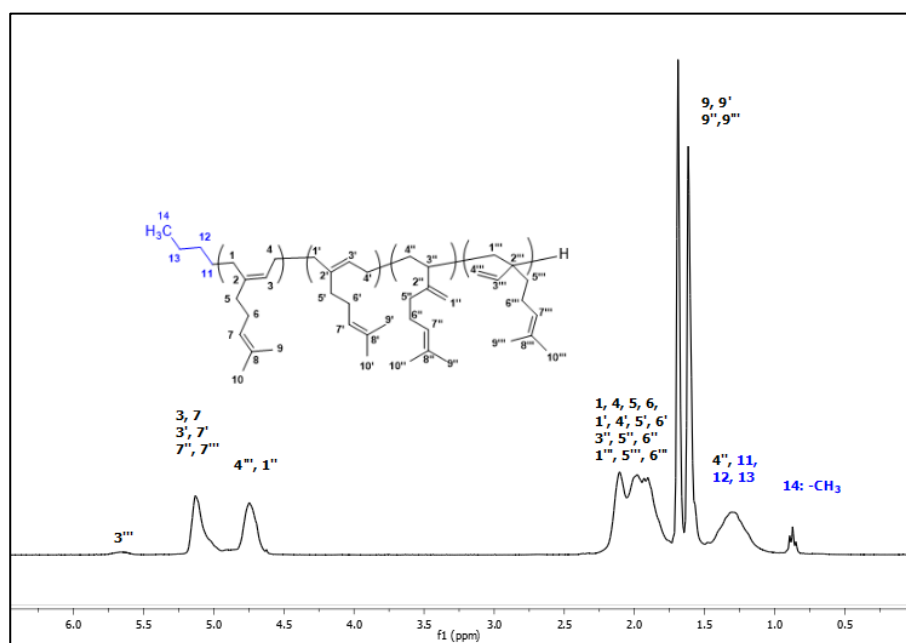


Figure 1.36:  $^1\text{H}$  NMR spectrum of polymyrcene with its attributions.

### Infrared spectroscopy (IR)

Based on the concept of the interaction of infrared light with matter either by emission, reflection or absorption the infrared spectroscopy is quite used in the characterization of polymers. In polymers, infrared spectroscopy has been used to characterize polymyrcene. In the figure below it shows the infrared spectrum of Myrcene and polymyrcene (Figure 1.37).

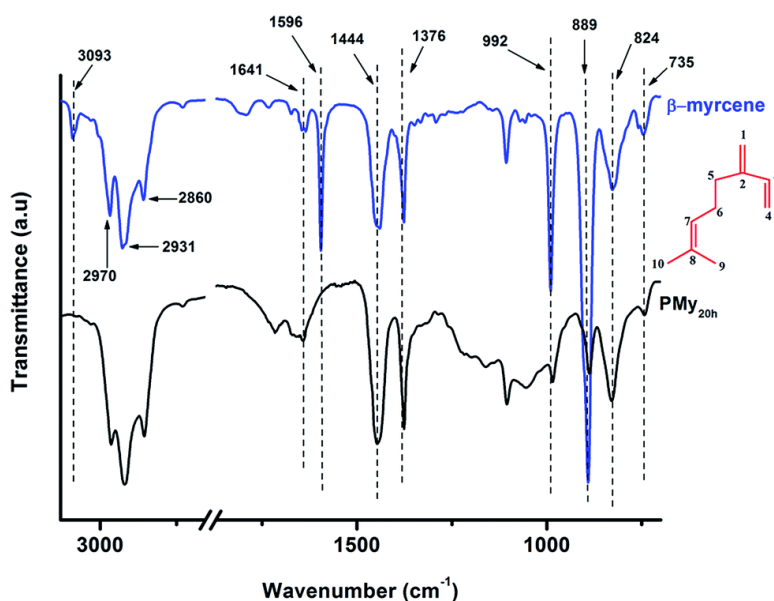


Figure 1.37: Infrared spectrum of Polymyrcene (excerpt from Preetom Sarkar and Anil K. Bhowmick. *RSC Adv.* 4, no. 106 (2014): 61343–54).

This interesting analysis technique allows identifying the functions present in polymers. For example, myrcene exhibits two distinctive CH bending vibrations at 992 and 889  $\text{cm}^{-1}$ , as well as specific absorption bands of the vinyl substituent at 1641  $\text{cm}^{-1}$ .

## 1.5 Conclusions

Flow chemistry continues to advance toward the frontiers of equipment innovation, optimization, and production of new materials. The use of equipment allowing online analysis makes process automation a reality in research laboratories and the industry.

It has been demonstrated that control of polymerization in a continuous process is possible thanks to the features of microfluidics systems. Control of the molecular mass of the polymers, control of temperature, good reproducibility, and improvement in process safety these features make microfluidics systems more attractive, not only in the field of research but also in the industry.

This bibliography research also showed that myrcene polymerization has been only developed in batch process herein comes the interest of using a novel approach as continuous flow.

Some interesting characteristics of myrcene have been presented with the aim of showing the benefits of using this monomer. These features intervene in the use of this monomer for the production of biobased polymers. Several types of research have shown that Myrcene polymerization can be done in different pathways such as cationic, anionic, coordinative, and free and controlled radical polymerization. This work is based on anionic polymerization due to its living characteristic.

It has been also shown the existence of different techniques of polymer analysis that allow a good characterization of polymers. Notably, this information about these techniques will help to the analysis of polymyrcene and its end-functionalization developed in this work.



## 1.6 Bibliography

- (1) Geyer, R.; Jambeck, J. R.; Law, K. L. Production, Use, and Fate of All Plastics Ever Made. *Sci. Adv.* **2017**, *3* (7), e1700782. <https://doi.org/10.1126/sciadv.1700782>.
- (2) Global Myrcene Market Growth 2019-2024.
- (3) Tiseo, I. Global Plastic Market Size Value 2021-2030. March 31, 2022.
- (4) Sahu, P.; Bhowmick, A. K.; Kali, G. Terpene Based Elastomers: Synthesis, Properties, and Applications. *Processes* **2020**, *8* (5), 553. <https://doi.org/10.3390/pr8050553>.
- (5) Bauer, N.; Brunke, J.; Kali, G. Controlled Radical Polymerization of Myrcene in Bulk: Mapping the Effect of Conditions on the System. *ACS Sustainable Chem. Eng.* **2017**, *5* (11), 10084–10092. <https://doi.org/10.1021/acssuschemeng.7b02091>.
- (6) Hulnik, M. I.; Vasilenko, I. V.; Radchenko, A. V.; Peruch, F.; Ganachaud, F.; Kostjuk, S. V. Aqueous Cationic Homo- and Co-Polymerizations of  $\beta$ -Myrcene and Styrene: A Green Route toward Terpene-Based Rubbery Polymers. *Polym. Chem.* **2018**, *9* (48), 5690–5700. <https://doi.org/10.1039/C8PY01378K>.
- (7) González-Villa, J.; Saldívar-Guerra, E.; León-Gómez, R. E. D.; López González, H. R.; Infante-Martínez, J. R. Kinetics of the Anionic Homopolymerizations of  $\beta$ -Myrcene and 4-Methylstyrene in Cyclohexane Initiated by *n*-Butyllithium. *J. Polym. Sci. Part A: Polym. Chem.* **2019**, *57* (21), 2157–2165. <https://doi.org/10.1002/pola.29487>.
- (8) Loughmari, S.; Hafid, A.; Bouazza, A.; El Bouadili, A.; Zinck, P.; Visseaux, M. Highly Stereoselective Coordination Polymerization of B-myrcene from a Lanthanide-based Catalyst: Access to Bio-sourced Elastomers. *J. Polym. Sci. A Polym. Chem.* **2012**, *50* (14), 2898–2905. <https://doi.org/10.1002/pola.26069>.
- (9) Bauer, N.; Brunke, J.; Kali, G. Controlled Radical Polymerization of Myrcene in Bulk: Mapping the Effect of Conditions on the System. *ACS Sustainable Chem. Eng.* **2017**, *5* (11), 10084–10092. <https://doi.org/10.1021/acssuschemeng.7b02091>.
- (10) Trumbo, D. L. Free Radical Copolymerization Behavior of Myrcene: I. Copolymers with Styrene, Methyl Methacrylate or p-Fluorostyrene. *Polymer Bulletin* **1993**, *31* (6), 629–636. <https://doi.org/10.1007/BF00300120>.
- (11) Loughmari, S.; Hafid, A.; Bouazza, A.; El Bouadili, A.; Zinck, P.; Visseaux, M. Highly Stereoselective Coordination Polymerization of B-myrcene from a Lanthanide-based Catalyst: Access to Bio-sourced Elastomers. *J. Polym. Sci. A Polym. Chem.* **2012**, *50* (14), 2898–2905. <https://doi.org/10.1002/pola.26069>.
- (12) Natalello, A.; Morsbach, J.; Friedel, A.; Alkan, A.; Tonhauser, C.; Müller, A. H. E.; Frey, H. Living Anionic Polymerization in Continuous Flow: Facilitated Synthesis of High-Molecular Weight Poly(2-Vinylpyridine) and Polystyrene. *Org. Process Res. Dev.* **2014**, *18* (11), 1408–1412. <https://doi.org/10.1021/op500149t>.
- (13) Plutschack, M. B.; Pieber, B.; Gilmore, K.; Seeberger, P. H. The Hitchhiker's Guide to Flow Chemistry. *Chem. Rev.* **2017**, *117* (18), 11796–11893. <https://doi.org/10.1021/acs.chemrev.7b00183>.
- (14) Whitesides, G. M. The Origins and the Future of Microfluidics. *Nature* **2006**, *442* (7101), 368–373. <https://doi.org/10.1038/nature05058>.

- (15) Nagaki, A.; Tomida, Y.; Yoshida, J. Microflow-System-Controlled Anionic Polymerization of Styrenes. *Macromolecules* **2008**, *41* (17), 6322–6330. <https://doi.org/10.1021/ma800769n>.
- (16) Nagaki, A.; Miyazaki, A.; Yoshida, J. Synthesis of Polystyrenes–Poly(Alkyl Methacrylates) Block Copolymers via Anionic Polymerization Using an Integrated Flow Microreactor System. *Macromolecules* **2010**, *43* (20), 8424–8429. <https://doi.org/10.1021/ma101663x>.
- (17) Liao, D.; Pang, W.; Bashir, M. S.; Chen, C. A Continuous Flow-through Strategy to Produce Highly Isotactic Poly(Isobutyl Vinyl Ether) via Cationic Polymerization. *Polym. Chem.* **2022**, 10.1039.D2PY00203E. <https://doi.org/10.1039/D2PY00203E>.
- (18) Karanassios, V. Microfluidics and Nanofluidics: Science, Fabrication Technology (From Cleanrooms to 3D Printing) and Their Application to Chemical Analysis by Battery-Operated Microplasmas-On-Chips. In *Microfluidics and Nanofluidics*; Kandelousi, M. S., Ed.; InTech, 2018. <https://doi.org/10.5772/intechopen.74426>.
- (19) Yoshida, J.; Nagaki, A.; Yamada, D. Continuous Flow Synthesis. *Drug Discovery Today: Technologies* **2013**, *10* (1), e53–e59. <https://doi.org/10.1016/j.ddtec.2012.10.013>.
- (20) Pérez, K.; Picard, B.; Vuluga, D.; Burel, F.; Hreiz, R.; Falk, L.; Commenge, J.-M.; Nagaki, A.; Yoshida, J.; Chataigner, I.; Maddaluno, J.; Legros, J. Bromine–Lithium Exchange on a Gem -Dibromoalkene, Part 2: Comparative Performance of Flow Micromixers. *Org. Process Res. Dev.* **2020**, *24* (5), 787–791. <https://doi.org/10.1021/acs.oprd.0c00203>.
- (21) Yoshida, J.; Kim, H.; Nagaki, A. Green and Sustainable Chemical Synthesis Using Flow Microreactors. *ChemSusChem* **2011**, *4* (3), 331–340. <https://doi.org/10.1002/cssc.201000271>.
- (22) Commenge, J.-M.; Falk, L. Villermaux–Dushman Protocol for Experimental Characterization of Micromixers. *Chemical Engineering and Processing: Process Intensification* **2011**, *50* (10), 979–990. <https://doi.org/10.1016/j.cep.2011.06.006>.
- (23) Wang, X.; Liu, Z.; Pang, Y. Concentration Gradient Generation Methods Based on Microfluidic Systems. *RSC Adv.* **2017**, *7* (48), 29966–29984. <https://doi.org/10.1039/C7RA04494A>.
- (24) Plutschack, M. B.; Pieber, B.; Gilmore, K.; Seeberger, P. H. The Hitchhiker’s Guide to Flow Chemistry. *Chem. Rev.* **2017**, *117* (18), 11796–11893. <https://doi.org/10.1021/acs.chemrev.7b00183>.
- (25) Falk, L.; Commenge, J.-M.; Portha, J.-F. Principes théoriques de la chimie en flux. *Médicaments et produits pharmaceutiques* **2019**, *Techniques de l’Ingénieur*. <https://doi.org/10.51257/a-v1-j8025>.
- (26) Gobby, D.; Angeli, P.; Gavriilidis, A. Mixing Characteristics of T-Type Microfluidic Mixers. *J. Micromech. Microeng.* **2001**, *11* (2), 126–132. <https://doi.org/10.1088/0960-1317/11/2/307>.
- (27) Hessel, V.; Löwe, H.; Schönfeld, F. Micromixers—a Review on Passive and Active Mixing Principles. *Chemical Engineering Science* **2005**, *60* (8–9), 2479–2501. <https://doi.org/10.1016/j.ces.2004.11.033>.

- (28) Janz, G. J.; Wait Jr, S. C. Space-time Yield and Reaction Rate. *The Journal of Chemical Physics* **1955**, *23* (8), 1550–1551.
- (29) Schenk, R.; Hessel, V.; Hofmann, C.; Kiss, J.; Löwe, H.; Ziogas, A. Numbering-up of Micro Devices: A First Liquid-Flow Splitting Unit. *Chemical Engineering Journal* **2004**, *101* (1–3), 421–429. <https://doi.org/10.1016/j.cej.2003.11.034>.
- (30) Monbaliu, J.-C. M.; Legros, J. Will the next Generation of Chemical Plants Be in Miniaturized Flow Reactors? *Lab on a Chip* **2022**.
- (31) Liebner, C.; Fischer, J.; Heinrich, S.; Lange, T.; Hieronymus, H.; Klemm, E. Are Micro Reactors Inherently Safe? An Investigation of Gas Phase Explosion Propagation Limits on Ethene Mixtures. *Process safety and environmental protection* **2012**, *90* (2), 77–82.
- (32) Picard, B.; Gouilleux, B.; Lebleu, T.; Maddaluno, J.; Chataigner, I.; Penhoat, M.; Felpin, F.-X.; Giraudeau, P.; Legros, J. Oxidative Neutralization of Mustard-Gas Simulants in an On-Board Flow Device with In-Line NMR Monitoring. *Angew Chem Int Ed Engl* **2017**, *56* (26), 7568–7572. <https://doi.org/10.1002/anie.201702744>.
- (33) Yasukouchi, H.; Nishiyama, A.; Mitsuda, M. Safe and Efficient Phosgenation Reactions in a Continuous Flow Reactor. *Organic Process Research & Development* **2018**, *22* (2), 247–251.
- (34) Zheng, J. L.; Wärnå, J.; Salmi, T.; Burel, F.; Taouk, B.; Leveneur, S. Kinetic Modeling Strategy for an Exothermic Multiphase Reactor System: Application to Vegetable Oils Epoxidation Using Prileschajew Method. *AIChE J.* **2016**, *62* (3), 726–741. <https://doi.org/10.1002/aic.15037>.
- (35) Liu, R. H.; Yang, J.; Pindera, M. Z.; Athavale, M.; Grodzinski, P. Bubble-Induced Acoustic Micromixing. *Lab Chip* **2002**, *2* (3), 151. <https://doi.org/10.1039/b201952c>.
- (36) Lu, L.-H.; Ryu, K. S.; Liu, C. A Novel Microstirrer and Arrays for Microfluidic Mixing. In *Micro Total Analysis Systems 2001*; Springer, 2001; pp 28–30.
- (37) Voldman, J.; Gray, M. L.; Schmidt, M. A. Liquid Mixing Studies with an Integrated Mixer/Valve. In *Micro Total Analysis Systems '98*; Harrison, D. J., van den Berg, A., Eds.; Springer Netherlands: Dordrecht, 1998; pp 181–184. [https://doi.org/10.1007/978-94-011-5286-0\\_44](https://doi.org/10.1007/978-94-011-5286-0_44).
- (38) Niu, X.; Lee, Y.-K. Efficient Spatial-Temporal Chaotic Mixing in Microchannels. *J. Micromech. Microeng.* **2003**, *13* (3), 454–462. <https://doi.org/10.1088/0960-1317/13/3/316>.
- (39) Bessoth, F. G.; deMello, A. J.; Manz, A. Microstructure for Efficient Continuous Flow Mixing. *Analytical communications* **1999**, *36* (6), 213–215.
- (40) Schönfeld, F.; Hessel, V.; Hofmann, C. An Optimised Split-and-Recombine Micro-Mixer with Uniform 'Chaotic' Mixing. *Lab Chip* **2004**, *4* (1), 65–69. <https://doi.org/10.1039/B310802C>.
- (41) Jen, C.-P.; Wu, C.-Y.; Lin, Y.-C.; Wu, C.-Y. Design and Simulation of the Micromixer with Chaotic Advection in Twisted Microchannels. *Lab Chip* **2003**, *3* (2), 77. <https://doi.org/10.1039/b211091a>.

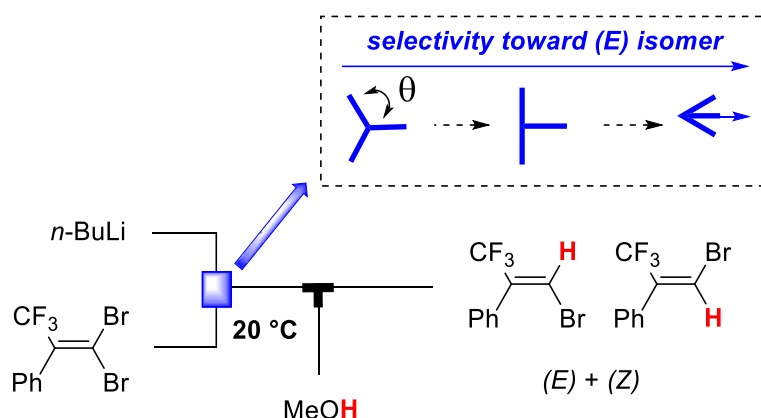
- (42) Nagaki, A.; Imai, K.; Ishiuchi, S.; Yoshida, J. Reactions of Difunctional Electrophiles with Functionalized Aryllithium Compounds: Remarkable Chemoselectivity by Flash Chemistry. *Angewandte Chemie International Edition* **2015**, *54* (6), 1914–1918.
- (43) Asano, S.; Yatabe, S.; Maki, T.; Mae, K. Numerical and Experimental Quantification of the Performance of Microreactors for Scaling-up Fast Chemical Reactions. *Org. Process Res. Dev.* **2019**, *23* (5), 807–817. <https://doi.org/10.1021/acs.oprd.8b00356>.
- (44) Oosthoek-de Vries, A. J.; Bart, J.; Tiggelaar, R. M.; Janssen, J. W.; van Bentum, P. J. M.; Gardeniers, H. J.; Kentgens, A. P. Continuous Flow <sup>1</sup>H and <sup>13</sup>C NMR Spectroscopy in Microfluidic Stripline NMR Chips. *Analytical chemistry* **2017**, *89* (4), 2296–2303.
- (45) Eyring, M. B.; Martin, P. Spectroscopy in Forensic Science☆. In *Reference Module in Chemistry, Molecular Sciences and Chemical Engineering*; Elsevier, 2013. <https://doi.org/10.1016/B978-0-12-409547-2.05455-X>.
- (46) Usutani, H.; Tomida, Y.; Nagaki, A.; Okamoto, H.; Nokami, T.; Yoshida, J. Generation and Reactions of *o*-Bromophenyllithium without Benzyne Formation Using a Microreactor. *J. Am. Chem. Soc.* **2007**, *129* (11), 3046–3047. <https://doi.org/10.1021/ja068330s>.
- (47) Natalello, A.; Morsbach, J.; Friedel, A.; Alkan, A.; Tonhauser, C.; Müller, A. H. E.; Frey, H. Living Anionic Polymerization in Continuous Flow: Facilitated Synthesis of High-Molecular Weight Poly(2-Vinylpyridine) and Polystyrene. *Org. Process Res. Dev.* **2014**, *18* (11), 1408–1412. <https://doi.org/10.1021/op500149t>.
- (48) Nagaki, A.; Tomida, Y.; Yoshida, J. Microflow-System-Controlled Anionic Polymerization of Styrenes. *Macromolecules* **2008**, *41* (17), 6322–6330. <https://doi.org/10.1021/ma800769n>.
- (49) Endo, Y.; Furusawa, M.; Shimazaki, T.; Takahashi, Y.; Nakahara, Y.; Nagaki, A. Molecular Weight Distribution of Polymers Produced by Anionic Polymerization Enables Mixability Evaluation. *Org. Process Res. Dev.* **2019**, *23* (4), 635–640. <https://doi.org/10.1021/acs.oprd.8b00403>.
- (50) Behr, A.; Johnen, L. Myrcene as a Natural Base Chemical in Sustainable Chemistry: A Critical Review. *ChemSusChem* **2009**, *2* (12), 1072–1095. <https://doi.org/10.1002/cssc.200900186>.
- (51) Kusari, S.; Lamshöft, M.; Zühlke, S.; Spitteller, M. An Endophytic Fungus from *Hypericum Perforatum* That Produces Hypericin. *J. Nat. Prod.* **2008**, *71* (2), 159–162. <https://doi.org/10.1021/np070669k>.
- (52) Omura, H.; Honda, K.; Feeny, P. From Terpenoids to Aliphatic Acids: Further Evidence for Late-Instar Switch in Osmeterial Defense as a Characteristic Trait of Swallowtail Butterflies in the Tribe Papilionini. *J Chem Ecol* **2006**, *32* (9), 1999–2012. <https://doi.org/10.1007/s10886-006-9124-x>.
- (53) Surendran, S.; Surendran, G. Myrcene—What Are the Potential Health Benefits of This Flavouring and Aroma Agent? *Frontiers in Nutrition* **2021**, *8*, 14.
- (54) Qiao, Z.; Hu, H.; Shi, S.; Yuan, X.; Yan, B.; Chen, L. An Update on the Function, Biosynthesis and Regulation of Floral Volatile Terpenoids. *Horticulturae* **2021**, *7* (11), 451. <https://doi.org/10.3390/horticulturae7110451>.

- (55) Kolicheski, M. B.; Cocco, L. C.; Mitchell, D. A.; Kaminski, M. Synthesis of Myrcene by Pyrolysis of  $\beta$ -Pinene: Analysis of Decomposition Reactions. *Journal of Analytical and Applied Pyrolysis* **2007**, *80* (1), 92–100. <https://doi.org/10.1016/j.jaap.2007.01.005>.
- (56) Bolton, J. M.; Hillmyer, M. A.; Hoye, T. R. Sustainable Thermoplastic Elastomers from Terpene-Derived Monomers. *ACS Macro Lett.* **2014**, *3* (8), 717–720. <https://doi.org/10.1021/mz500339h>.
- (57) <https://www.sigmaaldrich.com/FR/Fr/Product/Aldrich/W276200>. myrcene. January 7, 2022.
- (58) Paumgarten, F. J.; Delgado, I. F.; Alves, E. N.; Nogueira, A. C.; de-Farias, R. C.; Neubert, D. Single Dose Toxicity Study of Beta-Myrcene, a Natural Analgesic Substance. *Braz J Med Biol Res* **1990**, *23* (9), 873–877.
- (59) Opdyke, D. L. J. Myrcene. *Food and Cosmetics Toxicology* **1976**, *14* (6), 615.
- (60) Sarkar, P.; Bhowmick, A. K. Synthesis, Characterization and Properties of a Bio-Based Elastomer: Polymyrcene. *RSC Adv.* **2014**, *4* (106), 61343–61354. <https://doi.org/10.1039/C4RA09475A>.
- (61) Díaz de León Gómez, R. E.; Enríquez-Medrano, F. J.; Maldonado Textle, H.; Mendoza Carrizales, R.; Reyes Acosta, K.; López González, H. R.; Olivares Romero, J. L.; Lugo Uribe, L. E. Synthesis and Characterization of High *Cis* -Polymyrcene Using Neodymium-Based Catalysts. *Can. J. Chem. Eng.* **2016**, *94* (5), 823–832. <https://doi.org/10.1002/cjce.22458>.
- (62) Banda-Villanueva, A.; González-Zapata, J. L.; Martínez-Cartagena, M. E.; Magaña, I.; Córdova, T.; López, R.; Valencia, L.; Medina, S. G.; Rodríguez, A. M.; Soriano, F.; Díaz de León, R. Synthesis and Vulcanization of Polymyrcene and Polyfarnesene Bio-Based Rubbers: Influence of the Chemical Structure over the Vulcanization Process and Mechanical Properties. *Polymers* **2022**, *14* (7), 1406. <https://doi.org/10.3390/polym14071406>.
- (63) Zinelabidine Otmane Elabed; Kherroub, D. E.; Derdar, H.; Belbachir, M. Novel Cationic Polymerization of  $\beta$ -Myrcene Using a Proton Exchanged Clay (Maghnite-H<sup>+</sup>). *Polym. Sci. Ser. B* **2021**, *63* (5), 480–487. <https://doi.org/10.1134/S1560090421050043>.
- (64) Bordwell, F. G. Equilibrium Acidities in Dimethyl Sulfoxide Solution. *Accounts of Chemical Research* **1988**, *21* (12), 456–463.
- (65) Fetters, L. J.; EM, F. PARTIAL CHAIN COUPLING OF ANIONICALLY PREPARED POLYMERS BY AIR TERMINATION. **1977**.
- (66) Li, N. R.; Oalkyl, O. Chemistry of the Alkaline Earth Metal Enolates. *Organic Mechanisms* **2010**, 519.
- (67) Ovaska, T. V. *S* -Butyllithium. In *Encyclopedia of Reagents for Organic Synthesis*; John Wiley & Sons, Ltd., Ed.; John Wiley & Sons, Ltd: Chichester, 2001; p rb397. <https://doi.org/10.1002/047084289X.rb397>.
- (68) Tai, O.; Hopson, R.; Williard, P. G. Aggregation and Solvation of *n* -Butyllithium. *Org. Lett.* **2017**, *19* (15), 3966–3969. <https://doi.org/10.1021/acs.orglett.7b01644>.

- (69) Georges, S.; Hashmi, O. H.; Bria, M.; Zinck, P.; Champouret, Y.; Visseaux, M. Efficient One-Pot Synthesis of End-Functionalized Trans-Stereoregular Polydiene Macromonomers. *Macromolecules* **2019**, *52* (3), 1210–1219.
- (70) Newmark, R. A.; Majumdar, R. N. <sup>13</sup>C-NMR Spectra of Cis-Polymyrcene and Cis-Polyfarnesene. *J. Polym. Sci. A Polym. Chem.* **1988**, *26* (1), 71–77. <https://doi.org/10.1002/pola.1988.080260107>.
- (71) Ávila-Ortega, A.; Aguilar-Vega, M.; Loría Bastarrachea, M. I.; Carrera-Figueiras, C.; Campos-Covarrubias, M. Anionic Synthesis of Amine  $\omega$ -Terminated  $\beta$ -Myrcene Polymers. *J Polym Res* **2015**, *22* (11), 226. <https://doi.org/10.1007/s10965-015-0856-6>.
- (72) Alfred L. Rummelsburg, Wilmington, DeL, assignor to Hercules Powder Company, Wilmington, Del., a corporation of Delaware No Drawing. Polymerized Acyclic Terpenes and Method of Production. US2373419A.
- (73) Dupont, M.; Marianne, S. *Adhesive Compositions Containing a Block Copolymer with Polymyrcene*; Google Patents, 2016.
- (74) Sahu, P.; Bhowmick, A. K.; Kali, G. Terpene Based Elastomers: Synthesis, Properties, and Applications. *Processes* **2020**, *8* (5), 553. <https://doi.org/10.3390/pr8050553>.
- (75) Gellerstedt, G. Gel Permeation Chromatography. In *Methods in Lignin Chemistry*; Lin, S. Y., Dence, C. W., Eds.; Timell, T. E., Series Ed.; Springer Series in Wood Science; Springer Berlin Heidelberg: Berlin, Heidelberg, 1992; pp 487–497. [https://doi.org/10.1007/978-3-642-74065-7\\_34](https://doi.org/10.1007/978-3-642-74065-7_34).
- (76) Zhang, J.; Aydogan, C.; Patias, G.; Smith, T.; Al-Shok, L.; Liu, H.; Eissa, A. M.; Haddleton, D. M. Polymerization of Myrcene in Both Conventional and Renewable Solvents: Postpolymerization Modification via Regioselective Photoinduced Thiol–Ene Chemistry for Use as Carbon Renewable Dispersants. *ACS Sustainable Chem. Eng.* **2022**, *10* (29), 9654–9664. <https://doi.org/10.1021/acssuschemeng.2c03755>.
- (77) Maglic, K. D.; Cezairliyan, A.; Peletsky, V. E. Compendium of Thermophysical Property Measurement Methods: Vol. 1, Survey of Measurement Techniques. **1984**.
- (78) Zhang, Y.; Adams, R. D.; Da Silva, L. F. A Rapid Method of Measuring the Glass Transition Temperature Using a Novel Dynamic Mechanical Analysis Method. *The Journal of Adhesion* **2013**, *89* (10), 785–806.
- (79) Saalwächter, K. Chapter 1. Applications of NMR in Polymer Characterization – An Introduction. In *New Developments in NMR*; Zhang, R., Miyoshi, T., Sun, P., Eds.; Royal Society of Chemistry: Cambridge, 2019; pp 1–22. <https://doi.org/10.1039/9781788016483-00001>.
- (80) Georges, S.; Bria, M.; Zinck, P.; Visseaux, M. Polymyrcene Microstructure Revisited from Precise High-Field Nuclear Magnetic Resonance Analysis. *Polymer* **2014**, *55* (16), 3869–3878. <https://doi.org/10.1016/j.polymer.2014.06.021>.

# Chapter 2

## Controlled organolithium chemistry in flow microreactors: comparative performance of micromixers



## 2.1 Introduction

Miniaturized continuous flow reactors offer various leverage to control the course of chemical reactions, and researchers have been trying for years to enhance flow systems, in order to produce the desired product with the highest selectivity (including stereochemistry). Whereas the efficiency of the reactions depends on various parameters, reaction with fast kinetics are closely connected to the mixing performance.<sup>1</sup> For this reason, in the field of chemistry in continuous flow and, specifically, in microfluidics, researchers have focused on micromixer features providing methods to quantify the mixing quality in micromixers, as well as applications in organic synthesis.<sup>2</sup>

Indeed, micromixers have the critical role of homogenizing the medium prior to its response because they constitute the only feasible mixing location.<sup>3</sup> This will cause laminar flow to be interrupted in this area (often called local instationarity). On a general standpoint, micromixers can be classified as “active” or “passive”. Passive micromixer creates the combination of molecules by passing the reagents through a certain geometry system using only the reagents flow rate. In contrast, active micromixer uses an external energy source in a variety of ways (*e.g.* mechanical, acoustic...) in order to mix the reagents. Whereas active micromixers are quite efficient they are often expensive and passive micromixer are by far the most common (most accessible and robust). These latter are mostly based on different geometries, the T-shaped micromixer being the most popular since it is also commonly used in gas and liquid chromatography. Also, to maximize mixing, the use of mixers with very small diameter channels can be a solution by forming a «bottleneck». This reduces the diffusion length of the species, and allow a rapid mixing in this way. Some geometries, such as multilamellar mixers (Figure 2.1) are based entirely on this principle.



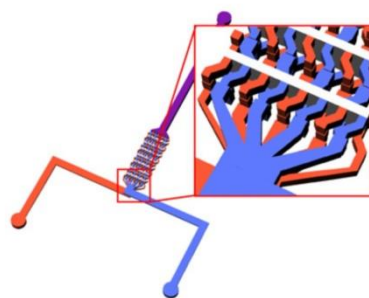
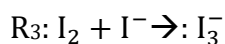
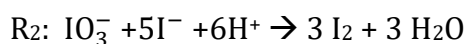
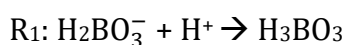


Figure 2.1 Multilamellar mixer (excerpt from “Microfluidic mixers: a short review,” Elveflow. [Online]. Available: <https://www.elveflow.com/microfluidic-tutorials/microfluidic-reviews-and-tutorials/microfluidic-mixers-short-review/>. [Accessed: 07-Nov-2022]).<sup>4</sup>

Thus, the mixing performance of micromixers depends on their intrinsic features and can be difficult to anticipate. There are thus several methods to quantify the mixing performance either experimental or *in silico*. In this line, there are several softwares to perform computational fluid dynamics (*e.g.* Ansys Fluent or Dassault Systems XFlow) based on the shape of the micromixers, the viscosity of the fluids, the flow rates, *etc*<sup>5-6</sup> According to Oddy, *et al.*,<sup>7</sup> the performance of various micromixers and, subsequently, the quality of the micromixing, can be studied using multiple of methods simultaneously.

An interesting experimental method is the characterization by yield and/or reaction selectivity.<sup>8-9</sup> For example, the Villermaux–Dushman reaction (VD) is based on a parallel and competitive reactions taking place in a single reactor.<sup>10</sup> This VD reaction, allows to establish a relationship between the quantity of triiodide ions ( $I_3^-$ ) produced during the reaction, and the efficacy of the mixture according to:<sup>2</sup>



The first reaction ( $R_1$ ) is a neutralization reaction and  $R_2$  is a redox reaction.  $R_1$  is almost instantaneous and much faster than  $R_2$ . Adding a sulfuric acid solution with a precise  $H^+$  proton concentration allows a stoichiometric deficiency in borate ions: an ideal mixture is thus obtained when the protons are completely consumed by the first reaction  $R_1$ . So, the acid stoichiometric deficiency will prevent the redox reaction  $R_2$  to occur. Since  $R_2$

generates iodine as a product, the measurement of the concentration of this compound provides indications of the state of segregation of the fluid. In addition, the iodine formed reacts with the iodide ions in a balanced and almost instantaneous reaction to give colored triiodide ions ( $I_3^-$ ). The concentration of triiodide ions is obtained by measuring the optical density (OD) of the outgoing fluid by UV/visible spectrophotometry at a wavelength of 353 nm. A high concentration in triiodide ions reveals an ineffectiveness in mixing and consequently in the micromixer or, to put it another way, *the worse the mixture, the more the solution becomes colored*.

## 2.2 Flash chemistry

Yoshida coined the phrase "flash chemistry" to describe uncontrollable short-time reactions (<1 second). Flash chemistry refers to reactions with periods so brief that they become unpredictable under classical conditions. Yoshida group has also published many pioneering works in the use of highly unstable intermediates in synthesis, especially organolithium species. For example, the reaction of alkyl iodophenones in presence of organolithium reagents (Figure 2.2). Actually, three competitive reactions may occur: 1) I-Li exchange, 2) addition onto the C=O group and 3) deprotonation in a of the C=O group. Usually, in order to selectively perform the path 1) without 2) and 3), the protection of the carbonyl as an acetal is required. In contrast, microflow allows to selectively perform 1), directly on the substrate, without further modification. Mesityllithium (MesLi) is generated in flow from MesBr and *n*-BuLi at only 0 °C in the R1 reactor. The key I-Li exchange step between the iodophenone and MesLi then occurs at -70 °C in the R2 reactor. To be fully effective and avoid any competitive side reaction, it is necessary to perform this step at very short times (1.5 to 3 ms) before adding electrophile E. Noteworthy, simple T-shape micromixers are used (Figure 2.2).

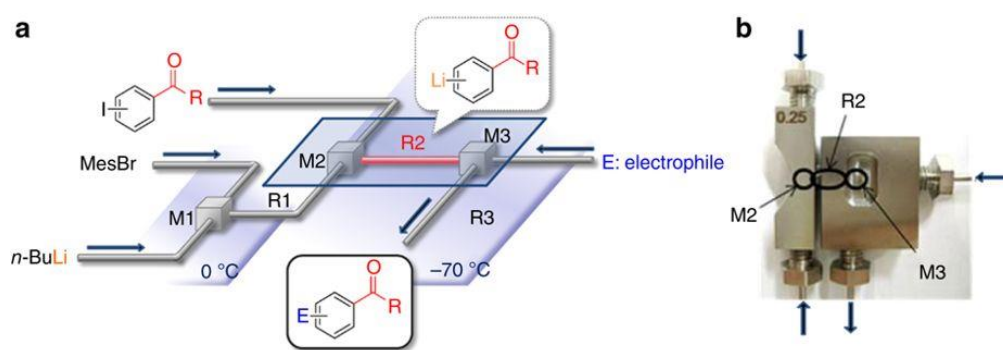


Figure 2.2 : Organolithium chemistry with unprotected alkyl iodophenones a) Setup of fluidic assembly b) Photo of the assembly with the M2 and M3 T-shape mixers and the R2 reactor (Excerpt from Kim, H., Nagaki, A., & Yoshida, J. I. (2011). *Nature communications*, 2(1), 1-6.).<sup>11</sup>

Another relevant example is the reaction of 3-bromo-2,5-dimethoxynitrobenzene with phenyl lithium (Figure 2.3). Using microfluidic systems, it is possible to take advantage of controlling the balances between kinetic and thermodynamic reactions. Thus, the substrate **3** (3-bromo-2,5-dimethoxynitrobenzene) will react preferentially by Br-Li exchange (0.06 s at 48 °C) to give the product **4**, after trapping isobutyraldehyde in the second micromixer (M2). When the residence time between PhLi and substrate **3** increases, isomerization to the lithiated product occurs progressively toward migration of the Li atom on the more acidic position, with a total isomerization in 63 s and a yield of 66% of the desired alcohol **5**.

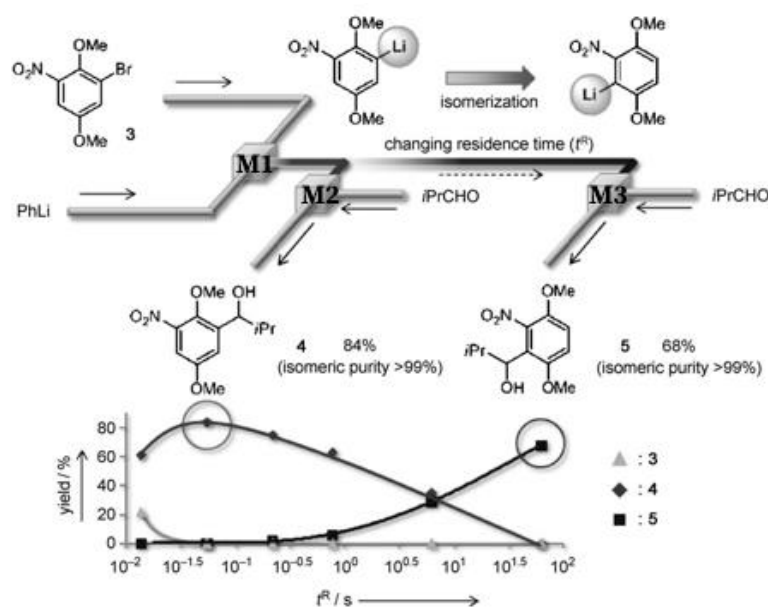


Figure 2.3 Reactivity of halogenated nitrobenzenes with microfluidic organolithies: switching between kinetic and thermodynamic products (excerpt from Nagaki, A., Kim, H., & Yoshida, J. I. (2009). *Angewandte Chemie*, 121(43), 8207-8209).<sup>12</sup>

In one of his numerous works on flash organolithium chemistry,<sup>13</sup> Yoshida found that the circular section T-shaped and W-shaped (sometimes referred to as V- or anchor-shaped) micromixers significantly differed in their ability to react with organolithium. However, this result is simply presented as an observation, without particular remark on this finding. The angle between the channels, which is = 90° for T-shaped mixers and = 45° for W-shaped mixers (the inlets are always 2 units apart, and the outlet is positioned in between in a "frontal encounter" configuration), is what distinguishes these mixers from one another. In this work, we aim at studying how the angle of the micromixer can influence the distribution of reaction products. Thus, the influence of sixteen passive mixers with eight different angles of 135°, 120°, 105° (Y mixers), 90° (T mixer), 75°, 60°, 45° and 30° (W mixers), and two internal diameters (ID = 0.5 and 0.25 mm) will be studied in a typical flash chemistry reaction. Parameters, such as flow rate, will also be varied to determine the most efficient micromixer for the reaction both in terms of chemical selectivity (one of a number of possible products) and geometric selectivity (one of two isomers).

### 2.3 Results and discussion

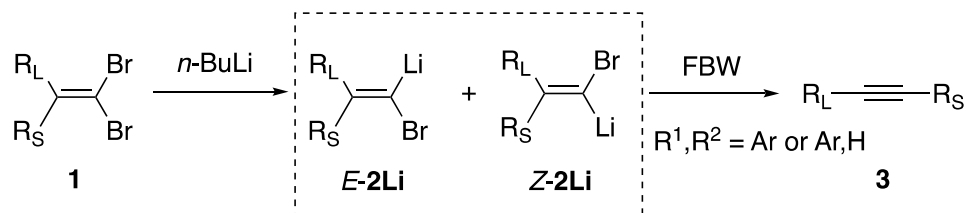
- Stability of vinyl carbenoid

Among unstable compounds in batch that could possibly be tamed by microflow reactors, vinyl carbenoids constitute an attractive target. Indeed, such compounds are known to rearrange according to the Fritsch-Buttemberg-Wiechell rearrangement (FBW).<sup>14</sup>

Carbenoids are defined as compounds whose reactivity is similar to that of carbenes, but which do not have the very particular electronic configuration of the latter.<sup>14</sup> Indeed, a carbenoid carbon atom will be substituted in such a way as to undergo both an accepting inductive effect and a powerful donor inductive effect from its substituents. Because of the large variety of possible substituents, carbenoids can display a dramatic change in behavior and reactivity. Common carbenoids are those bearing both an electronegative heteroatom and an alkali or alkaline earth metal. In this case, as a rule of the thumb, metal electropositivity correlates with the carbenoid reactivity, and the lability of the electronegative group further enhances this trend. As such, bromo-lithiated carbenoids<sup>15</sup> are mostly unstable and vinyl carbenoids **2** obtained by lithium-halogen exchange from **1** may undergo fast Fritsch-Buttemberg-Wiechell (FBW) rearrangement into alkynes **3**.<sup>14</sup> This ability to undergo FBW rearrangement is highly dependent on the nature of the

electronegative substituent, the metal and the migrating group R. Vinyl carbenoids bearing aryl groups, or an arene and a hydrogen atom, are particularly susceptible to this transformation (Figure 2.4).

In the case of stable carbenoids from *gem*-dibromovinyl systems,<sup>16</sup> the metal-halogen exchange is often driven by steric decompression (Figure 2.4),<sup>17</sup> through direct metalation can be favored with a metal-chelating group (*e.g.* R = MOM).<sup>18</sup> Carbenoids of this type have occasionally been used in synthesis,<sup>18,19</sup> though most lithium/bromine vinyl carbenoids **2** are used in FBW rearrangements (Corey-Fuchs protocol) and knowledge of their properties remains fragmentary. The use of vinyl carbenoids **2** would provide a means to quickly build a trisubstituted alkene bearing a bromine atom and with a defined configuration, opening up many synthetic possibilities. In a preliminary work, we have shown that microflow conditions allow: 1) better control of regioselectivity when there is no clear discriminating R group, and 2) trapping of the carbenoid intermediates **2** before the fast FBW rearrangement or decomposition occurs.<sup>20</sup>



**Flask**  $\dashrightarrow$   $\left[ \begin{array}{l} - \text{stereochemistry driven by steric hindrance} \\ - \text{non-observable with } R^1, R^2 = \text{Ar or Ar,H} \end{array} \right.$

**Flow**  $\dashrightarrow$  carbenoid generation and trapping with controlled geometry

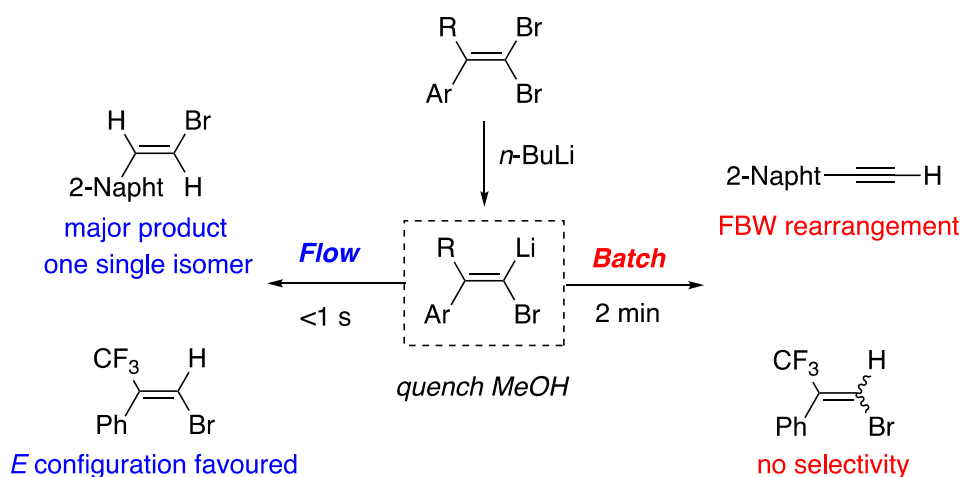
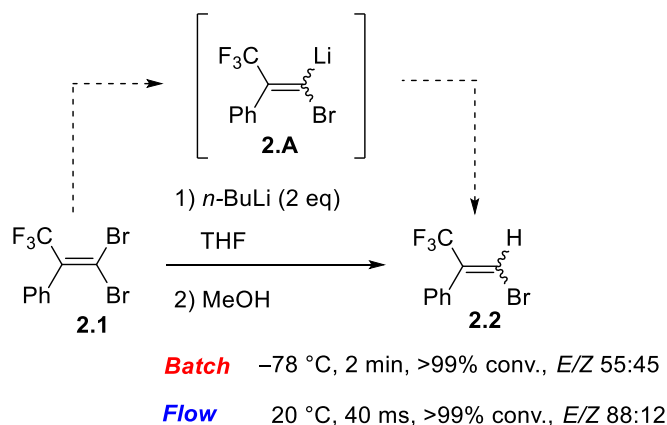


Figure 2.4: Synthesis and reactivity of vinylcarbenoids 2 from gem-dibromoalkenes 1.

Notably, it was shown that gem-dibromoalkene **2.1** was able to undergo lithium-bromine exchange and that the corresponding carbenoid intermediate **2.A** was stable enough to trap a proton to generate the corresponding monobromoolefin **2.2** (Figure 2.5).



T-shaped micromixer,  $Q(n\text{-BuLi} + \mathbf{2.1}) = 9.4 \text{ mL/min}$ , ID 0.5 mm

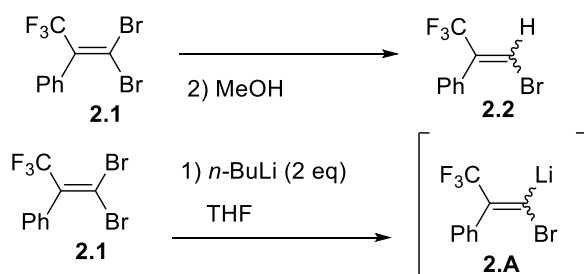


Figure 2.5: Generation and trapping of a carbenoid A from gem-dibromoalkene (2.1) under batch and continuous flow conditions.

Whereas the reaction was unselective under classical batch conditions, even at  $-78\text{ }^{\circ}\text{C}$  (Figure 2.6), a 88:12 E/Z ratio could be attained on a single run by using a continuous flow microreactor equipped with a T-shaped micromixer ( $\theta = 90\text{ }^{\circ}$ , ID mixer  $500\text{ }\mu\text{m}$ , tubing =  $500\text{ }\mu\text{m}$ , reactor tubing ID =  $500\text{ }\mu\text{m}$ , L = 3 cm (Figure 2.6), flow rate  $Q(2.1+n\text{-BuLi}) = 9.4\text{ mL/min}$ ), even at  $20\text{ }^{\circ}\text{C}$  within 30 milliseconds (ms).



Figure 2.6 : Reactor tubing ID =  $500\text{ }\mu\text{m}$ , L = 3 cm.

Besides the fundamental aspect of the finding of flow micromixing effect on the stereoselectivity of the Li-Br exchange, this could also be of interest to access some high-value targets. Indeed trapped with a convenient electrophile, such a compound afford a simple path to access a selective estrogen receptor modulator called Panomifene (Figure 2.7).<sup>21,22</sup> For example, generating **A** with a specific diastereoselectivity and using as an electrophile trimethyl borate  $(\text{BOMe})_3$ , would afford **B** that could be involved in a sequence of Suzuki cross-couplings to yield the target Panomifene.

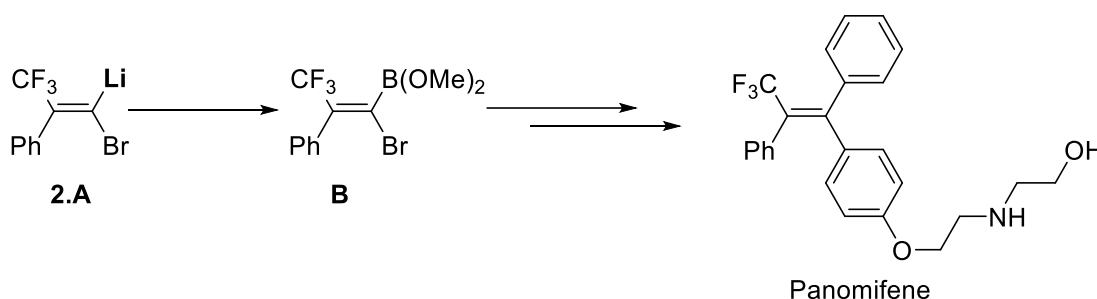


Figure 2.7: Proposed path for the synthesis of Panomifene from a vinyl carbenoid.

## 2.4 Micromixers

The W micromixers ( $45^{\circ}$ ) used in this study were first given by Yoshida during the stay of the PhD student Baptiste Picard at the University of Kyoto at the fall 2017, and then sent to MG63 company to manufacture several micromixers with various angles.

## 2.5 Influence of the design and sizing of the flow micromixer

We now extend this study to the influence of the design and sizing of the flow micromixer in the reaction between **2.1** (in THF) and *n*-BuLi (in hexanes) at 20 °C (Figure 2.8).

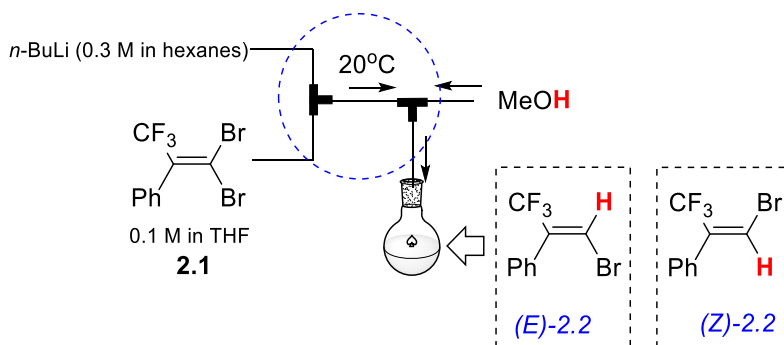


Figure 2.8: Set up of Lithium-halogen exchange on gem-dibromoalkene.

Our first investigations are reported in table 2.1 with the measurement of the conversion rate of **2.1**, the selectivity of the transformation toward product **2.2** and the corresponding *E/Z* ratio, by using two micromixers (ID = 500 μm) with respective angles of 90° (Table 2.1, entries 1-6) and 45° (Table 2.1, entries 7-12) at various flow rates *Q*.

Table 2.1: Effect of T-shaped (90°) and W-shaped (45°) micromixers and flow rates on the conversion of **2.1** into **2.2**.<sup>a</sup>

Entry	ID (μm)	Angle (°)	Flow rate <i>Q</i> (mL/min)		<i>t</i> <sup>R</sup> (ms)	Conversion (%) <sup>b</sup>	Product selectivity for <b>2.2</b> <sup>b,c</sup>	<i>E/Z</i> ratio <sup>b</sup>
			Substrate	<i>n</i> -BuLi				
1	500	90	1	0.625	220	59	98	93:07
2						31	64	71:29
3						30	91	84:16
4						71	72	88:12
5			6	3	40	98	99	77:23
6						99	99	72:28
7	500	45	1	0.625	220	88	70	55:45
8 <sup>d</sup>						-	-	-
9			4	2	60	100	95	65:35



10				100	97	61:39
11	5	2	50	100	96	64:36
12				98	99	69:31

<sup>a</sup> Experiments were performed with: [2.1] = 0.1 M in THF, [n-BuLi] = 0.3 M in hexane.

Reactor tubing: ID = 500  $\mu$ m, L = 3 cm.

<sup>b</sup> Measured by GC-MS and <sup>19</sup>F NMR.

<sup>c</sup> Product selectivity = [2.2]/([2.2] + [other products]) $\times$ 100.

<sup>d</sup> Clogging occurred

First experiments were conducted with the T-shaped mixer at a low flow rate  $Q = 1.625$  mL/min ( $t^R = 220$  ms; entries 1-4). The first assay gave a satisfactory result: 59% conversion of **2.1** almost exclusively into target product **2.2** and with an excellent *E* selectivity (93%). Unfortunately, these results were not reproducible. Under the same conditions, the three following experiments (entries 2-4) gave significantly different results: conversion varied from 31 to 71% and selectivity for **2.2** could drop down to 64% (GC-MS suggesting some other products such as the incorporation of a butyl chain instead of the methanolic proton, as previously observed in batch mode). Moreover, the stereoisomeric ratio was still in favor of the *E* compound but never exceeded 88% (entry 4). In contrast, entries 5 and 6 shows that increasing the flow rate by >5-fold ( $Q = 9$  mL/min) with the same reactor ( $t^R = 40$  ms) afforded reproducible results: >98% conversion and selective formation of **2.2** albeit with a disappointing stereoisomeric selectivity (<77% *E*). This shows that high flow values are required to ensure flow stability and therefore reproducibility of reaction conditions.

Switching to a micromixer with  $\theta = 45^\circ$  also demonstrated the importance of the flow rate conditions. At  $Q = 1.625$  mL/min, the reaction could either take place or the flow system could clog (entries 7 and 8). Increasing  $Q$  to 6 and 7 mL/min brought reproducible results with full conversion into the desired monobrominated product with slight variations in the *E/Z* ratio from 61:39 to 69:31.

From these experiments with two different micromixers the following conclusions could be drawn: 1) high flow rates ensure reproducibility of the experiments, 2) both 90 and 45° angles guarantee high conversions of the substrate **2.1** into the carbenoid **2.A** with subsequent trapping of a methanolic proton, 3) a clear tendency toward *E*-selectivity can

be observed. 4) Despite some small discrepancies between identical experiments, *E*-selectivity seems significantly higher with a T-shape mixer rather than with a 45° W-shape in those conditions.

### 2.6 Effect of micromixers with an angle ranging from 135 to 30°

We extended the scope of the study to a broader range of eight micromixers from 135 to 30° (see Figure 2.9, Figure 2.10, Table 2.1 and Supporting information).








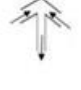
Y, 135°		W, 75°	
Y, 120°		W, 60°	
Y, 105°		W, 45°	
T, 90°		W, 30°	

Figure 2.9 : Micromixers angles design.

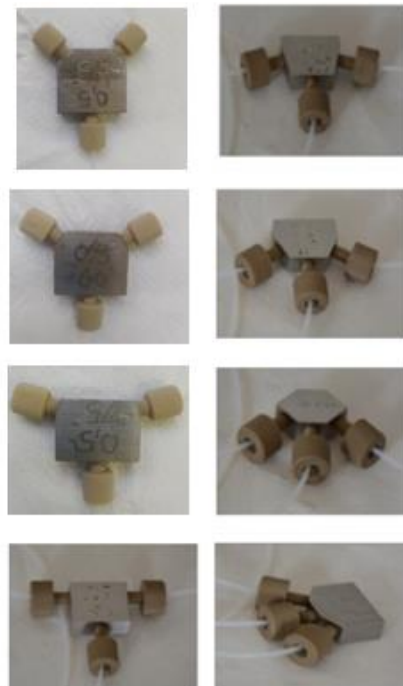


Figure 2.10: Micromixers angles.

These micromixers with an ID = 500 and 250  $\mu\text{m}$ , where associated with the same reactor tubing as in table 1, ( $L = 3 \text{ cm}$ , ID = 500  $\mu\text{m}$ ) at an intermediate flow rate  $Q = 3.5 \text{ mL/min}$ . Results are depicted in Table 2.2.

Table 2.2: Effect of micromixers with an angle ranging from 135 to 30° at moderate flow rate (3.5 mL/min) on the conversion of 1 into 2.2.<sup>a</sup>

Entry	ID ( $\mu\text{m}$ )	Angle ( $^\circ$ )	Flow rate Q (mL/min)		$t^R$ (ms)	Conversion (%) <sup>b</sup>	Product selectivity for 2.2 <sup>b,c</sup> (%)	E/Z ratio <sup>b</sup>
			Substrate	<i>n</i> -BuLi				
1	500	135	2.5	1	100	46	79	80:20
2		105				22	82	77:23
3		90				60	85	90:10
4		75				41	84	79:21
5		60				56	89	84:16
6		45				63	93	86:14
7		30				56	88	86:14
8	250	135	2.5	1	100	98	99	77:23
9		120				49	98	89:11
10		105				84	89	98:02
11		90				91	90	80:20
12		75				80	98	81:19
13		60				69	>99	92:08
<b>14</b>		<b>45</b>				<b>92</b>	<b>&gt;99</b>	<b>92:08</b>
15		30				95	88	82:18

<sup>a</sup> Experiments were performed with: [2.1] = 0.1 M in THF, [n-BuLi] = 0.3 M in hexane. Reactor tubing: ID = 0.5 mm, L = 3 cm.

<sup>b</sup> Measured by GC-MS and <sup>19</sup>F NMR. Average value over 2 runs (reproducibility is  $\pm 2\%$ ).

<sup>c</sup> Product selectivity =  $[2.2]/([2.2] + [\text{other products}]) \times 100$ .

With ID = 500  $\mu\text{m}$  and  $t^R = 100 \text{ ms}$  (entries 1-7), conversions were below 60% for each microreactor except for an angle = 90 and 45° (60 and 63% respectively) who also afforded the best E/Z selectivity (90:10 and 86:14 respectively; entries 3 and 7). Performing the experiments with a thinner ID (250  $\mu\text{m}$ ) had an enormous effect on the Br-Li exchange with five reactors affording conversions >90% and in all eight cases affording the desired trapped carbenoid 2.2 >88% (entries 8-15).

Regarding E/Z selectivity, the Y-shaped  $\theta = 105^\circ$  and the W-shaped  $\theta = 45^\circ$  microreactors led to the best isomeric ratios (entries 10 and 14, respectively). However, when considering

the overall selectivity toward *E*-2.2, the micromixer W-45 led to 84% whereas Y-105 only provided 73% of *E*-2.2. These experiments therefore demonstrate the beneficial effect of small diameters for conversion and selectivity. Final assessments at a high flow rate (8.4 mL/min,  $t^R = 40$  ms) are reported in Table 2.3.

Table 2.3: Effect of micromixers with angle ranging from 135 to 30° at high flow rate (8.4 mL/min) on the conversion of 2.1 into 2.2.<sup>a</sup>

Entry	ID ( $\mu\text{m}$ )	Angle ( $^\circ$ )	Flow rate Q		$t^R$ (ms)	Conversion (%) <sup>b</sup>	Product selectivity for 2.2 <sup>b,c</sup> (%)	<i>E/Z</i> ratio <sup>b</sup>
			Substrate	<i>n</i> -BuLi				
1	250	135	6	2.4	40	97	>99	77:23
2		120				78	>99	94:06
3		105				>99	>99	64:36
4		90				>99	>99	65:35
5 <sup>d</sup>		75				–	–	–
6		60				98	>99	68:32
7		45				90	>99	93:07
8		30				98	>99	68:32

<sup>a</sup> Experiments were performed with: [2.1] = 0.1 M in THF, [n-BuLi] = 0.3 M in hexane. Reactor tubing: ID = 500  $\mu\text{m}$ , L = 3 cm.

<sup>b</sup> Measured by GC-MS and <sup>19</sup>F NMR. Average value over 2 runs (reproducibility is  $\pm 2\%$ ).

<sup>c</sup> Product selectivity = [2.2]/([2.2] + [other products]) $\times 100$ . <sup>d</sup> Clogging occurred

Higher flow rates unquestionably improved the conversion toward 2.2, despite the longer residence time, all mixers yielded a greater or comparable conversion compared to lower flow rates (Table 2.4), despite the shorter residence time (as reactor length and width were kept constant).

Table 2.4: Yields of 2.2 using different micromixers ID 0.25 and 0.5 mm, Q 3.5 and 8.4 mL/min.<sup>a</sup>

Angle ( $^\circ$ )	ID 0.25 mm, Q 3.5 mL/min	ID 0.25 mm, Q 8.4 mL/min	ID 0.5 mm, Q 3.5 mL/min
	Yield %	Yield %	Yield %
135	96	96	36

<b>120</b>	49	78	- <sup>b</sup>
<b>105</b>	78	99	18
<b>90</b>	83	99	51
<b>75</b>	78	- <sup>b</sup>	35
<b>60</b>	69	96	50
<b>45</b>	92	89	58
<b>30</b>	85	98	49

<sup>a</sup> Experiments were performed with: [2.1] = 0.1 M in THF, [n-BuLi] = 0.3 M in hexane. Reactor tubing: ID = 500  $\mu$ m, L = 3 cm.

<sup>b</sup> Clogging occurred

This substantially corroborates the concept of a diffusion-ordered response and demonstrates the utmost significance of mixing. However, such a clear trend could not be observed concerning stereoselectivity as the previous best ratio at lower flow rate was attained with Y-105 at 98:02 and now dropped to 64:36 while Y-120 increases from 89:11 to 94:06. The only clear conclusion that can be drawn is that the W-45 high efficiency remained constant (83% overall for E-2). A histogram, of the results from Table 2.4, is represented in Figure 2.11.

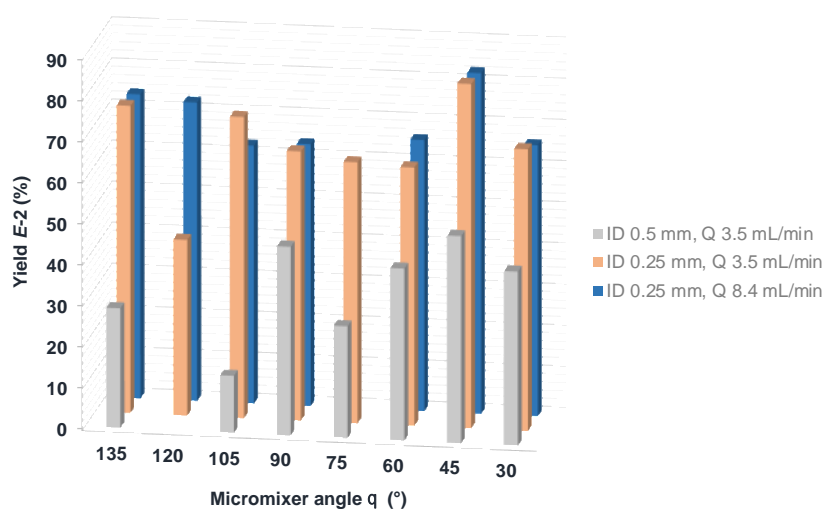


Figure 2.11 : Yield of 2.2 according to the angle of the micromixer.

If the increased conversion in a shorter time can be adequately explained by an enhanced mixing, how this mixing affects the stereochemistry of the reaction remains unclear at this point. At least two non-exclusive hypotheses could explain the observed selectivities: the first could be a fast equilibrium between *Z* and *E* form of the intermediate carbenoid. One of the isomers would be the kinetic product, while the other, which is thermodynamically preferred, would form gradually. The second idea is supported by the specific reactivity of

organolithium species linked with their aggregation state. This state strongly depends on the chemical environment, including solvents, additives, etc.<sup>23,24</sup> It was postulated that depending on the mixing quality, the chemical environment of limited species would be of various compositions. This hypothesis is based on the particular reactivity of organolithium species associated with their aggregation state. This state strongly depends on the chemical environment, including solvents and additives. For example, *n*-BuLi is hexameric in hexane, whereas it is found under a mixture of tetramer/dimer in THF (Figure 2.12).<sup>25</sup>

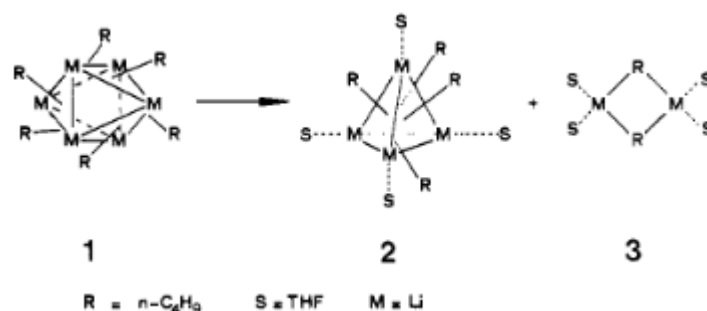


Figure 2.12: Lithium aggregates, (1) Hexamer, (2) Tetramer (3) Dimer, (excerpt from McGarrity and Ogle, 1985).<sup>14</sup>

It could be postulated that, depending on the quality of mixing, the chemical environment of lithiated species will be of various composition. In the worst case, laminar regime and bad mixing would force THF and hexane to flow side by side as well-defined domains, whereas in the best case of perfect mixing, the whole solution would be homogeneous before reaction occurs. This would have a deep impact on the aggregation state of organolithium species *n*-BuLi and/or carbenoid **2.A** eventually modifying their reactivity. In order to check this, several experiments were performed by using the same solvent for the two streams. With hexane as common solvent (and *i*-PrOH used as protic quench to keep the reaction mixture homogeneous), the system immediately clogged whatever the angle of micromixer, probably due to Lithium bromide (LiBr) precipitation. Preparing a solution of *n*-BuLi in THF proved very challenging, as THF solutions of *n*-BuLi are prone to rapid degradation at room temperature through deprotonation of the  $\alpha$ -position of THF followed by reverse (3+2) cycloaddition of the heterocycle.<sup>26,27</sup>

The equilibrium hypothesis, on the other hand, was ruled out by dedicated experiments: a microflow set-up was implemented with fixed flow rate  $Q(2.1+n\text{-BuLi})$  (9 mL/min) and

micromixer ( $\theta = 90^\circ$ , ID = 500  $\mu\text{m}$ ), and only the length of the reactor tube was modified (with fixed ID = 500  $\mu\text{m}$ ; Figure 2.13).

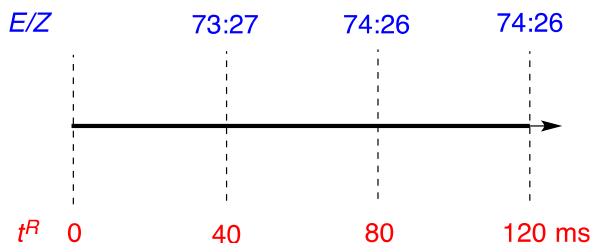


Figure 2.13 Evolution of E/Z ratio of 2.2 according to time in a flow set up.

With  $L = 3$  cm ( $t^R = 40$  ms), 6 cm ( $t^R = 80$  ms) and 9 cm ( $t^R = 120$  ms), full conversion into **2.2** was observed with almost no evolution in the E/Z ratio over time. Thus, it seems unlikely that the variations of stereoselectivity observed in a similar reaction time in experiments with various micromixers stems from a purely thermodynamic driven isomerization.

Finally, the potential of this set-up for the synthesis of functionalized scaffolds was assessed by trapping a solution of methyl benzoylformate in THF as an electrophile under best previous conditions reported in Table 2.3, entry 7 (Figure 2.14).

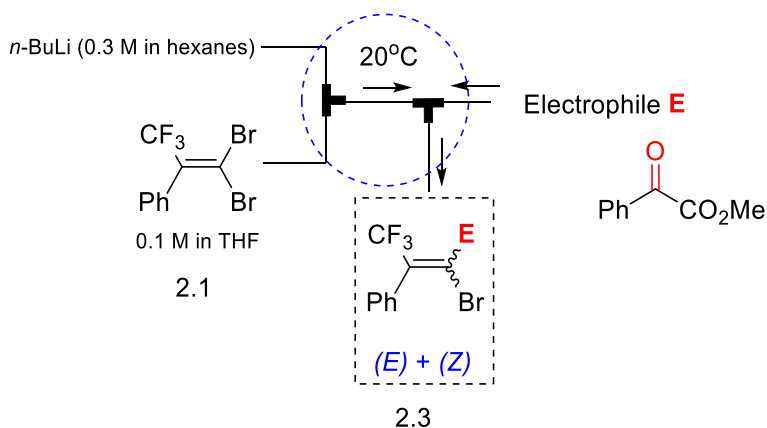


Figure 2.14 : Reaction in MF with methylbenzoylformate.

The reactor outlet was then collected into a flask containing methanol to afford product **2.3** (Figure 2.15).

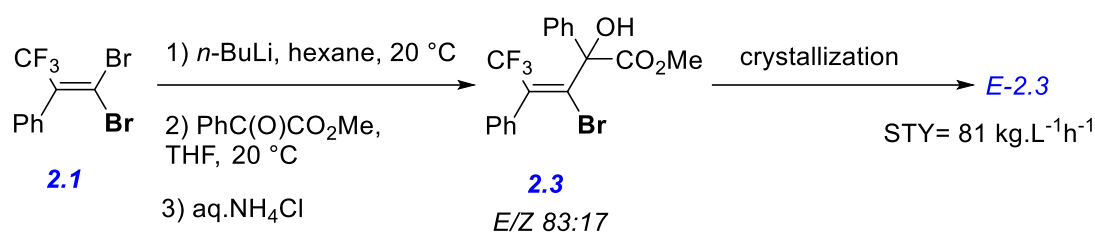


Figure 2.15: Synthesis of compound (*E*)-2.3 under microflow conditions (see Supporting information for details).

This reaction offered a >99% conversion of **2.1** with a 95% selectivity for **2.3** (*E/Z* ratio 84:16). Collecting the reactor outlet for 3 minutes followed by crystallization of the crude product yielded 338 mg of pure (*E*)-**2.3** with a productivity of 6.7 g/h and a high space-time yield (STY) of 81 kg.L<sup>-1</sup>.h<sup>-1</sup> due to the very small sizing of the global microreactor (83 μL). Further experiments with other electrophiles (such as boronates) to synthesize valuable molecular targets could be envisioned in future studies, outside the scope of this thesis.

## 2.7 Computational fluid dynamics study (CFD) of 45° micromixer

The above analysis is supported by a computational fluid dynamic study (CFD) carried out by Laurent Falk, Jean-Marc Commenge, Rainier Hreiz and Assile Ayoud at Laboratory of Reactions and Process Engineering (LRGP) from Nancy, France. CFD is an analysis of fluid flows using numerical solution techniques. This analysis was performed with the objective of corroborate the experimental results obtained to.

The results presented below (Figure 2.16) correspond to a V-shaped micromixer, with an angle of 45° between the inlet and outlet pipes. The pipes diameter is 250 μm.

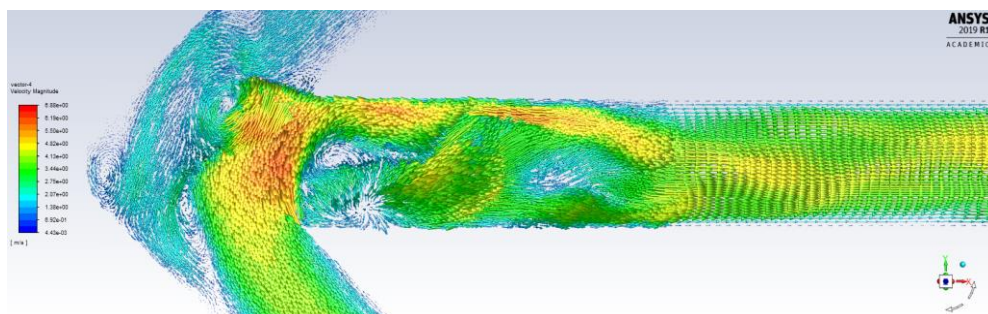
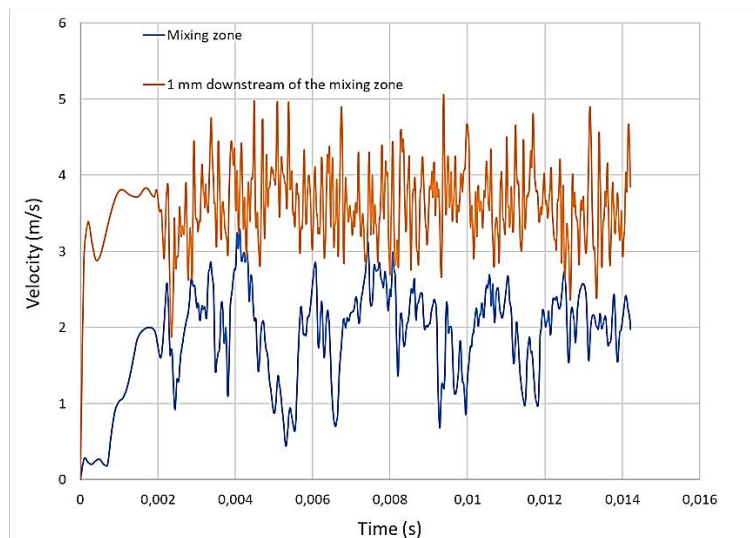


Figure 2.16 CFD of a V-shaped micromixer, with an angle of 45°; ID 0.25mm. Courtesy of LRGP



A flow rate of 2.4 mL/min of *n*-BuLi solution is set at the upper inlet, which corresponds to a Re about 200. The substrate is fed from the lower inlet with a flow rate of 6 mL/min corresponding to a Re of nearly 500. Hence, the Reynolds number at the outlet pipe flow is about 700.

Direct Numerical Simulation of the flow was carried out by solving the Navier-Stokes equations using ANSYS Fluent 19.1 commercial CFD code. The numerical results revealed that the flow is highly unsteady and extremely chaotic, which corresponds to a turbulent flow regime. The figure below (Figure 2.17), depicts the velocity field (at and arbitrarily instant) in the mid-plane of the micromixer, with the color levels corresponding to the velocity magnitude.



*Figure 2.17: Velocity temporal variations at two points, micromixer 45°, ID 0.25 mm. Courtesy of LRGP*

To be sure that the flow is indeed turbulent and not only chaotic, the velocity temporal variations at two points were recorded and are shown in the Figure 2.17. The blue curve represents the velocity magnitude at the point located at the center of the mixing zone, and the orange one represents the velocity at a point located 1 mm downstream in the outlet pipe.

Both curves reveal that the flow undergoes high frequency fluctuations which clearly characterize a turbulent flow regime at both the mixing zone and the outlet pipe.

## 2.8 Conclusion

We have investigated the stereoselectivity of lithium-bromine exchange on a *gem*-dibromo alkene in a microflow system with sixteen passive mixers that have two internal diameters of 500  $\mu\text{m}$  and 250  $\mu\text{m}$  and eight variable angles (from 135 to 30°). At 20 °C and different flow rates, the 45° W-shaped mixer with a narrower ID provided the best selectivity for the *E*-monobrominated product. This micromixer effect, which probably help disaggregating the organolithium species, is thought to result from a good mixing of the two streams of *n*-BuLi (in hexanes) and substrate (in THF). It is possible to obtain functionalized molecules with regulated geometry and a very high space-time yield by trapping a relevant electrophile under these conditions. This work opens the door to access more complex structures, such as active pharmaceutical ingredients or polymers.

## 2.9 Bibliography

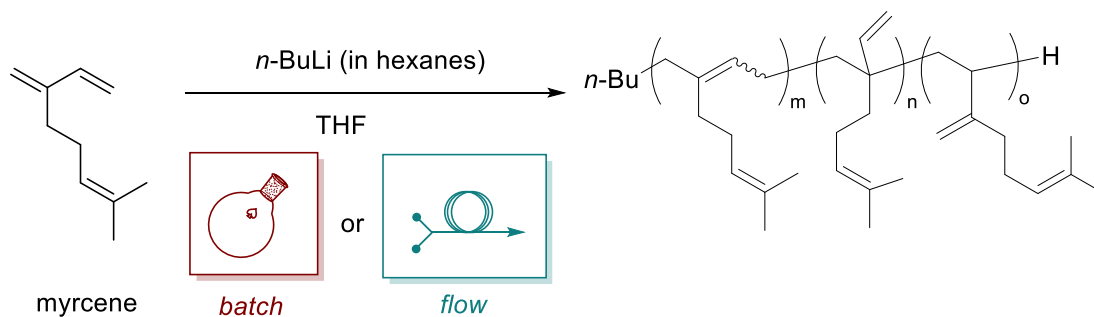
- (1) Panić, S.; Loebbecke, S.; Tuercke, T.; Antes, J.; Bošković, D. Experimental Approaches to a Better Understanding of Mixing Performance of Microfluidic Devices. *Chemical Engineering Journal* **2004**, *101* (1–3), 409–419.
- (2) Falk, L.; Commenge, J.-M. Performance Comparison of Micromixers. *Chemical Engineering Science* **2010**, *65* (1), 405–411.
- (3) Taheri, R. A.; Goodarzi, V. Numerical Investigation of Mixing Improvement in a Novel Spiral Microchannel with Baffles. *Engineering Analysis with Boundary Elements* **2022**, *144*, 518–529.
- (4) Microfluidic Mixers : A Short Review, Elveflow. [Online]., 2022.
- (5) Sakurai, R.; Yamamoto, K.; Motosuke, M. Concentration-Adjustable Micromixers Using Droplet Injection into a Microchannel. *Analyst* **2019**, *144* (8), 2780–2787.
- (6) Gobby, D.; Angeli, P.; Gavriilidis, A. Mixing Characteristics of T-Type Microfluidic Mixers. *J. Micromech. Microeng.* **2001**, *11* (2), 126–132. <https://doi.org/10.1088/0960-1317/11/2/307>.
- (7) Oddy, M. H.; Santiago, J. G.; Mikkelsen, J. C. Electrokinetic Instability Micromixing. *Analytical chemistry* **2001**, *73* (24), 5822–5832.
- (8) Fournier, M.-C.; Falk, L.; Villermaux, J. A New Parallel Competing Reaction System for Assessing Micromixing Efficiency—Experimental Approach. *Chemical Engineering Science* **1996**, *51* (22), 5053–5064.
- (9) Endo, Y.; Furusawa, M.; Shimazaki, T.; Takahashi, Y.; Nakahara, Y.; Nagaki, A. Molecular Weight Distribution of Polymers Produced by Anionic Polymerization Enables Mixability Evaluation. *Org. Process Res. Dev.* **2019**, *23* (4), 635–640. <https://doi.org/10.1021/acs.oprd.8b00403>.
- (10) Commenge, J.-M.; Falk, L. Villermaux–Dushman Protocol for Experimental Characterization of Micromixers. *Chemical Engineering and Processing: Process Intensification* **2011**, *50* (10), 979–990. <https://doi.org/10.1016/j.cep.2011.06.006>.
- (11) Kim, H.; Nagaki, A.; Yoshida, J. A Flow-Microreactor Approach to Protecting-Group-Free Synthesis Using Organolithium Compounds. *Nature communications* **2011**, *2* (1), 1–6.
- (12) Nagaki, A.; Kim, H.; Yoshida, J. Nitro-Substituted Aryl Lithium Compounds in Microreactor Synthesis: Switch between Kinetic and Thermodynamic Control. *Angewandte Chemie* **2009**, *121* (43), 8207–8209.
- (13) Nagaki, A.; Imai, K.; Ishiuchi, S.; Yoshida, J. Reactions of Difunctional Electrophiles with Functionalized Aryllithium Compounds: Remarkable Chemoselectivity by Flash Chemistry. *Angewandte Chemie International Edition* **2015**, *54* (6), 1914–1918.
- (14) Knorr, R. Alkylidenecarbenes, Alkylidenecarbenoids,<sup>†</sup> and Competing Species: Which Is Responsible for Vinylic Nucleophilic Substitution, [1 + 2] Cycloadditions, 1,5-CH Insertions, and the Fritsch–Buttenberg–Wiechell Rearrangement? *Chem. Rev.* **2004**, *104* (9), 3795–3850. <https://doi.org/10.1021/cr030616h>.

- (15) Capriati, V.; Florio, S. Anatomy of Long-Lasting Love Affairs with Lithium Carbenoids: Past and Present Status and Future Prospects. *Chemistry – A European Journal* **2010**, *16* (14), 4152–4162. <https://doi.org/10.1002/chem.200902870>.
- (16) Chelucci, G. Synthesis and Metal-Catalyzed Reactions of Gem-Dihalovinyl Systems. *Chem. Rev.* **2012**, *112* (3), 1344–1462. <https://doi.org/10.1021/cr200165q>.
- (17) Harada, T.; Katsuhira, T.; Hattori, K.; Oku, A. Stereochemistry in Carbenoid Formation by Bromine/Lithium and Bromine/Zinc Exchange Reactions of Gem-Dibromo Compounds. *Tetrahedron* **1994**, *50* (27), 7987–8002. [https://doi.org/10.1016/S0040-4020\(01\)85284-4](https://doi.org/10.1016/S0040-4020(01)85284-4).
- (18) Fürst, R.; Rinner, U. Synthesis of an Advanced Intermediate of the Jatrophone Diterpene Pl-4: A Dibromide Coupling Approach. *J. Org. Chem.* **2013**, *78* (17), 8748–8758. <https://doi.org/10.1021/jo401480t>.
- (19) Mizuta, S.; Otaki, H.; Kitamura, K.; Nishi, K.; Watanabe, K.; Makau, J. N.; Hashimoto, R.; Usui, T.; Chiba, K. 3,3-Dibromo-2-Trifluoromethyl Acrylic Acid Ethyl Ester: A Versatile Platform for the Stereoselective Preparation of Functionalized- $\alpha$ -Trifluoromethyl  $\alpha,\beta$ -Unsaturated Lactones and Trifluoromethyl Pyrazolinones. *Org. Chem. Front.* **2016**, *3* (12), 1661–1667. <https://doi.org/10.1039/C6QO00360E>.
- (20) Picard, B.; Pérez, K.; Lebleu, T.; Vuluga, D.; Burel, F.; Harrowven, D. C.; Chataigner, I.; Maddaluno, J.; Legros, J. Bromine-Lithium Exchange on Gem-Dibromoalkenes Part 1: Batch vs Microflow Conditions. *J. Flow Chem* **2020**, *10* (1), 139–143. <https://doi.org/10.1007/s41981-019-00057-6>.
- (21) Konno, T.; Daitoh, T.; Noiri, A.; Chae, J.; Ishihara, T.; Yamanaka, H. A Highly Regio- and Stereoselective Carbocupration of Fluoroalkylated Internal Alkynes: A Short Total Synthesis of the Antiestrogenic Drug Panomifene. *Organic Letters* **2004**, *6* (6), 933–936.
- (22) Liu, X.; Shimizu, M.; Hiyama, T. A Facile Stereocontrolled Approach to CF<sub>3</sub>-Substituted Triarylethenes: Synthesis of Panomifene. *Angewandte Chemie International Edition* **2004**, *43* (7), 879–882.
- (23) Hamdoun, G.; Sebban, M.; Cossoul, E.; Harrison-Marchand, A.; Maddaluno, J.; Oulyadi, H. <sup>1</sup>H Pure Shift DOSY: A Handy Tool to Evaluate the Aggregation and Solvation of Organolithium Derivatives. *Chem. Commun.* **2014**, *50* (31), 4073–4075. <https://doi.org/10.1039/C4CC00111G>.
- (24) Reich, H. J. Role of Organolithium Aggregates and Mixed Aggregates in Organolithium Mechanisms. *Chem. Rev.* **2013**, *113* (9), 7130–7178. <https://doi.org/10.1021/cr400187u>.
- (25) McGarrity, J. F.; Ogle, C. A. High-Field Proton NMR Study of the Aggregation and Complexation of n-Butyllithium in Tetrahydrofuran. *J. Am. Chem. Soc.* **1985**, *107* (7), 1805–1810. <https://doi.org/10.1021/ja00293a001>.
- (26) Stanetty, P.; Mihovilovic, M. D. Half-Lives of Organolithium Reagents in Common Ethereal Solvents. *J. Org. Chem.* **1997**, *62* (5), 1514–1515. <https://doi.org/10.1021/jo961701a>.

- (27) Rivera, N. R.; Kassim, B.; Grigorov, P.; Wang, H.; Armenante, M.; Bu, X.; Lekhal, A.; Variankaval, N. Investigation of a Flow Step Clogging Incident: A Precautionary Note on the Use of THF in Commercial-Scale Continuous Process. *Org. Process Res. Dev.* **2019**, *23* (11), 2556–2561. <https://doi.org/10.1021/acs.oprd.9b00366>.
- (28) Uno, H.; Nibu, N.; Misobe, N. Re-Investigation of the Coupling Reaction of 2-Aryl-1,1-Dibromo-3,3,3-Trifluoropropenes. Preparation of Perfluoroalkylated [3]Cumulenes. *BCSJ* **1999**, *72* (6), 1365–1375. <https://doi.org/10.1246/bcsj.72.1365>.

# Chapter 3

## Anionic polymerization of myrcene under batch and flow conditions



### 3.1 Introduction

This chapter deals with the comparative anionic polymerization of myrcene under discontinuous macrobatch and continuous microflow conditions: the main objective of this work being the synthesis of polymyrcene oligomers with a precisely controlled molar mass under conditions allowing perfect reproducibility at various scales.

### 3.2 General reaction parameters

As explained below, key parameters were fixed to develop this model reaction and to compare batch and continuous flow results, such as monomer and initiator choice, solvent used, or the influence of concentration and temperature.

#### 3.2.1 Myrcene as monomer

As mentioned in chapter 1, myrcene is found in nature, and it is commercially available at reasonable cost. Its homopolymerization affords polymyrcene (PMYR), an elastomer exhibiting good properties. Indeed, such biobased polymers constitute an alternative solution to replace polymers synthesized from fossil resources (*e.g.*, isoprene in this case). Among all the methods, polymyrcene can be easily synthesized by anionic polymerization.<sup>1</sup>

#### 3.2.2 Anionic polymerization

Anionic polymerization is a chain-growth polymerization which involves vinyl monomers with significant electronegative groups (such as acrylates), but also dienes. As this anionic path is typically used to produce synthetic polydiene rubbers, this type of polymerization has also been used to synthesize polymyrcene.<sup>2</sup>

## General considerations

Pure monomers and solvents, as well as dry conditions, are needed in anionic polymerization to prevent any undesired consumption of the active center. The active center is the site on a chain carrier where reaction takes place.

## Monomers

Apart from heterocyclic molecules, monomers susceptible to anionic polymerization usually have substituents that stabilize the electronegative charge of the active center (electronegative withdrawing groups, p-systems). These include non-polar monomers such as styrene, butadiene or isoprene (or others 1,3 dienes) and polar monomers<sup>12</sup> such as vinylpyridine, acrylates or vinyl ketones.

Solvents used are essentially hydrocarbons and ethers which will not interfere with the active center contrary to alcohols, esters or halogenated solvents. However, their solvation power can influence the final microstructure of the polymer.

Thus, this project started by studying the anionic polymerization of myrcene under batch conditions. After that, myrcene polymerization in continuous flow is carried out. Batch and continuous flow were finally compared.

As a reminder, the reaction of anionic myrcene polymerization is as follows (Figure 3.1):

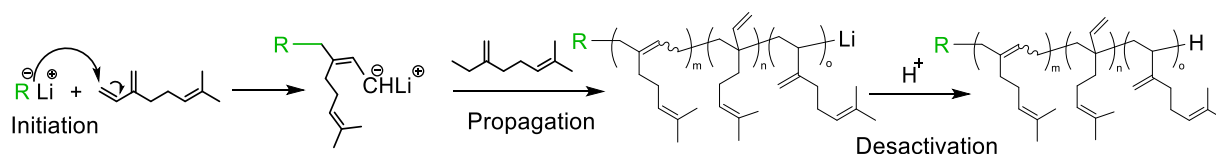


Figure 3.1: Anionic polymerization of myrcene with an alkyl-lithium (for sake of clarity, the scheme was drawn starting with a 1,4-addition).

In this work, we were interested in the anionic polymerization due to two interesting features exhibited by this type of reactions: 1) a “living” polymerization, and 2) a very narrow molecular weight distribution (Poisson distribution), since all growing chains have the same growth probability (if initiation time is short compared to that of propagation).<sup>3</sup>



Anionic polymerization allows a lower index of polymerization, compared with other types of polymerization, and consequently allows the prediction of the degree of polymerization (Equation 3.1).<sup>4</sup>

$$\bar{X}n_{th} = \frac{\Delta M}{[I]_o} \quad \text{Equation 3.1}$$

Where:

$\bar{X}n_{th}$  = degree of polymerization

$\Delta M$  = consumed monomer (mol)

$[M]_o$  = initial concentration of monomer (mol/L)

$[I]_o$  = initial concentration of initiator (mol/L)

$\bar{M}n_{th}$  = theoretical molar mass (g/mol)

$M_{unit}$  = monomer unit

If we assume there is a total reaction, the theoretical molar mass can be calculated by Equation 3.2 :

$$\bar{M}n_{th} = \frac{[M]_o}{[I]_o} * M_{unit} \quad \text{Equation 3.2}$$

Telechelic oligomers (see Chapter 4) industrially used have  $1000 < \bar{M}n < 5000$ .<sup>5</sup> These liquid polymers are usually attractive to prepare materials with specific architectures and properties. Thus, our aim was to prepare oligomers having a maximum  $\bar{M}n$  of 2500. Hence, all experiments (batch and continuous flow) were performed with a (monomer/initiator) ratio of 17/1, to allow  $\bar{M}n_{th} = 17 * 136 = 2312 \text{ g/mol}$ .

### 3.2.3 Initiator

The anionic polymerization of myrcene can be done with a large family of alkyl-lithiums initiators<sup>6</sup> among which the butyl family is prominent. In this work, *sec*-BuLi and *tert*-BuLi, were quickly excluded due to several issues. Among these problems, we identified the presence of lithium hydroxide (LiOH) which will be an issue in microfluidic systems, pyrophoricity or flammability, and the cost of experiments (cryogenic conditions). We finally decided to use *n*-BuLi as the initiator in our polymerization reaction because it was more manageable and affordable than the others but also more stable in ethereal solvents in a broader range of temperatures.

### 3.2.4 Solvents

The effect of the solvent used in the anionic polymerization of myrcene is not well known nor clearly defined. However, it is widely recognized that polar and non-polar solvents can affect the distribution of the polymer and, consequently, its microstructure.<sup>3</sup>

*n*-Butyllithium is commercialized in hexanes. In such solvent, alkylolithiums are known to be aggregated. Thus, to afford a fast initiation step, we decided to use the deaggregating THF as solvent to prepare the reacting solutions of myrcene. Thus, when the reaction was performed at 10 °C in a THF/hexane mixture as solvent, it yielded the desired polymer with low polydispersity, even in batch conditions, as it will be described later in the manuscript. This results can be explained by the fact that ethereal solvents are not only diluents but also have effects on dissociation and solvation of organometallic species (Section 2.6, page 81).<sup>4</sup>

### 3.2.5 Temperature

According to studies on the stability of organolithiums in ethereal solvents, Stanetty *et al.* reported that *n*-BuLi content remained stable for 107 min at 20 °C.<sup>7</sup> In order to evaluate the effect of temperature on the initiator, we decided to perform a study of the degradation of *n*-BuLi at 30 °C.

To do this, we prepared a *n*-BuLi/hexane/THF solution under stirring in a round-bottom flask. This solution was titrated with a solution of menthol/bipyridine in THF at 0°C along time. Figure 3.2 shows that *n*-BuLi content decreases just after 3 min at 30 °C. After 5 min half of *n*-BuLi is consumed.

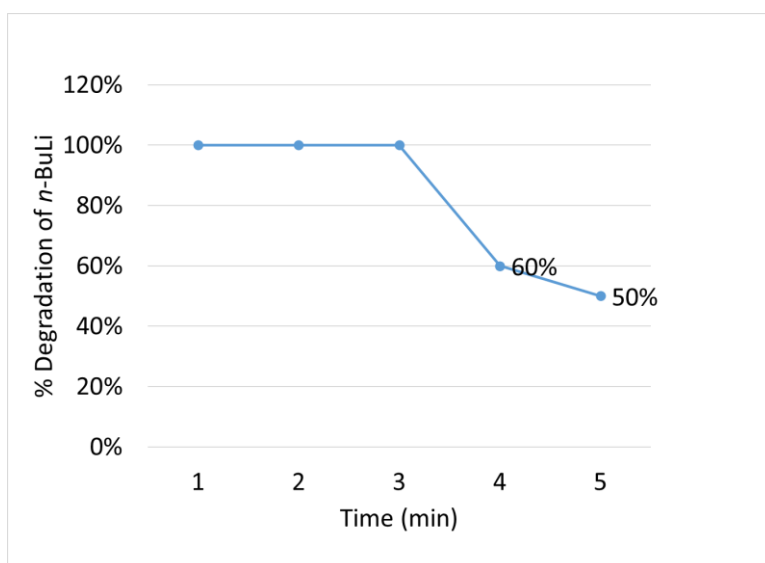


Figure 3.2: Study of degradation of *n*-BuLi at 30 °C in a THF/hexane solution.

This is related to the well-known decomposition of THF via reverse (3+2) cycloaddition (Figure 3.3).<sup>8</sup>

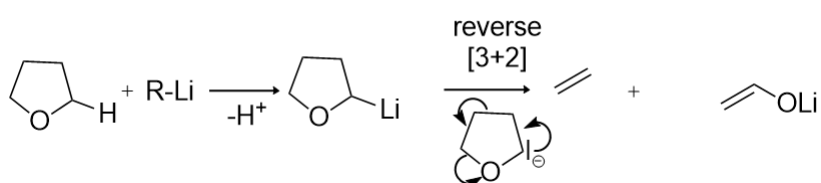


Figure 3.3: Decomposition of THF with organolithium.

For this reason, we finally decided to set the temperature of the reaction at a lower value: 10 °C.

### 3.2.6 Scale

To see the effect of the scale in batch, the polymerization of myrcene was carried out using different scales, from 110 mg to 17 g, but keeping constant the same (monomer/initiator) molar ratio (17:1) and the concentration of reagents. *n*-BuLi was used at 2.5 M in hexanes (directly from the bottle) for the higher scale (17 g), and as 0.3 M solution in hexanes for the smaller batch scale and in flow reactions.

Firstly, the reaction was performed using 0.11 g of myrcene (in 0.26 mL of THF in a 5 mL round flask). As shown in Table 3.1, molar mass was monitored according to time by quenching aliquots with methanol. After 30 min,  $\overline{M}_n = 2400$  and it is considered that

myrcene polymerization reaches the maximum value estimated of molar mass ( $\overline{Mn}_{th}=2312$  g/mol).

Table 3.1: Polymerization reaction using 0.1 g of myrcene.

Entry	Time (min)	$\overline{Mn}$ (g/mol)		$\overline{D}$	Yield (%) <sup>a</sup>	Conv. (%) <sup>b</sup>	$\overline{Mn}_{th}$ <sup>c</sup>
		<sup>1</sup> H NMR	GPC				
1	1	410	550	1.23	11	17	255
2	2	650	600	1.23	28	28	648
3	10	1050	1300	1.26	53	45	1227
4	20	2200	1850	1.19	71	95	1644
5	30	2400	1900	1.23	91	104	2107

<sup>a</sup> Based on the mass of PMYR recovered after full removal of volatiles (including myrcene). <sup>b</sup> based on the  $\overline{Mn}$  (<sup>1</sup>H NMR)/2316×100. <sup>c</sup> Theoretical  $\overline{Mn} = \text{yield} \times 2316 / 100$

By increasing the scale (myrcene 1 g, in 2.6 mL of THF in a 10 mL round flask), the time required to reach  $\overline{Mn}_{th}$  drop to 8 minutes (Table 3.2).

Table 3.2: Polymerization reaction using 1 g of myrcene.<sup>a</sup>

Entry	Time (min)	$\overline{Mn}$ (g/mol)		$\overline{D}$	Yield (%) <sup>a</sup>	Conv. (%) <sup>b</sup>	$\overline{Mn}_{th}$ <sup>c</sup>
		<sup>1</sup> H NMR	GPC				
1	1	950	900	1.24	20	42	463
2	2	800	950	1.14	32	35	741
3	4	1750	1550	1.12	61	73	1412
4	8	2300	2050	1.14	90	101	2084
5	10	2200	2800	1.24	59	95	1366
6	30	2700	3250	1.23	68	117	1574
7	60	2600	3000	1.35	65	112	1505

<sup>a</sup> Based on the mass of PMYR recovered after full removal of volatiles (including myrcene). <sup>b</sup> based on the  $\overline{Mn}$  (<sup>1</sup>H NMR)/2316×100. <sup>c</sup> Theoretical  $\overline{Mn} = \text{yield} \times 2316 / 100$

Noteworthy, we noticed that at the highest scale of monomer we used (17 g of myrcene), the polymerization reaction was rapidly achieved, *i.e.* the molar mass remains stable with time, (Table 3.3). In this case, a single-minute reaction allowed to reach  $\overline{Mn} = 2050$  g/mol.

Table 3.3: Polymerization reaction using 17 g of myrcene.<sup>a</sup>

Entry	Time (min)	$\overline{Mn}$ (g/mol)		Đ	Yield (%) <sup>a</sup>	Conv. (%) <sup>b</sup>	$\overline{Mn}_{th}$ <sup>c</sup>
		<sup>1</sup> H NMR	GPC				
1	1	2050	2250	1.13	88	89	2038
2	10	2050	1950	1.17	92	91	2130

<sup>a</sup> Based on the mass of PMYR recovered after full removal of volatiles (including myrcene). <sup>b</sup> based on the  $\overline{Mn} = (^1H\ NMR)/2316 \times 100$ . <sup>c</sup> Theoretical  $\overline{Mn} = yield \times 2316/100$

Overall, the dispersity values (Đ) obtained are regular and in the classical range for anionic polymerization (< 1.5) but lower final molar masses are observed compared to experiments performed on lower scales (0.1 and 1.0 g).

The polymerization of myrcene in a batch is thus affected by the scale/quantity used. Focusing on a 1 min reaction time, when the reaction volume increases, yield and molar mass increases, which is not kinetically expected since monomer and initiator concentration are kept constant (Table 3.4). These results suggested that the uncontrolled increase of polymers molar mass is linked to the fact that we do not have a firm grip on the temperature when the scale of starting material increases.

Table 3.4: Batch polymerization of myrcene at different scales after 1 min reaction (filled up to 60%).

Entry	Scale (g)	S/V	$\overline{Mn}$ (g/mol)	Yield (%)
		(cm <sup>-1</sup> )	<sup>1</sup> H NMR	<sup>1</sup> H NMR
1	17.0	0.86	2050	88
2	1.0	3.32	950	20
3	0.1	6	410	11

By calculating the S/V under all three conditions (Figure 3.4, entry 1-3), we can see that this value decreases when the quantity of material increases, resulting in less good heat removal. This corroborates the previous observation. By calculating the same S/V for a tubular system (S/V = 80 cm<sup>-1</sup>, ID = 0.5 mm), we immediately see the interest of microfluidics in controlling the temperature of the reaction medium.

### 3.2.7 Temperature

One of the main problems in batch conditions is temperature control. To evaluate this parameter, the polymerization of myrcene was performed in batch using a 17.0 g scale for

1 minute at 10 °C. Temperature was controlled using two K-Thermocouples HANNA. The first thermocouple was used to control external temperature with a bath at 10°C, and the internal temperature was measured using the second thermocouple (Figure 3.4).

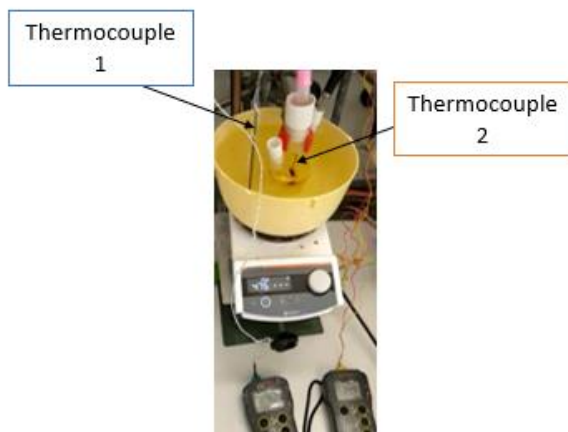


Figure 3.4: Experimental setup for batch polymerization of myrcene with temperature control.

We noticed that even when using a bath at 10 °C, the internal temperature reaction quickly rises to 45 °C in less than 1 minute (Figure 3.5).

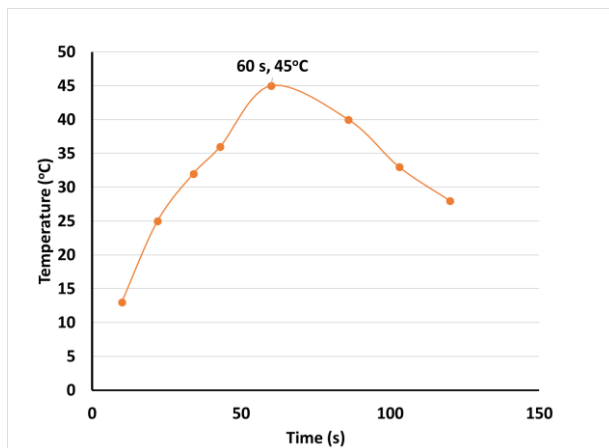


Figure 3.5: Temperature inside the reactor (17 g myrcene, bath 10 °C)

As showed in the Figure 3.5, we were not able to control the internal temperature on a large scale in batch. However, this could be controlled when using the smallest scale, but at the expense of production.

### 3.2.8 Microstructure

As previously indicated, it is well known that the reaction solvent can have an impact on the microstructure. Regarding the microstructure of PMYR obtained by anionic polymerization, the effect of the solvent has been highlighted in two distinct papers: Avila-Ortega reported that the reaction of myrcene in pure benzene with *sec*-BuLi afforded 1,4 microstructure as major isomer (85%), Wahlen, C did  $\beta$ -myrcene polymerization in pure cyclohexane and obtained 94% 1,4 and 6% 1,2 units,<sup>9</sup> while Hillmeyer and Hoyer described the 3,4 isomer as major product (60%) along with 1,4 (30%) and 1,2 (10%) adducts in THF with *sec*-BuLi (1.4 M in hexanes).<sup>10,11</sup> Thus, 1,4 cis/trans, 3,4, and 1,2 unit content was determined by means of <sup>1</sup>H NMR in our reaction conditions (Figure 3.6).

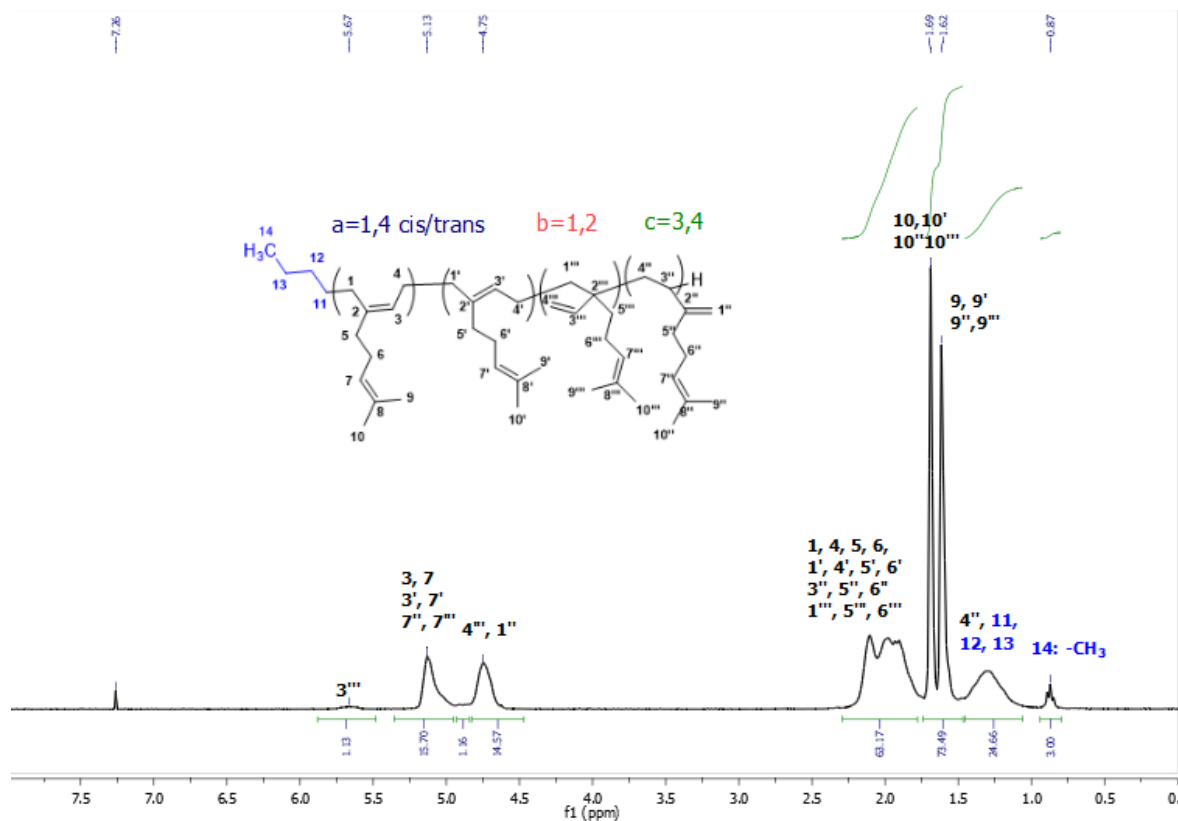


Figure 3.6: <sup>1</sup>H NMR (300 MHz, CDCl<sub>3</sub>) spectrum of polymyrcene in batch at 10 °C in THF/hexane. Microstructure calculations:  $b=1.13(1H)$ ;  $c=(14.57-1.13)/2=6.72(1H)$ ;  $a=(15.70-6.72-1.13)/2=3.92(1H)$ ;  $a=3.92/11.77=33\%$ ,  $b=1.13/11.77=10\%$ ,  $c=6.72/11.77=57\%$

Table 3.5 shows the microstructure of polymyrcene in batch at different scales. No significant difference was noticed at 0.1 g (entry 1) and 1 g (entry 2), since percentage of hexane was the same.

Table 3.5: Microstructure of polymyrcene under batch conditions at 10 °C.

Entry	Batch scale (g)	Hexane (%)	1,2- (%)	3,4- (%)	1,4- (%)
1	0.1	38	15	62	23
2	1.0	38	11	62	27
3	17.0	14	10	57	33

A well-marked difference was not observed either for the larger batch scale (17g) even if the solvent mixture was richer in THF. Results were similar to Hillmeyer and Hoye.

### 3.3 Continuous flow reactors

As it was mentioned in the bibliography, continuous flow reactors allow control over many reaction parameters. In this part, some of these parameters such as flow rate, reactors length, temperature, mixer type, were varied to study their effect on the polymerization reaction.

#### 3.3.1 Setup

All the stainless-steel reactors in this work were made inhouse and dried overnight in an oven at 120 °C before use. This part is essential to avoid moisture in the system. Once each part is dried, the system is assembled. Figure 3.7 shows the setup used in microflow conditions.

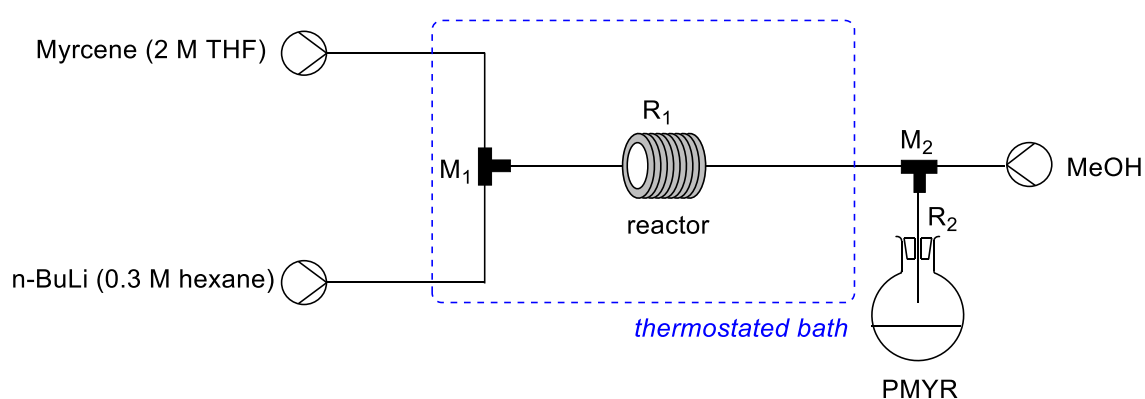
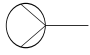


Figure 3.7: Diagram of the setup used in microflow conditions for the synthesis of polymyrcene. Flow rate of myrcene/n-BuLi/ MeOH (mL/min): 0.25/0.1/0.1 respectively, 1 min reaction. Reactor geometry: 0.75 mm ID, 1-meter length.



Basically, the flow system includes different elements such as syringe-pumps , stainless-steel tubing and connections/junctions (PFA and stainless steel), mixers (M), reactors (R) (750  $\mu\text{m}$  Internal Diameter ID, various length), and a thermostated water bath.

Solutions are pumped with syringe pumps. The system has a first inlet containing a solution of myrcene in THF (2 M) and a second inlet with *n*-BuLi solution (0.3 M in hexanes). The solutions are passed through a first T-shaped micromixer M1 (stainless steel, 500  $\mu\text{m}$  of internal diameter (ID)) connected to a tubular microreactor (stainless steel, 750  $\mu\text{m}$  ID, 1 m length) at the desired flow rate. This microreactor is immersed in a water bath thermostated at 10 °C. The reaction mixture then feeds the second T-shaped micromixer M2 (500  $\mu\text{m}$  ID) to be quenched with methanol. The quenched mixture is passed through a second tube (300 mm length and 750  $\mu\text{m}$  ID) before collection in a vial containing 2 mL of HCl 2 M. Three dead volumes were run through the system before collection to ensure reactor equilibrium, then 2 to 5 mL of reaction solution were collected at the outlet for analysis.

### 3.3.2 Mixers and mixing

In contrast with what was observed in Chapter 2,<sup>12</sup> where micromixers angle was evaluated, no significant influence was observed when testing the reaction with W- and T-shaped micromixers in our conditions (Table 3.6).

*Table 3.6: Results after polymerization using W and T micromixers ( $R_1=1$  m,  $T=10$  °C).*

Entry	Angle ( $\theta$ )	$\overline{M}_n$ (g/mol)		D
		$^1\text{H NMR}$	GPC	
1	45	1000	750	1.14
2	90	950	700	1.14

Thus, we decided to stick with the more affordable ***T-shaped mixers*** of 0.5 mm ID for all reactions (Figure 3.8).



*Figure 3.8: T- and W-shaped micromixers.*

### 3.3.3 Flow rate

Based on preliminary works in organolithium chemistry under microflow conditions during my Master training,<sup>12-13</sup> and after several studies, starting conditions were as follows: *myrcene/n-BuLi/MeOH*, were injected at flow rates of **0.25/0.1/0.1 (mL/min)** *respectively* in a stainless-steel tube reactor of 0.75 mm internal diameter (ID) and 1-meter length.

### 3.3.4 Reactor size and flow rate

Changing the size of the flow reactor or the flow rate allows access to different residence times and, consequently, to oligomers with different molar mass. Figure 3.10 shows different sizes of stainless steel microreactors used in this work. The shape of the reactors was adapted to the workspace. A typical setup used in continuous flow is shown (Figure 3.9).

Different experiments using the same flow rate, *myrcene/n-BuLi* (mL/min): **0.25/0.1** at 10 °C with different reactors size, were performed (Table 3.7). These results showed that by

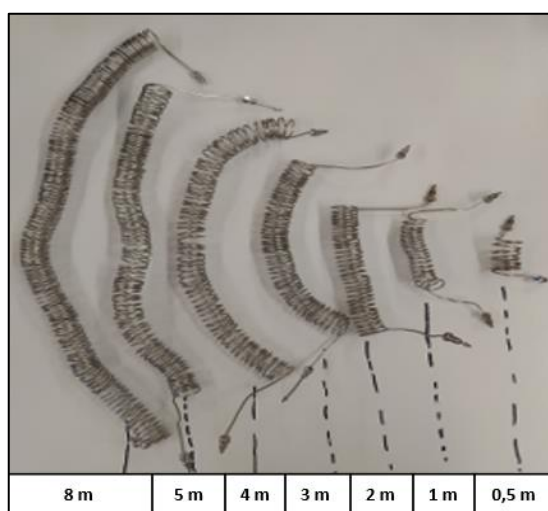


Figure 3.10: Stainless steel microreactors

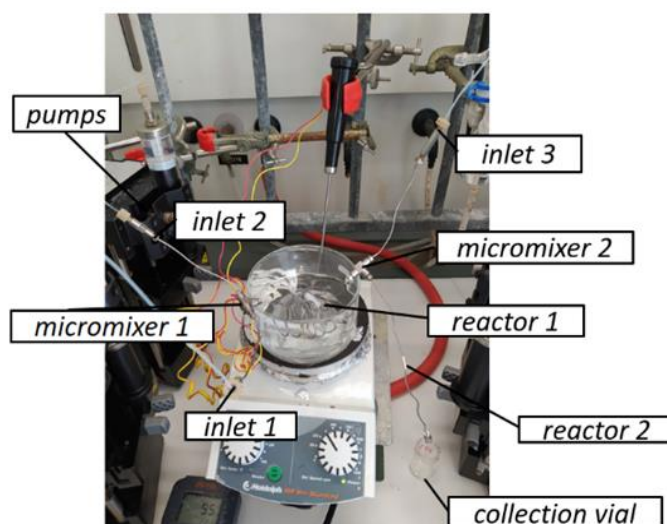


Figure 3.9: Microflow Setup.

increasing the residence time, it was possible to obtain polymers with a higher molar mass. As well, fine control of the molar mass and reproducibility was achieved in continuous flow.

Table 3.7: Different experiments with 0.25/0.1 myrcene/*n*-BuLi (mL/min) flow rate at 10°C.

Entry	Reactor length (m)	Residence time (s)	$\overline{Mn}$ (g/mol)		$\overline{D}$	Yield (%) <sup>a</sup>	Conv. (%) <sup>b</sup>	$\overline{Mn}_{th}$ <sup>c</sup>
			<sup>1</sup> H NMR	GPC				
1	0.5	38	450	400	1.44	13	19	301
2	1.0	75	700	600	1.27	28	30	648
3	1.6	120	1000	850	1.33	42	43	972
4	2.0	157	1150	900	1.19	54	50	1250
5	2.4	180	1300	1050	1.16	57	56	1320
6	3.0	227	1050	1200	1.43	47	45	1088
7	4.0	302	1500	1400	1.20	69	65	1598
8	8.0	600	2100	1700	1.36	54	91	1250

<sup>a</sup> based on the mass of PMYR recovered after full removal of volatiles (including myrcene). <sup>b</sup> based on the  $\overline{Mn} = (^1H\ NMR)/2316 \times 100$ . <sup>c</sup> Theoretical  $\overline{Mn} = yield \times 2316/100$

### Residence time fixed

Reactions using different reactors sizes (0.5, 1 and 8 m), different flow rates, for a residence time fixed (75 s) were performed. Results showed that there is no significant difference in the obtained molar mass (Table 3.8). This is important because it allows us to change the flow rate or the reactor size. This means that mixing (influenced by the flow rate in the mixing zone) does not seem to be a major parameter in this reaction between *n*-BuLi (in hexane) and myrcene (in THF). Probably because an instantaneous anionic initiation of myrcene by *n*-BuLi occurs even at low flow rates in our conditions (THF). Thus, the  $t^R$  can be tuned either through the flow rate or the reactor size, indifferently (each experiment was performed twice).

Table 3.8: Experiments using 0.5, 1 and 8 m reactor with various flow rates ( $t^R$  fixed at 75 s).

Entry	Flow rate Myr/ <i>n</i> -BuLi (mL/min)	Reactor Size (m)	Molar mass ( $\overline{Mn}$ ) (g/mol)		$\overline{D}$	Yield (%) <sup>a</sup>	Conv. (%) <sup>b</sup>	$\overline{Mn}_{th}$ <sup>c</sup>
			<sup>1</sup> H NMR	GPC				
1	0.125/0.05	0.5	800	650	1.10	26	35	602
2	0.25/0.1	1.0	700	650	1.27	28	32	648
3	2/0.8	8.0	850	550	1.23	47	37	1088

<sup>a</sup> based on the mass of PMYR recovered after full removal of volatiles (including myrcene). <sup>b</sup> based on the  $\overline{Mn} = (^1H\ NMR)/2316 \times 100$ . <sup>c</sup> Theoretical  $\overline{Mn} = yield \times 2316/100$

## Reactor size fixed

Keeping constant the reactor size (8 m) and changing the flow rate (Table 3.9) led to different residence time. Comparing Table 3.7 and Table 3.8 shows that similar results were obtained to those shown in Table 3.9.

Table 3.9: Experiments using 8 m reactor at 10°C with different flow rates.

Entry	Flow rate Myr/ <i>n</i> - BuLi (mL/min)	Residence time (s)	$\overline{Mn}$ (g/mol)		$\mathbb{D}$	Yield (%) <sup>a</sup>	Conv. (%) <sup>b</sup>	$\overline{Mn}_{th}$ <sup>c</sup>
			<sup>1</sup> H NMR	GPC				
1	4/1.6	38	600	350	1.16	29	26	671
2	2/0.8	75	900	550	1.23	47	39	1088
3	0.25/0.1	600	2100	1700	1.36	54	91	1250

<sup>a</sup> based on the mass of PMYR recovered after full removal of volatiles (including myrcene). <sup>b</sup> based on the  $\overline{Mn} = (^1H\ NMR)/2316 \times 100$ . <sup>c</sup> Theoretical  $\overline{Mn} = yield \times 2316/100$

With the flow system it is therefore possible to precisely select the number of monomer units with  $\overline{Mn} = 600$  ( $t^R = 38$  s; entry 1) to 2100 ( $t^R = 600$  s; entry 3). It is worth to note that such a fine  $t^R$  tuning (and therefore  $\overline{Mn}$  of PMYR) was unreachable in a conventional batch reactor.

Therefore, by comparing all these results (Figure 3.11) a relationship between residence time and the obtained molar mass of the polymer can be established, from Equation 3.3.

$$t^R = \frac{V}{Q} = \frac{\pi r^2 L}{Q}$$

Equation 3.3

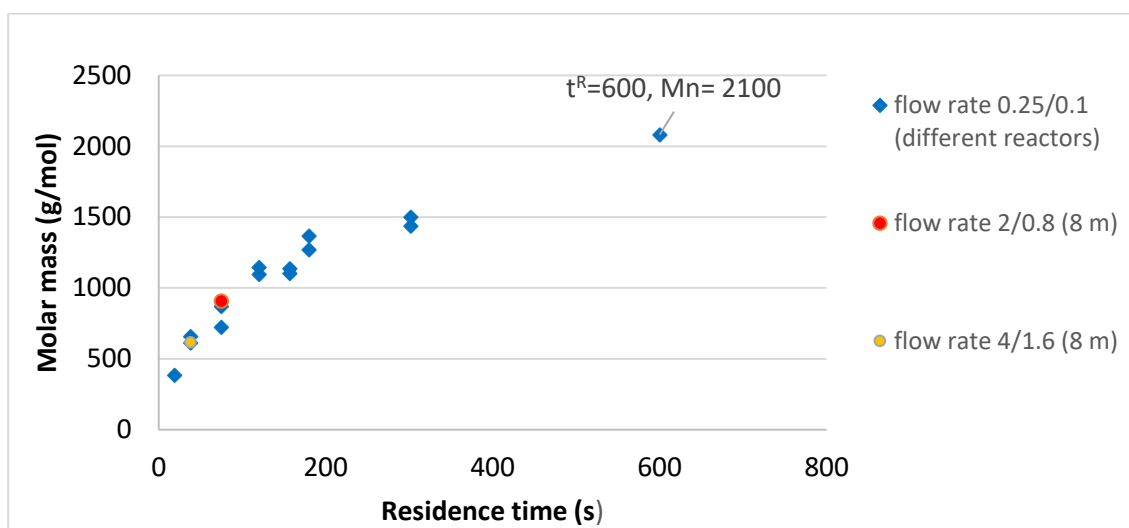


Figure 3.11 Comparison between different length reactors at 10°C.

Thus, from these results it can be concluded that the polymerization of myrcene under microfluidic conditions is finely controlled, conversely to macrobatch polymerization that depends on the amount of material used.

### 3.3.5 Influence of temperature

According to experiments analyzed by  $^1\text{H}$  NMR and GPC, we have observed that temperature plays an important role in the propagation of the reaction. Comparing the results obtained previously at 10 °C (Table 3.7) with those obtained at 20 °C (Table 3.10) showed that increasing the temperature by 10 degrees slightly increases the molar mass of the polymer.

Table 3.10: Experiments with the same flow rate, myrcene /n-BuLi (mL / min): 0.25 / 0.1, different length of reactors at 20 °C.

Entry	Reactor size (m)	Residence time (s)	$\overline{Mn}$ (g/mol)		$\overline{D}$	Yield (%) <sup>a</sup>	Conv. (%) <sup>b</sup>	$\overline{Mn}_{th}$ <sup>c</sup>
			$^1\text{H}$ NMR	GPC				
1	0.5	38	0.5	900	600	40	39	926
2	1.0	75	1.0	1100	850	51	47	1181
3	1.6	120	1.6	1450	1050	78	63	1806
4	2.0	157	2.0	1650	1450	73	71	1690
5	2.4	180	2.4	1500	1500	78	65	1806
6	4.0	302	4.0	1700	1800	74	73	1713

<sup>a</sup> based on the mass of PMYR recovered after full removal of volatiles (including myrcene). <sup>b</sup> based on the  $\overline{Mn}$  = ( $^1\text{H}$  NMR)/2316×100. <sup>c</sup> Theoretical  $\overline{Mn}$  = yield×2316/100

To further determine the influence of temperature, experiments were performed at constant  $t^R = 75$  s (Table 3.11). At this short reaction time, a temperature of 10 °C allowed to reach a short  $\overline{Mn} = 700$  (i.e., 5 monomer units) whereas 20 °C led to  $\overline{Mn} = 1100$  (8 units)

with a plateau at 30 °C with  $\overline{Mn} = 1350$  (10 units). This is likely connected to the consumption of *n*-BuLi in the deprotonation/decomposition of THF that arises very fast when the temperature increases, with a  $[myrcene]/[n\text{-BuLi}]$  increase also.

Therefore, performing the reaction at a temperature close to room temperature (10 to 20 °C) is energy saving and allows fine control of the  $\overline{Mn}$  of PMYR with no competitive degradation of the initiator.

Table 3.11: Polymerization of myrcene in microflow conditions at different temperatures.  $t_R=75s$

Entry	Temp (°C)	$\overline{Mn}$ (g/mol)		D	Yield (%) <sup>a</sup>	Conv. (%) <sup>b</sup>	$\overline{Mn}_{th}$ <sup>c</sup>
		<sup>1</sup> H NMR	GPC				
1	10	700	650	1.37	28	30	648
2	20	1100	1000	1.23	43	47	996
3	30	1350	1050	1.18	65	58	1505
4	40	1500	1200	1.19	73	65	1690
5	50	1350	1200	1.21	58	58	1343

<sup>a</sup> based on the mass of PMYR recovered after full removal of volatiles (including myrcene). <sup>b</sup> based on the  $\overline{Mn}({}^1\text{H NMR})/2316 \times 100$ . <sup>c</sup> Theoretical  $\overline{Mn} = \text{yield} \times 2316/100$

### 3.3.6 Microstructure

As depicted in Figure 3.1 and 3.6, the anionic polymerization of myrcene occurs through 3 possible addition reactions: 1,2 addition, 3,4 addition and 1,4-addition. Therefore, the PMYR obtained exhibit a microstructure with a statistical repartition of the 3 motifs stemming from these additions. The percentage of each motif can be determined by <sup>1</sup>H NMR analysis according to the specific chemical shifts of the corresponding vinyl H.<sup>10,11</sup>

The effect of the solvent on the microstructure has been highlighted in two distinct papers: Avila-Ortega reported that the reaction of myrcene in pure benzene with *s*-BuLi afforded 1,4 microstructure as major isomer (85%) while Hillmeyer and Hoyer described the 3,4 isomer as major product (60%) along with 1,4 (30%) and 1,2 (10%) adducts in THF with *s*-BuLi (1.4 M in hexanes).<sup>10,11</sup> An NMR comparison of the structures obtained herein under batch and flow conditions were also performed. In batch, it showed that the 3,4 isomer is the major adduct (57%) along with 1,4 (33%) and 1,2 isomers (10%). In flow, the proportion of the 3,4 isomer rises to 66% accompanied with 1,4 (22%) and 1,2 (12%). However, this is hardly assignable to the nature of the reactor, but rather to the proportion

of hexanes in the polymerization medium. Whereas, in batch, *n*-BuLi was used as provided (2.5 M in hexanes), the commercial solution was diluted to 0.3 M for practical reasons in the flow inlet. This results in a significant variation of the V/V percentage of hexanes in the reaction medium (hexanes/THF): 14% (batch) and 29% (flow) with obvious consequences on the reactivity and selectivity.<sup>14</sup> <sup>1</sup>H NMR of the resulting PMYR obtained in microflow reaction at 10°C is shown hereafter. Microstructure was determined and compared to PMYR obtained in batch conditions.

Table 3.12: Microstructure batch vs flow.

Entry	Conditions	V/V% Hexane	%1,2	%3,4	%1,4
1	BATCH (17 g)	14	10	57	33
2	FLOW	29	12	66	22

As expected, since hexane/THF mixture were similar (Table 3.12), continuous flow did not affect *in se* polymyrcene microstructure since solvent properties mainly govern it.<sup>15</sup>

### 3.3.7 Space-time yield and parallelization

Continuous flow chemistry allows direct calculation of space-time yield. Simply knowing the quantity in grams obtained, the volume of the reactor used, and the collection time of the samples, a simple yield calculation can be made. The calculation corresponds to the following Equation 3.4.

$$\text{Space - time yield} = \frac{\text{Productivity} \left( \frac{\text{kg}}{\text{h}} \right)}{\text{Volume of reactor (L)}} \quad \text{Equation 3.4}$$

For example, with a single monomer inlet, at a concentration of 2 M, *n*-BuLi at a concentration of 0.3 M, and using an 8-meter-long reactor, ID 0.75 mm, and a flow rate of myrcene/*n*-BuLi (mL/min): 0.25/0.1, we will have a productivity of 68 mg/min of myrcene for a reactor volume of 3.53 mL. For a 90 % conversion, space-time yield is then 1.04 kg/L/h.

### 3.3.8 Kinetic modeling of myrcene polymerization in continuous flow

To the best of our knowledges, only kinetics modeling of myrcene polymerization in batch has been performed. Table 3.13 is a comparison of kinetics values found in the literature for polyisoprene, polybutadiene, and polymyrcene. In 2008, Benvenuta Tapia reported isoprene polymerization in diethyl ether at 20 °C and 1,3-butadiene polymerization at 0 °C<sup>1617</sup>. Gonzalez-Villa *et al.* performed the study of anionic myrcene polymerization in batch conditions in 2019.<sup>1</sup> This study was carried out in cyclohexane initiated by *n*-butyllithium at different temperatures (55, 63, and 71 °C). In this study, at 55 °C a propagation constant of  $k_p = 1.24 \text{ L/mol/min}$  was evaluated.

Table 3.13: Comparison of kinetic values found for different polymers.

Monomer	Initiator	Solvent	Reaction Temp. (°C)	$k_p$ (L/(mol*s))	$E_a$ (kJ/mol)
Isoprene	<i>n</i> -BuLi	Diethyl ether	20	0.003	66.1
1,3 Butadiene	<i>s</i> -BuLi	Cyclohexane	0	0.002	89.6
β-Myrcene	<i>n</i> -BuLi	Cyclohexane	55	0.02	85.5

Non-ideal mixing conditions could occur in batch conditions, decreasing the accuracy of kinetic constant evaluation. To overcome such issue, microfluidic conditions were used to estimate kinetic constants for myrcene polymerization.

The reaction rates of step 1 and 2 were expressed as (Equation 3.5,3.6):

$$\text{Reaction 1: } R_1 = k_1[nBuLi][myrcene] \quad \text{Equation 3.5}$$

$$\text{Reaction 2: } R_2 = k_2[Intermediate][myrcene] \quad \text{Equation 3.6}$$

We assumed a plug flow model for the continuous reactor. The material balances are expressed as (Equation 3.7):

$$\frac{\partial C_i}{\partial \tau} = r_i \quad \text{Equation 3.7}$$

By using this equation, the four ODEs used for this work are (Equation 3.8,9,10 and 11):

$$\frac{\partial [M]}{\partial \tau} = -R_1 - R_2 \quad \text{Equation 3.8}$$



$$\frac{\partial[Int]}{\partial\tau} = R_1 - R_2 \quad \text{Equation 3.9}$$

$$\frac{\partial[Dim]}{\partial\tau} = +R_2 \quad \text{Equation 3.10}$$

$$\frac{\partial[nBuLi]}{\partial\tau} = -R_1 \quad \text{Equation 3.11}$$

Where:

$C_i$  = initial concentration

$\tau$  = residence time

[myrcene] = [M]

[Dim] = [Dimer]

[Int] = [Intermediate]

The kinetic modeling was performed in ModEst software; ODEs were solved by ODESSA solver.<sup>18,19</sup> Myrcene concentration was used as an observable. The objective function was defined as  $OF = ([M]_{\text{experimental}} - [M]_{\text{simulation}})^2$ . The minimization of the objective function was done by the simplex and Levenberg-Marquardt algorithm.<sup>20</sup>

The estimated kinetic constants:  $k_1(T)$ ,  $k_1(T_{ref})$ ,  $k_2(T)$ ,  $k_2(T_{ref})$ , and a modified Arrhenius equation was expressed as follows:

$$k_1(T) = A_1 * e^{\left(\frac{-E_{a1}}{RT}\right)} \quad \text{Equation 3.12}$$

$$k_1(T_{ref}) = A_2 * e^{\left(\frac{-E_{a1}}{RT_{ref}}\right)} \quad \text{Equation 3.13}$$

$T$  is the absolute temperature (Kelvin)

$T_{ref}$  reference temperature (Kelvin)

$$\frac{k_1(T)}{k_1(T_{ref})} = \frac{A_1}{A_2} * e^{\left[\frac{-E_{a1}}{R}\left(\frac{1}{T} - \frac{1}{T_{ref}}\right)\right]} \quad \text{Equation 3.14}$$

$A$  is the pre-exponential factor (unitless)

$k$  is the rate constant (frequency of collisions leading to a reaction) (L/(mol\*s)).

$R$  is the universal gas constant (L \*atm / K\* mol)

$E_a$  is the reaction's activation energy (kJ/mol)

Equation 3.15 and Equation 3.16 are modified Arrhenius equation, so  $a_1=a_2$ .

$$k_1(T) = k_1(T_{ref}) * e^{\left[\frac{-E_{a1}}{R}\left(\frac{1}{T} - \frac{1}{T_{ref}}\right)\right]} \quad \text{Equation 3.15}$$

$$k_2(T) = k_2(T_{ref}) * e^{\left[\frac{-E_{a1}}{R}\left(\frac{1}{T} - \frac{1}{T_{ref}}\right)\right]} \quad \text{Equation 3.16}$$

From Table 3.14, one can notice that the credible interval for  $k_1$  is quite large, which could be explained by the fact that we do not measure the initiator's intermediate concentration.

Table 3.14: Estimated kinetic constants and statistical data.

Parameters estimated at 15 ° C	Values	Credible interval	Credible interval in %
$k_1$ (Tref :15°C) (L/mol/s)	0.14	+/- 0.14	97.50
$E_{a1}$ (J/mol)	0	-	-
$k_p$ (Tref :15°C) (L/mol/s)	0.08	+/- 0.01	9.10
$E_{ap}$ (J/mol)	48700.00	+/- 7760.0	15.90

From the preliminary modeling, it seems that the rate constant  $k_1$  was temperature independent, for that reason we put  $E_{a1}=0$  J/mol. It seems to be logical since to anionic polymerization the initiation in THF could be faster than propagation ( $k_I > k_p$ ).<sup>21 22</sup>

The credible intervals for the other kinetic constants are narrow, meaning that the parameters are well identified.

The correlation matrix (Table 3.15) shows that the correlations are negligible in this case. According to Toch *et al.*,<sup>23</sup> two parameters are correlated if their binary correlation coefficient is higher than 0.95.

Table 3.15: Parameter correlation matrix.

Parameters	k1 (L/mol/s)	kp (L/mol/s)	Eap (J/mol)
k1 (L/mol/s)	1.00	0.00	0.0
kp (L/mol/s)	-0.84	1.00	0.0
Eap (J/mol)	-0.49	0.49	1.0

Globally, and Figure 3.13 show that the model can fit the experimental concentration of myrcene.

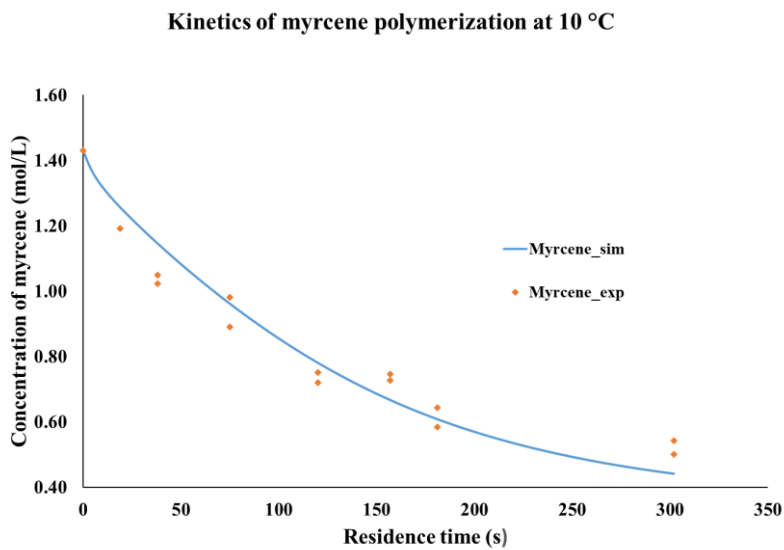


Figure 3.12: Simulation vs experimental trend of concentration vs residence time at 10 °C.

Kinetics of myrcene polymerization at 20°C

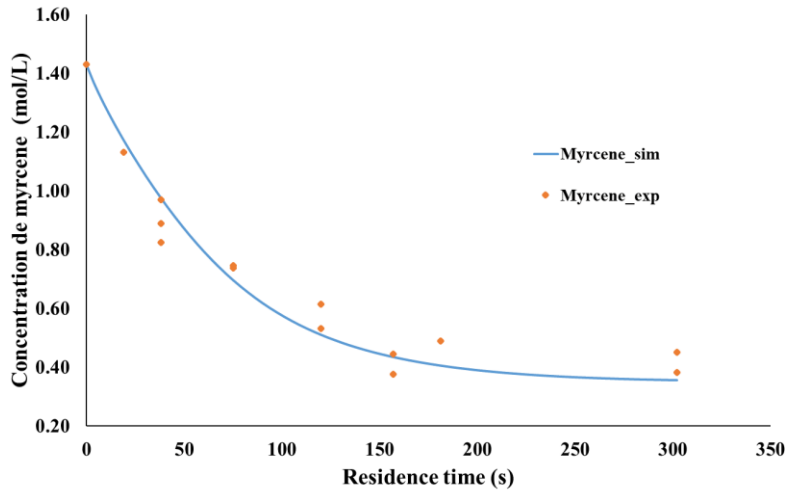


Figure 3.13 Simulation vs experimental trend of concentration vs residence time at 20 °C.

Figure 3.14 (parity plot) shows that the model can predict the experimental concentrations.

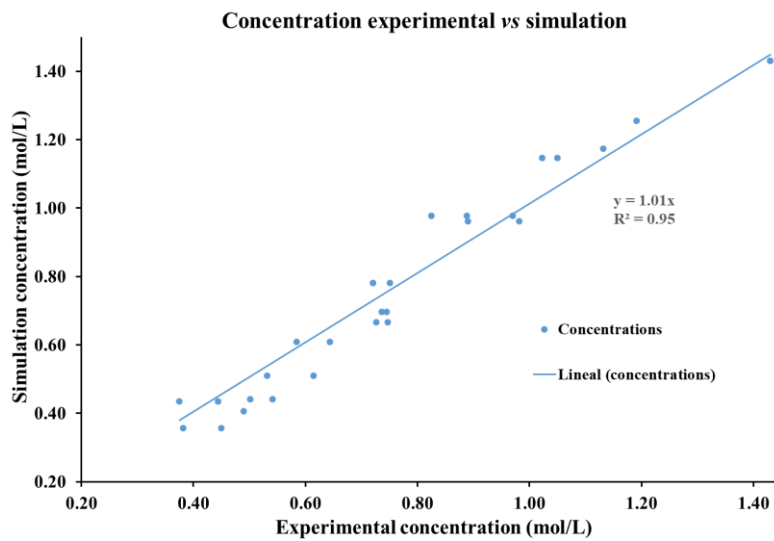


Figure 3.14: Experimental concentration vs simulation concentration of myrcene (10 and 20 °C).

If we return to the literature's results (Table 3.16), we find that the values are in the same order of magnitude. This is a fact that ensures the reliability of the values obtained.

Table 3.16 Comparison between kinetics values of myrcene's polymerization at different conditions.

<b>Monomer</b>	<b>Initiator</b>	<b>Solvent</b>	<b>Reaction Temp. (°C)</b>	<b><math>k_p</math> (L/(mol*s))</b>	<b><math>E_a</math> (kJ/mol)</b>
$\beta$ -Myrcene	n-BuLi	Cyclohexane	55	0.02	85,5
		THF	15	0.08	48,7

### 3.4 Conclusions

In this chapter anionic polymerization of myrcene was conducted in THF using *n*-BuLi at 10°C in batch conditions and using flow chemistry.

Polymerization of myrcene is an exothermic reaction. As a consequence, in batch conditions the reaction is affected by the scale/quantity used, and decomposition of THF via reverse (3+2) cycloaddition may occur, while in microfluidic conditions polymerization was finely controlled. In this case, molecular weight was directly linked to the residence time  $t^R$  and a living polymerization was observed.

Microfluidic conditions did not have a major effect on microstructure. The latter was mainly governed by solvent composition.

A kinetic model assuming a very rapid initiation step was developed and could fit very well experimental data.

### 3.5 Bibliography

- (1) González-Villa, J.; Saldívar-Guerra, E.; León-Gómez, R. E. D.; López González, H. R.; Infante-Martínez, J. R. Kinetics of the Anionic Homopolymerizations of  $\beta$ -Myrcene and 4-Methylstyrene in Cyclohexane Initiated by *n*-Butyllithium. *J. Polym. Sci. Part A: Polym. Chem.* **2019**, *57* (21), 2157–2165. <https://doi.org/10.1002/pola.29487>.
- (2) Banda-Villanueva, A.; González-Zapata, J. L.; Martínez-Cartagena, M. E.; Magaña, I.; Córdova, T.; López, R.; Valencia, L.; Medina, S. G.; Rodríguez, A. M.; Soriano, F.; Díaz de León, R. Synthesis and Vulcanization of Polymyrcene and Polyfarnesene Bio-Based Rubbers: Influence of the Chemical Structure over the Vulcanization Process and Mechanical Properties. *Polymers* **2022**, *14* (7), 1406. <https://doi.org/10.3390/polym14071406>.
- (3) Flory, P. J. *Principles of Polymer Chemistry*; Cornell university press, 1953.
- (4) Fontanille, M. G., Y. *Chimie et Physico-Chimie Des Polymères*; Dunod, 2014.
- (5) Ebdon, J. R. Terminally Reactive Oligomers: Telechelic Oligomers and Macromers. In *New Methods of Polymer Synthesis*; Ebdon, J. R., Ed.; Springer US: Boston, MA, 1991; pp 162–196. [https://doi.org/10.1007/978-1-4684-1530-8\\_6](https://doi.org/10.1007/978-1-4684-1530-8_6).
- (6) Quirk, R. P.; Huang, T.-L. Alkylolithium-Initiated Polymerization of Myrcene New Block Copolymers of Styrene and Myrcene. In *New Monomers and Polymers*; Culbertson, B. M., Pittman, C. U., Eds.; Springer US: Boston, MA, 1984; pp 329–355. [https://doi.org/10.1007/978-1-4684-4619-7\\_19](https://doi.org/10.1007/978-1-4684-4619-7_19).
- (7) Stanetty, P.; Mihovilovic, M. D. Half-Lives of Organolithium Reagents in Common Ethereal Solvents. *J. Org. Chem.* **1997**, *62* (5), 1514–1515. <https://doi.org/10.1021/jo961701a>.
- (8) Clayden, J.; Yasin, S. A. Pathways for Decomposition of THF by Organolithiums: The Role of HMPA. *New J. Chem.* **2002**, *26* (2), 191–192. <https://doi.org/10.1039/b109604d>.
- (9) Wahlen, C.; Rauschenbach, M.; Blankenburg, J.; Kersten, E.; Ender, C. P.; Frey, H. Myrcenol-Based Monomer for Carbanionic Polymerization: Functional Copolymers with Myrcene and Bio-Based Graft Copolymers. *Macromolecules* **2020**, *53* (20), 9008–9017.
- (10) Ávila-Ortega, A.; Aguilar-Vega, M.; Loría Bastarrachea, M. I.; Carrera-Figueiras, C.; Campos-Covarrubias, M. Anionic Synthesis of Amine  $\omega$ -Terminated  $\beta$ -Myrcene Polymers. *J Polym Res* **2015**, *22* (11), 226. <https://doi.org/10.1007/s10965-015-0856-6>.
- (11) Bolton, J. M.; Hillmyer, M. A.; Hoye, T. R. Sustainable Thermoplastic Elastomers from Terpene-Derived Monomers. *ACS Macro Lett.* **2014**, *3* (8), 717–720. <https://doi.org/10.1021/mz500339h>.
- (12) Pérez, K.; Picard, B.; Vuluga, D.; Burel, F.; Hreiz, R.; Falk, L.; Commenge, J.-M.; Nagaki, A.; Yoshida, J.; Chataigner, I.; Maddaluno, J.; Legros, J. Bromine–Lithium Exchange on a Gem -Dibromoalkene, Part 2: Comparative Performance of Flow Micromixers. *Org. Process Res. Dev.* **2020**, *24* (5), 787–791. <https://doi.org/10.1021/acs.oprd.0c00203>.

- (13) Picard, B.; Pérez, K.; Lebleu, T.; Vuluga, D.; Burel, F.; Harrowven, D. C.; Chataigner, I.; Maddaluno, J.; Legros, J. Bromine-Lithium Exchange on Gem-Dibromoalkenes Part 1: Batch vs Microflow Conditions. *J Flow Chem* **2020**, *10* (1), 139–143. <https://doi.org/10.1007/s41981-019-00057-6>.
- (14) Zhang, J.; Aydogan, C.; Patias, G.; Smith, T.; Al-Shok, L.; Liu, H.; Eissa, A. M.; Haddleton, D. M. Polymerization of Myrcene in Both Conventional and Renewable Solvents: Postpolymerization Modification via Regioselective Photoinduced Thiol–Ene Chemistry for Use as Carbon Renewable Dispersants. *ACS Sustainable Chem. Eng.* **2022**, *10* (29), 9654–9664. <https://doi.org/10.1021/acssuschemeng.2c03755>.
- (15) Bolton, J. M.; Hillmyer, M. A.; Hoye, T. R. Sustainable Thermoplastic Elastomers from Terpene-Derived Monomers. *ACS Macro Lett.* **2014**, *3* (8), 717–720. <https://doi.org/10.1021/mz500339h>.
- (16) Sinn, H.; Bandermann, F. The Kinetics of the Polyisoprene Formation Initiated with Lithium Organyl: POLYISOPRENE FORMATION. *J. polym. sci., C Polym. symp.* **1967**, *16* (8), 4515–4522. <https://doi.org/10.1002/polc.5070160828>.
- (17) Tapia, J. J. B.; López, J. A. T.; Nájera, R. H. Kinetics of the Anionic Polymerization of 1,3-Butadiene Using an Initiator Composed of Alkyl Aluminium, n-Butyllithium and Barium Alkoxide to Produce High Trans-1,4-Polybutadiene. *Macromolecular Reaction Engineering* **2008**, *2* (3), 222–232. <https://doi.org/10.1002/mren.200700048>.
- (18) Yang, X.; Wang, C.; Li, S.; Huang, K.; Li, M.; Mao, W.; Cao, S.; Xia, J. Study on the Synthesis of Bio-Based Epoxy Curing Agent Derived from Myrcene and Castor Oil and the Properties of the Cured Products. *RSC Adv.* **2017**, *7* (1), 238–247. <https://doi.org/10.1039/C6RA24818G>.
- (19) Leveneur, S.; Pinchard, M.; Rimbault, A.; Safdari Shadloo, M.; Meyer, T. Parameters Affecting Thermal Risk through a Kinetic Model under Adiabatic Condition: Application to Liquid-Liquid Reaction System. *Thermochimica Acta* **2018**, *666*, 10–17. <https://doi.org/10.1016/j.tca.2018.05.024>.
- (20) Marquardt, D. W. (1963). An Algorithm for Least-Squares Estimation of Nonlinear Parameters. *Journal of the Society for Industrial and Applied Mathematics*, *11*(2), 431–441. <http://www.jstor.org/stable/2098941>.
- (21) Morton, M. *Anionic Polymerization: Principles and Practice*; Academic Press: New York, 1983.
- (22) Hsieh, H.; Quirk, R. P. *Anionic Polymerization: Principles and Practical Applications*; CRC Press, 1996.
- (23) Toch, K.; Thybaut, J. W.; Marin, G. B. A Systematic Methodology for Kinetic Modeling of Chemical Reactions Applied to *n*-Hexane Hydroisomerization. *AIChE J.* **2015**, *61* (3), 880–892. <https://doi.org/10.1002/aic.14680>.
- (24) Tonhauser, C.; Frey, H. A Road Less Traveled to Functional Polymers: Epoxide Termination in Living Carbanionic Polymer Synthesis. *Macromol. Rapid Commun.* **2010**, *31* (22), 1938–1947. <https://doi.org/10.1002/marc.201000353>.

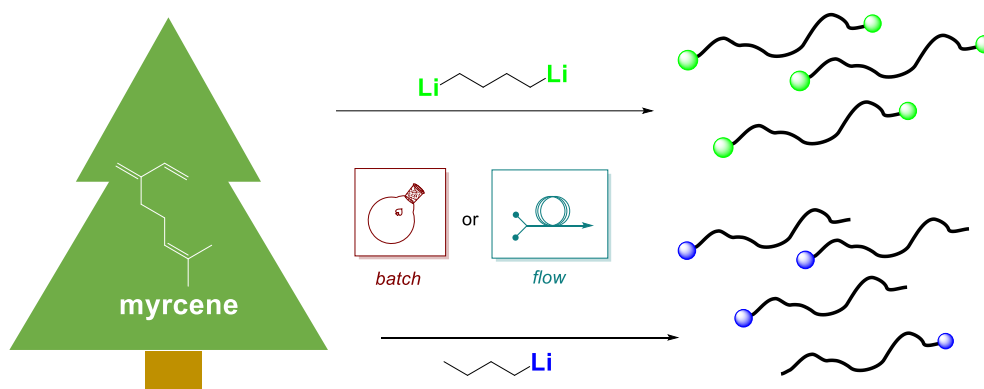
- (25) Quirk, R. P.; Ma, J.-J. Characterization of the Functionalization Reaction Product of Poly(Styryl)Lithium with Ethylene Oxide. *J. Polym. Sci. A Polym. Chem.* **1988**, *26* (8), 2031–2037. <https://doi.org/10.1002/pola.1988.080260804>.
- (26) Takahashi, Y.; Nagaki, A. Anionic Polymerization Using Flow Microreactors. *Molecules* **2019**, *24* (8), 1532. <https://doi.org/10.3390/molecules24081532>.
- (27) Takahashi, Y.; Nagaki, A. Anionic Polymerization Using Flow Microreactors. *Molecules* **2019**, *24* (8), 1532. <https://doi.org/10.3390/molecules24081532>.
- (28) Ueda, K.; Hirao, A.; Nakahama, S. Synthesis of Polymers with Amino End Groups. 3. Reactions of Anionic Living Polymers with  $\alpha$ -Halo- $\iota$ -Aminoalkanes with a Protected Amino Functionality. *Macromolecules* **1990**, *23* (4), 939–945. <https://doi.org/10.1021/ma00206a006>.
- (29) Kim, J.; Lee, M.; Ryu, C.-Y.; Lee, J.; Hwang, S. S.; Park, T. S.; Kim, K. U.; Yoon, H. S.; Ahn, B. I.; Char, K. Synthesis of Dilithium  $\alpha$ ,  $\omega$ -Disulfonated Polystyrene by Anionic Polymerization. *Polymer journal* **1994**, *26* (10), 1111–1117.
- (30) Quirk, R. P.; Yin, J. Carbonation of Polymeric Organolithium Compounds: Effects of Chain End Structure. *J. Polym. Sci. A Polym. Chem.* **1992**, *30* (11), 2349–2355. <https://doi.org/10.1002/pola.1992.080301108>.
- (31) Quirk, R. P.; Yin, J.; Fetters, L. J. Carbonation and Related Reactions of Poly (Styryl) Lithium. *Macromolecules* **1989**, *22* (1), 85–90.
- (32) Schulz, D. N.; Halasa, A. F. Anionic Polymerization Initiators Containing Protected Functional Groups. II. *Journal of Polymer Science: Polymer Chemistry Edition* **1977**, *15* (10), 2401–2410.
- (33) Georges, S.; Hashmi, O. H.; Bria, M.; Zinck, P.; Champouret, Y.; Visseaux, M. Efficient One-Pot Synthesis of End-Functionalized Trans-Stereoregular Polydiene Macromonomers. *Macromolecules* **2019**, *52* (3), 1210–1219.
- (34) Ruiz Martínez, E.; Sánchez Hervás, J. M. Chemical Valorization of CO<sub>2</sub>. In *Carbon Dioxide Utilization to Sustainable Energy and Fuels*; Inamuddin, Boddula, R., Ahamed, M. I., Khan, A., Eds.; Springer International Publishing: Cham, 2022; pp 1–30. [https://doi.org/10.1007/978-3-030-72877-9\\_1](https://doi.org/10.1007/978-3-030-72877-9_1).
- (35) SciencesRoundtable, N. R. C. (US) C. *Carbon Dioxide as a Feedstock*; National Academies Press (US), 2001.
- (36) Seo, H.; Nguyen, L. V.; Jamison, T. F. Using Carbon Dioxide as a Building Block in Continuous Flow Synthesis. *Advanced Synthesis & Catalysis* **2019**, *361* (2), 247–264.
- (37) Nagaki, A.; Takahashi, Y.; Yoshida, J. Extremely Fast Gas/Liquid Reactions in Flow Microreactors: Carboxylation of Short-Lived Organolithiums. *Chem. Eur. J.* **2014**, *20* (26), 7931–7934. <https://doi.org/10.1002/chem.201402520>.
- (38) Wu, J.; Yang, X.; He, Z.; Mao, X.; Hatton, T. A.; Jamison, T. F. Continuous Flow Synthesis of Ketones from Carbon Dioxide and Organolithium or Grignard Reagents. *Angew. Chem. Int. Ed.* **2014**, *53* (32), 8416–8420. <https://doi.org/10.1002/anie.201405014>.
- (39) Nagaki, A.; Takahashi, Y.; Yoshida, J. Extremely Fast Gas/Liquid Reactions in Flow Microreactors: Carboxylation of Short-Lived Organolithiums. *Chemistry – A European Journal* **2014**, *20* (26), 7931–7934. <https://doi.org/10.1002/chem.201402520>.



- (40) Monbaliu, J.-C. M.; Legros, J. Will the next Generation of Chemical Plants Be in Miniaturized Flow Reactors? *Lab Chip* **2022**. <https://doi.org/10.1039/D2LC00796G>.
- (41) Cawse, J. L.; Stanford, J. L.; Still, R. H. Polymers from Renewable Sources: 5. Myrcene-Based Polyols as Rubber-Toughening Agents in Glassy Polyurethanes. *Polymer* **1987**, *28* (3), 368–374.
- (42) Negishi, E.; Swanson, D. R.; Rousset, C. J. Clean and Convenient Procedure for Converting Primary Alkyl Iodides and .Alpha.,.Omega.-Diodoalkanes into the Corresponding Alkylolithium Derivatives by Treatment with Tert-Butyllithium. *J. Org. Chem.* **1990**, *55* (19), 5406–5409. <https://doi.org/10.1021/jo00306a022>.

# Chapter 4

## End-functionalization and Telechelic polymyrcene in a continuous flow system



## 4.1 Introduction

There are two main ways to introduce functionalities at one end of a polymer chain. Either, a chain-end functionalization achieved through a post-polymerization reaction of the living anionic chain-end with desired functional electrophilic species or, by using a protected functionalized initiator.

### Post-polymerization

Many functionalities may be introduced by the selected termination of living polymers. For example, hydroxyl-terminated polymers can be obtained by reaction with the highly toxic ethylene oxide (Figure 4.1).

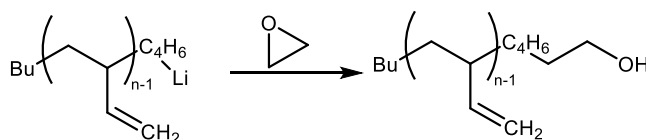


Figure 4.1: Synthesis of hydroxyl-terminated polyisoprene.<sup>24,25</sup>

It is also possible to introduce multiple OH groups by acetal-protected functional epoxides followed by acidic hydrolysis as demonstrated by Löwe, H., & Frey, H. *et al.* after an anionic polymerization of styrene at room temperature in flow reactor (Figure 4.2).<sup>26</sup>

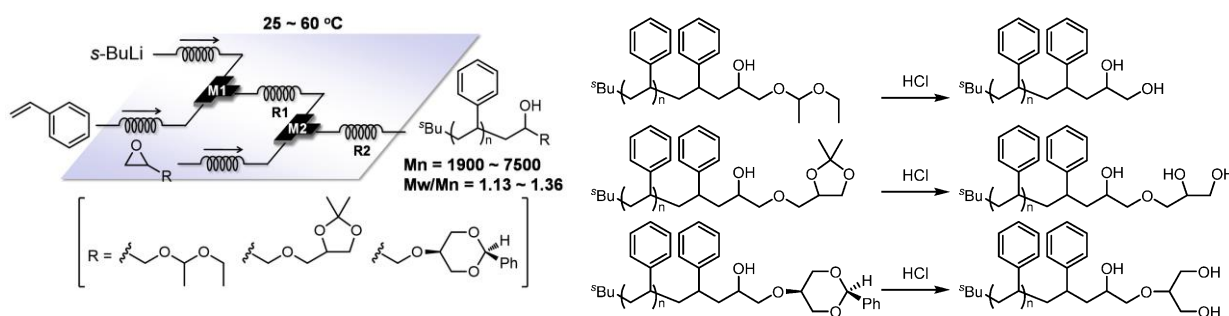


Figure 4.2: Poly hydroxyl-terminated polystyrene (excerpt from Takahashi, Y.; Nagaki, A. *Anionic Polymerization Using Flow Microreactors. Molecules* **2019**, *24* (8), 1532. <https://doi.org/10.3390/molecules24081532>).<sup>27</sup>

An amino group can be added through protected  $\alpha$ -halo- $\omega$ -aminoalkanes (Figure 4.3).<sup>28</sup>

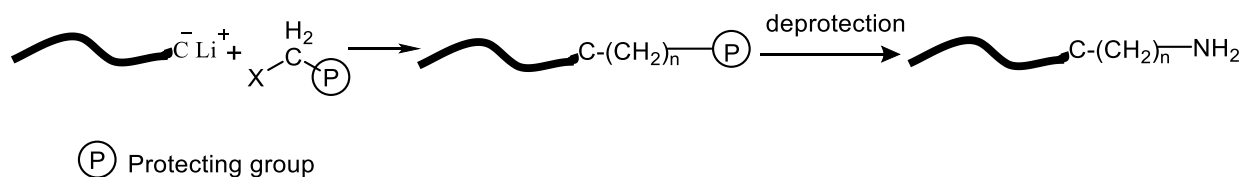


Figure 4.3: Functionalization of dienes with  $\alpha$ -halo- $\omega$ -aminoalkanes

Sulfonate end-capped polymers have been synthesized through the reaction of polymeric organolithium compounds directly with sultones (Figure 4.4).

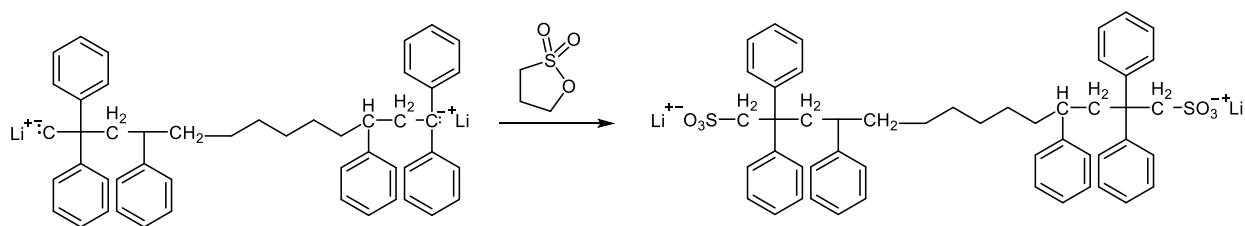


Figure 4.4: Synthesis of Sulfonate end-capped polymers.<sup>29</sup>

A carboxylic acid group can be introduced by the addition of carbon dioxide to the living polymer solution (Figure 4.5).<sup>30,31</sup> Quirk *et al.* showed carbonation in benzene at room temperature of polyisoprenyl lithium, and polystyrene lithium was possible. However, the carboxylic compound was systematically contaminated by the formation of a dimeric ketone and a trimeric alcohol.

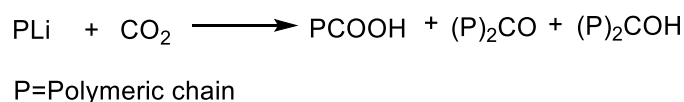


Figure 4.5: Addition of a carboxylic acid group to polymers with  $\text{CO}_2$ .

### Use of functionalized initiators

Organolithium protected functionalized initiators, are also used to obtain end-functionalized polymers.<sup>32</sup> Two suitable compounds are listed below (Figure 4.6).

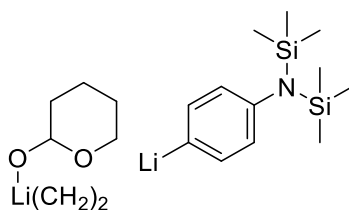


Figure 4.6: Protected functionalized initiator.

Even though quantitative functionalization is effective with a protected functionalized initiator, limited availability and limited solubility of the initiators, may impact on the practical application of this strategy.<sup>22</sup>

## Diene functionalization

To transform polydienes into reactive entities able to be integrated into the materials, it is necessary to introduce functional groups. Recent studies by Visseaux *et al.*, reported coordinative polymerization and the end-functionalization of isoprene, and myrcene by trapping benzophenone to introduce an alcohol moiety as a polar end-functionality (Figure 4.7).<sup>33</sup>

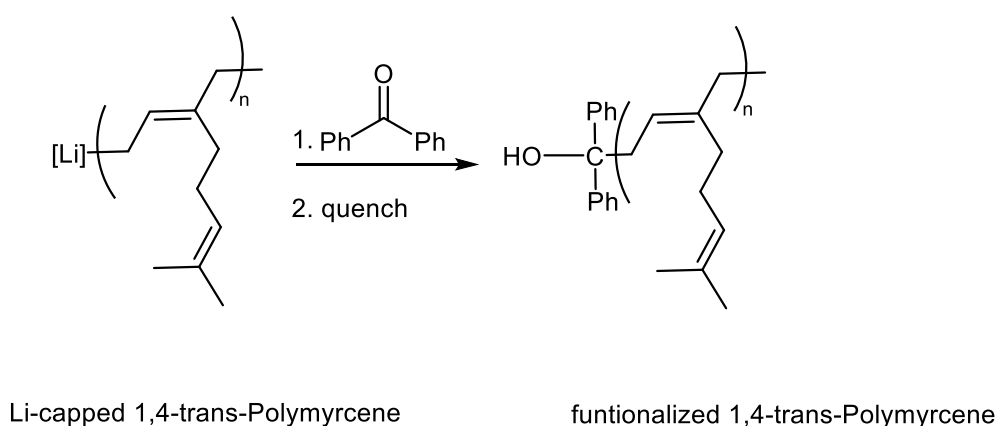


Figure 4.7: End-functionalization of polymyrcene by trapping benzophenone.

Visseaux' work shows that it is possible to obtain 97% of functional (FD%) polyisoprene and 65 to 83 % of functional polymyrcene after 24 to 72 hours of reaction in toluene at 50 °C (Table 4.1).<sup>33</sup>

Table 4.1: Stereoselective polymerization and functionalization of polymyrcene and isoprene at 50 °C by Visseaux *et al.*<sup>33</sup>

Monomer	Monomer (eq)	<i>n</i> -BuLi (eq)	Yield (%)	$\overline{M}_n$ (g/mol)	$\overline{D}$	1,4 <i>cis</i> / <i>trans</i>	3,4	FD (%)
Isoprene	50	20	>99	1000	-	96.7	3.3	97
Myrcene	200	-	82	22300	1.7	98.8	1.2	65
Myrcene	200	20	76	18800	1.5	98	2.0	83

<sup>a</sup>GPC analysis not performed.

According to flow results at 10 °C, in chapter 3, the number average molecular weight is a linear function of conversion (Figure 4.8). However, it was demonstrated that this is not a sufficient criterion to attest for living anionic polymerization.

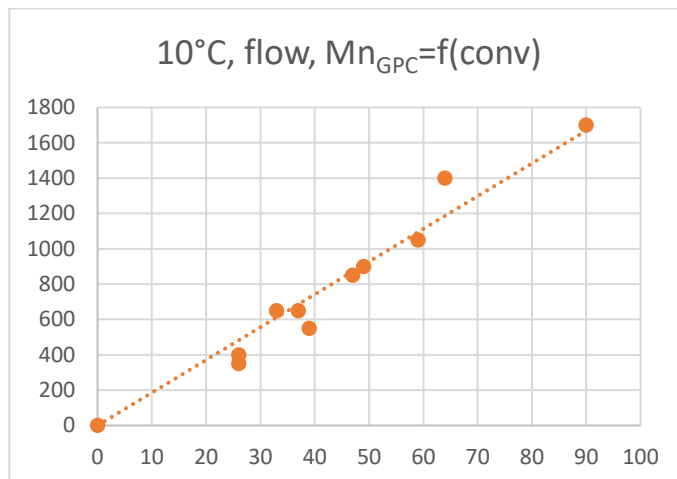


Figure 4.8: Results obtained in the anionic polymerization in flow conditions at 10 °C

On the other hand, controlled termination of living polymerization systems can, in principle, result in chain-end functionalized polymers. However, as a diagnostic test of perfect living polymerizations it may be also limited since the functionalization reactions need to be quantitative, which very often is not the case.

The objective of this chapter is thus to present the end-functionalization of polymyrcene with different endings in continuous flow reactors.

First, TMSCl was used as electrophile, to produce TMS endings. Then, CO<sub>2</sub> was used in the polymerization reaction to introduce carboxylic moieties. To evaluate the presence of the carboxylic function in polymyrcene, an esterification reaction was also performed. Glass transition temperature and solubility of different end-functionalized polymyrcene are also presented. Then, to extend this study, the use of 1,4 dilithium butane was evaluated, to have access to telechelic or bifunctional polymyrcene.

## 4.2 Living polymerization

As mentioned, the character of living polymerization is one of the advantages of an anionic polymerization. In order to confirm the living character of the polymerization, it was decided to trap a relevant group instead of a simple hydrogen atom. Indeed, whereas this

hydrogen should come from the methanol inlet, competitive processes could also occur (such as deprotonation of THF) and quench the polymerization in an early manner.

#### 4.2.1. Synthesis of polymyrcene TMS end-functionalized in flow conditions

By introducing an inlet of chlorotrimethylsilane at the end of the system before precipitation in acidic solution (HCl 2N), polymyrcene with a TMS end-group can be synthesized (Figure 4.9).

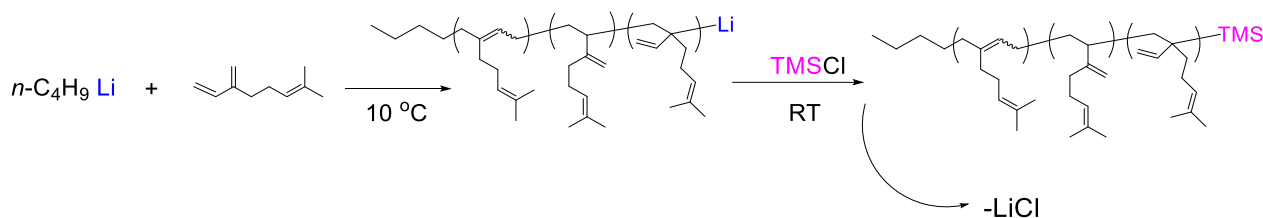


Figure 4.9: Functionalization of polymyrcene TMS-end group.

The quenched mixture is extracted with dichloromethane (3 x 10 mL), washed with water (20 mL), dried over magnesium sulfate, and concentrated under vacuum to afford a crude mixture, analyzed by mean of NMR. Figure 4.10 shows the experimental setup used in this case.

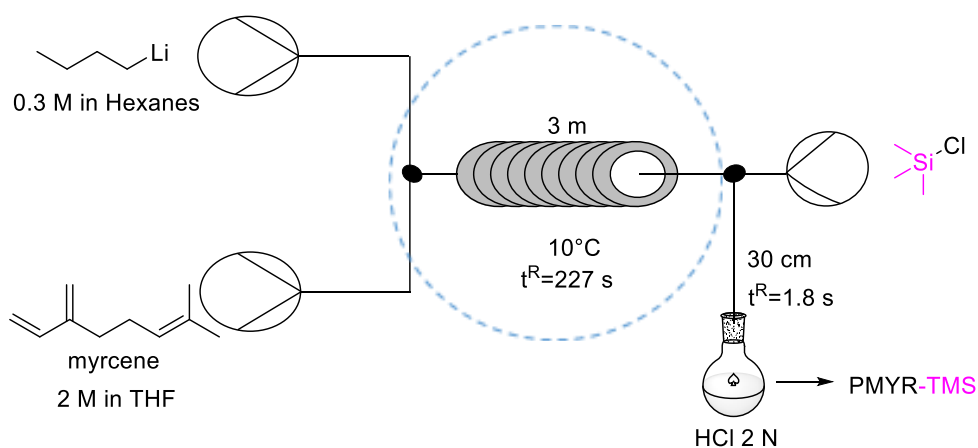


Figure 4.10: Experimental set up for TMS end-functionalization with mix THF/TMSCl.

A representative experiment was performed with  $t^R = 227\text{ s}$ , and the degree of functionalization was determined by  $^1\text{H}$  NMR analyses by comparing the  $(\text{CH}_3)_3$  groups from TMS with the  $\text{CH}_3$  group from the  $n\text{-Bu}$  initiator (Figure 4.10). A 73% degree of

functionalization was measured, showing thus the living character of this process. It should be noted that the incomplete functionalization of the polymer with the TMS group is much likely due to the traces of HCl in the TMSCl (injected neat).

The dispersity and molar mass values ( $\overline{M}_w/\overline{M}_n=1.9$ ,  $\overline{M}_n=1500$ ) remains reasonable as those obtained before (section 3.3.4). These results confirm the living polymerization of PMYR, resulting in a fashion method to obtain functional oligomer.

### 4.3 Telescoped anionic polymerization of myrcene/functionalization with CO<sub>2</sub> in a flow system

Nowadays, carbon dioxide is used in the production of functional molecules and polymers.<sup>34-35</sup> However, the methods to reuse CO<sub>2</sub> are still a challenge, since the two-phase reactions are difficult to carry out by conventional batch methods.<sup>36</sup>

Yoshida *et al.* reported a gas-liquid carboxylation reaction under batch and flow conditions (Figure 4.11). The carboxylation reaction was performed first under batch conditions, yielding 28% of desired product at 0 °C. In contrast, doing the same reaction in continuous flow, led to 87% of the desired carboxylic acid product at the same temperature.<sup>37</sup>

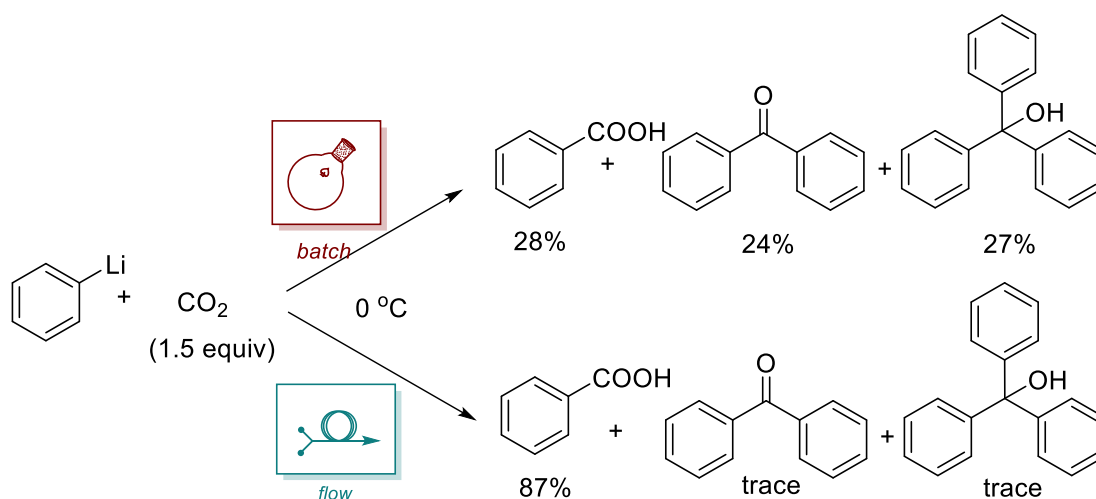


Figure 4.11: Reaction of phenyl-lithium with carbon dioxide.

These results are not surprising since continuous flow systems have been shown to be generally more efficient than conventional batch conditions for biphasic gas/liquid reactions, especially for the challenging trapping of 1H, which often suffers from



unselective consecutive competitive additions (carboxylic acid – ketone- tertiary alcohol). Thus, a flow reactor system fed with an organometallic reagent (R-Li or R-MgX) in a first inlet, and a CO<sub>2</sub> tank connected to a mass flow controller in a second inlet provided the selective mono-addition product R-CO<sub>2</sub>H without over-addition products, even without cryogenic conditions. Conversely, consecutive competitive over-addition occurred in batch reactors.<sup>38,39</sup>

Concatenated polymerization/CO<sub>2</sub>H functionalization in flow would be a mean to overcome all the drawbacks associated with the analogous batch synthesis: 1) as shown in chapter 3 the  $\overline{Mn}$  of PMYR can be finely tuned, 2) the higher interfacial contact between gas and liquid phases should enhance the selectivity of carboxylation.



Figure 4.12: Interphase in batch (left) vs continuous flow (right).

Moreover, it is possible to use stoichiometric amounts of CO<sub>2</sub> in flow, whereas it is generally much challenging under batch conditions. Using a mass flow controller (MFC) we become able to control the inlet of CO<sub>2</sub> and know the quantity dissolved. Thus, CO<sub>2</sub> was introduced in the previous flow set up (Figure 4.13:) implemented for the controlled anionic polymerization of myrcene with a third inlet linked to the CO<sub>2</sub> tank and controlled by mean of a mass flow controller (constant flow rate of 1.36 mL/min under 1 bar). The outlet was collected in an aqueous acidic solution.

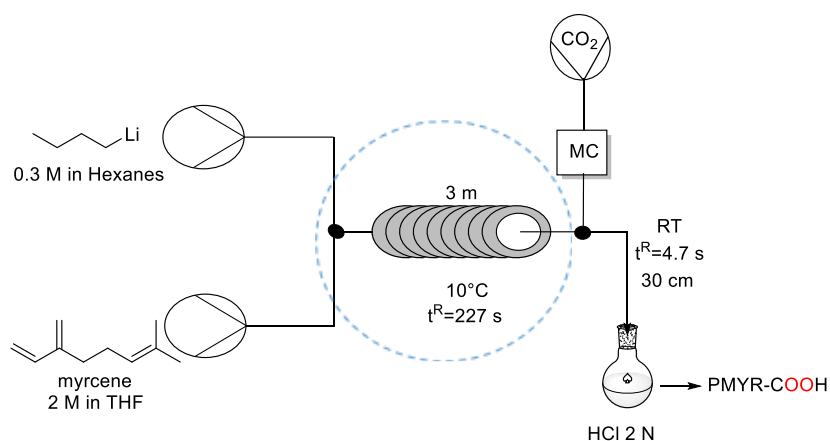


Figure 4.13: Set up of telescoped anionic polymerization of myrcene/functionalization with  $\text{CO}_2$  in a flow system (MFC = mass flow controller).

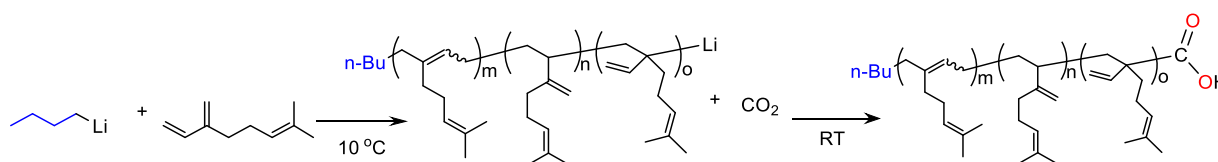


Figure 4.14: Synthesis of polymyrcene acid end-functionalized with  $\text{CO}_2$  in flow conditions.

Thus, after polymerization of myrcene in a stainless-steel flow microreactor (ID = 0.75 mm, L = 3 m) as described above [ $Q(\text{myrcene}) = 0.25 \text{ mL/min}$ ,  $Q(n\text{-BuLi}) = 0.1 \text{ mL/min}$ ,  $t^R = 227 \text{ s}$ ],  $\text{CO}_2$  was delivered in a further inlet (Reactor 2: ID = 0.75 mm, L = 30 cm). Delightfully, this telescoped process afforded the target PMYR terminated by a useful  $\text{CO}_2\text{H}$  functional moiety: PMYR- $\text{CO}_2\text{H}$  (Table 4.2, entries 3-5). Increasing the mass flow rate -and therefore increasing the number of equivalents of  $\text{CO}_2$  allowed to reach a functionalization degree  $\text{FD} = 95\%$  with 3 equiv. of gas with regard to  $n\text{-BuLi}$ .

Table 4.2: Experiments for the end-functionalization of PMYR with CO<sub>2</sub> at 10 °C.<sup>a</sup>

Entry	Conditions	<i>t</i> (s) <sup>b</sup>	Mass flow rate (mg/min)	Molar flow rate (mmol/min)	Molar ratio <i>n</i> - BuLi/CO <sub>2</sub>	$\overline{Mn}$ (g/mol)		<i>D</i>	Product	FD (%) <sup>c</sup>
						<sup>1</sup> H NMR	GPC			
1	batch	60	–	–	bubbled gas	1750	950	2.50	ketone	–
2	batch	120	–	–	bubbled gas	1800	1350	2.17	ketone	–
3	flow	7.6	1.32	0.03	1:1	1000	1200	1.58	acid	30
4	flow	4.6	2.64	0.06	1:2	1050	850	1.69	acid	64
5	flow	3.6	3.96	0.09	1:3	1415	1100	1.19	acid	95

<sup>a</sup> According to set-up described in Fig. 7. <sup>b</sup> Entries 1,2: bubbling time of CO<sub>2</sub> in the batch reactor; Entries 3-5: residence time in reactor 2 (*t*<sup>R2</sup>). <sup>c</sup> Functionalization degree (FD) calculated by <sup>1</sup>H NMR by comparing the relative intensity of CH(CO<sub>2</sub>H) ( $\delta = 3.05$  ppm) with the CH<sub>3</sub> group of butyl chain initiator of PMYR ( $\delta = 0.86$  ppm).

It is worth to note that a parallel experiment was conducted under batch conditions (Table 4.2, entries 1 and 2) which afforded a different result: a ketone connected to two PMYR moieties was obtained as major product as attested by <sup>13</sup>C NMR in which a signal at  $\delta = 207.19$  ppm (Figure 4.15), typical of a -C(=O)- moiety appeared (in contrast to  $\delta(\text{CO}_2) = 178.48$  and 177.89 ppm detected in the flow experiment (Figure 4.16)).

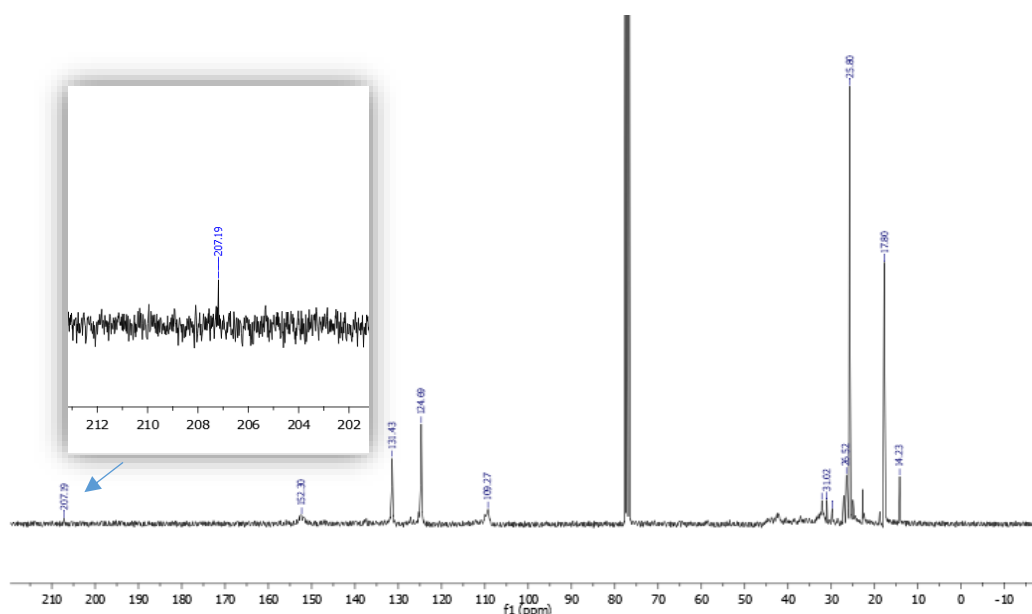


Figure 4.15: <sup>13</sup>C NMR (300 MHz, CDCl<sub>3</sub>) of polymyrcene ketone in batch at 10°C.

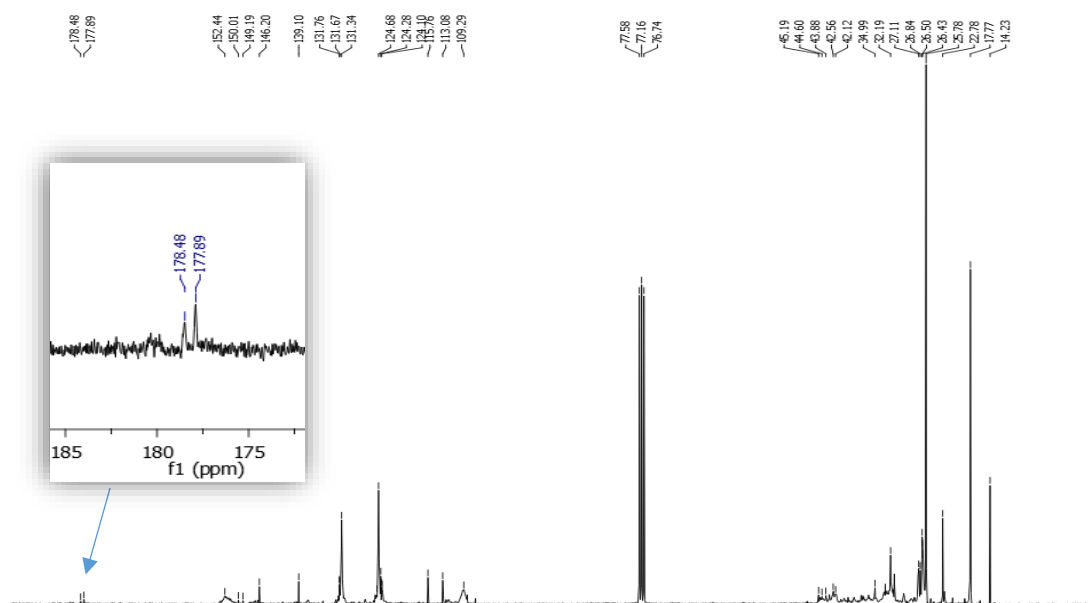


Figure 4.16:  $^{13}\text{C}$  NMR of polymyrce end-group acid, MF conditions: flow rate myrcene/ $n\text{-BuLi}/\text{CO}_2$  0.25:0.1:1.36 mL/min respectively at  $10^\circ\text{C}$ .

This difference of reactivity (confirming thus the previous observations by Yoshida and Jamison with small organometallics) is depicted in Figure 4.17, along with the corresponding reaction paths.

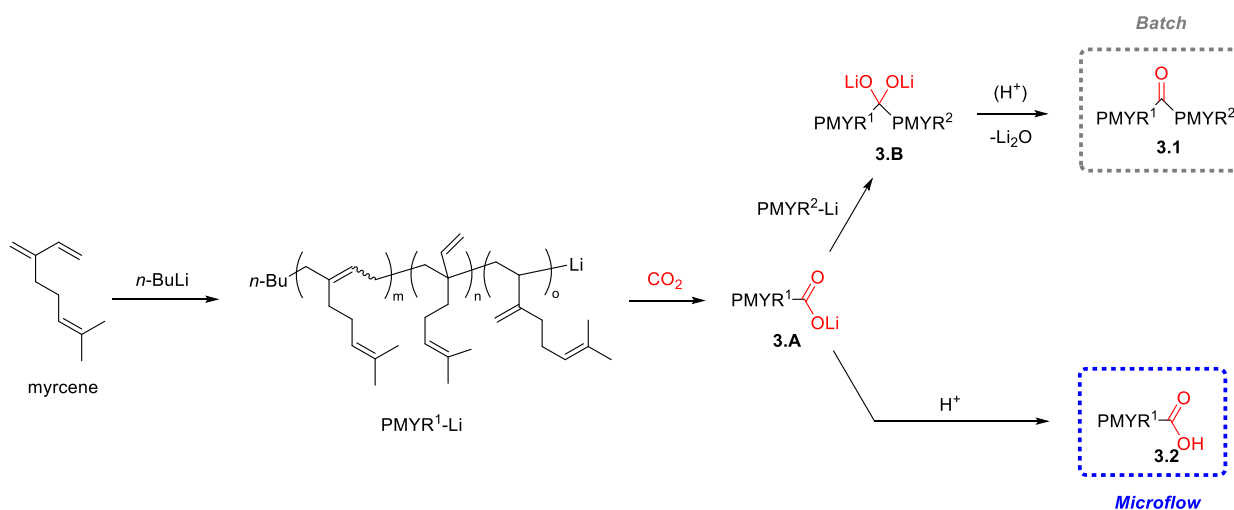


Figure 4.17: End-functionalization of PMYR: reactivity according to batch or flow conditions.

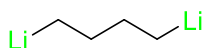
Thus, in any reactor, PMYR-Li adds onto  $\text{CO}_2$  to afford the intermediate **3.A**. Due to lower liquid/gas mass transfer in the batch reactor, there is, in this case, coexistence between PMYR-Li and **3.A** that can undergo a second addition to yield **3.B**. This latter, upon elimination of Lithium oxide ( $\text{Li}_2\text{O}$ ), provides the ketone  $(\text{PMYR})_2\text{C}=\text{O}$  **3.1**. Beside mixing

issues, a plausible explanation for this divergence of reactivity lies on a major dichotomy between batch and flow conditions: the composition of the reaction medium according to space and time.

In a batch reactor, the chemical composition of the reaction medium evolves with time as the conversion of reagents/substrates to products increases. In contrast, under flow conditions, the conversion increases along the reactor: thus, any point of the flow reactor corresponds to a specific state of the progress of the reaction, with -ideally- a completion at the outlet of the reactor. In our case, this major feature avoids reactions between PMYR-Li and the primary product A, and thus undesired competitive products, with high benefits for chemical selectivity toward PMYR-CO<sub>2</sub>H 3.2.<sup>40</sup>

#### 4.4 Telechelic polymyrcene

Feedstock-derived functional oligomers are attractive as molecular building blocks. Among polyterpene derivatives amine  $\omega$ -terminated  $\beta$ -myrcene polymers have been synthesized as well as hydroxytelechelic PMYR, these last being used as toughening agents.<sup>41</sup> Another application of bifunctionalized polymyrcene would be the synthesis of biobased polyurethane. To do this, it is necessary to develop methods to synthesize bifunctionalized polymers, called telechelic polymers. This kind of polymers has two reactive end-groups in  $\alpha$  and  $\omega$  positions. To obtain bifunctionalized polymyrcene our interest turns towards the challenging, and thus underexploited, 1,4 dilithiobutane as initiator (Figure 4.18).



Chemical Formula: C<sub>4</sub>H<sub>8</sub>Li<sub>2</sub>

Exact Mass: 70.09

Molecular Weight: 69.99

Figure 4.18: 1,4 dilithiobutane

With this initiator in hand, it becomes possible to afford symmetric oligomers of structure HO<sub>2</sub>C-PMYR-(CH<sub>2</sub>)<sub>4</sub>-PMYR-CO<sub>2</sub>H, which could then be used for further developments.

Similar to the polymerization with *n*-BuLi (chapter 3), the myrcene/Li(CH<sub>2</sub>)<sub>4</sub>Li chosen was  $\left(\frac{\text{monomer}}{\text{initiator}} : \frac{17}{1}\right)$ , which gives low molecular weights for the polymers (initiator standing for

reactive center). The theoretical molecular masses for polymyrcene were obtained through  $\overline{Mn}_{th} = 2316 \text{ g/mol}$

For the anionic polymerization of myrcene in batch, different conditions were used such as: temperature change, various organic solvents, different mass quantities of the monomer.

The polymerization reaction of myrcene was then passed to microflow conditions. Reactions with TMS and CO<sub>2</sub> as electrophiles were carried out.

#### 4.4.1 Initiator synthesis

All reactions were performed under very dry conditions and inert atmosphere to avoid any possible residue with traces of water, which was detrimental to the process, creating side reactions between lithiated species and water.

As said above, to get access to telechelic polymyrcene, 1,4-dilithiobutane was chosen as the initiator for the polymerization reaction. This product was prepared for every experiment according to the procedure used by Negishi *et al.*<sup>42</sup> The reaction is performed in batch under cryogenic conditions (-78 °C) (Figure 4.19).

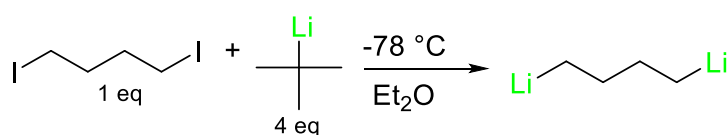


Figure 4.19: Transformation reaction of 1,4-diiodobutane into 1,4-dilithiobutane by treatment with *tert*-butyllithium

To remove the excess of *tert*-BuLi present in the medium, we took advantage of the fact that *tert*-BuLi is more sensitive to thermal degradation compared to 1,4-dilithiobutane. Thus, we followed the overall lithium base content along time at 20 °C by titration with menthol/2,2'-bipyridine.

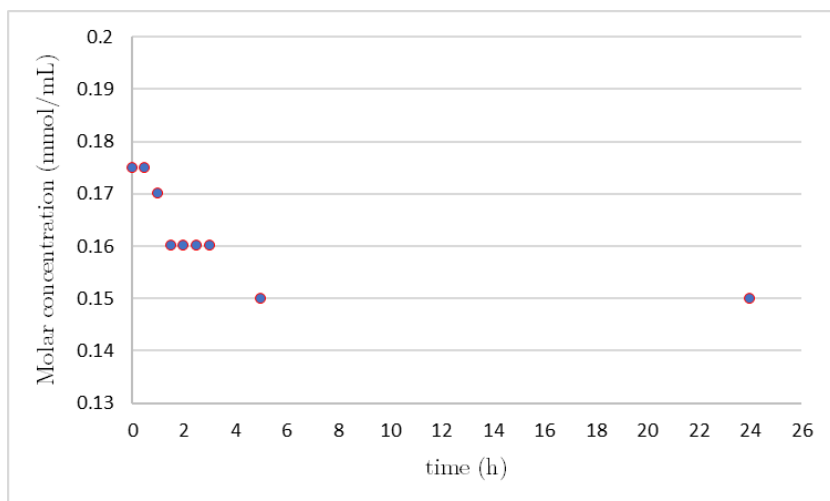


Figure 4.20: Degradation of *tert*-butyllithium and concentration of 1,4-dilithiobutane over time at 20°C.

In Figure 4.20, the degradation of *tert*-butyllithium residues is observed between 0-1h, from 1-1.5h a plateau is observed showing the ideal concentration of the product ([Li]=0.16 M). After 5 h the concentration was still 0.15 M. The product was then stored at -25 °C overnight and analyzed after 24 h. Result, demonstrated its stability over time when kept at low temperature and in the dark. This study helped us to obtain the optimal parameters for the synthesis of the 1,4-dilithiobutane initiator.

#### 4.4.2 Results for bifunctionalized polymycene with TMS ending under batch

The bifunctionalized initiator was introduced into the system to obtain telechelic polymycene. By quenching with TMSCl it is obtained a bifunctionalized polymycene, that can be used to characterize the microstructure of the final polymer (Figure 4.21).

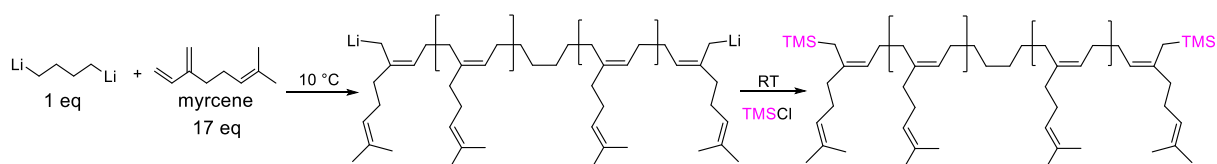


Figure 4.21: Anionic polymerization of polymycene bifunctionalized with TMS (for sake of clarity, the scheme was drawn starting with a 1,4-addition).

The conditions were settled in relation with the previous experience (Table 4.3).

Table 4.3: Molar concentration and number of equivalents of reagents for anionic polymerization of myrcene in batch.

Reagent	Concentration (mmol/mL)	Eq. (mmol)
Myrcene	2	17
1,4-DiLi	0.16	1
TMScI	pure	3

#### 4.4.3 Effects of different variables on the polymer

In this study different variables were modified to see their influence in the final molecular mass of the polymer. The parameters studied were the temperature, the mass quantity, and the solvent.

##### Temperature effect

For the experiment different temperature conditions were tried to arrive to the best possible control of the molecular mass. Temperatures under 20°C were the best suited for the reaction to avoid rapid degradation of the alkyllithium compound. Tetrahydrofuran was used as solvent for the reaction.

Table 4.4: Temperature effect on the polymerization of myrcene in batch. (1 g Myrcene).

No	Temp (°C)	Time (h)	$\overline{Mn}$ NMR (g/mol)	$\overline{Mn}$ GPC (g/mol)	Đ
1 <sup>a</sup>	-78°C	24	-	-	-
2 <sup>a</sup>	0°C	5	-	-	-
3	10°C	1.5	4070	1530	3.3

<sup>a</sup>No data of GPC analysis.

No polymerization of myrcene was observed for temperatures below 10 °C (Table 4.4), even when the time was increased. At 10°C the conversion was total but, high values of molecular weight <sup>1</sup>H NMR and Đ were observed.

#### 4.4.4 Results for bifunctionalized polymyrcene with TMS ending under flow conditions

We have optimized the continuous flow polymerization reactions by using an assembly similar to the previous one (Figure 4.22).



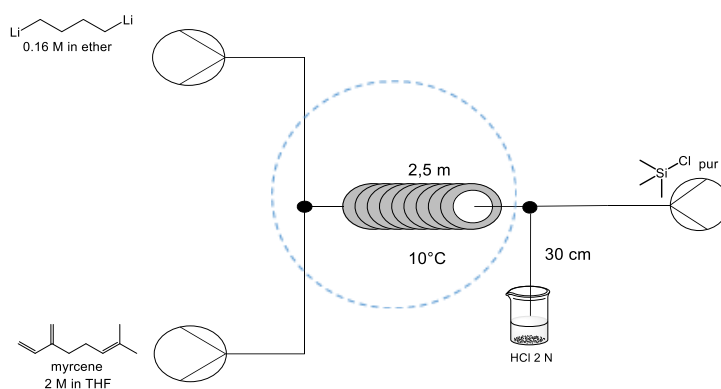


Figure 4.22: Setup for bifunctionalization of polymyrcene TMS end-group.

To continue studying the control of the molar mass of the polymyrcene, the reaction was now made in a microflow reactor. The volumetric flow rate was established in the three pumps depending on the concentration of the solutions used for the reaction (Table 4.5).

Table 4.5: Results for anionic polymerization of myrcene with TMS endings in a continuous flow reactor.

No.	$Q_{\text{myrcene/THF}}$ (mL/min)	$Q_{1,4 \text{ DiI/Et}_2\text{O}}$ (mL/min)	$Q_{\text{TMSCl}}$ (mL/min)	$\overline{M}_n$ NMR (g/mol)	$\overline{M}_n$ GPC (g/mol)	$\overline{D}$
1 <sup>a</sup>	0.25	0.20	0.20	2600	-	-
2	0.25	0.20	0.20	2700	1500	1.2

<sup>a</sup> No data of GPC analysis.

As the parameters for the reaction were well managed, the values of molecular weight in <sup>1</sup>HNMR for samples 1 and 2 correspond to the values expected if we consider that the functionalization with TMS is not full (FD = 75% as shown in the previous chapter).

#### 4.4.5 Results for the synthesis of bifunctionalized polymyrcene with CO<sub>2</sub>H ending under microflow conditions

Following the molar mass control already obtained for the polymyrcene with TMS endings, a reaction with carbon dioxide in continuous flow was done to obtain CO<sub>2</sub>H endings. For the microflow conditions it was necessary to keep the same molar ratio already established for the study (Myr/DiLi 17:1). To do so the volumetric flow rates for the solution of 1,4-dilithiumbutane and the solution Myrcene/THF were set-up in each pump based on the molar concentration of each reagent.

The selected temperature for the reaction was 10 °C with 2 initial cooling loops at 0 °C for each reactive. After several experiments the reactor length established was of 2.5 m.

As before, to control the volumetric flow of CO<sub>2</sub>, a mass flow controller was used. This instrument was connected to a CO<sub>2</sub> gas tank and allowed to control the mass flow of the gas through a software by opening and closing a valve. The following tables show the parameters for the polymerization in continuous flow conditions established during the study.

Table 4.6: Molar concentration and volumetric flows of reagents used in microflow conditions.

Reagent	Concentration (mmol/mL)	Q <sub>v</sub> (mL/min)
1,4-dilithiumbutane	0.16	0.20
Myrcene/THF	2	0.25
TMSCl	Pure	0.20
CO <sub>2</sub>	Pure	1.3

Table 4.7: Dimensions and residence time of reactors used in microflow conditions.

Reactor	Material	Dimensions	Length (m)	t <sup>R</sup> (min)
1	Stainless steel	1/16" in * 0.75 mm	2.5	2.45
2	Stainless steel	1/16" in * 0.75 mm	0.03	0.02

After having optimized the parameters in continuous flow, we have introduced the end-group CO<sub>2</sub>H (Figure 4.23).

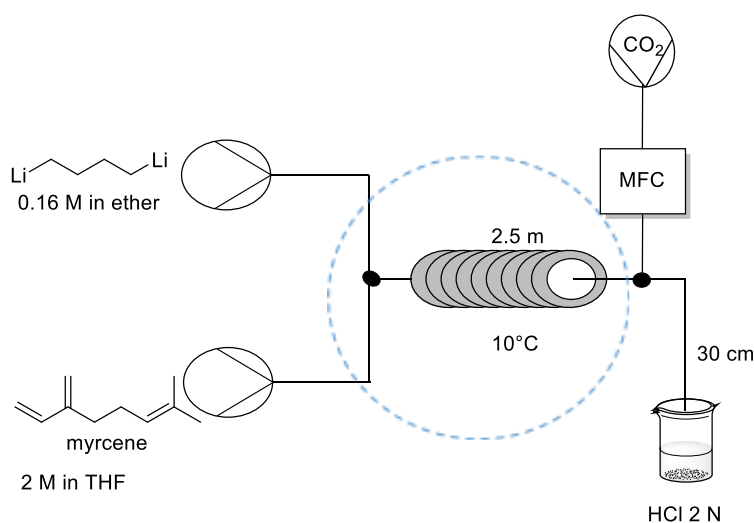


Figure 4.23 : Setup for bifunctionalization of polymycene CO<sub>2</sub>H end-group.

Table 4.8: Results for anionic polymerization of myrcene with CO<sub>2</sub>H endings in a continuous flow reactor.

$Q_{\text{myrcene/THF}}$ (mL/min)	$Q_{1,4 \text{ Dil/Et}_2\text{O}}$ (mL/min)	$Q_{\text{CO}_2}$ (mL/min)	$\overline{Mn}$ <sup>1</sup> HNMR (g/mol)	$\overline{Mn}$ GPC (g/mol)	$\overline{D}$
0.25	0.20	1.3	2200	1500	1.2

Better control over molar mass in microfluidic conditions was again observed (Table 4.8).  $\overline{Mn}$  <sup>1</sup>HNMR was calculated based on a telechelic structure and gave a close value to  $\overline{Mn}_{\text{th}}$ . This shows that we have the same FD close to 95% that we observed before.

Microstructure analysis in the ether/THF mixture gave the following: 33%1,4; 55%3,4; 12% 1,2-unit content.

#### 4.5 Conclusions

In this chapter, living chains were either initiated using *n*-BuLi or using a new alkyl dilithium. In a post-polymerization strategy, functionalities were introduced using TMSCl, and CO<sub>2</sub> was selected termination on the living polymers.

When reactions were conducted in batch, yields were not quantitative with TMSCl while ketone structures were mainly observed instead of the expected CO<sub>2</sub>H end groups when CO<sub>2</sub>.

In flow conditions TMSCl addition was effective (73%). Concerning CO<sub>2</sub> addition in flow conditions the functionalization degree reached high yields (95%). This could be ascribed to a better control of the CO<sub>2</sub> addition in the process probably optimizing the gas-liquid mixing as well as the absence of secondary reactions between reagents and product in microfluidic conditions, thus leading to CO<sub>2</sub>H endings. Thus, new carboxy-telechelic oligomers could be obtained using a new sustainable controlled microfluidic process

## 4.6 Bibliography

- (1) González-Villa, J.; Saldívar-Guerra, E.; León-Gómez, R. E. D.; López González, H. R.; Infante-Martínez, J. R. Kinetics of the Anionic Homopolymerizations of  $\beta$ -Myrcene and 4-Methylstyrene in Cyclohexane Initiated by *n*-Butyllithium. *J. Polym. Sci. Part A: Polym. Chem.* **2019**, *57* (21), 2157–2165. <https://doi.org/10.1002/pola.29487>.
- (2) Banda-Villanueva, A.; González-Zapata, J. L.; Martínez-Cartagena, M. E.; Magaña, I.; Córdova, T.; López, R.; Valencia, L.; Medina, S. G.; Rodríguez, A. M.; Soriano, F.; Díaz de León, R. Synthesis and Vulcanization of Polymyrcene and Polyfarnesene Bio-Based Rubbers: Influence of the Chemical Structure over the Vulcanization Process and Mechanical Properties. *Polymers* **2022**, *14* (7), 1406. <https://doi.org/10.3390/polym14071406>.
- (3) Flory, P. J. *Principles of Polymer Chemistry*; Cornell university press, 1953.
- (4) Fontanille, M. G., Y. *Chimie et Physico-Chimie Des Polymères*; Dunod, 2014.
- (5) Ebdon, J. R. Terminally Reactive Oligomers: Telechelic Oligomers and Macromers. In *New Methods of Polymer Synthesis*; Ebdon, J. R., Ed.; Springer US: Boston, MA, 1991; pp 162–196. [https://doi.org/10.1007/978-1-4684-1530-8\\_6](https://doi.org/10.1007/978-1-4684-1530-8_6).
- (6) Quirk, R. P.; Huang, T.-L. Alkylolithium-Initiated Polymerization of Myrcene New Block Copolymers of Styrene and Myrcene. In *New Monomers and Polymers*; Culbertson, B. M., Pittman, C. U., Eds.; Springer US: Boston, MA, 1984; pp 329–355. [https://doi.org/10.1007/978-1-4684-4619-7\\_19](https://doi.org/10.1007/978-1-4684-4619-7_19).
- (7) Stanetty, P.; Mihovilovic, M. D. Half-Lives of Organolithium Reagents in Common Ethereal Solvents. *J. Org. Chem.* **1997**, *62* (5), 1514–1515. <https://doi.org/10.1021/jo961701a>.
- (8) Clayden, J.; Yasin, S. A. Pathways for Decomposition of THF by Organolithiums: The Role of HMPA. *New J. Chem.* **2002**, *26* (2), 191–192. <https://doi.org/10.1039/b109604d>.
- (9) Wahlen, C.; Rauschenbach, M.; Blankenburg, J.; Kersten, E.; Ender, C. P.; Frey, H. Myrcenol-Based Monomer for Carbanionic Polymerization: Functional Copolymers with Myrcene and Bio-Based Graft Copolymers. *Macromolecules* **2020**, *53* (20), 9008–9017.
- (10) Ávila-Ortega, A.; Aguilar-Vega, M.; Loría Bastarrachea, M. I.; Carrera-Figueiras, C.; Campos-Covarrubias, M. Anionic Synthesis of Amine  $\omega$ -Terminated  $\beta$ -Myrcene Polymers. *J Polym Res* **2015**, *22* (11), 226. <https://doi.org/10.1007/s10965-015-0856-6>.
- (11) Bolton, J. M.; Hillmyer, M. A.; Hoye, T. R. Sustainable Thermoplastic Elastomers from Terpene-Derived Monomers. *ACS Macro Lett.* **2014**, *3* (8), 717–720. <https://doi.org/10.1021/mz500339h>.
- (12) Pérez, K.; Picard, B.; Vuluga, D.; Burel, F.; Hreiz, R.; Falk, L.; Commenge, J.-M.; Nagaki, A.; Yoshida, J.; Chataigner, I.; Maddaluno, J.; Legros, J. Bromine–Lithium Exchange on a Gem -Dibromoalkene, Part 2: Comparative Performance of Flow Micromixers. *Org. Process Res. Dev.* **2020**, *24* (5), 787–791. <https://doi.org/10.1021/acs.oprd.0c00203>.

- (13) Picard, B.; Pérez, K.; Lebleu, T.; Vuluga, D.; Burel, F.; Harrowven, D. C.; Chataigner, I.; Maddaluno, J.; Legros, J. Bromine-Lithium Exchange on Gem-Dibromoalkenes Part 1: Batch vs Microflow Conditions. *J Flow Chem* **2020**, *10* (1), 139–143. <https://doi.org/10.1007/s41981-019-00057-6>.
- (14) Zhang, J.; Aydogan, C.; Patias, G.; Smith, T.; Al-Shok, L.; Liu, H.; Eissa, A. M.; Haddleton, D. M. Polymerization of Myrcene in Both Conventional and Renewable Solvents: Postpolymerization Modification via Regioselective Photoinduced Thiol–Ene Chemistry for Use as Carbon Renewable Dispersants. *ACS Sustainable Chem. Eng.* **2022**, *10* (29), 9654–9664. <https://doi.org/10.1021/acssuschemeng.2c03755>.
- (15) Bolton, J. M.; Hillmyer, M. A.; Hoye, T. R. Sustainable Thermoplastic Elastomers from Terpene-Derived Monomers. *ACS Macro Lett.* **2014**, *3* (8), 717–720. <https://doi.org/10.1021/mz500339h>.
- (16) Sinn, H.; Banderhann, F. The Kinetics of the Polyisoprene Formation Initiated with Lithium Organyl: POLYISOPRENE FORMATION. *J. polym. sci., C Polym. symp.* **1967**, *16* (8), 4515–4522. <https://doi.org/10.1002/polc.5070160828>.
- (17) Tapia, J. J. B.; López, J. A. T.; Nájera, R. H. Kinetics of the Anionic Polymerization of 1,3-Butadiene Using an Initiator Composed of Alkyl Aluminium, n-Butyllithium and Barium Alkoxide to Produce High Trans-1,4-Polybutadiene. *Macromolecular Reaction Engineering* **2008**, *2* (3), 222–232. <https://doi.org/10.1002/mren.200700048>.
- (18) Yang, X.; Wang, C.; Li, S.; Huang, K.; Li, M.; Mao, W.; Cao, S.; Xia, J. Study on the Synthesis of Bio-Based Epoxy Curing Agent Derived from Myrcene and Castor Oil and the Properties of the Cured Products. *RSC Adv.* **2017**, *7* (1), 238–247. <https://doi.org/10.1039/C6RA24818G>.
- (19) Leveneur, S.; Pinchard, M.; Rimbault, A.; Safdari Shadloo, M.; Meyer, T. Parameters Affecting Thermal Risk through a Kinetic Model under Adiabatic Condition: Application to Liquid-Liquid Reaction System. *Thermochimica Acta* **2018**, *666*, 10–17. <https://doi.org/10.1016/j.tca.2018.05.024>.
- (20) Marquardt, D. W. (1963). An Algorithm for Least-Squares Estimation of Nonlinear Parameters. *Journal of the Society for Industrial and Applied Mathematics*, *11*(2), 431–441. [Http://www.jstor.org/stable/2098941](http://www.jstor.org/stable/2098941).
- (21) Morton, M. *Anionic Polymerization: Principles and Practice*; Academic Press: New York, 1983.
- (22) Hsieh, H.; Quirk, R. P. *Anionic Polymerization: Principles and Practical Applications*; CRC Press, 1996.
- (23) Toch, K.; Thybaut, J. W.; Marin, G. B. A Systematic Methodology for Kinetic Modeling of Chemical Reactions Applied to *n*-Hexane Hydroisomerization. *AIChE J.* **2015**, *61* (3), 880–892. <https://doi.org/10.1002/aic.14680>.
- (24) Tonhauser, C.; Frey, H. A Road Less Traveled to Functional Polymers: Epoxide Termination in Living Carbanionic Polymer Synthesis. *Macromol. Rapid Commun.* **2010**, *31* (22), 1938–1947. <https://doi.org/10.1002/marc.201000353>.

- (25) Quirk, R. P.; Ma, J.-J. Characterization of the Functionalization Reaction Product of Poly(Styryl)Lithium with Ethylene Oxide. *J. Polym. Sci. A Polym. Chem.* **1988**, *26* (8), 2031–2037. <https://doi.org/10.1002/pola.1988.080260804>.
- (26) Takahashi, Y.; Nagaki, A. Anionic Polymerization Using Flow Microreactors. *Molecules* **2019**, *24* (8), 1532. <https://doi.org/10.3390/molecules24081532>.
- (27) Takahashi, Y.; Nagaki, A. Anionic Polymerization Using Flow Microreactors. *Molecules* **2019**, *24* (8), 1532. <https://doi.org/10.3390/molecules24081532>.
- (28) Ueda, K.; Hirao, A.; Nakahama, S. Synthesis of Polymers with Amino End Groups. 3. Reactions of Anionic Living Polymers with  $\alpha$ -Halo- $\iota$ -Aminoalkanes with a Protected Amino Functionality. *Macromolecules* **1990**, *23* (4), 939–945. <https://doi.org/10.1021/ma00206a006>.
- (29) Kim, J.; Lee, M.; Ryu, C.-Y.; Lee, J.; Hwang, S. S.; Park, T. S.; Kim, K. U.; Yoon, H. S.; Ahn, B. I.; Char, K. Synthesis of Dilithium  $\alpha$ ,  $\omega$ -Disulfonated Polystyrene by Anionic Polymerization. *Polymer journal* **1994**, *26* (10), 1111–1117.
- (30) Quirk, R. P.; Yin, J. Carbonation of Polymeric Organolithium Compounds: Effects of Chain End Structure. *J. Polym. Sci. A Polym. Chem.* **1992**, *30* (11), 2349–2355. <https://doi.org/10.1002/pola.1992.080301108>.
- (31) Quirk, R. P.; Yin, J.; Fetters, L. J. Carbonation and Related Reactions of Poly (Styryl) Lithium. *Macromolecules* **1989**, *22* (1), 85–90.
- (32) Schulz, D. N.; Halasa, A. F. Anionic Polymerization Initiators Containing Protected Functional Groups. II. *Journal of Polymer Science: Polymer Chemistry Edition* **1977**, *15* (10), 2401–2410.
- (33) Georges, S.; Hashmi, O. H.; Bria, M.; Zinck, P.; Champouret, Y.; Visseaux, M. Efficient One-Pot Synthesis of End-Functionalized Trans-Stereoregular Polydiene Macromonomers. *Macromolecules* **2019**, *52* (3), 1210–1219.
- (34) Ruiz Martínez, E.; Sánchez Hervás, J. M. Chemical Valorization of CO<sub>2</sub>. In *Carbon Dioxide Utilization to Sustainable Energy and Fuels*; Inamuddin, Boddula, R., Ahamed, M. I., Khan, A., Eds.; Springer International Publishing: Cham, 2022; pp 1–30. [https://doi.org/10.1007/978-3-030-72877-9\\_1](https://doi.org/10.1007/978-3-030-72877-9_1).
- (35) SciencesRoundtable, N. R. C. (US) C. *Carbon Dioxide as a Feedstock*; National Academies Press (US), 2001.
- (36) Seo, H.; Nguyen, L. V.; Jamison, T. F. Using Carbon Dioxide as a Building Block in Continuous Flow Synthesis. *Advanced Synthesis & Catalysis* **2019**, *361* (2), 247–264.
- (37) Nagaki, A.; Takahashi, Y.; Yoshida, J. Extremely Fast Gas/Liquid Reactions in Flow Microreactors: Carboxylation of Short-Lived Organolithiums. *Chem. Eur. J.* **2014**, *20* (26), 7931–7934. <https://doi.org/10.1002/chem.201402520>.
- (38) Wu, J.; Yang, X.; He, Z.; Mao, X.; Hatton, T. A.; Jamison, T. F. Continuous Flow Synthesis of Ketones from Carbon Dioxide and Organolithium or Grignard Reagents. *Angew. Chem. Int. Ed.* **2014**, *53* (32), 8416–8420. <https://doi.org/10.1002/anie.201405014>.
- (39) Nagaki, A.; Takahashi, Y.; Yoshida, J. Extremely Fast Gas/Liquid Reactions in Flow Microreactors: Carboxylation of Short-Lived Organolithiums. *Chemistry – A European Journal* **2014**, *20* (26), 7931–7934. <https://doi.org/10.1002/chem.201402520>.

- (40) Monbaliu, J.-C. M.; Legros, J. Will the next Generation of Chemical Plants Be in Miniaturized Flow Reactors? *Lab Chip* **2022**. <https://doi.org/10.1039/D2LC00796G>.
- (41) Cawse, J. L.; Stanford, J. L.; Still, R. H. Polymers from Renewable Sources: 5. Myrcene-Based Polyols as Rubber-Toughening Agents in Glassy Polyurethanes. *Polymer* **1987**, *28* (3), 368–374.
- (42) Negishi, E.; Swanson, D. R.; Rousset, C. J. Clean and Convenient Procedure for Converting Primary Alkyl Iodides and .Alpha.,.Omega.-Diodoalkanes into the Corresponding Alkylolithium Derivatives by Treatment with Tert-Butyllithium. *J. Org. Chem.* **1990**, *55* (19), 5406–5409. <https://doi.org/10.1021/jo00306a022>.

## 5 General conclusions and perspectives

### General conclusions

Chemistry in miniaturized reactors operating in continuous flow makes it possible to progress towards the frontiers of innovation, optimization and production of new materials. The space-resolution of reaction in such fluidic reactors allows a fine control of the molar mass of the polymers to access tailored oligomers. Moreover, the superior thermal transfer in microflow reactors compared to macrobatch reactors leads to significant improvement in process safety.

In a first part, we studied the stereoselectivity of the lithium bromine exchange on a *gem*-dibromo alkene in a microflow system with sixteen passive mixers that have two internal diameters (500  $\mu\text{m}$  and 250  $\mu\text{m}$ ) and eight variable angles (135 to 30°). As a result, a high flow rate in a fine W micro-mixer (45°, ID = 0.25 mm) achieves *E*-stereoselectivity exceeding 90% without any cryogenic conditions (20 °C here).

In the second part, the anionic polymerization of the biobased analogue of isoprene, myrcene, with *n*-BuLi at various scales using batch and flow reactor with various sizes. Conversely to batch conditions, flow conditions allowed a fully living polymerization, without reproducibility and scale-up issues. Notably, we were also able to control a low molar mass of polymyrcene with the help of a homogeneous and controlled temperature inside the reactor. Also, thanks to the microfluidic system, it was possible to trap carbon dioxide (CO<sub>2</sub>) at the end of polymerization and 95% functionalization was obtained, in a totally selective manner thus introducing a useful carboxyl function.

Finally, preliminary results in the flow synthesis of telechelic polymyrcene bearing CO<sub>2</sub>H endings were obtained. In this study, we used the challenging and underexploited 1,4 dilithiumbutane as an initiator.

Such results in microflow confirm the effectiveness of these reactors in anionic chemistry. Among the beneficial impacts of flow technology, the possibility to handle pyrophoric reagents at friendlier temperatures is worth noting. Another important point to mention is



the great reproducibility of the reactions can be reproduced allowing easy scale-up of the quantity of products yielded.

This work opens the door to a new sustainable process to obtain controlled and functionalized oligomers. For example, hydrogenation of the bifunctional polymer CO<sub>2</sub>H would lead to novel macro diols of interest.

### Perspectives

This project opens doors to further interesting perspectives:

- Hydrogenation of the telechelic polymyrcene with CO<sub>2</sub>H endings to eliminate double bonds and obtain OH endings. Promising results have already been obtained.
- This know-how could be extended to other terpenes such ocimene, farnesene or alloocimene in continuous flow reactors.
- Multibloc copolymers may be considered by using flow chemistry using multiple inlets.

### Green solvents

- To carry out a more environmentally friendly process, the use of green solvents could be an option.
- The use of 2-methyltetrahydrofuran (2-MeTHF) in continuous flow, can be consider in the future.
- Limonene also can be an option as a solvent in the anionic polymerization of myrcene.<sup>1</sup>

(1) Dev, A.; Rösler, A.; Schlaad, H. Limonene as a Renewable Unsaturated Hydrocarbon Solvent for Living Anionic Polymerization of  $\beta$ -Myrcene. *Polym. Chem.* 2021, 12 (21), 3084–3087. <https://doi.org/10.1039/D1PY00570G>.

## 6 Résumé general

Dans la recherche de méthodes flexibles et durables pour la synthèse des structures moléculaires, les systèmes à flux continu offrent une grande adaptabilité sur les volumes, de l'échelle laboratoire à la production. Étant donné que les systèmes à flux continu permettent de manipuler des composés dangereux sans exposer l'opérateur, l'utilisation de composés organométalliques devient plus simple et sécurisée. Les réactions choisies pour cette étude sont du domaine de la chimie des composés organolithiens : (1) réaction sélective d'échange brome-lithium sur un composé vinylique, pour étudier l'influence de différentes géométries de micro-mélangeurs sur le cours des réactions chimiques et (2) polymérisation du myrcène, un monomère biosourcé. Dans un premier temps, seize mélangeurs passifs avec huit angles différents de 135°, 120°, 105° (mélangeurs en Y), 90° (mélangeur en T), 75°, 60°, 45° et 30° (mélangeurs en W) et deux diamètres internes (DI = 0,5 et 0,25 mm) associés à un réacteur tubulaire de diamètre interne (DI) = 0,5 mm seront étudiés. Différents paramètres seront mis à point (débit, concentration notamment) pour sélectionner le micro-mélangeur le plus efficace pour la réaction en termes de sélectivité chimique (un produit parmi plusieurs possibles) et de sélectivité géométrique (un isomère parmi deux). Dans une deuxième partie la polymérisation anionique du myrcène en flux continu sera réalisée. Dans une dernière partie, une fonctionnalisation du polymyrcène par un piégeage in situ en flux continu à l'aide de dioxyde de carbone sera étudiée dans le but d'obtenir un polymyrcène fonctionnel.

## Une alternative : les réacteurs à flux continu

La chimie en flux continu consiste à faire passer un ou plusieurs fluides différents à travers des tubes, un seul microréacteur ou un système microfluidique. Dans les systèmes à flux continu, il existe différentes désignations d'échelles telles que nano, micro, milli et mésofluidique, selon les diamètres intérieurs des réacteurs considérés. Cependant, ces désignations ne sont pas soumises à des règles strictes parce que la complexité des systèmes à flux continu peut conduire à l'utilisation d'objets de tailles différentes dans un même assemblage, ce qui rend une nomenclature stricte non pertinente.

Ce concept de microfluidique est basé sur l'utilisation de petits volumes de fluides et d'un ou plusieurs dispositifs de moins de 1 millimètre de diamètre interne. Il n'y a aucune restriction sur l'utilisation des unités, donc dans ce manuscrit nous parlerons indistinctement en mm ou en  $\mu\text{m}$  de diamètre interne.

Parmi les avantages de l'utilisation du flux continu en chimie, on peut citer : synthétiser des produits de manière plus sûre et plus rapide,<sup>1</sup> effectuer des réactions efficaces en terme d'efficacité et sélectivité,<sup>2</sup> limiter la consommation d'énergie des installations (refroidissement, chauffage,...).<sup>3</sup> Les systèmes microfluidiques sont un outil puissant pour les études mécanistiques de réactions impliquant des intermédiaires très instables. Il y a certaines caractéristiques générales du flux continu qu'il est nécessaire de connaître pour pouvoir maîtriser le système, parmi eux se trouvent, le débit, la concentration, la viscosité, la température, la pression, le mélange *etc.*

### Caractéristiques générales

**Débit (Q) :** Le débit est un paramètre essentiel afin de contrôler précisément le temps de séjour des molécules à l'intérieur du microréacteur. Selon la bibliographie,<sup>4</sup> en modifiant le débit uniquement, il est possible d'obtenir une variation de résultats au niveau de la conversion, du rendement ou de la sélectivité. Si la même concentration est conservée mais que le débit est modifié, on peut avoir différents rapports molaires entre les réactifs

**Concentration (C) :** dans les réacteurs à flux continu, la concentration des réactifs est un autre paramètre crucial pour caractériser les réactions chimiques, car elle influe sur la miscibilité des fluides et la vitesse de la réaction.

**Viscosité ( $\mu$ ) :** Le fait que les deux fluides aient des viscosités différentes donne lieu à des profils de vitesse non symétriques à l'entrée du canal et par conséquent au centre du mélangeur.<sup>5</sup> En d'autres termes, cela pourrait influencer le mélange. En plus, dans les réactions de polymérisation, la viscosité peut augmenter en raison de la masse molaire croissante des polymères.

**Volume (V) :** Les faibles dimensions des réacteurs en flux permet l'utilisation de faible volume de réactifs à un instant donné à l'intérieur du dispositif, ce qui permet de limiter les risques liés à l'utilisation d'espèces dangereuses. De plus, il permet d'envisager des réactions à des échelles moléculaires minuscules. Le volume dans un réacteur à micro flux est calculé en fonction du diamètre interne (DI) et de la longueur du réacteur tubulaire.

$$V = \frac{\pi d_t^2 L}{4}$$

*Équation 1*

Où :

$d_t$ , est le diamètre interne du réacteur tubulaire(m).

$L$ , longueur du réacteur tubulaire (m).

**Température (T) :** Les systèmes de microfluidique sont plus efficaces dans le transfert d'énergie thermique comparé aux réacteurs conventionnels car le transfert d'énergie est directement lié à la géométrie du réacteur. L'utilisation de microréacteurs permet d'évacuer la chaleur plus rapidement et maintenir des conditions plus proches de l'isotherme, grâce à la capacité des microréacteurs à échanger la chaleur avec son environnement. Pour évaluer la différence entre le dégagement de chaleur d'un réacteur en batch et en flux continu, il faut d'abord considérer le cas d'une réaction exothermique.<sup>6</sup> Dans une réaction exothermique de l'ordre 1, le rapport entre le flux de chaleur libéré par la réaction et le flux de chaleur évacué par échange est le suivant :

$$\frac{\text{heat flux released by the reaction}}{\text{heat flux removed by exchange}} = \frac{kC_A(-\Delta_r H)V}{US(T - T_{ex})} \quad \text{Équation 2}$$

Où :

$k$  est la constante de vitesse spécifique pour une réaction de premier ordre ( $s^{-1}$ )

$C_A$  est la concentration du composé A (mmol/mL)

$\Delta_r H$  est l'enthalpie (Joules)

$S$  est la surface (m<sup>2</sup>)

$U$  est le coefficient d'échange global (W.m<sup>2</sup>/K)

$(T - T_{ex})$  est la différence de température entre le milieu de réaction et le milieu de refroidissement (K).

Cette équation fait référence au rapport de transfert de chaleur entre le milieu de réaction et l'extérieur. Si le flux de chaleur dissipé par la réaction est plus grand que le flux de chaleur retiré par l'échange, le système augmentera la température. Ceci est exprimé par le rapport  $\frac{S}{V}$ , où la surface de transfert ( $S$ ) a une relation inverse avec le diamètre du réacteur.<sup>6</sup>

Le coefficient d'échange  $U$ , qui se réfère à la façon dont la chaleur peut être menée à travers la paroi du réacteur et le milieu de refroidissement. Ce coefficient dépend des conditions hydrodynamiques, des performances de conduction thermique du matériau de paroi entre le réfrigérant et le milieu de réaction.  $U$  est également inversement proportionnel à la taille du réacteur.

Les réacteurs à flux continu cylindriques, permettent le transfert de chaleur sur toute sa surface selon l'Équation 3 :

$$\frac{S}{V} = \frac{2\pi hr}{\pi hr^2} = \frac{2}{r} = \frac{4}{d} \quad \text{Équation 3}$$

Où :  $V$  : volume (m<sup>3</sup>),  $S$  : surface (m<sup>2</sup>),  $r$  : rayon(m),  $h$  : hauteur(m)  $d$  : diamètre(m)

Cependant, dans les réacteurs conventionnels comme un ballon à fond rond ; la zone d'échange spécifique est totalement différente et est calculée en utilisant cette Équation 4 :

$$\frac{S}{V} = \frac{6\pi r h}{\pi h^2 (3r - h)} \quad \text{Équation 4}$$

Où : **V** : volume (m<sup>3</sup>), **S** : surface (m<sup>2</sup>), **r** : rayon(m), **h** : hauteur(m)

Cela montre que la zone d'échange spécifique du réacteur influence l'évacuation de la chaleur et que, par conséquent, cela a une influence sur le contrôle de la température de la réaction. Ceci permet d'expliquer pourquoi le contrôle de la température en systèmes microstructurés est meilleur comparé aux réacteurs conventionnels. De ce fait, pour avoir une bonne méthode de comparaison entre les systèmes conventionnels et les systèmes microfluidiques, il est important de prendre en compte les dimensions de chacun des dispositifs.

**Mélange** : Dans plusieurs réactions, principalement celles qui sont très rapides, le mélange représente un défi dans les conditions au niveau de réacteurs conventionnels. Idéalement, le temps de mélange doit être plus court que le temps de réaction et ce n'est pas toujours le cas pour les réactions ultra-rapides comme l'échange halogène-métal. Dans la plupart des dispositifs à flux continu, les fluides ne changent -en apparence- jamais leurs conditions d'écoulement laminaire, raison pour laquelle, dans le cas d'un réacteur tubulaire, le mélange pourrait être considéré comme reposant uniquement sur l'inter-diffusion moléculaire.

Dans les conditions de flux continu en réacteurs miniaturisés, l'écoulement peut être considéré comme laminaire, car il n'y a pas de turbulence et que le mélange est strictement dû à la diffusion.

Par exemple, la Fig 2 montre comment se réalise la mélange dans un réacteur microfluidique.<sup>7</sup> Si nous considérons le cas d'une réaction comme :  $A + B \rightarrow C + A \rightarrow D$

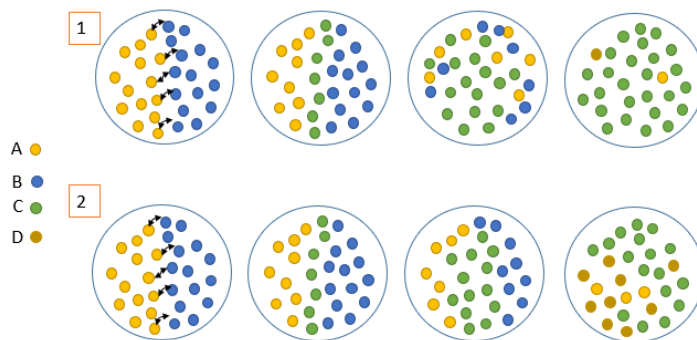


Fig 2 : Évolution du mélange dans un réacteur à flux continu.

Ce phénomène s'explique par la cinétique de la réaction. S'il y a un bon mélange, les règles cinétiques qui s'appliquent dans des conditions homogènes sont respectées. Ainsi, la réaction 1 (avec  $r_1 = k_1[A][B]$ ), pourrait se produire sélectivement sans réaction 2, ( $r_2 = k_2[A][C]$ ) si  $k_1 > k_2$ . Au contraire, si le mélange n'est pas bon la réaction 2 peut se produire, entraînant la formation du produit non désirée D, même si  $k_1 > k_2$ . Cependant, la réalité n'est souvent pas si simple, et il peut avoir de multiples possibilités de réactions secondaires.

**Diamètre interne des réacteurs et géométrie des mélangeurs :** Un petit changement dans le diamètre du micromélangeur peut affecter significativement. La vitesse du fluide diminue à mesure que le diamètre du micro-mélangeur augmente et vice versa. Selon Kolbl *et coll.* les temps de mélange ne peuvent pas être déduits des réactions d'essais chimiques en appliquant des modèles de mélange simples qui ne tiennent pas compte de la géométrie spécifique de l'appareillage.<sup>8</sup>

Dans une simulation sur les profils de vitesses dans les micro-mélangeurs T et Y, Gobby *et coll.* montrent que l'angle semble avoir un léger effet sur le mélange et sur la perte de pression.<sup>5</sup>

**Pression (P) :** c'est un paramètre qui peut influencer davantage le mélange puisque la diminution de la pression est directement liée à l'énergie dissipée au cours du processus de mélange. La perte de charges peut également réduire l'efficacité du pompage des fluides à travers le réacteur, en particulier si celui-ci est long.

Temps de séjour ( $t^R$ ) : Le temps de réaction est contrôlé par le temps de séjour dans les réacteurs à flux continu. Le temps de séjour est le temps moyen nécessaire pour faire passer un fluide ou une solution dans le microréacteur. Le temps de résidence est calculé à partir de l'Équation 5 :

- Temps de réaction = *temps de séjour* =  $t^R = f(V_{reactor}, Q_1 + Q_2)$

$$t^R = \frac{V}{Q}$$

Équation 5

V : volume (mL)

Q : débit volumique (mL/min)

Étant donné que le temps de séjour est dépendant du volume du réacteur, ce dernier augmente en fonction de l'allongement de la longueur du canal et diminue en fonction de l'augmentation du débit. La précision sur le contrôle du temps de séjour en système fluide est extrêmement utile pour la réalisation de réaction impliquant un réactif instable de courte durée de vie.

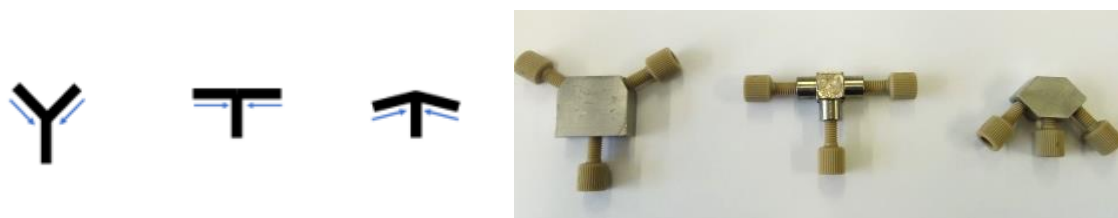
### Dispositifs dans les systèmes à flux continu

Il existe différents types d'outils permettant d'agir sur les dispositifs en flux continu, tels que : les réacteurs, les micromélangeurs, les pompes, les vannes, les connectiques, les appareils d'analyse (RMN et IR), régulateurs de débit massique (MFC), et d'autres appareils supplémentaires. Dans cette partie on va se focaliser sur les microréacteurs et les micromélangeurs. Afin de maintenir une définition cohérente, nous allons définir la microfluidique comme tout système contenant au moins un dispositif fluide, qui a un diamètre de section inférieur à 1 millimètre (au moins une des zones).

Dans les systèmes de microfluidique, les **microréacteurs** sont des microcanaux dans lesquels la réaction a lieu. Un réacteur à flux continu peut avoir différentes formes selon l'utilisation. Il peut également être fabriqué à partir de divers matériaux comme le verre, l'acier inoxydable, ou à partir de différents polymères.



Les micromélangeurs représentent un dispositif largement utilisé. Il existe deux types de micromélangeurs selon la source d'énergie : le mélangeur actif et le mélangeur passif. Le mélangeur passif utilise l'énergie de l'action de pompage continu ou du potentiel hydrostatique<sup>9</sup>. La Fig 3 montre les mélangeurs passifs typiques, T, W et Y. La différence entre ces mélangeurs réside dans l'angle entre les canaux,  $\theta = 90^\circ$  pour la forme T et pour la forme W et Y l'angle est variable.<sup>10</sup>



*Fig 3: Mélangeurs passifs tels que Y, T et W et ses symboles.*

Yoshida a observé une différence significative de réactivité des organolithiums entre les micromélangeurs en forme de T et en forme de W (également appelés micromélangeurs en forme de V ou d'ancre).<sup>11</sup> En raison de ses travaux, différents micromélangeurs nous ont été envoyés par son groupe (micromélangeurs passifs avec des angles  $45^\circ$  et  $90^\circ$ ). Ils ont ensuite été envoyés à la société MG63 pour avoir différents micromélangeurs avec différents angles.

### **Chimie contrôlée des organolithiums dans les microréacteurs à flux : effet de micromélangeur.**

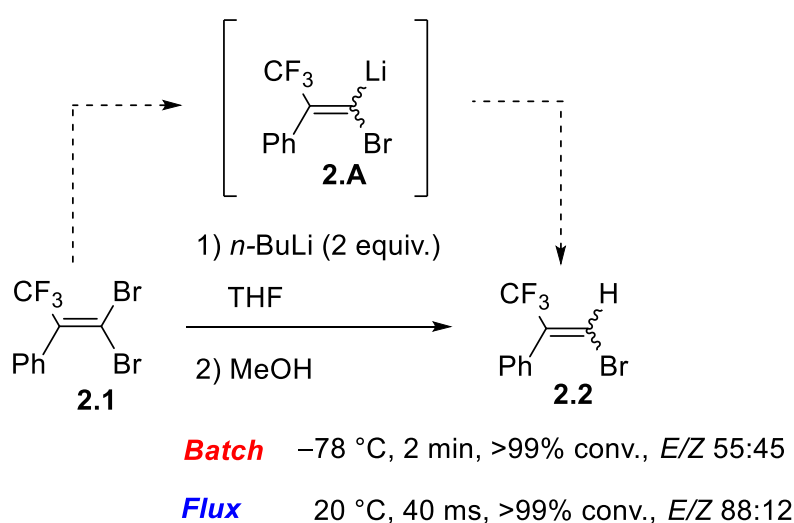
Avant de passer à la polymérisation en flux continu, l'influence de seize mélangeurs passifs avec huit angles différents de  $135^\circ$ ,  $120^\circ$ ,  $105^\circ$  (mélangeurs en Y),  $90^\circ$  (mélangeur en T),  $75^\circ$ ,  $60^\circ$ ,  $45^\circ$  et  $30^\circ$  (mélangeurs en W) et deux diamètres internes (DI = 0,5 et 0,25 mm) a été étudiée. Certains paramètres, tels que le débit, ont été modifiés pour déterminer le micromélangeur le plus efficace pour la réaction en termes de sélectivité chimique (l'un des nombreux produits possibles) et de sélectivité géométrique (l'un des deux isomères).

### **Influence de la conception et du dimensionnement du micromélangeur**

Les carbénoïdes de vinyle lithiés peuvent être facilement obtenus par échange halogène-métal à partir de l'alcène gem-dihalogène correspondant dans des conditions

cryogéniques. Cependant, ces carbénoïdes sont souvent particulièrement instables, car ils peuvent subir un réarrangement rapide de Fritsch-Buttemberg-Wiechell (FBW) ainsi que diverses réactions secondaires.<sup>11-13</sup>

Dans une étude préliminaire,<sup>13</sup> nous avons montré que le *gem*-dibromo alcène **2.1** pouvait subir un échange brome-lithium et que le carbénoïde intermédiaire **2.A** correspondant était suffisamment stable pour piéger un proton pour produire l'oléfine **2.2** monobromée correspondante (Figure 4.24).



*Micromelangeur en T, Q(n-BuLi + 1) = 9.4mL/min, ID 0.5 mm*

Figure 4.24: Génération et piégeage d'un carbénoïde 2.A à partir du *gem*-dibromoalcène (2.1) en batch et en flux continu.

Alors que la réaction n'était pas sélective dans des conditions de batch classiques, même à -78 °C (Figure 4.24), un rapport 88:12 E/Z pouvait être atteint en un seul essai en utilisant un microréacteur à flux continu équipé d'un micromélangeur en forme de T ( angle= 90°, DI micro mélangeur  $\theta = 500 \mu\text{m}$ , taille du réacteur DI = 500  $\mu\text{m}$ , L = 3 cm (Figure 4.24), débit  $Q_{(2.1+n\text{-BuLi})} = 9,4 \text{ mL/min}$ ), même à 20 °C dans les 30 millisecondes (ms).

Nous étendons maintenant cette étude à l'influence de la conception et du dimensionnement du micromélangeur dans la réaction entre 2.1 (en THF) et *n*-BuLi (en hexanes) à 20 °C (Fig 4).



<sup>a</sup> Des expériences ont été réalisées avec : [2.1] = 0,1 M en THF, [n-BuLi] = 0,3 M en hexane. Taille du réacteur : DI = 0,5 mm, L = 3 cm.

<sup>b</sup> Mesuré par GC-MS et <sup>19</sup>F RMN. Valeur moyenne sur 2 cycles (reproductibilité de ± 2 %).

<sup>c</sup> Sélectivité des produits = [2.2]/([2.2] + [autres produits]) 100.

Avec DI = 500 μm et  $t^R$  = 100 ms (entrées 1 à 7), les conversions étaient inférieures à 60 % pour chaque microréacteur à l'exception d'un angle = 90 et 45° (60 et 63 % respectivement) qui offrait également la meilleure sélectivité E/Z (90:10 et 86:14 respectivement ; entrées 3 et 7). La réalisation des expériences avec un DI plus petit (250 μm) a eu un effet énorme sur l'échange Br-Li avec cinq réacteurs permettant des conversions >90% et dans les huit cas offrant le carbénoïde piégé désiré 2 >88% (entrées 8-15).

En ce qui concerne la sélectivité E/Z, les microréacteurs en forme de Y,  $\theta = 105^\circ$  et en forme de W,  $\theta = 45^\circ$  ont conduit aux meilleurs rapports isomériques (entrées 10 et 14, respectivement). Cependant, lorsqu'on considère la sélectivité globale vers E-2.2, le micromélangeur W-45 a mené à 84 %, tandis que Y-105 n'a fourni que 73 % de E-2.2. Ces expériences démontrent donc l'effet bénéfique des petits diamètres pour la conversion et la sélectivité. Les évaluations finales à un débit élevé (8,4 mL/min,  $t^R = 40$  ms) sont présentées dans le Tableau 2.

Tableau 2: Effet des micromélangeurs dont l'angle varie de 135 à 30° à débit élevé (8,4 ml/min) sur la conversion de 2.1 en 2.2.<sup>a</sup>

Entrée	DI (μm)	Angle (°)	Débit Q (mL/min)		$t^R$ (ms)	Conversion (%) <sup>b</sup>	Sélectivité des produits 2.2 <sup>b,c</sup> (%)	Ratio E/Z
			Substrat	n-BuLi				
1	250	135	6	2.4	40	97	>99	77:23
2		120				78	>99	94:06
3		105				>99	>99	64:36
4		90				>99	>99	65:35
5 <sup>d</sup>		75				–	–	–
6		60				98	>99	68:32
7		45				90	>99	93:07
8		30				98	>99	68:32

<sup>a</sup> Des expériences ont été réalisées avec : [2.1] = 0,1 M en THF, [n-BuLi] = 0,3 M en hexane. Taille du réacteur : DI = 500 μm, L = 3 cm.

<sup>b</sup> Mesuré par GC-MS et <sup>19</sup>F RMN. Valeur moyenne sur 2 cycles (reproductibilité de ± 2 %).

---

<sup>c</sup> *Sélectivité des produits* =  $[2.2]/([2.2] + [\text{autres produits}]) \cdot 100$ .

<sup>d</sup> *Il y a eu obstruction*

Des débits plus élevés ont incontestablement amélioré la conversion vers 2.2 : malgré le temps de séjour plus long, tous les mélangeurs ont produit une conversion plus grande ou comparable par rapport à des débits plus faibles, malgré le temps de séjour plus court (la longueur et la largeur du réacteur étant maintenue constante). Cela corrobore substantiellement le concept de réponse ordonnée par diffusion et démontre la plus grande importance du mélange. Cependant, une tendance aussi claire n'a pas pu être observée en ce qui concerne la stéréosélectivité, car le précédent meilleur rapport à débit inférieur a été atteint avec Y-105 à 98:02 (tableau 1, entrée 10) et est maintenant tombé à 64:36 (tableau 2, entrée 3) tandis que Y-120 augmente de 89:11 à 94:06 (tableau 1, entrée 9 ; tableau 2, entrée 2). La seule conclusion claire qui peut être tirée est que le rendement élevé du W-45 est demeuré constant (83 % dans l'ensemble pour le E-2.2).

Si l'augmentation de la conversion dans un temps plus court peut être correctement expliquée par un mélange amélioré, la manière dont le mélange affecte la stéréochimie de la réaction reste floue à ce stade. Au moins deux hypothèses non exclusives pourraient expliquer les sélectivités observées : la première pourrait être un équilibre rapide entre la forme *Z* et *E* du carbénoïde intermédiaire.

L'un des isomères serait le produit cinétique, tandis que l'autre, qui est préféré thermodynamiquement, se formerait progressivement. La deuxième idée est soutenue par la réactivité spécifique des espèces organolithiées liée à leur état d'agrégation. Cet état dépend fortement de l'environnement chimique, y compris les solvants, les additifs, etc.<sup>14,15</sup>

Il a été postulé que selon la qualité du mélange, l'environnement chimique des espèces limitées serait de diverses compositions. Cette hypothèse repose sur la réactivité particulière des espèces organolithiées associées à leur état d'agrégation. Cet état dépend fortement de l'environnement chimique, y compris les solvants et les additifs. Par exemple, le *n*-BuLi est hexamérique dans l'hexane, alors qu'il se trouve sous un mélange tétramère/dimère dans le THF.<sup>16</sup> On pourrait supposer que, selon la qualité du mélange, l'environnement chimique des espèces lithiées sera de composition différente. Dans le pire

des cas, un régime laminaire et un mauvais mélange forceraient le THF et l'hexane à s'écouler côte à côte dans des domaines bien définis, alors que dans le meilleur cas de mélange parfait, la solution entière serait homogène avant que la réaction ne se produise. Cela aurait un impact profond sur l'état d'agrégation des espèces d'organolithium, *n*-BuLi et/ou carbénoïde **2.A** modifiant finalement leur réactivité. Pour vérifier cela, plusieurs expériences ont été réalisées en utilisant le même solvant pour les deux flux. Avec l'hexane comme solvant commun (et *l*'-PrOH utilisé pour garder le mélange de réaction homogène), le système s'est immédiatement bouché quel que soit l'angle du micromélangeur, probablement en raison de la précipitation du bromure de lithium (LiBr). Préparer une solution de *n*-BuLi dans le THF s'est avéré très difficile, car les solutions de *n*-BuLi entraîne une dégradation rapide du THF à température ambiante.<sup>15-17</sup>

L'hypothèse de l'équilibre, par contre, a été écartée par des expériences dédiées : une configuration de flux continu a été mise en œuvre avec un débit fixe  $Q_{(2.1+n-BuLi)}$  (9 ml/min) et un micromélangeur ( $\theta = 90^\circ$ , DI = 500  $\mu\text{m}$ ), et seule la longueur du tube du réacteur a été modifiée avec un DI fixe = 500  $\mu\text{m}$  ; Figure 4.25 :

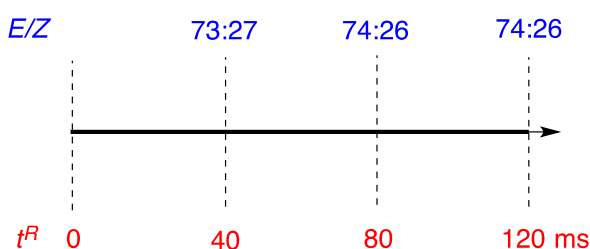


Figure 4.25: Evolution du rapport E/Z de **2** en fonction du temps dans une configuration de flux.

Avec  $L = 3$  cm ( $t^R = 40$  ms), 6 cm ( $t^R = 80$  ms) et 9 cm ( $t^R = 120$  ms), la conversion complète en **2.2** a été observée avec presque aucune évolution du rapport E/Z dans le temps. Ainsi, il semble peu probable que les variations de stéréosélectivité observées dans un temps de réaction similaire lors d'expériences avec divers micromélangeurs proviennent d'une isomérisation purement thermodynamique.

## Conclusion de la première partie

Nous avons étudié la stéréosélectivité de l'échange lithium-brome sur le gem-dibrome alcène dans un système à flux continu, avec seize mélangeurs passifs qui ont deux diamètres internes de 500  $\mu\text{m}$  et 250  $\mu\text{m}$  et huit angles variables (de 135 à 30°). À 20 °C et à différents débits, le mélangeur en forme de W de 45° a fourni la meilleure sélectivité pour le produit E-monobromé. Ce travail montre qu'il est possible d'obtenir des molécules fonctionnalisées avec une géométrie régulée. Ce travail ouvre la porte à l'accès à des structures plus complexes, comme c'est le cas des polymères.

## Polymérisation anionique dans les réacteurs à flux continu

Des dispositifs comme les microréacteurs peuvent être utilisés pour la synthèse organique, la production de médicaments et comme moyen de contrôler les structures polymères dans la réaction. Pour la synthèse des polymères, il est essentiel de contrôler précisément la masse molaire et sa distribution, en utilisant une polymérisation hautement contrôlée.

Basé sur le concept de microréacteur à flux continu, la polymérisation contrôlée a été développée pour divers composés, tels que : styrène, méthacrylates d'alkyle et isobutyl vinyl éther. Par exemple, Nagaki *et coll.* (2010) ont travaillé à la polymérisation anionique du styrène en flux continu (Fig 5).<sup>18</sup>

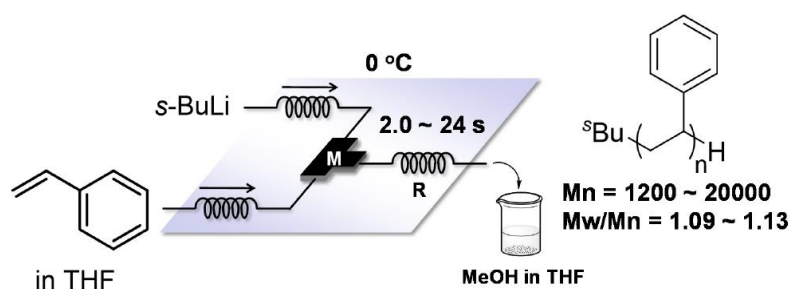


Fig 5: Polymérisation anionique du styrène en flux continu (extrait de Nagaki *et coll.*, 2019).<sup>18</sup>

Ces résultats montrent qu'il est possible d'effectuer une polymérisation anionique en flux continu et qu'il est facile de contrôler de grandes à petites masses molaires ( $\overline{Mn}$ ) de polymère comme  $\overline{Mn}$ =1200-20000 g/mol.

Voulant associer la microfluidique, qui permet le contrôle de la polymérisation, à l'utilisation de ressources renouvelables nous proposons la polymérisation du Myrcène, un analogue de l'isoprène, par voie anionique.

### Un terpène intéressant : le Myrcène

Le myrcène est connu pour son utilisation comme agent aromatisant. En raison de ses caractéristiques, il est utilisé dans différentes applications dans les industries alimentaires telles que les boissons.<sup>19</sup>

Le myrcène appartient à la famille des monoterpènes, et il se présente sous deux formes :  $\alpha$ -myrcène et  $\beta$ -myrcène (Figure 4.26).

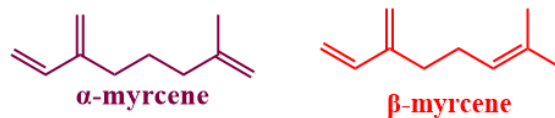


Figure 4.26: Structure alpha et  $\beta$ -Myrcène et propriétés chimiques.

Les deux formes se trouvent dans la nature, mais le  $\alpha$ -myrcène n'est pas abondant, et à cause de cela le  $\beta$ -myrcène est souvent simplement appelé myrcène dans la littérature.<sup>19</sup> En raison de sa structure, le Polymyrcène peut facilement être considéré comme un substitut du polybutadiène ; et du polyisoprène (Figure 4.27).

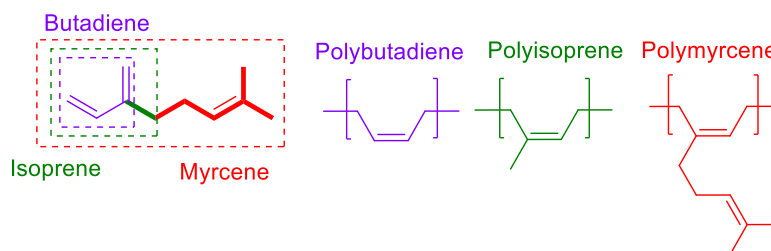


Figure 4.27 : Similitudes de structure entre le butadiène, isoprène et le Myrcène.

Le myrcène est un composé que l'on trouve dans la nature et qui est disponible dans le commerce. En comparant les prix du  $\beta$ -myrcène avec d'autres monomères similaires, le myrcène est peu coûteux. De plus, le myrcène peut être polymérisé par voie anionique, et comme matériau de départ, il n'est relativement pas cher. Toutes ces caractéristiques font de ce terpène,  $\beta$ -Myrcène, l'objet de nombreuses recherches et y compris dans ce travail.



## Synthèse du Polymyrcène

Le Polymyrcène a été synthétisé par différentes voies, comme par polymérisation radicalaire libre<sup>20</sup> ou contrôlé,<sup>21</sup> mais aussi par polymérisation coordinative,<sup>22</sup> cationique<sup>23</sup> et anionique.<sup>24</sup> La microstructure du Polymyrcène est composée de différents isomères, dont la présence est fonction des conditions de réaction (Fig 6). Si l'addition est 1,4 l'apparition de deux isomères, cis et trans peut être observée. La structure 3,4 et le vinyle 1,2 sont également présents.

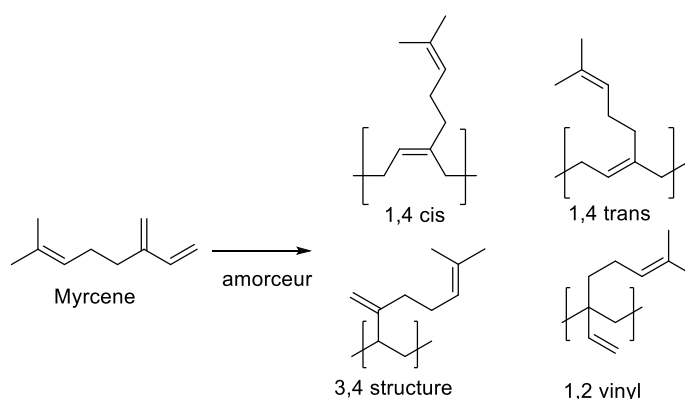


Fig 6 : Polymérisation du Myrcène et ses différentes microstructures.

## Polymérisation anionique du Myrcène

Dans ces travaux on est intéressé par la polymérisation anionique du Myrcène en flux continu.

La polymérisation anionique du Myrcène a été réalisée de plusieurs façons. En 1988, Newmark et Majumdar ont synthétisé de façon anionique le cis-Polymyrcène et le cis-polyfarnésène avec le *sec*-butyllithium comme amorceur pour déterminer leur microstructure par <sup>13</sup>C-RMN.<sup>25</sup> De la même façon, Ávila-Ortega *et coll.* ont rapporté la synthèse anionique d'amine  $\omega$ -terminaison pour le Polymyrcène, en utilisant le *sec*-butyllithium comme amorceur de la polymérisation.<sup>26</sup>

Parmi les différents types de polymérisation, la polymérisation anionique est l'une des méthodes utilisées industriellement pour polymériser les diènes. Certaines des caractéristiques de ce type de polymérisation sont : pureté des réactifs et solvants requis (pas d'humidité dans le solvant), degré de réactivité du carbanion : solvants limités aux hydrocarbures et aux éthers (hexane, THF, etc.), polymérisation sous atmosphère inerte (azote, argon).

Dans le cas de la polymérisation anionique, l'étape initiale est atteinte lorsque le transfert électronique a lieu. L'étape de propagation commence par l'ajout des monomères, puis se termine par la désactivation ou l'arrêt de la réaction (Fig 7).

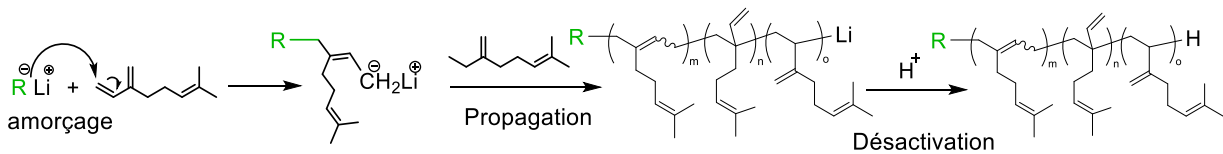


Fig 7:Étapes de la polymérisation anionique du Myrcène (seulement la structure 1,4 est présentée pour faire une simplification du schéma).

Ce type de polymérisation est intéressant en raison de sa faible polydispersité et de son caractère vivant. Dans le cas du Polymyrcène il produit des élastomères (homopolymères ou copolymères).

### Les organolithiums

Les organolithiums sont utilisés comme amorceurs dans les réactions de polymérisation anionique, car ils sont composés de liaisons carbone-lithium. Cette liaison C-Li est polaire car il y a une énorme différence d'électronégativité entre le carbone (2,55) et le lithium (0,98).<sup>27</sup> Ces composés sont de très bons nucléophiles ou bases fortes.<sup>28</sup>

### Polymérisation du myrcène en réacteur conventionnel et en flux continu

Une fois que on a bien maîtrisée les conditions d'un système à flux continu, tels que mélange, température, débit etc., la polymérisation du myrcène en flux continu a été développée. Le principal objectif de la réaction de polymérisation est d'obtenir des oligomères à masse molaire contrôlée et de déterminer la limite de la stratégie à flux continu.

## Paramètres de réaction généraux

Comme expliqué ci-dessus, des paramètres clés ont été fixés pour développer cette réaction, tels que le monomère, l'amorceur, solvant et température.

## Polymérisation anionique

Des monomères et des solvants purs, ainsi que des conditions anhydres, sont nécessaires dans la polymérisation anionique pour empêcher toute consommation indésirable du centre actif. Le centre actif étant le site sur une chaîne où la réaction a lieu.

**Monomères :** En dehors des molécules hétérocycliques, les monomères sensibles à la polymérisation anionique ont généralement des substituants qui stabilisent la charge électronégative (groupes de retrait électronégatif) du centre actif. Il s'agit de monomères non polaires comme le styrène, le butadiène ou l'isoprène (ou d'autres 1,3 diènes) et de monomères polaires comme la vinylpyridine, et les acrylates.

Dans ce projet nous avons souhaité étudier la polymérisation anionique du myrcène dans des réacteurs conventionnels et la comparer à la polymérisation du myrcène en flux continu.

Les oligomères télchéliques utilisés industriellement ont  $1000 < \bar{M}_{th} < 5000$ .<sup>29</sup> Ainsi, notre objectif a été de préparer des oligomères ayant un  $\bar{M}_n$  maximum de 2500. Par conséquent, toutes les expériences (batch et flux continu) ont été réalisées avec un ratio de 17/1 (monomère/amorceur) pour permettre  $\bar{M}_{th} = 17 * 136 = 2312 \text{ g/mol}$ .

**Solvants :** Un mélange THF/hexane a été utilisé afin d'avoir une initiation rapide de la polymérisation, et des temps de réaction rapide à 10 °C.

**Température :** Selon la bibliographie,<sup>30</sup> la dégradation d'alkyllithiums devrait se produire lorsque la température est supérieure à 30 °C dans le THF. En effet, une réaction de décomposition du THF avec les organolithiens est généralement observée (après 100 min à 20°C pour le *n*-BuLi, dès 5 min à 30 °C).<sup>31</sup> De ce fait on a fixé la température à 10 °C pour les réactions en batch.

## Etude de la polymérisation anionique du myrcène en batch

L'effet de taille a été étudié en réacteur conventionnel, cela nous a permis de mettre en évidence la difficile régulation de la température dans ces conditions. En effet, à même concentration en monomère et amorceur nous avons observé une variation de la cinétique de polymérisation selon que l'on travaillait avec des batch de 0.1 g, 1 g ou 17g en monomères. Cela est clairement observé en suivant l'évolution des masses molaires au cours du temps (Tableau 3).

Tableau 3: Polymérisation anionique du Myrcène avec *n*-BuLi en batch à différentes échelles.<sup>a</sup>

Entrée	Myrcène (g)	t (min)	$\overline{M}_n$ RMN (g/mol) <sup>b,c</sup>	$\overline{M}_n$ GPC (g/mol) <sup>b</sup>	Đ	Rdt (%) <sup>d</sup>	Conv. (%) <sup>e</sup>	$\overline{M}_n$ th. <sup>f</sup>
1	0.110	2	650	600	1.23	28	28	648
2		10	1050	1300	1.26	53	45	1227
3		20	2200	1850	1.19	71	95	1644
4		30	2400	1900	1.23	91	104	2107
5	1	1	970	900	1.24	20	42	463
6		2	800	950	1.14	32	35	741
7		4	1700	1600	1.12	61	73	1412
8		8	2330	2050	1.14	90	101	2084
9		10	2200	2800	1.24	59	95	1366
10		30	2700	3250	1.23	68	117	1574
11		60	2600	3000	1.35	65	112	1505
12	17	1	2060	2300	1.13	88	89	2038
13		10	2100	2000	1.17	92	91	2130

<sup>a</sup> Chaque expérience a été réalisée deux fois. Effectué à 10 °C avec du Myrcène/*n*-BuLi = 17:1. <sup>b</sup> Masse moléculaire moyenne. <sup>c</sup> Les rendements de RMN <sup>1</sup>H sont calculés en comparant l'intensité relative du groupe CH<sub>3</sub> de l'amorceur ( $\delta = 0,87$  ppm) avec celle du vinyle CH de PMYR ( $\delta = 4,75$  ppm). <sup>d</sup> d'après la quantité matière de PMYR récupérée après l'élimination complète des composés volatils (y compris le Myrcène). <sup>e</sup> basé sur le  $\overline{M}_n$  (<sup>1</sup>H RMN)/2316×100. <sup>f</sup>  $\overline{M}_n$  théorique = rendement×2316/100

Par ailleurs, la réaction reproduite en présence d'une sonde thermique à l'intérieur du milieu réactionnel (dans le cas batch à 17g) montre que dès que le *n*-BuLi a été ajouté au milieu la réaction a bondi de 10 à 45 °C en 1 minute.

En calculant le S/V dans les trois conditions, on s'aperçoit que cette valeur diminue lorsque la quantité de matière augmente traduisant une moins bonne évacuation de la chaleur. Ceci vient corroborer l'observation précédente. En calculant de même S/V pour un système tubulaire (S/V=80 cm<sup>-1</sup>, DI 0,5 mm), on entrevoit immédiatement l'intérêt de la microfluidique concernant le contrôle de la température du milieu réactionnel (Tableau 4).

Tableau 4: Polymérisation du myrcène en batch à différentes échelles après 1 min de réaction (rempli jusqu'à 60%).

Entrée	Echelle (g)	S/V	$\overline{Mn}$ (g/mol)	Rendement (%)
		(cm <sup>-1</sup> )	<sup>1</sup> H NMR	<sup>1</sup> H NMR
1	17.0	0.86	2050	88
2	1.0	3.6	950	20
3	0.1	6	410	11

### Etude de la polymérisation anionique du myrcène en microfluidique

**Installation :** Tous les réacteurs en acier inoxydable ont été fabriqués en interne et séchés pendant la nuit dans un four à 120 °C avant leur utilisation. Cette partie est essentielle pour éviter l'humidité dans le système. Une fois chaque pièce séchée, le système est assemblé. La Fig 8 montre un schéma du montage expérimental.

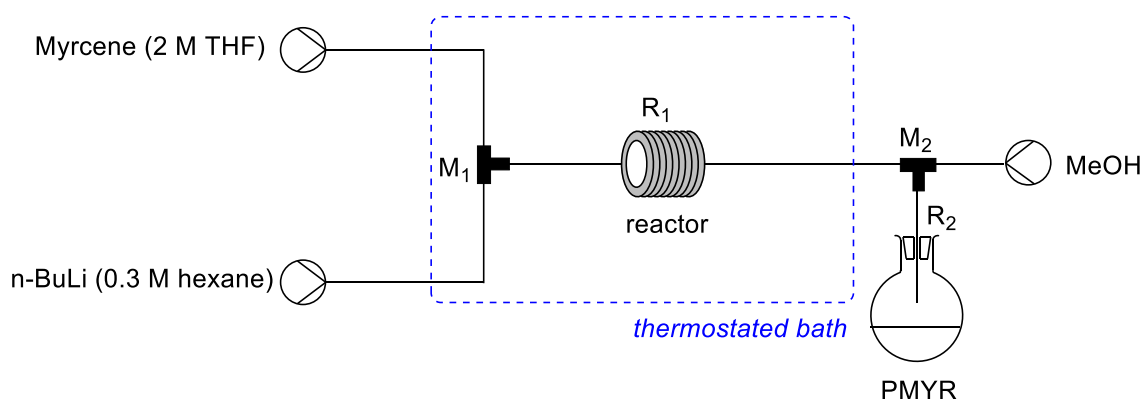


Fig 8: Schéma de la configuration utilisée dans les conditions de flux continu pour la synthèse de Polymyrcène.

Le système comprend différents éléments tels que des pompes à seringues, des tubes en acier inoxydable et des connexions/jonctions (PFA et acier inoxydable), des mélangeurs (M), des réacteurs (R) (750µm DI, de différentes longueurs) et un bain thermostaté.

Les solutions sont pompées avec des pousse seringues. Le système possède une première entrée contenant une solution de Myrcène dans le THF (2 M) et une seconde entrée avec une solution *n*-BuLi (0,3 M en hexanes). Les solutions sont d'abord passées par un micromélangeur en forme de T (acier inoxydable, 500 µm de diamètre interne (DI) connecté à un microréacteur tubulaire (acier inoxydable, 750 µm DI, 1 m de longueur) au

débit souhaité. Ce microréacteur est immergé dans un bain thermostaté à 10 °C. Le deuxième micromélangeur en forme de T (500 µm DI) sert à terminer la réaction avec du méthanol. Le mélange est passé par un deuxième tube de 300 mm de longueur et 750 µm DI avant collecte dans un flacon contenant 2 ml de HCl 2 M. Avant tout prélèvement trois volumes morts de réactifs ont été passés dans le système pour assurer l'équilibre du réacteur. Ensuite entre 2 et 5 mL ont été prélevés pour analyse.

**Choix du débit :** Les matières premières, le Myrcène/*n*-BuLi/MeOH, ont été injectées à des débits de 0,25/0,1/0,1 mL.min<sup>-1</sup> respectivement dans un réacteur à tubes en acier inoxydable de 0,75 mm de diamètre interne (DI) et de 1 m de longueur.

### Taille et débit des réacteurs

Le temps de séjour ( $t^R$ ) est d'importance en microfluidique. Il peut être contrôlé en modifiant la longueur du réacteur tubulaire ou le débit de la pompe. Dans notre cas, ( $t^R$ ) devrait influencer la longueur de la chaîne macromoléculaire.

### Temps de séjour contrôlé par la longueur du réacteur tubulaire (débit fixe)

Des réacteurs tubulaires de 0,5 à 8m ont été utilisés en utilisant le même débit, Myrcène/*n*-BuLi (mL/min) : **0,25/0,1 à 10 °C**. Les résultats montrent que contrôlant le temps de séjour il est possible de contrôler aussi la masse molaire du polymyrcène (Tableau 5).

Tableau 5: Différentes expériences avec un débit de 0,25/0,1 Myrcène/*n*-BuLi (mL/min) à 10 °C.<sup>a</sup>

Entrée	Longueur du réacteur (m)	$t^R$ (s)	$\overline{Mn}$ (g/mol)		$D$	Rdt (%) <sup>d</sup>	Conv. (%) <sup>e</sup>	$\overline{Mn}_{th}$ <sup>f</sup>
			<sup>1</sup> H RMN	GPC				
1	0,5	38	450	400	1,44	13	19	301
2	1,0	75	700	600	1,27	28	30	648
3	1,6	120	1000	850	1,33	42	43	972
4	2,0	157	1150	900	1,19	54	50	1250
5	2,4	180	1300	1050	1,16	57	56	1320
6	3,0	227	1050	1200	1,43	47	45	1088
7	4,0	302	1500	1400	1,20	69	65	1598
8	8,0	600	2100	1700	1,36	54	91	1250

<sup>a</sup> Chaque expérience a été réalisée deux fois. Effectué à 10 °C avec du Myrcène/*n*-BuLi = 17:1. <sup>b</sup> Masse moléculaire moyenne. <sup>c</sup> Les rendements de RMN <sup>1</sup>H sont calculés en comparant l'intensité relative du groupe CH<sub>3</sub> de l'amorceur ( $\delta = 0,87$  ppm) avec celle du vinyle CH de PMYR ( $\delta = 4,75$  ppm). <sup>d</sup> d'après la quantité matière de PMYR récupérée après l'élimination complète des composés volatils ( $\gamma$  compris le Myrcène). <sup>e</sup> basé sur le  $\overline{Mn} = (^1H\text{ RMN})/2316 \times 100$ . <sup>f</sup>  $\overline{Mn}_{th} = \text{rendement} \times 2316/100$

## Temps de séjour fixé

Des réactions utilisant des réacteurs de tailles différentes (0,5, 1, 8 m), des débits différents, pour une durée de résidence fixée (75 s) ont été réalisées. Les résultats ont montré qu'il n'y a pas de différence significative dans la masse molaire obtenue (Tableau 6). Cela est important parce qu'il nous permet de modifier le débit ou la taille du réacteur. Cela signifie que le mélange (influencé par le débit dans la zone de mélange) ne semble pas être un paramètre majeur dans cette réaction entre *n*-BuLi (en hexane) et Myrcène (en THF). Probablement parce qu'une initiation anionique instantanée du Myrcène par *n*-BuLi se produit même à faible débit dans nos conditions (THF). Ainsi, le  $t^R$  peut être réglé soit par le débit, soit par la taille du réacteur, indifféremment (chaque expérience a été réalisée deux fois).

Tableau 6: Expériences utilisant des réacteurs de 0,5, 1 et 8 m.<sup>a</sup>

Entrée	Débit Myr/ <i>n</i> -BuLi (mL/min)	Longueur du réacteur (m)	$\overline{Mn}$ (g/mol)		$\overline{D}$	Rdt (%) <sup>d</sup>	Conv. (%) <sup>e</sup>	$\overline{Mn}_{th.}$ <sup>f</sup>
			<sup>1</sup> H RMN	GPC				
1	0,125/0,05	0,5	800	650	1,10	26	35	602
2	0,25/0,1	1,0	700	650	1,27	28	32	648
3	2/0,8	8,0	850	550	1,23	47	37	1088

<sup>a</sup> Chaque expérience a été réalisée deux fois. Effectué à 10 °C avec du Myrcène/*n*-BuLi = 17:1. <sup>b</sup> Masse moléculaire moyenne. <sup>c</sup> Les rendements de RMN <sup>1</sup>H sont calculés en comparant l'intensité relative du groupe CH<sub>3</sub> de l'amorceur ( $\delta = 0,87$  ppm) avec celle du vinyle CH de PMYR ( $\delta = 4,75$  ppm). <sup>d</sup> d'après la quantité matière de PMYR récupérée après l'élimination complète des composés volatils (*y* compris le Myrcène). <sup>e</sup> basé sur le Mn (<sup>1</sup>H RMN)/2316×100. <sup>f</sup> Mn théorique = rendement×2316/100

## Taille du réacteur fixée

Le fait de maintenir la taille du réacteur constante (8 m) et de modifier le débit a entraîné un temps de séjour différent (Tableau 7). En faisant la comparaison avec de tableaux précédentes Les résultat montrent que contrôlant le temps de séjour il est possible de contrôler aussi la masse molaire du polymyrcène (Tableau 5) il est montré que des résultats similaires ont été obtenus.

Tableau 7: Expériences utilisant un réacteur de 8 m à 10 °C avec différents débits. <sup>a</sup>

Entrée	Débit Myr/ <i>n</i> -BuLi (mL/min)	$t^R$ (s)	$\overline{Mn}$ (g/mol)		$D$	Rdt (%) <sup>d</sup>	Conv. (%) <sup>e</sup>	$\overline{Mn}_{th}$ <sup>f</sup>
			<sup>1</sup> H RMN	GPC				
1	4/1,6	38	600	350	1,16	29	26	671
2	2/0,8	75	900	550	1,23	47	39	1088
3	0,25/0,1	600	2100	1700	1,36	54	91	1250

<sup>a</sup> Chaque expérience a été réalisée deux fois. Effectué à 10 °C avec du Myrcène/*n*-BuLi = 17:1. <sup>b</sup> Masse moléculaire moyenne. <sup>c</sup> Les rendements de RMN <sup>1</sup>H sont calculés en comparant l'intensité relative du groupe CH<sub>3</sub> de l'amorceur ( $\delta = 0,87$  ppm) avec celle du vinyle CH de PMYR ( $\delta = 4,75$  ppm). <sup>d</sup> d'après la quantité matière de PMYR récupérée après l'élimination complète des composés volatils (*y* compris le Myrcène). <sup>e</sup> basé sur le  $\overline{Mn}({}^1H\text{ RMN})/2316 \times 100$ . <sup>f</sup>  $\overline{Mn}_{th} = \text{rendement} \times 2316/100$

Avec le système à flux continu, il est possible de sélectionner précisément le nombre d'unités monomères avec  $\overline{Mn}=450$  ( $t^R = 19$  s; entrée 4) à 2100 ( $t^R = 600$  s; entrée 19). Il convient de noter qu'un tel réglage de  $t^R$ , et donc  $\overline{Mn}$  de PMYR, est inaccessible dans un réacteur en batch.

Par conséquent, en comparant tous ces résultats, on peut établir une relation entre le temps de résidence et la masse molaire obtenue du polymère. Ainsi, à partir de ces résultats, on peut conclure que la polymérisation du Myrcène dans des conditions microfluidique est finement contrôlée à l'inverse de la polymérisation par batch, qui présente des problèmes de transfert de masse et de chaleur.

### Microstructure dans des conditions de flux continu

Les expériences sur la réaction de polymérisation en milieu THF/hexane montrent que la configuration moléculaire du polymère observée est de l'ordre ~10% pour 1,2 vinyle, ~60 % pour 3,4 structure et ~30 % pour 1,4 que ce soit en batch ou en microfluidique et en accord avec la littérature.<sup>32</sup>

Tableau 8: Microstructure batch vs flux continu.

Entrée	Conditions	Hexane V/V%	1,2- %	3,4- %	1,4- %
1	BATCH (17 g)	14	10	57	33
2	FLUX	29	12	66	22

### Fonctionnalisation finale et Polymyrcène téléchélique dans un système à flux continu

Comme mentionné, le caractère de polymérisation vivante est un des avantages de la polymérisation anionique. Afin de confirmer le caractère vivant de la polymérisation, il a



été décidé de piéger une fonction pertinente au lieu d'un simple atome d'hydrogène. Cette fois-ci la fonctionnalisation du Polymyrcène est réalisée avec du TMSCl et du CO<sub>2</sub> gaz.

### Synthèse du Polymyrcène TMS fonctionnalisé en conditions de flux continu

En introduisant une entrée de chlorotriméthylsilane à la fin du système avant la précipitation en solution acide (HCl 2 N), on peut synthétiser le Polymyrcène avec une terminaison TMS (Fig 9).

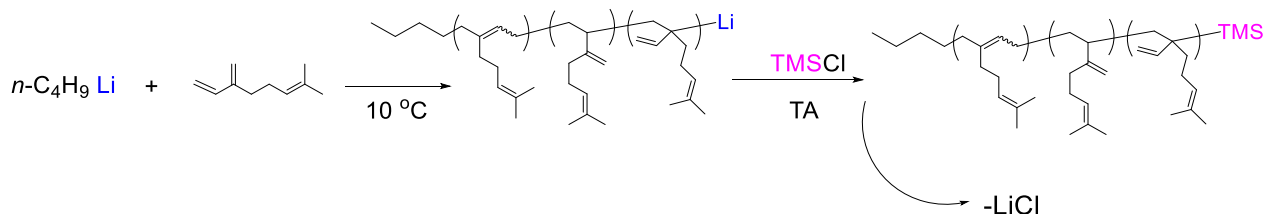


Fig 9: Fonctionnalisation du Polymyrcène avec terminaison TMS.

Le mélange est extrait avec du dichlorométhane (3 x 10 mL), lavé avec de l'eau (20 mL), séché sur du sulfate de magnésium et concentré sous vide pour permettre un mélange brut, analysé au moyen de RMN. Fig 10 montre la configuration expérimentale utilisée dans ce cas.

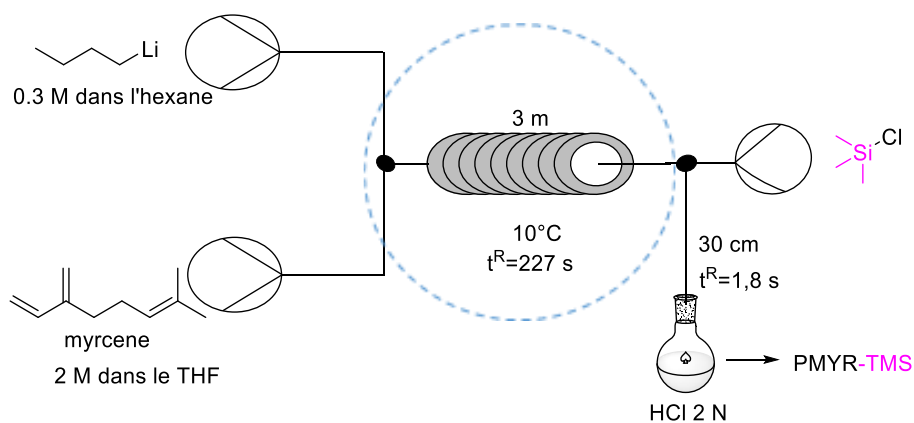


Fig 10: Configuration expérimentale pour la fonctionnalisation finale de TMS avec mix THF/TMSCl.

Une expérience représentative a été réalisée avec  $t^R = 229$  s, et le degré de fonctionnalisation a été déterminé par des analyses <sup>1</sup>H RMN en comparant les signaux (CH<sub>3</sub>)<sub>3</sub> de TMS avec le signal CH<sub>3</sub> de l'amorceur *n*-BuLi : un degré de fonctionnalisation de 73 % a été mesuré, En montrant ainsi le caractère vivant de ce processus. Il convient de

noter que la fonctionnalisation incomplète du polymère avec la terminaison TMS est très probablement due aux traces de HCl dans le TMSCl (injecté pur).

Certaines conclusions peuvent être tirées, la fonctionnalisation finale de PMYR avec TMS est réalisée en flux continu dans un rendement raisonnable. Les valeurs de dispersion et de masse molaire ( $\mathcal{D}=1.9$ ,  $\overline{Mn} = 1500$ ) demeurent raisonnables comme celles obtenues auparavant. Ces résultats confirment la polymérisation vivante du PMYR, aboutissant à une méthode de mode pour obtenir un oligomère fonctionnel.

Une fois le Polymyrcène fonctionnalisé au TMS obtenu, nous nous sommes intéressés à la fonctionnalisation en utilisant le CO<sub>2</sub> gaz.

### **Polymérisation anionique du Myrcène/fonctionnalisation avec du CO<sub>2</sub> dans un système d'écoulement**

De nos jours, le dioxyde de carbone est utilisé dans la production de molécules et de polymères fonctionnels.<sup>33-34</sup> Cependant, les méthodes de réutilisation du CO<sub>2</sub> demeurent un défi, car les réactions en deux phases sont difficiles à réaliser.<sup>35</sup>

Yoshida *et coll.* ont signalé une réaction de carboxylation gaz-liquide dans des conditions de batch et en microflux (Fig 11). La réaction de carboxylation a d'abord été effectuée dans des conditions de batch, donnant 28 % du produit désiré à 0 °C. En revanche, en faisant la même réaction en flux continu, 87 % du produit d'acide carboxylique a été obtenu à la même température.<sup>36</sup>

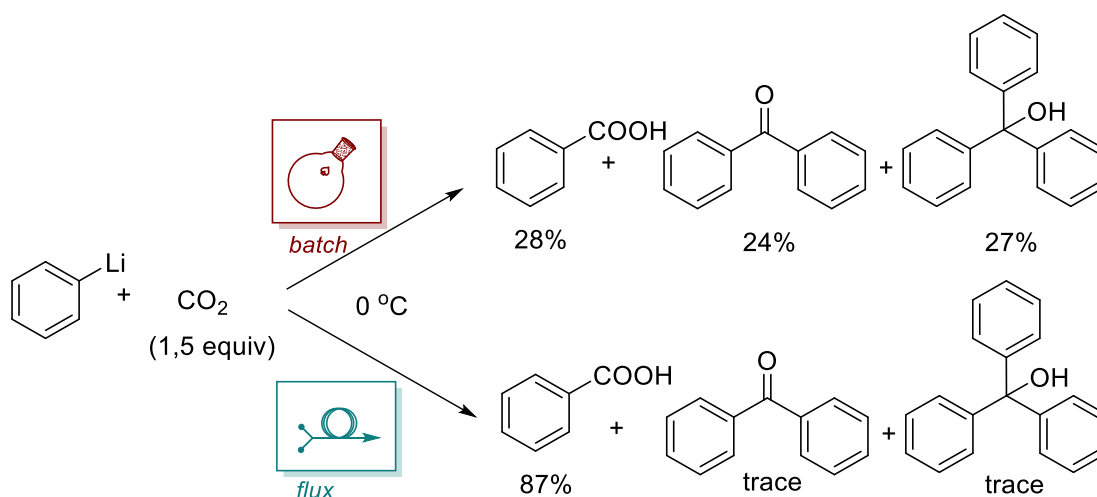


Fig 11: Réaction du phényllithium avec le dioxyde de carbone.

Ces résultats ne sont pas surprenants étant donné que les systèmes à flux continu se sont révélés généralement plus efficaces que les conditions de batch classiques pour les réactions gaz/liquide biphasiques, en particulier pour le piégeage difficile du  $\text{CO}_2$ , qui souffre souvent d'ajouts concurrents consécutifs non sélectifs (acide carboxylique – cétone – alcool tertiaire). Ainsi, un système de réacteur à flux alimenté avec un réactif organométallique ( $\text{R-Li}$  ou  $\text{R-MgX}$ ) dans une première entrée, et un réservoir de  $\text{CO}_2$  connecté à un régulateur de débit massique dans une seconde entrée ont fourni le produit sélectif mono-addition  $\text{R-CO}_2\text{H}$  sans produits en trop, même sans conditions cryogéniques. Inversement, des ajouts concurrentiels consécutifs se sont produits en batch.<sup>37,38</sup>

La polymérisation concaténée/fonctionnalisation  $\text{CO}_2\text{H}$  en flux serait un moyen de surmonter tous les inconvénients associés à la synthèse par batch analogue : 1) comme a été montré le  $\overline{M}_n$  de PMYR peut être finement réglé, 2) le contact interfacial plus élevé entre les phases gazeuse et liquide devrait améliorer la sélectivité de la carboxylation. En plus, il est possible d'utiliser des quantités stœchiométriques de  $\text{CO}_2$  en flux continu, alors qu'il est généralement très difficile dans des conditions de batch.

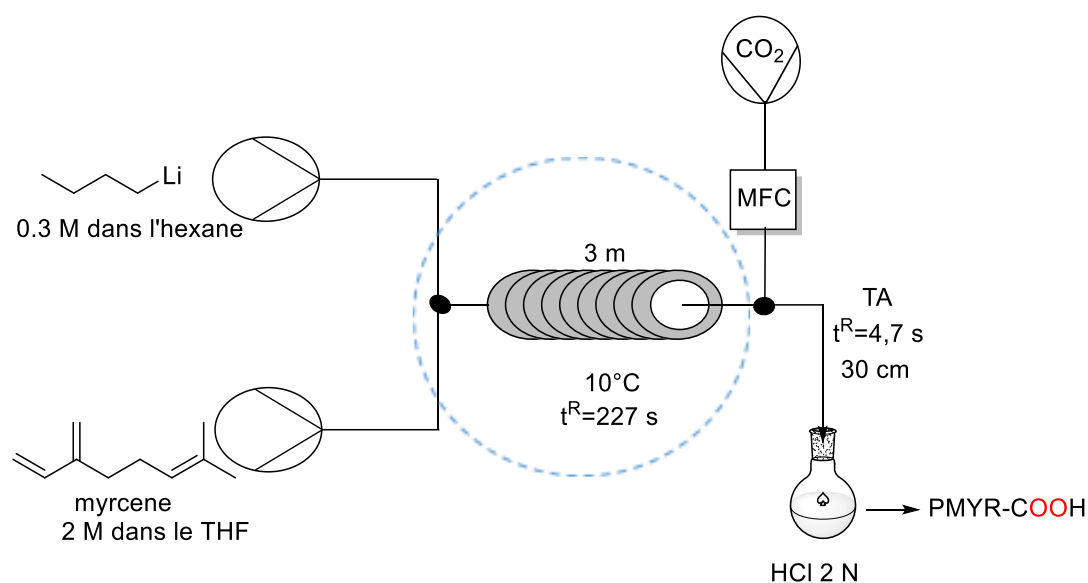


Fig 12: Montage pour la polymérisation du Myrcène/fonctionnalisation avec du CO<sub>2</sub> dans un système de débit (MFC = contrôleur de débit massique).

Ainsi, le CO<sub>2</sub> a été introduit dans le circuit précédent (Fig 12), mis en œuvre pour la polymérisation anionique contrôlée du Myrcène en raccordant une troisième entrée reliée au réservoir de CO<sub>2</sub> et contrôlé au moyen d'un régulateur de débit massique (débit constant de 1,36 mL/min sous 1 bar). La sortie a été recueillie dans une solution acide aqueuse.

Ainsi, après polymérisation du Myrcène dans un microréacteur à écoulement en acier inoxydable (DI = 0,75 mm, L = 3 m) tel que décrit ci-dessus [ $Q(\text{Myrcène}) = 0,25 \text{ mL/min}$ ,  $Q(n\text{-BuLi}) = 0,1 \text{ mL/min}$ ,  $t^R = 227 \text{ s}$ ] et le CO<sub>2</sub> a été livré dans une entrée supplémentaire (réacteur 2 : DI = 0,75 mm, L = 30 cm). Heureusement, ce processus a permis au PMYR cible de se terminer par un groupement fonctionnel PMYR-COOH utile (Tableau 9) a permis d'atteindre un degré de fonctionnalisation DF = 95% avec 3 équivalents.

Tableau 9: Expériences de fonctionnalisation finale de PMYR avec du CO<sub>2</sub> à 10 °C.<sup>a</sup>

Entrée	Reacteur	t (s) <sup>b</sup>	Débit massique (mg/min)	Débit molaire (mmol/min)	Rapport molaire n-BuLi/CO <sub>2</sub>	M <sub>n</sub> (g/mol)		D	Produit	DF (%) <sup>c</sup>
						<sup>1</sup> H RMN	GPC			
1 <sup>b</sup>	batch	60	–	–	–	1750	950	2,50	cétone	–
2 <sup>b</sup>	batch	120	–	–	–	1800	1350	2,17	cétone	–
3	MF	7,6	1,32	0,03	1:1	1000	1200	1,58	acide	30
4	MF	4,6	2,64	0,06	1:2	1050	850	1,69	acide	64
5	MF	3,6	3,96	0,09	1:3	1415	1100	1,19	acide	95

<sup>a</sup> Selon l'installation décrite à la fig. 7. <sup>b</sup> Entrées 1,2 : temps de ajout de CO<sub>2</sub> dans le ballon; Entrées 3-5 : temps de séjour dans le réacteur 2 (t<sup>R2</sup>). <sup>c</sup> Degré de fonctionnalisation (DF) calculé par RMN <sup>1</sup>H en comparant l'intensité relative de CH(CO<sub>2</sub>H) (δ = 3,05 ppm) avec le groupe CH<sub>3</sub> de l'amorceur de la chaîne butylique de PMYR (δ = 0,86 ppm).

Il convient de noter qu'une expérience parallèle a été menée dans des conditions de batch (Tableau 9, entrées 1 et 2) qui ont donné un résultat différent : une cétone connectée à deux groupes de PMYR a été obtenue comme produit principal, comme l'atteste la RMN <sup>13</sup>C dans laquelle un signal à δ = 207,19 ppm, typique d'un fonction -C(=O)- est apparu (contrairement à δ (CO<sub>2</sub>) = 178,48 et 177,89 ppm détectés pour le polymyrcene en flux continu.

Cette différence de réactivité (confirmant ainsi les observations précédentes de Yoshida et de Jamison avec de petits organométalliques) est représentée dans la Fig 13 avec les trajectoires de réaction correspondantes.

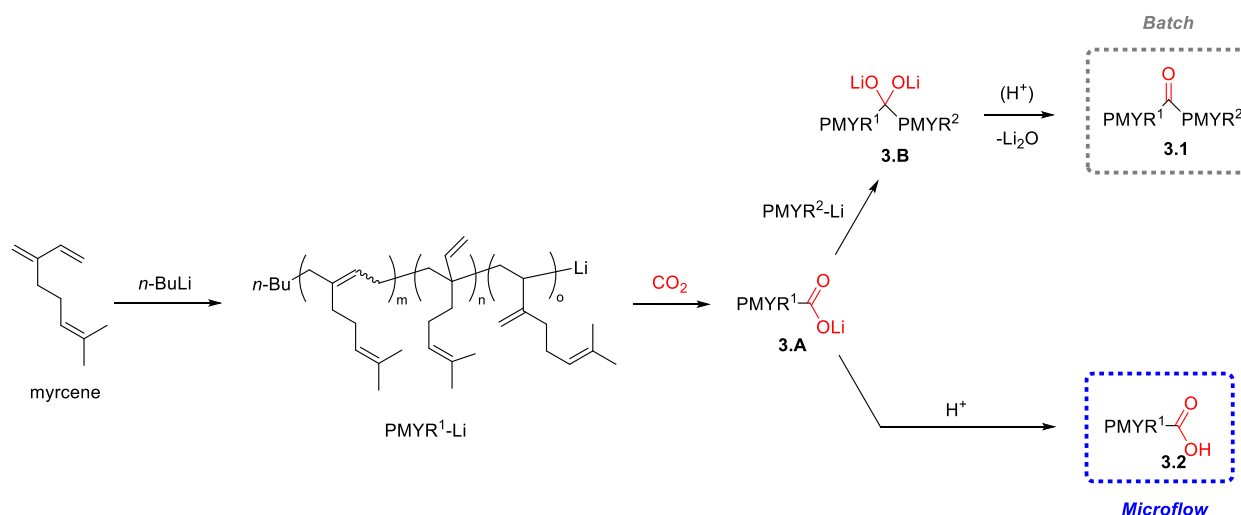


Fig 13: Fonctionnalisation finale du PMYR : réactivité selon les conditions de batch ou flux continu.

Ainsi, dans n'importe quel réacteur, le PMYR-Li s'ajoute au CO<sub>2</sub> pour permettre l'intermédiaire. En raison d'un transfert de masse liquide/gaz plus faible dans le réacteur en batch, il y a, dans ce cas, une coexistence entre le PMYR-Li et le **3.A** qui peut subir une seconde addition pour produire du **3.B**. Cette dernière, après élimination de l'oxyde de lithium (Li<sub>2</sub>O), fournit la cétone (PMYR)<sub>2</sub>C=O. Outre les problèmes de mélange, une explication plausible de cette divergence de réactivité réside dans une dichotomie majeure entre les conditions de batch et flux continu : la composition du milieu de réaction selon l'espace et le temps.

Dans un réacteur en batch, la composition chimique du milieu de réaction évolue avec le temps à mesure que la conversion des réactifs/substrats en produits augmente. En revanche, dans les conditions de flux continu, la conversion augmente le long du réacteur, et les produits normalement ne rencontrent pas les substrats. Dans notre cas, cette caractéristique majeure évite les réactions entre PMR-Li et le produit primaire **3.A**, et donc les produits concurrents indésirables, avec des avantages pour la sélectivité chimique vers PMYR-CO<sub>2</sub>H.<sup>39</sup>

## Polymyrcène téléchélique

Une fois que la fonctionnalisation du polymyrcène a été maîtrisée en flux, on a décidé d'utiliser un amorceur bifonctionnel pour arriver à des polymères téléchéliques. Une application de Polymyrcène bifonctionnel serait la synthèse de polyesters ou, après hydrogénation, de polyuréthane biosourcé plus hydrophobes. Pour obtenir un Polymyrcène bifonctionnel, nous avons effectué plusieurs réactions en utilisant le 1,4 dilithiumbutane comme amorceur.

Comme pour la polymérisation avec le *n*-BuLi, le degré de polymérisation choisi était  $\left(\frac{\text{monomer}}{\text{initiator}} : \frac{17}{1}\right)$ , ce qui donne de petites masses moléculaires pour les polymères. Les masses moléculaires théoriques du Polymyrcène ont été obtenus à partir de  $\bar{M}_{th} = 17 * 136 = 2312$  g/mol

La réaction de polymérisation du myrcène a été transposée aux conditions microfluidiques. Des réactions avec TMS et CO<sub>2</sub>H comme électrophiles ont été effectuées.

## Résultats pour le Polymyrcène bifonctionnel avec de terminaisons TMS en flux continu

L'amorceur bifonctionnel a été introduit dans le système pour obtenir le Polymyrcène téléchélique. En utilisant le TMSCl, on obtient un Polymyrcène bifonctionnel, qui peut être utilisé pour caractériser la microstructure du polymère final (Fig 14).

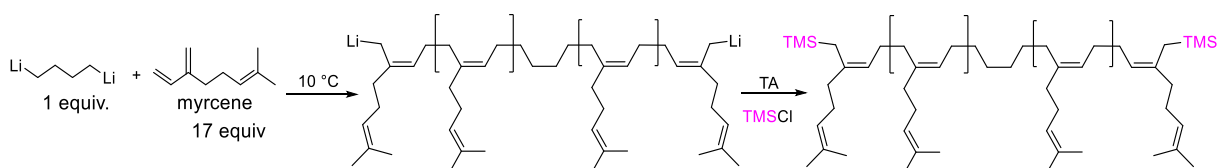


Fig 14: Polymérisation anionique du Polymyrcène bifonctionnel avec TMS (seulement la structure 1,4 est présentée pour faire une simplification du schéma).

Nous avons optimisé les réactions de polymérisation en continu. En utilisant un assemblage similaire au précédent, nous avons réalisé la synthèse du Polymyrcène bifonctionnel (Fig 15).

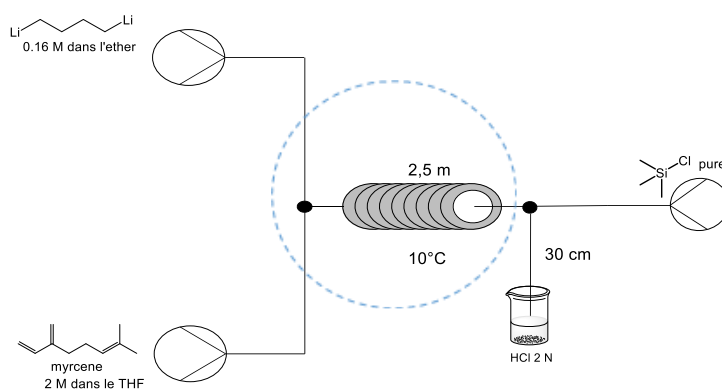


Fig 15: Montage pour la synthèse du Polymyrcène bifonctionnel.

Les conditions ont été établies en fonction de l'expérience antérieure (Tableau 10).

Tableau 10: Résultats de la polymérisation anionique du Myrcène avec des terminaisons TMS dans un réacteur à flux continu.

Non.	$Q_{\text{myrcene/THF}}$ (mL/min)	$Q_{1,4 \text{ Dil/Et}_2\text{O}}$ (mL/min)	$Q_{\text{TMSCl}}$ (mL/min)	$\overline{Mn}$ $^1\text{H RMN}$ (g/mol)	$\overline{Mn}$ GPC (g/mol)	$\overline{D}$
1 <sup>a</sup>	0,25	0,20	0,20	2600	-	-
2	0,25	0,20	0,20	2700	1500	1,2

<sup>a</sup> Aucune donnée d'analyse GPC.

Comme les paramètres de la réaction ont été bien gérés, les valeurs de la masse moléculaire en  $^1\text{H}$  NMR pour les échantillons 1 et 2 correspondent aux valeurs attendues avec une erreur de 10 %, éventuellement due à la manipulation ou à l'équipement. Les échantillons n'étaient pas très solubles dans le dichlorométhane après un séchage complet, ce qui a affecté l'analyse GPC.

### Résultats pour le Polymyrcène bifonctionnel avec $\text{CO}_2\text{H}$ en flux continu

Suite au contrôle de masse molaire déjà obtenu pour le Polymyrcène avec des terminaisons TMS, une réaction avec le dioxyde de carbone en flux continu a été effectuée pour obtenir des terminaisons  $\text{CO}_2\text{H}$ . Pour les conditions de flux continu, il était nécessaire de conserver le même rapport molaire déjà établi pour l'étude (Myr/DiLi:17/1). Pour ce faire, les débits volumétriques de la solution de 1,4-dilithiumbutane et de la solution Myrcène/THF ont été établis dans chaque pompe en fonction de la concentration molaire de chaque réactif (Fig 16).



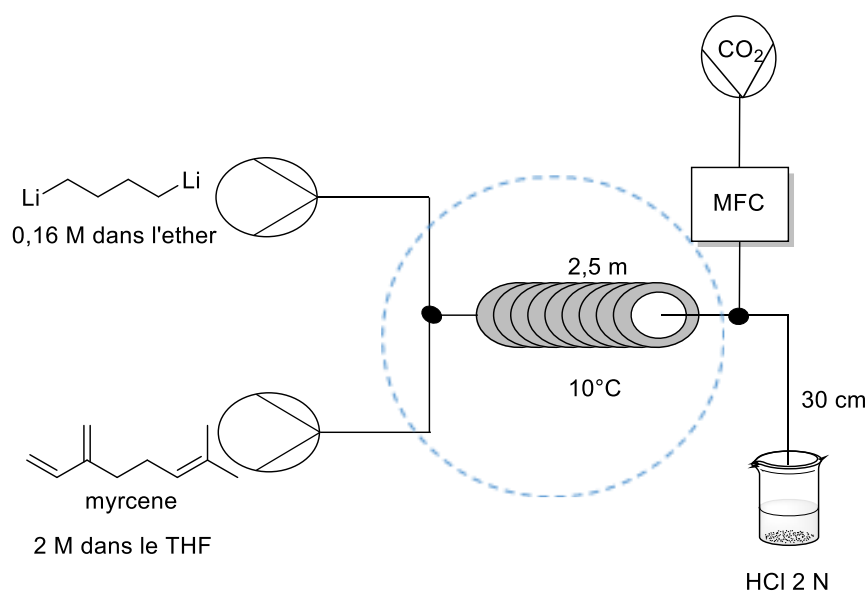


Fig 16: Montage pour la bifonctionnalisation du Polymyrcène avec CO<sub>2</sub>H.

Les résultats obtenus pour cette réaction ont donné de meilleurs résultats que dans des conditions de batch pour l'addition de terminaisons CO<sub>2</sub>H dans le polymère. Cela s'explique par le fait que la quantité en mmol de CO<sub>2</sub> dans le réacteur tubulaire a été contrôlée à l'aide d'un régulateur de débit massique. Après avoir optimisé les paramètres en flux continu, nous avons introduit la terminaison CO<sub>2</sub>H.

Tableau 11: Résultats de la polymérisation anionique du Myrcène avec des terminaisons CO<sub>2</sub>H dans un réacteur à flux continu.

$Q_{\text{myrcene/THF}}$ (mL/min)	$Q_{1,4 \text{ Dil/Et}_2\text{O}}$ (mL/min)	$Q_{\text{CO}_2}$ (mL/min)	$\overline{M}_n$ <sup>1</sup> H RMN (g/mol)	$\overline{M}_n$ GPC (g/mol)	$\overline{D}$
0,25	0,20	1,3	2400	1500	1,2

Un meilleur contrôle de la masse molaire en conditions microfluidiques a de nouveau été observé.  $\overline{M}_n$  <sup>1</sup>H NMR a été calculé sur la base d'une structure Telechelic et a donné une valeur proche de la  $\overline{M}_n^{\text{th}}$ . Cela montre que nous avons le même FD près de 95% que nous avons observé avant. L'analyse de microstructure dans le mélange éther/THF a donné les résultats suivants : 33% 1,4-; 55% 3,4- : 12% 1,2-unité de contenu.

## Conclusions du résumé

La chimie en flux continu permet de progresser vers les frontières de l'innovation, de l'optimisation et de la production de nouveaux matériaux.

Dans un premier temps avons étudié la stéréosélectivité de l'échange lithium-brome sur un *gem*-dibromoalcène dans un système de microfluidique avec seize mélangeurs passifs qui ont deux diamètres internes de 500  $\mu$ m et 250  $\mu$ m et huit angles variables (de 135 à 30°). Il en résulte qu'un débit élevé dans un micro-mélangeur en W fin (45°, DI = 0,25 mm) permet d'atteindre une sélectivité dépassant les 90% à 20 °C.

Dans la seconde partie, plusieurs expériences ont été réalisées avec Myrcène/*n*-BuLi en utilisant différentes tailles de réacteurs. Les résultats ont montré qu'en utilisant un système en flux continu, il est possible d'obtenir une polymérisation vivante et des résultats reproductibles. Nous avons également pu contrôler la masse molaire du Polymyrcène et la température à l'intérieur du réacteur. Également, grâce au réacteur microfluidique, il a été possible de piéger monoxyde de carbone (CO<sub>2</sub>), à la fin de la polymérisation (Degré de fonctionnalisation de 95%), de manière totalement sélective pour éviter les réactions concurrentielles consécutives et introduire une fonction carboxyle utile.

Finalement, la synthèse du Polymyrcène téléchélique avec 1,4 dilithiumbutane comme amorceur a été effectuée. Polymyrcène avec les terminaisons TMS en batch été faite pour étudier le degré de polymérisation et la masse moléculaire final du polymère. Toutefois, le contrôle de la masse moléculaire dans en batch n'a jamais été atteint. Les polymères obtenus la plupart du temps avaient une masse moléculaire plus élevé que prévu avec une polydispersité supérieure à 2. Des résultats similaires ont été obtenus pour le Polymyrcène avec des terminaisons CO<sub>2</sub>H, ce qui a donné une masse moléculaire élevé avec peu de piégeage des terminaisons CO<sub>2</sub>H. Les réactions en batch n'étaient pas reproductibles, contrairement à celles en flux continu. Ce qui s'explique par un manque de transfert de chaleur/masse rapide en raison de la forme du ballon et du mélange déficient.

Ce travail ouvre la porte à un nouveau processus durable pour obtenir des oligomères contrôlés et fonctionnalisés. Par exemple une hydrogénation du polymère bifonctionnel CO<sub>2</sub>H conduirait à de nouveaux macrodiols d'intérêt.

## Bibliographie

- (1) Yoshida, J.; Nagaki, A.; Yamada, D. Continuous Flow Synthesis. *Drug Discovery Today: Technologies* **2013**, *10* (1), e53–e59. <https://doi.org/10.1016/j.ddtec.2012.10.013>.
- (2) Pérez, K.; Picard, B.; Vuluga, D.; Burel, F.; Hreiz, R.; Falk, L.; Commenge, J.-M.; Nagaki, A.; Yoshida, J.; Chataigner, I.; Maddaluno, J.; Legros, J. Bromine–Lithium Exchange on a Gem -Dibromoalkene, Part 2: Comparative Performance of Flow Micromixers. *Org. Process Res. Dev.* **2020**, *24* (5), 787–791. <https://doi.org/10.1021/acs.oprd.0c00203>.
- (3) Yoshida, J.; Kim, H.; Nagaki, A. Green and Sustainable Chemical Synthesis Using Flow Microreactors. *ChemSusChem* **2011**, *4* (3), 331–340. <https://doi.org/10.1002/cssc.201000271>.
- (4) Commenge, J.-M.; Falk, L. Villiermaux–Dushman Protocol for Experimental Characterization of Micromixers. *Chemical Engineering and Processing: Process Intensification* **2011**, *50* (10), 979–990. <https://doi.org/10.1016/j.cep.2011.06.006>.
- (5) Gobby, D.; Angeli, P.; Gavriilidis, A. Mixing Characteristics of T-Type Microfluidic Mixers. *J. Micromech. Microeng.* **2001**, *11* (2), 126–132. <https://doi.org/10.1088/0960-1317/11/2/307>.
- (6) Falk, L.; Commenge, J.-M.; Portha, J.-F. Principes théoriques de la chimie en flux. *Médicaments et produits pharmaceutiques* **2019**, *Techniques de l'Ingénieur*. <https://doi.org/10.51257/a-v1-j8025>.
- (7) Plutschack, M. B.; Pieber, B.; Gilmore, K.; Seeberger, P. H. The Hitchhiker's Guide to Flow Chemistry. *Chem. Rev.* **2017**, *117* (18), 11796–11893. <https://doi.org/10.1021/acs.chemrev.7b00183>.
- (8) Kölbl, A.; Kraut, M. On the Use of the Iodide Iodate Reaction Method for Assessing Mixing Times in Continuous Flow Mixers. *AIChE J.* **2011**, *57* (4), 835–840. <https://doi.org/10.1002/aic.12313>.
- (9) Hessel, V.; Löwe, H.; Schönfeld, F. Micromixers—a Review on Passive and Active Mixing Principles. *Chemical Engineering Science* **2005**, *60* (8–9), 2479–2501. <https://doi.org/10.1016/j.ces.2004.11.033>.
- (10) Nagaki, A.; Imai, K.; Ishiuchi, S.; Yoshida, J. Reactions of Difunctional Electrophiles with Functionalized Aryllithium Compounds: Remarkable Chemoselectivity by Flash Chemistry. *Angewandte Chemie International Edition* **2015**, *54* (6), 1914–1918.
- (11) Knorr, R. Alkylidenecarbenes, Alkylidenecarbenoids,† and Competing Species: Which Is Responsible for Vinylic Nucleophilic Substitution, [1 + 2] Cycloadditions, 1,5-CH Insertions, and the Fritsch–Buttenberg–Wiechell Rearrangement? *Chem. Rev.* **2004**, *104* (9), 3795–3850. <https://doi.org/10.1021/cr030616h>.
- (12) Capriati, V.; Florio, S. Anatomy of Long-Lasting Love Affairs with Lithium Carbenoids: Past and Present Status and Future Prospects. *Chemistry – A European Journal* **2010**, *16* (14), 4152–4162. <https://doi.org/10.1002/chem.200902870>.
- (13) Picard, B.; Pérez, K.; Lebleu, T.; Vuluga, D.; Burel, F.; Harrowven, D. C.; Chataigner, I.; Maddaluno, J.; Legros, J. Bromine-Lithium Exchange on Gem-Dibromoalkenes. Part 1: Batch vs Microflow Conditions. *J. Flow Chem.* **in press**. <https://doi.org/10.1007/s41981-019-00057-6>.

- (14) Hamdoun, G.; Sebban, M.; Cossoul, E.; Harrison-Marchand, A.; Maddaluno, J.; Oulyadi, H. <sup>1</sup> H Pure Shift DOSY: A Handy Tool to Evaluate the Aggregation and Solvation of Organolithium Derivatives. *Chem. Commun.* **2014**, *50* (31), 4073–4075. <https://doi.org/10.1039/C4CC00111G>.
- (15) Reich, H. J. Role of Organolithium Aggregates and Mixed Aggregates in Organolithium Mechanisms. *Chem. Rev.* **2013**, *113* (9), 7130–7178. <https://doi.org/10.1021/cr400187u>.
- (16) McGarrity, J. F.; Ogle, C. A. High-Field Proton NMR Study of the Aggregation and Complexation of n-Butyllithium in Tetrahydrofuran. *J. Am. Chem. Soc.* **1985**, *107* (7), 1805–1810. <https://doi.org/10.1021/ja00293a001>.
- (17) Rivera, N. R.; Kassim, B.; Grigorov, P.; Wang, H.; Armenante, M.; Bu, X.; Lekhal, A.; Variankaval, N. Investigation of a Flow Step Clogging Incident: A Precautionary Note on the Use of THF in Commercial-Scale Continuous Process. *Org. Process Res. Dev.* **2019**, *23* (11), 2556–2561. <https://doi.org/10.1021/acs.oprd.9b00366>.
- (18) Takahashi, Y.; Nagaki, A. Anionic Polymerization Using Flow Microreactors. *Molecules* **2019**, *24* (8), 1532. <https://doi.org/10.3390/molecules24081532>.
- (19) Surendran, S.; Surendran, G. Myrcene—What Are the Potential Health Benefits of This Flavouring and Aroma Agent? *Frontiers in Nutrition* **2021**, *8*, 14.
- (20) Trumbo, D. L. Free Radical Copolymerization Behavior of Myrcene: I. Copolymers with Styrene, Methyl Methacrylate or p-Fluorostyrene. *Polymer Bulletin* **1993**, *31* (6), 629–636. <https://doi.org/10.1007/BF00300120>.
- (21) Bauer, N.; Brunke, J.; Kali, G. Controlled Radical Polymerization of Myrcene in Bulk: Mapping the Effect of Conditions on the System. *ACS Sustainable Chem. Eng.* **2017**, *5* (11), 10084–10092. <https://doi.org/10.1021/acssuschemeng.7b02091>.
- (22) Loughmari, S.; Hafid, A.; Bouazza, A.; El Bouadili, A.; Zinck, P.; Visseaux, M. Highly Stereoselective Coordination Polymerization of B-myrcene from a Lanthanide-based Catalyst: Access to Bio-sourced Elastomers. *J. Polym. Sci. A Polym. Chem.* **2012**, *50* (14), 2898–2905. <https://doi.org/10.1002/pola.26069>.
- (23) Zinelabidine Otmane Elabed; Kherroub, D. E.; Derdar, H.; Belbachir, M. Novel Cationic Polymerization of  $\beta$ -Myrcene Using a Proton Exchanged Clay (Maghnite-H<sup>+</sup>). *Polym. Sci. Ser. B* **2021**, *63* (5), 480–487. <https://doi.org/10.1134/S1560090421050043>.
- (24) Dev, A.; Rösler, A.; Schlaad, H. Limonene as a Renewable Unsaturated Hydrocarbon Solvent for Living Anionic Polymerization of  $\beta$ -Myrcene. *Polym. Chem.* **2021**, *12* (21), 3084–3087. <https://doi.org/10.1039/D1PY00570G>.
- (25) Newmark, R. A.; Majumdar, R. N. <sup>13</sup>C-NMR Spectra of Cis-Polymyrcene and Cis-Polyfarnesene. *J. Polym. Sci. A Polym. Chem.* **1988**, *26* (1), 71–77. <https://doi.org/10.1002/pola.1988.080260107>.
- (26) Ávila-Ortega, A.; Aguilar-Vega, M.; Loría Bastarrachea, M. I.; Carrera-Figueiras, C.; Campos-Covarrubias, M. Anionic Synthesis of Amine  $\omega$ -Terminated  $\beta$ -Myrcene Polymers. *J Polym Res* **2015**, *22* (11), 226. <https://doi.org/10.1007/s10965-015-0856-6>.
- (27) Flory, P. J. *Principles of Polymer Chemistry*; Cornell university press, 1953.

- (28) Ovaska, T. V. *S*-Butyllithium. In *Encyclopedia of Reagents for Organic Synthesis*; John Wiley & Sons, Ltd., Ed.; John Wiley & Sons, Ltd: Chichester, 2001; p rb397. <https://doi.org/10.1002/047084289X.rb397>.
- (29) Ebdon, J. R. Terminally Reactive Oligomers: Telechelic Oligomers and Macromers. In *New Methods of Polymer Synthesis*; Ebdon, J. R., Ed.; Springer US: Boston, MA, 1991; pp 162–196. [https://doi.org/10.1007/978-1-4684-1530-8\\_6](https://doi.org/10.1007/978-1-4684-1530-8_6).
- (30) Stanetty, P.; Mihovilovic, M. D. Half-Lives of Organolithium Reagents in Common Ethereal Solvents. *J. Org. Chem.* **1997**, *62* (5), 1514–1515. <https://doi.org/10.1021/jo961701a>.
- (31) Clayden, J.; Yasin, S. A. Pathways for Decomposition of THF by Organolithiums: The Role of HMPA. *New J. Chem.* **2002**, *26* (2), 191–192. <https://doi.org/10.1039/b109604d>.
- (32) Bolton, J. M.; Hillmyer, M. A.; Hoye, T. R. Sustainable Thermoplastic Elastomers from Terpene-Derived Monomers. *ACS Macro Lett.* **2014**, *3* (8), 717–720. <https://doi.org/10.1021/mz500339h>.
- (33) Ruiz Martínez, E.; Sánchez Hervás, J. M. Chemical Valorization of CO<sub>2</sub>. In *Carbon Dioxide Utilization to Sustainable Energy and Fuels*; Inamuddin, Boddula, R., Ahamed, M. I., Khan, A., Eds.; Springer International Publishing: Cham, 2022; pp 1–30. [https://doi.org/10.1007/978-3-030-72877-9\\_1](https://doi.org/10.1007/978-3-030-72877-9_1).
- (34) SciencesRoundtable, N. R. C. (US) C. *Carbon Dioxide as a Feedstock*; National Academies Press (US), 2001.
- (35) Seo, H.; Nguyen, L. V.; Jamison, T. F. Using Carbon Dioxide as a Building Block in Continuous Flow Synthesis. *Advanced Synthesis & Catalysis* **2019**, *361* (2), 247–264.
- (36) Nagaki, A.; Takahashi, Y.; Yoshida, J. Extremely Fast Gas/Liquid Reactions in Flow Microreactors: Carboxylation of Short-Lived Organolithiums. *Chem. Eur. J.* **2014**, *20* (26), 7931–7934. <https://doi.org/10.1002/chem.201402520>.
- (37) Wu, J.; Yang, X.; He, Z.; Mao, X.; Hatton, T. A.; Jamison, T. F. Continuous Flow Synthesis of Ketones from Carbon Dioxide and Organolithium or Grignard Reagents. *Angew. Chem. Int. Ed.* **2014**, *53* (32), 8416–8420. <https://doi.org/10.1002/anie.201405014>.
- (38) Nagaki, A.; Takahashi, Y.; Yoshida, J. Extremely Fast Gas/Liquid Reactions in Flow Microreactors: Carboxylation of Short-Lived Organolithiums. *Chemistry – A European Journal* **2014**, *20* (26), 7931–7934. <https://doi.org/10.1002/chem.201402520>.
- (39) Monbaliu, J.-C. M.; Legros, J. Will the next Generation of Chemical Plants Be in Miniaturized Flow Reactors? *Lab Chip* **2022**. <https://doi.org/10.1039/D2LC00796G>.

## **Experimental Section**

Controlled organolithium chemistry in flow microreactors: micromixer effect, synthesis and end-functionalization of polymyrcene

## Table of Contents

1.	General considerations	182
2.	Microreactor design	185
3.	Experimental procedures	191
a.	Synthesis of (1,1-Dibromo-3,3,3-trifluoroprop-1-en-2-yl)benzene (2.1):	191
b.	Synthesis of (E)-(1-bromo-3,3,3-trifluoroprop-1-en-2-yl)benzene (E-2.2):	192
c.	Data of (Z)-2; (Z)-(1-bromo-3,3,3-trifluoroprop-1-en-2-yl)benzene (Z-2.2):	193
d.	Synthesis of methyl 3-bromo-5,5,5-trifluoro-2-hydroxy-2,4-diphenyl-3-pentenoate (E-2.3):	193
e.	Protocol of titration reaction of <i>n</i> -Butyllithium	197
f.	Synthesis of PMYR under batch conditions	198
g.	Synthesis of PMYR under flow conditions	201
h.	Synthesis of PMYR quenched with TMSCl under flow conditions	203
i.	Synthesis of PMYR quenched with CO <sub>2</sub> under batch conditions	205
j.	Synthesis of PMYR quenched with CO <sub>2</sub> under flow conditions	208
k.	Synthesis of 1,4-dilithiumbutane	211
l.	Synthesis of telechelic PMYR with TMS end-functionalization under batch conditions	212
m.	Synthesis of telechelic PMYR with TMS end-functionalization under microflow conditions	214
n.	Synthesis of telechelic PMYR with CO <sub>2</sub> H end-functionalization under flow conditions	216
o.	Mass balance in polymerization reaction (batch)	218
p.	Volatility of myrcene	218



## Table of figures

Fig. 1: 250 $\mu\text{m}$ , $\theta$ 30° .....	185
Fig. 2: 500 $\mu\text{m}$ , $\theta$ 30° .....	185
Fig. 3 : 500 $\mu\text{m}$ , $\theta$ 45° .....	186
Fig. 4 : 500 $\mu\text{m}$ , $\theta$ 45° .....	186
Fig. 5:500 $\mu\text{m}$ , $\theta$ 60° .....	186
Fig. 6:250 $\mu\text{m}$ , $\theta$ 60° .....	187
Fig. 7:500 $\mu\text{m}$ , $\theta$ 75° .....	187
Fig. 8:250 $\mu\text{m}$ , $\theta$ 75° .....	187
Fig. 9 :500 $\mu\text{m}$ , $\theta$ 90° .....	188
Fig. 10: 250 $\mu\text{m}$ , $\theta$ 90° .....	188
Fig. 11 : 500 $\mu\text{m}$ , $\theta$ 105° .....	188
Fig. 12: 250 $\mu\text{m}$ , $\theta$ 105° .....	189
Fig. 13: 500 $\mu\text{m}$ , $\theta$ 120° .....	189
Fig. 14:250 $\mu\text{m}$ , $\theta$ 120° .....	189
Fig. 15:500 $\mu\text{m}$ , $\theta$ 135° .....	190
Fig. 16 : 250 $\mu\text{m}$ , $\theta$ 135° .....	190
Fig. 17:Spectrum $^1\text{H}$ NMR (300 MHz, $\text{CDCl}_3$ ) of E-2.3. ....	195
Fig. 18:Spectrum $^{19}\text{F}$ NMR of E-2.3.....	195
Fig. 19 : Spectrum $^{13}\text{C}$ { $^1\text{H}$ } NMR (75 MHz, $\text{CDCl}_3$ ) of E-2.3. ....	196
Fig. 20: Chromatogram of E-2.3 (GC (DB5)).....	196
Fig. 21:GPC of PMYR in batch at 10°C.....	199
Fig. 22: $^1\text{H}$ NMR (300 MHz, $\text{CDCl}_3$ ) spectrum of PMYR in batch at 10°C. Microstructure calculations: $b=1.13(1\text{H})$ ; $c=(14.57-1.13)/2=6.72(1\text{H})$ ; $a=(15.70-6.72-1.13)/2=3.92(1\text{H})$ ; $a=3.92/11.77=33\%$ , $b=1.13/11.77=10\%$ , $c=6.72/11.77=57\%$ ... ..	199
Fig. 23: $^{13}\text{C}$ NMR (75 MHz, $\text{CDCl}_3$ ) spectrum of PMYR in batch at 10°C.....	200
Fig. 24:Infrared spectrum of PMYR in batch at 10°C.....	200
Fig. 25:Experimental setup in microflow conditions .....	202
Fig. 26;GPC of PMYR in microflow conditions, flow rate myrcene/n-BuLi/Methanol: 0.25/0.1/0.1 mL/min respectively at 10°C. ....	202
Fig. 27: $^1\text{H}$ NMR (300 MHz, $\text{CDCl}_3$ ) of PMYR with TMS end-group, MF: flow rate myrcene/n-BuLi/TMScI: 0.25:0.1:0.1 mL.min <sup>-1</sup> respectively at 10°C. Functionalization degree: $6,56/9 \times 100=73\%$ .....	<b>Erreur ! Signet non défini.</b>
Fig. 28: $^{13}\text{C}$ NMR (75 MHz, $\text{CDCl}_3$ ) of PMYR with TMS end-group, MF: flow rate myrcene/n-BuLi/TMScI 0.25:0.1:0.1 mL.min <sup>-1</sup> respectively at 10°C. ....	<b>Erreur ! Signet non défini.</b>
.....	<b>Erreur ! Signet non défini.</b>
Fig. 29:GPC of PMYR ketone in batch at 10°C. ....	206
Fig. 30: $^1\text{H}$ NMR (300 MHz, $\text{CDCl}_3$ ) of PMYR ketone in batch at 10°C.....	206
Fig. 31: $^{13}\text{C}$ NMR (300 MHz, $\text{CDCl}_3$ ) of PMYR ketone in batch at 10°C. ....	<b>Erreur ! Signet non défini.</b>
Fig. 32 : FTIR of PMYR ketone in batch (carbonyl group signal 1707.18 $\text{cm}^{-1}$ ) at 10°C.....	<b>Erreur ! Signet non défini.</b>

Fig. 33:GPC of PMYR end-group acid, MF conditions: flow rate myrcene/n-BuLi/CO <sub>2</sub> 0.25:0.1:1.36 mL.min <sup>-1</sup> respectively at 10°C.....	<b>Erreur ! Signet non défini.</b>
Fig. 34: <sup>1</sup> H NMR of PMYR end-group acid, MF conditions: flow rate myrcene/n-BuLi/CO <sub>2</sub> 0.25:0.1:1.36 mL.min <sup>-1</sup> respectively, at 10°C. Functionalization degree: 95%.....	209
Fig. 35: <sup>13</sup> C NMR of PMYR end-group acid, MF conditions: flow rate myrcene/n-BuLi/CO <sub>2</sub> 0.25:0.1:1.36 mL.min <sup>-1</sup> respectively at 10°C.....	<b>Erreur ! Signet non défini.</b>
Fig. 36: FT IR of PMYR end-group acid (carbonyl group signal 1708.07 cm <sup>-1</sup> ). MF conditions: flow rate myrcene/n-BuLi/CO <sub>2</sub> 0.25:0.1:1.36 mL.min <sup>-1</sup> respectively at 10°C.....	<b>Erreur ! Signet non défini.</b>
Fig. 37:GPC of Telechelic PMYR with TMS end-functionalization under batch conditions.....	213
Fig. 38: <sup>1</sup> H NMR of Telechelic PMYR with TMS end-functionalization under batch conditions.....	213
Fig. 39: <sup>1</sup> H NMR of Telechelic PMYR with TMS end-functionalization under microflow conditions.....	215
Fig. 40:GPC of Telechelic PMYR with TMS end-functionalization under microflow conditions.....	215
Fig. 41: <sup>1</sup> H NMR Telechelic PMYR with CO <sub>2</sub> H end-functionalization under flow conditions.....	217
Fig. 42:FT IR spectrum of polymyrcene with CO <sub>2</sub> H endings. CO <sub>2</sub> H signal at 1707 cm <sup>-1</sup> .....	217
Fig. 43:Entries and outlets in the reaction process (scale, 0.1 g of myrcene).....	218
Fig. 44:Study of the evaporation of myrcene at room temperature.....	219
Fig. 45:Myrcene evaporation under different pressures.....	220

## 1. General considerations

### Reagents and materials

Dibromoalkene **1** was prepared according to Corey-Fuchs protocol (*vide infra*). Myrcene was purchased from Sigma-Aldrich or Acros (distilled from  $\text{CaH}_2$ ). 1,4-diiodobutane (99% stabilized with copper) and 2,2'-bipyridine (98%) were obtained from Alfa Aesar and used as received. Menthol (99.5%) was obtained from Acros Organics. Chlorotrimethylsilane (TMSCl  $\geq 98\%$  GC), trimethylsilyldiazomethane (TMSDM, 2.0 M in hexane) were obtained from Aldrich. TMSCl was freshly distilled and (trimethylsilyl)diazomethane was used as received.

Carbon dioxide ( $\text{CO}_2$  purity  $> 99.995$  vol%,  $\text{H}_2\text{O} < 5$  ppm) was purchased from Linde.

Organolithiums were purchased from Sigma-Aldrich or Acros as a 2.6 M solution in hexanes and diluted to the wanted titer with n-hexane (distilled from  $\text{CaH}_2$ ) and titrated by menthol/bipyridine method before usage.

### Solvents

Methanol (MeOH) was purchased from Sigma-Aldrich or Acros and was used as received. Tetrahydrofuran (THF) was distilled from benzophenone/sodium for the reaction. Deuterated Chloroform ( $\geq 99.8\%$  analytical reagent grade) and calcium hydride ( $\text{CaH}_2$ -90-55% reagent grade) were obtained from Fischer Scientific and used as received. Dichloromethane (DCM) (for analysis stabilized with ethanol) and molecular sieves 3A were bought from Carlo Erba reagents and used as received. Methylene chloride  $\text{D}_2$  (99.8%  $\text{D}$ ) was obtained from Eurisotop and used as received. Diethyl Ether ( $\text{Et}_2\text{O}$ ) was filtered through  $\text{Al}_2\text{O}_3$  under vacuum conditions at room temperature (RT) and dried in molecular sieves 3A for several hours before its use. The water content of the solvents was determined by coulometric Karl Fischer titration.

## **Glassware and stainless-steel materials**

All instruments were cleaned up. Glass and stainless-steel instrumentation were kept in the oven for 24h at 140°C to eliminate any water residues. Flasks were kept for several hours in a Schlenk line *in vacuo* before use.

## **Microflow reactors**

Microflow reactors were cut from stainless steel tubing purchased either from CIL. Micromixers were custom manufactured by MG-63 (vide infra for schematics). Reagents were fed in the reactors by mean of Harvard Apparatus PHD Ultra syringe pumps, and SGE glass syringes.

**Reaction conditions:** All experiments were run in oxygen and moisture-free environment. Glassware was dried under vacuum using a Schlenk line by heating the flask with a heat-gun before cycling dry argon and vacuum. Stainless steel reactors were dried overnight in a 120 °C oven, before cooling in a desiccator over silica gel under vacuum.

**Comparative performance of flow micromixers:** Flow experiments at room temperature were run in a bath of tap water at roughly 20 °C. Flow experiments: three dead volumes of reagents were run through the system before collection to ensure reactor equilibrium, then 15 mL were collected for analysis.

**Synthesis and Functionalization of polymyrcene (PMYR):** Flow experiments were run in a tap water bath cooled at 10 °C. Flow experiments: three dead volumes of reagents were run through the system before collection to ensure reactor equilibrium, then approximately between 2-5 mL were collected for analysis.

**NMR Analysis:** NMR Spectra were recorded on a Bruker 300 MHz spectrometer and worked with MestReNova software, chemical shifts are given in part per millions in regard to SiMe<sub>4</sub> for <sup>1</sup>H and <sup>13</sup>C, and FCCL<sub>3</sub> for <sup>19</sup>F. Spectra were calibrated on residual non-deuterated solvent peaks.

**Gas Chromatography Analysis:** GC-MS analyses were recorded on a Shimadzu QP2010SE apparatus, operating in EI (70 eV) with a quadrupole analyser in scan mode (m/z = 50 to 500) and a DB-5MS (30 m, 0.25 mm, 0.25 μm) column. Quantitative GC were run on a Scion

436 chromatograph. Analyses of the conversion of **1** were performed on a DB-5 (30 m, 0.25 mm, 0.25  $\mu\text{m}$ ) column at 1.7 mL/min He carrier gas flowrate. Oven program starts at 50 °C for 2 min, then heat up to 250 °C at 20 K/min followed by a final isotherm of 5 min.

**Gel Permeation Chromatography (GPC):** GPC chromatograms were recorded on a PL-GPC 50 Plus, treated with GPC offline software. GPC was calibrated with polymethyl methacrylate (PMMA) a pre-weighed polymer standard from Agilent. Samples were diluted in dichloromethane and injected into the GPC (30°C, 1mL/min, 2 mixed-C column).

**Infrared analysis:** Infrared spectra were recorded on a Perkin Elmer ATR universal sampler 100 spectrum.

## 2. Microreactor design

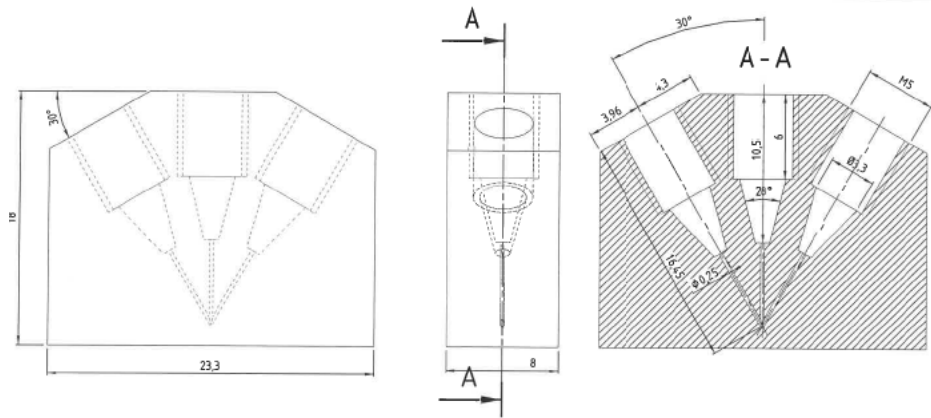


Fig. 1: 250  $\mu\text{m}$ ,  $\theta$  30°

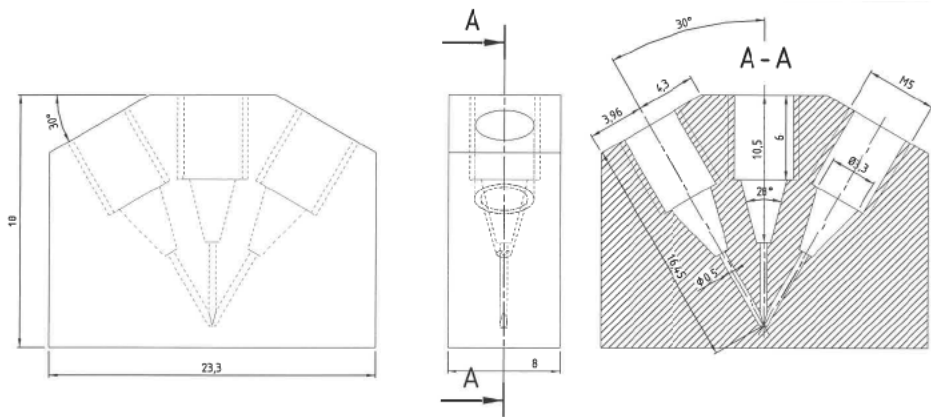


Fig. 2: 500  $\mu\text{m}$ ,  $\theta$  30°

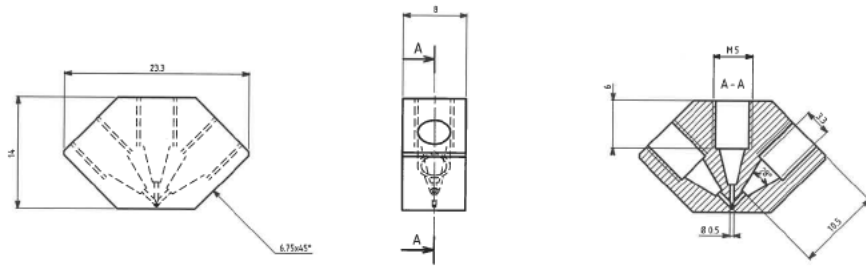


Fig. 3 : 500  $\mu\text{m}$ ,  $\theta$  45°

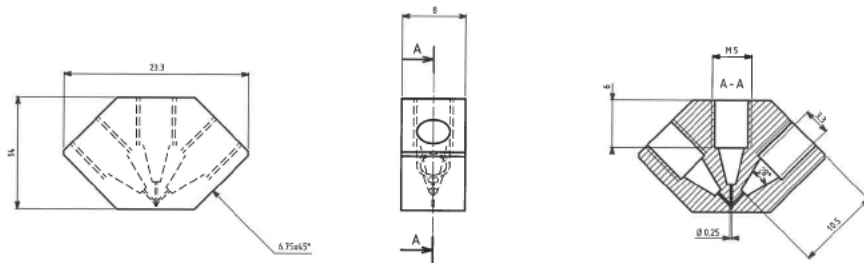


Fig. 4 : 500  $\mu\text{m}$ ,  $\theta$  45°

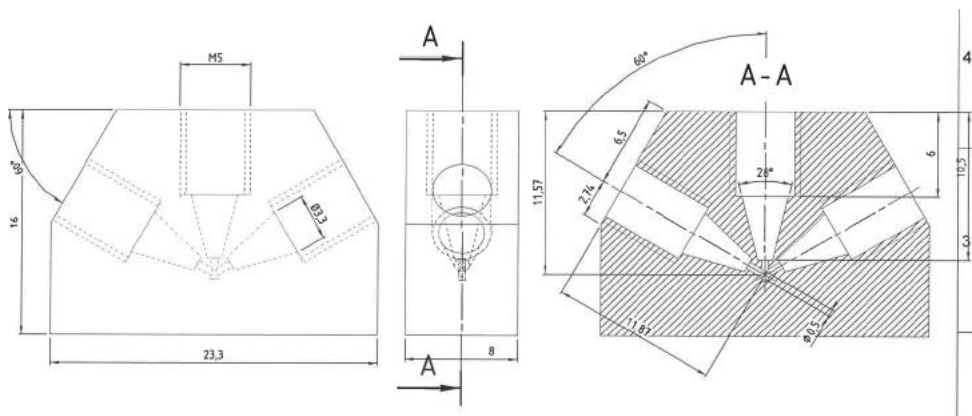


Fig. 5: 500  $\mu\text{m}$ ,  $\theta$  60°

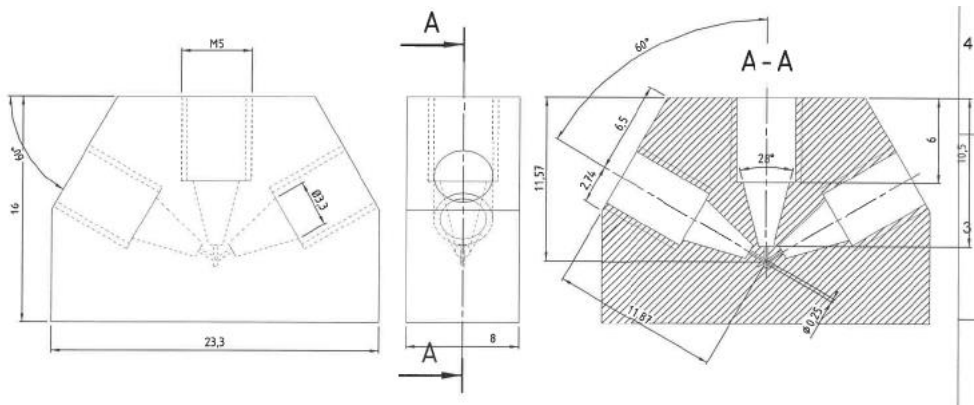


Fig. 6:250  $\mu\text{m}$ ,  $\theta$  60°

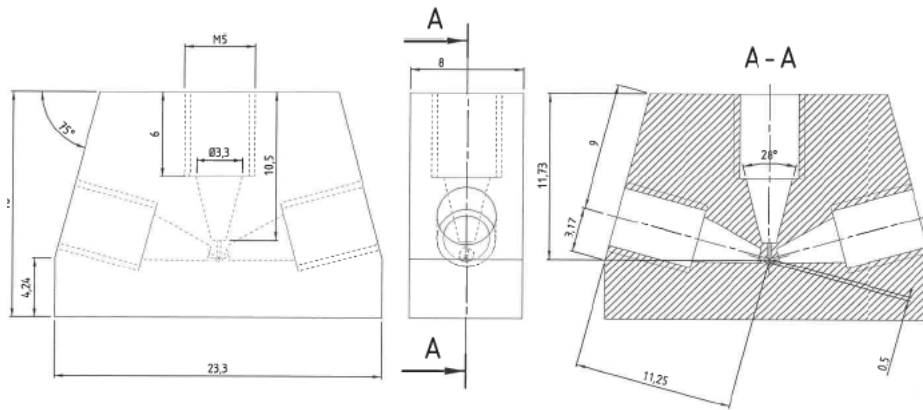


Fig. 7:500  $\mu\text{m}$ ,  $\theta$  75°

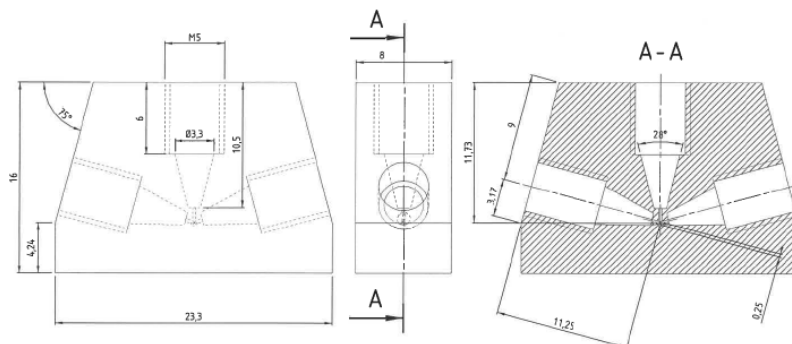


Fig. 8:250  $\mu\text{m}$ ,  $\theta$  75°



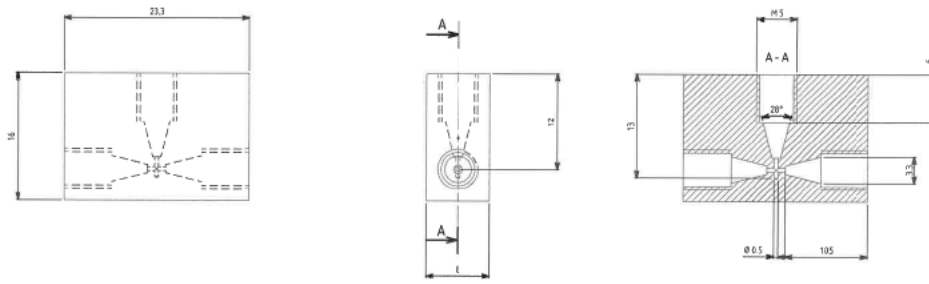


Fig. 9 : 500  $\mu\text{m}$ ,  $\theta$  90°

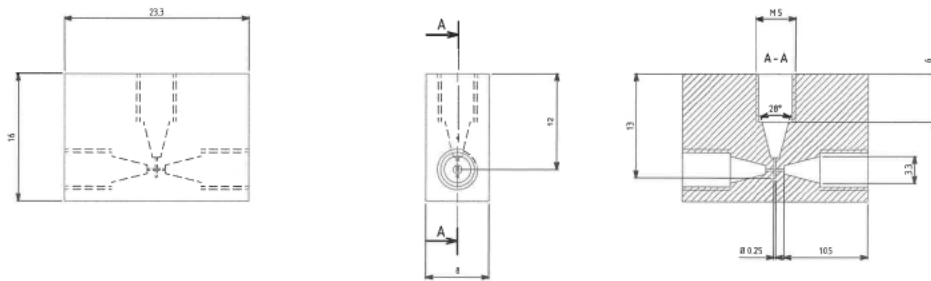


Fig. 10: 250  $\mu\text{m}$ ,  $\theta$  90°

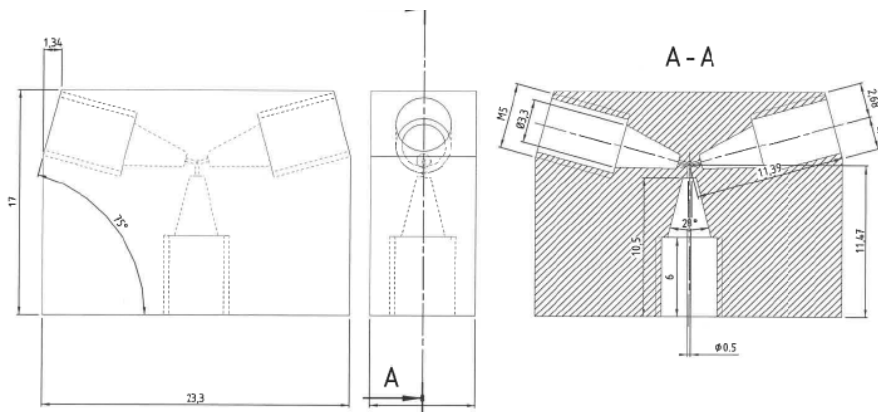


Fig. 11 : 500  $\mu\text{m}$ ,  $\theta$  105°

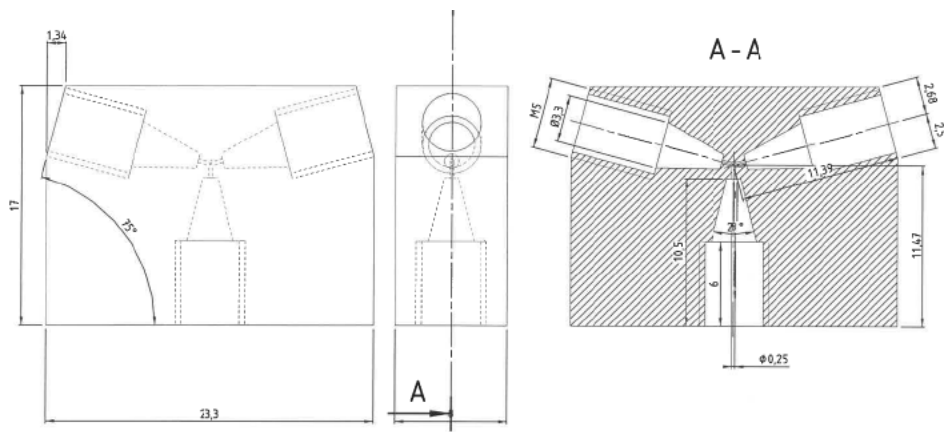


Fig. 12: 250  $\mu\text{m}$ ,  $\theta$  105°

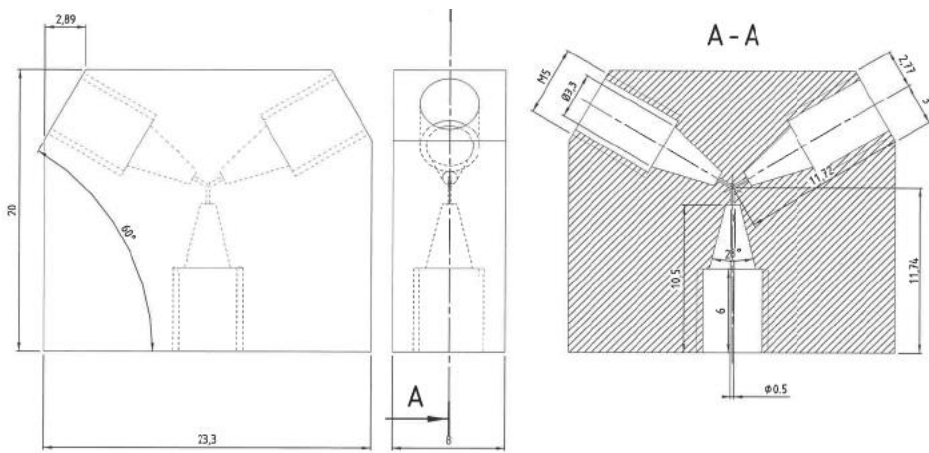


Fig. 13: 500  $\mu\text{m}$ ,  $\theta$  120°

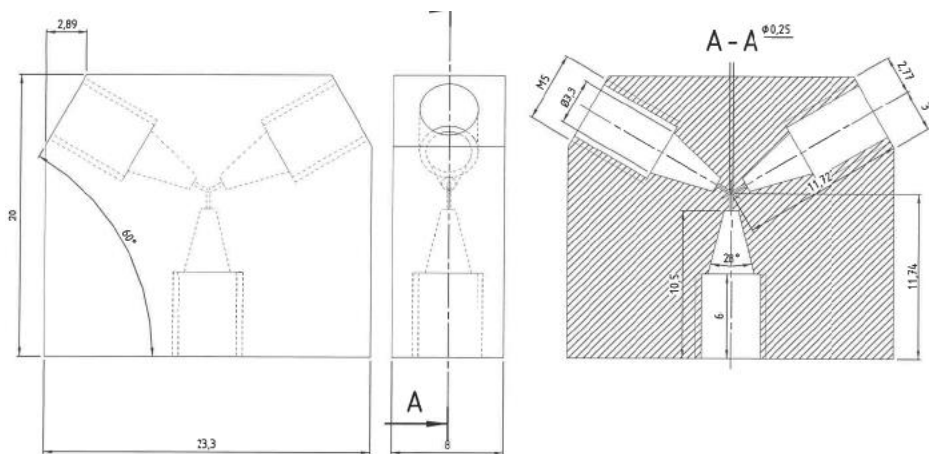


Fig. 14: 250  $\mu\text{m}$ ,  $\theta$  120°

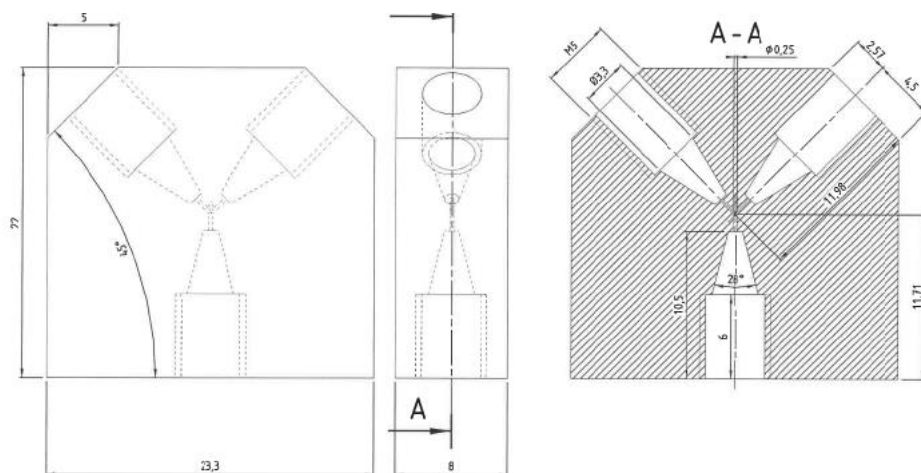


Fig. 15:  $500 \mu\text{m}$ ,  $\theta 135^\circ$

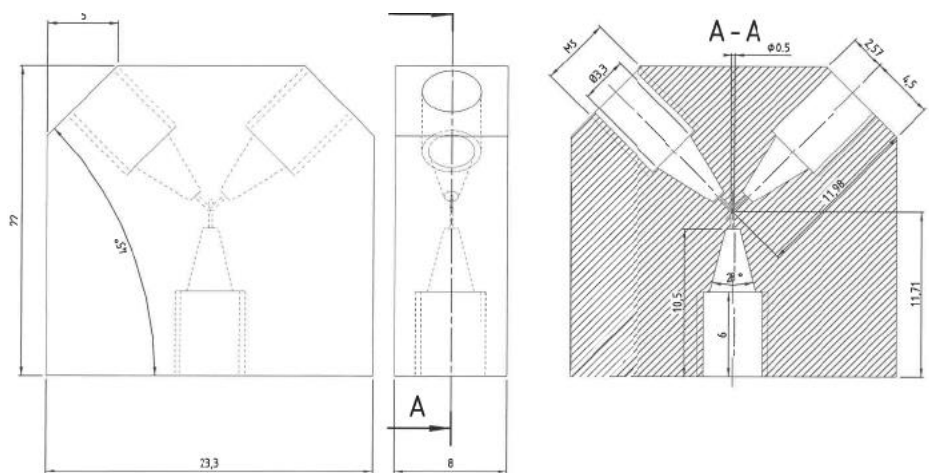
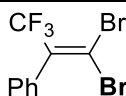


Fig. 16 :  $250 \mu\text{m}$ ,  $\theta 135^\circ$

### 3. Experimental procedures

#### a. Synthesis of (1,1-Dibromo-3,3,3-trifluoroprop-1-en-2-yl)benzene (2.1):



#### 2.1

A  $\text{CBr}_4$  (19 g, 2 eq.) solution in dichloromethane is cooled by an ice bath,  $\text{PPh}_3$  (30.5 g, 4 eq.) is then added portion wise. Bright orange coloration is observed as phosphorous ylide is formed, and this compound was observed to sometime precipitate without influence on the reaction. After two minutes, trifluoroacetophenone (4.03 mL, 1 eq.) is added dropwise. The ice bath is removed a minute after addition. The reaction is let warm up to room temperature for a night, and is finally quenched with water. The mixture is poured in a separation funnel, and the aqueous phase is extracted with dichloromethane, and organic phases are assembled and dried over  $\text{MgSO}_4$ . The obtained phases are filtered and concentrated *in vacuo* yielding a yellow gum containing the product, phosphine oxide and residual solvent. Purification is achieved by adding water to this crude gum, which is then slowly distilled. The aqueous distillate is then extracted with dichloromethane. Dichloromethane is removed in vacuum to yield 84% of **2.1** as a colourless oil with very specific odour.

$^1\text{H NMR}$  (300 MHz,  $\text{CDCl}_3$ )  $\delta$  = 7.46 – 7.39 (m, 3H), 7.26 – 7.21 (m, 2H).

$^{13}\text{C}$   $\{^1\text{H}\}$  NMR (75 MHz,  $\text{CDCl}_3$ )  $\delta$  = 137.6 (q,  $J$  = 32.7 Hz), 135.5 (q,  $J$  = 1 Hz), 129.4, 128.8 (2C), 128.7 (2C), 121.9 (q,  $J$  = 276.1 Hz), 101.6 (q,  $J$  = 3.2 Hz).

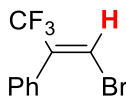
$^{19}\text{F}$   $\{^1\text{H}\}$  NMR (282 MHz,  $\text{CDCl}_3$ )  $\delta$  = -58.4 (s).

GC (DB5): 7.72 min. MS,  $m/z$  (%) = 151(20), 169(40), 170(70), 229(30), 231(30), 249(35), 251(35), 328(55), 330(100), 332(50). Data concordant with literature.<sup>1</sup>

---

<sup>1</sup> Djawed Nauroozi et al., "Microwave-Assisted Dibromoolefination of Aromatic and Heteroaromatic Aldehydes and Ketones," *Journal of Heterocyclic Chemistry* 53, no. 2 (2016): 615–19, <https://doi.org/10.1002/jhet.2332>.

b. **Synthesis of (E)-(1-bromo-3,3,3-trifluoroprop-1-en-2-yl)benzene (E-2.2):**



(E)-2.2

Obtained as the main product of lithiation of **2.1** under flow conditions. **2.1** in THF (at 0.1 M) was introduced in a micromixer (variable angle from 135 to 30°, with two internal diameters 500 and 250  $\mu\text{m}$ ), and mixed with a *n*-BuLi solution (0.3 M in hexanes). The resulting solution was passed through a microreactor, 30 mm length (total volume 6  $\mu\text{L}$ ) and introduced in a second T-shape micromixer (500  $\mu\text{m}$  ID) to be quenched with methanol. The quenched mixture was then passed through a second tube of 300 mm length and 700  $\mu\text{m}$  ID before collection in a vial and then diluted HCl was added (0.1 M). The resulting mixture is extracted with dichloromethane, dried over magnesium sulfate, and concentrated under vacuum to afford a crude mixture, analyzed by mean of GC. GC analysis indicates the ratio for the two isomers (*E* and *Z*). Unambiguous attribution of the main product geometry was possible thanks to a NMR  $^1\text{H}$ - $^{19}\text{F}$  hetero-NOESY experiment run on an isomer mixture in acetone- $d_6$ , displaying a strong correlation of the -66.4 ppm (from the major product) fluorine signal with the 7.74 ppm proton signal, confirming previous literature report<sup>2</sup>.

**$^1\text{H}$  NMR (300 MHz,  $\text{C}_3\text{D}_6\text{O}$ )**  $\delta$  = 7.74 (q,  $J$  = 1.7 Hz), 7.55 – 7.26 (m).

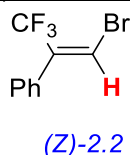
**$^{19}\text{F}$  NMR (262 MHz,  $\text{C}_3\text{D}_6\text{O}$ )**  $\delta$  = -65.6 (d,  $J$  = 1.7 Hz)

**GC (DB5)** : 5.82 min. **MS**,  $m/z$  (%) = 50(20), 76(20), 102(90), 151(70), 171(50), 250(100), 252(98).

---

<sup>2</sup> Peter A. Morken et al., "Synthesis of Fluorinated 1,2,3-Butatrienes from .Alpha.-Halovinyl Organometallic Reagents," *Journal of the American Chemical Society* 115, no. 13 (June 1993): 5430–39, <https://doi.org/10.1021/ja00066a011>.

c. **Data of (Z)-2: (Z)-(1-bromo-3,3,3-trifluoroprop-1-en-2-yl)benzene (Z-2.2):**



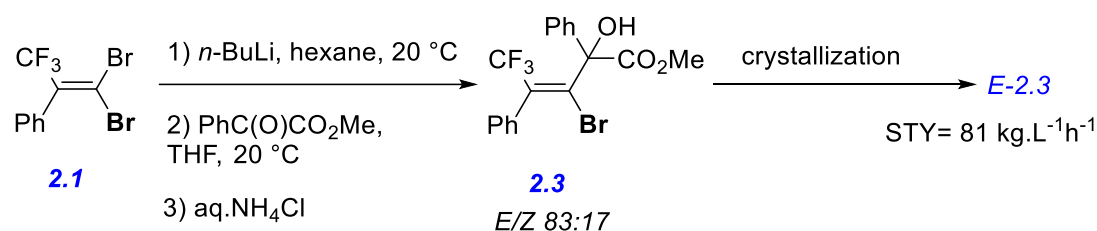
Obtained as a mixture along with (*E*)-2.2 by lithiation of **2.1**.

<sup>1</sup>H NMR (300 MHz, C<sub>3</sub>D<sub>6</sub>O) δ = 7.55 – 7.26 (m)

<sup>19</sup>F NMR (262 MHz, C<sub>3</sub>D<sub>6</sub>O) δ = -60.1

GC (DB5) : 6.61 min. MS, m/z (%) = 50(20), 76(20), 102(90), 151(70), 171(50), 250(100), 252(98).

d. **Synthesis of methyl 3-bromo-5,5,5-trifluoro-2-hydroxyl-2,4-diphenyl-3-pentenoate (E-2.3):**



Obtained as the main product of lithiation of **1** under flow conditions. **1** in THF (at 0.1 M) was introduced with a flow rate of 6 mL.min<sup>-1</sup> in a micromixer angle 45°, with internal diameter 250 μm, and mixed with a *n*-BuLi solution, 2.4 mL.min<sup>-1</sup> (0.3 M in hexanes). The resulting solution was passed through a microreactor, 30 mm length (500 μm ID, total volume 6 μL) and introduced in a second T-shape micromixer (500 μm ID) to be quenched with methyl benzoylformate (at 0.5 M in THF) with a flow rate of 3 mL.min<sup>-1</sup>. The quenched mixture was then passed through a second tube of 200 mm length and 700 μm ID (total volume 77 μL) before collection in a flask at 0°C and then saturated NH<sub>4</sub>Cl was added (10 ml).

The resulting mixture is extracted with dichloromethane, dried over magnesium sulfate, and concentrated under vacuum to afford a crude mixture, analyzed by mean of GC.

The crude mixture is diluted in DCM and then it is evaporated slowly until the crystallization of *E-2.3*. The crystals are washed several times with pentane to remove impurities.

**<sup>1</sup>H NMR (300 MHz, CDCl<sub>3</sub>)**  $\delta$  = 3.75 (3H, s, OMe), 4.25 (1H, s, OH), 7.13 (2H, m, Ar), 7.23-7.30 (6H, m, Ar), 7.45 (2H, m, Ar).

**<sup>19</sup>F NMR (262 MHz, CDCl<sub>3</sub>)**  $\delta$  = -56.54

**<sup>13</sup>C {<sup>1</sup>H} NMR (75 MHz, CDCl<sub>3</sub>)**  $\delta$  = 53.96 (OMe), 83.10 (C<sup>2</sup>), 126.66 (Ar), 128.17(Ar), 128.69 (Ar), 128.80 (Ar), 128.85 (Ar), 138.67 (q, J = 3.3 Hz), 137.93 (d, J = 1.7 Hz), 135.49 (q, J = 33.1 Hz), 127.28 – 115.75 (m), 141.01 (ipso C of 2-Ph) and 172.66 (CO<sub>2</sub>).

**GC (DB5)** : 12.62 min. **MS**, m/z (%) = 105(95), 129(44), 227(52), 277(56), 317(50), 335(33), 355(70).

**Mp**= 138°C

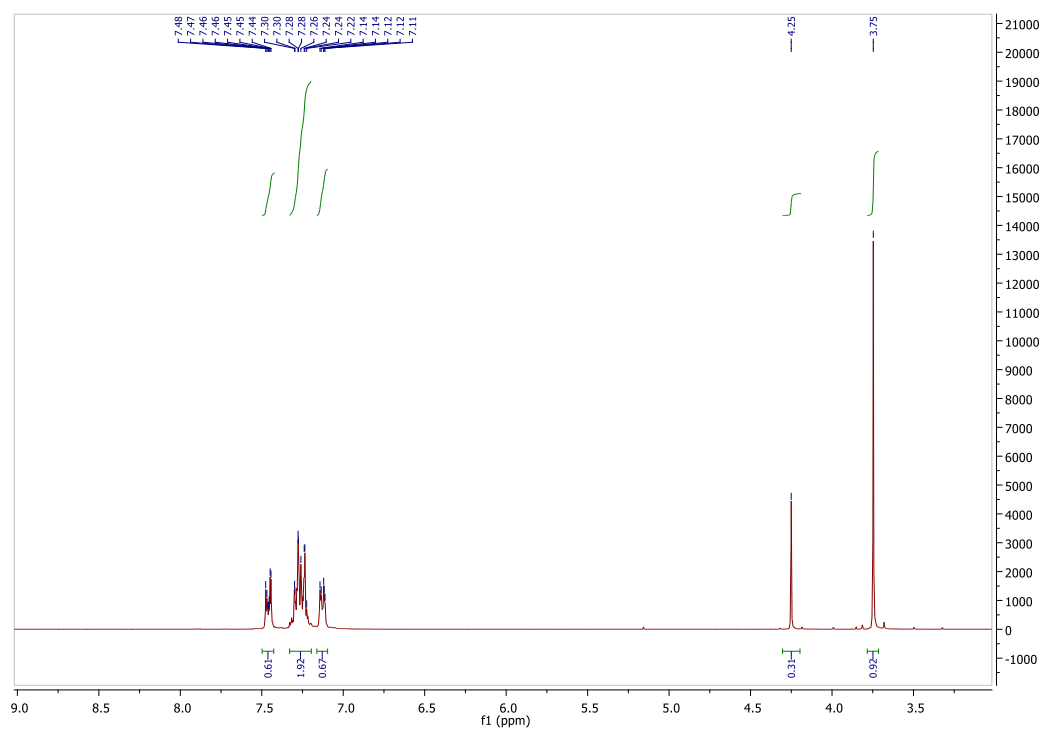


Fig. 17: Spectrum  $^1\text{H}$  NMR (300 MHz,  $\text{CDCl}_3$ ) of E-2.3.

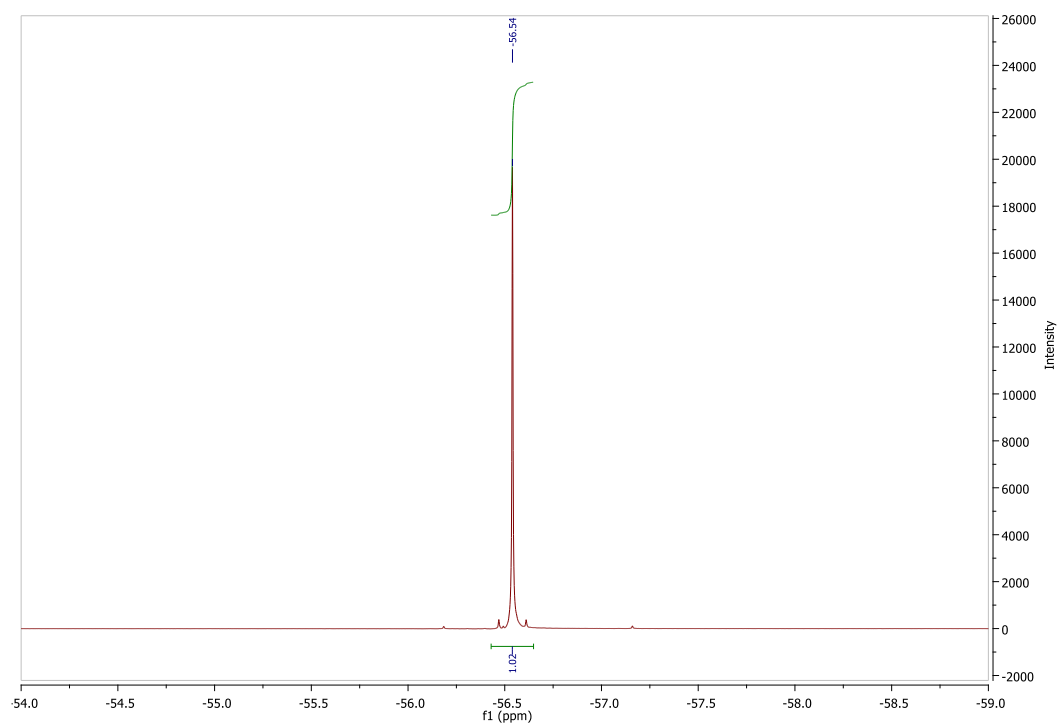


Fig. 18: Spectrum  $^{19}\text{F}$  NMR of E-2.3.



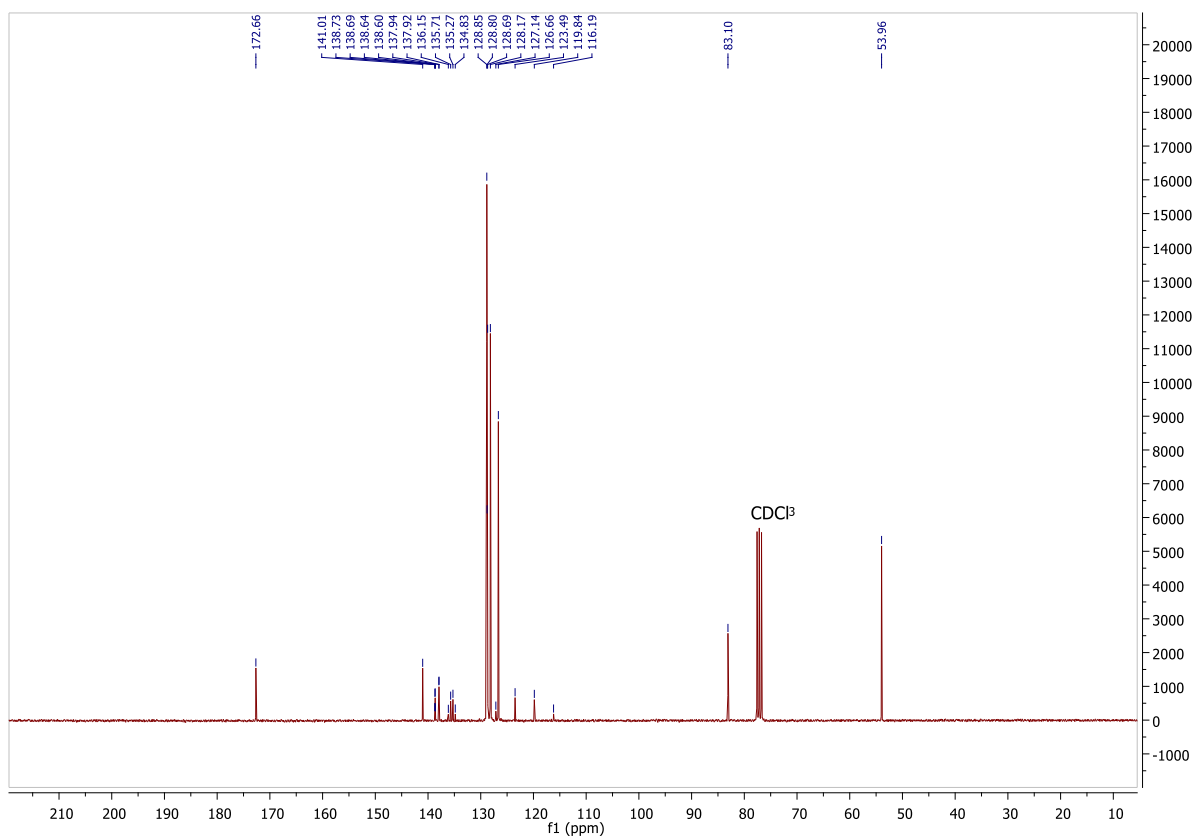


Fig. 19 : Spectrum  $^{13}\text{C}\{^1\text{H}\}$  NMR (75 MHz,  $\text{CDCl}_3$ ) of E-2.3.

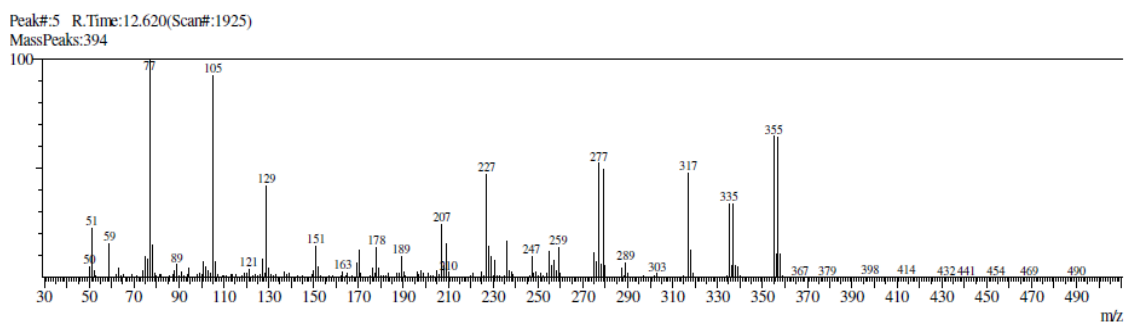
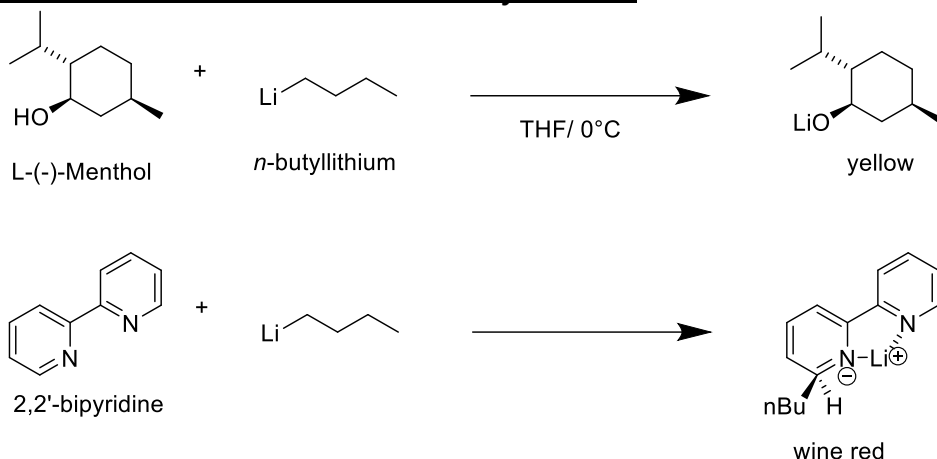


Fig. 20: Chromatogram of E-2.3 (GC (DB5)).

e. **Protocol of titration reaction of *n*-Butyllithium**

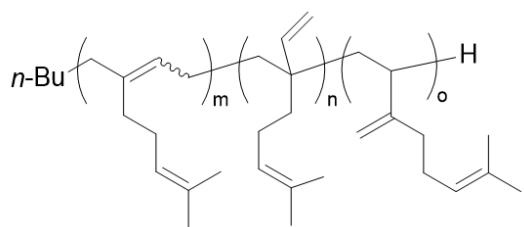


**Procedure :**

- Under an inert atmosphere (Ar), 1 mmol (152 mg) of L-(-)-menthol, 5 mL of THF and, 5 mg of 2,2'-bipyridine are added at 0°C.
- Organolithium (*n*-butyllithium) is added dropwise until the color changes from yellow to wine red.
- The concentration (C) is calculated from the quantity of menthol moles (n) and the volume of organolithium (V) used until the solution turns to wine red.

$$C = n \cdot V^{-1}$$

**f. Synthesis of PMYR under batch conditions**



2.6 mL of anhydrous THF is introduced in a reactor under inert atmosphere (Ar) and then cooled with a 10° C water bath. Then, 1.4 mL of hexane is introduced and 0.19 mL of *n*-BuLi (2.5 M in hexanes) is injected. After 5 minutes, 1.4 mL of myrcene (8 mmol) is introduced in one portion. After the time selected (1, 2, 8 min, etc.), the reaction is quenched with methanol: water (2/2 mL). The quenched mixture is extracted with dichloromethane (3 x 10 mL), washed with water (20 mL), dried over magnesium sulfate, and concentrated under vacuum to afford a crude mixture, analyzed by mean of NMR (data in accordance with the literature.<sup>3</sup>).

**<sup>1</sup>H NMR (300 MHz, CDCl<sub>3</sub>)** δ (ppm)= 5.67, 5.13, 4.75, 1.69, 1.62 and 0.87 (3 H).

**<sup>13</sup>C NMR (75 MHz, CDCl<sub>3</sub>)** δ (major isomer) (ppm) = 139.04, 131.21, 124.51, 36.96, 30.67, 27.01, 26.83, 25.71, and 17.73.

<sup>3</sup> (a) J.M. Bolton, M.A. Hillmyer, T.R. Hoyer, Sustainable Thermoplastic Elastomers from Terpene-Derived Monomers, ACS Macro Lett. 3 (2014) 717–720. <https://doi.org/10.1021/mz500339h>. (b) S. Loughmari, A. Hafid, A. Bouazza, A. El Bouadili, P. Zinck, M. Visseaux, Highly stereoselective coordination polymerization of β-myrcene from a lanthanide-based catalyst: Access to bio-sourced elastomers, Journal of Polymer Science Part A: Polymer Chemistry. 50 (2012) 2898–2905. <https://doi.org/10.1002/pola.26069>.

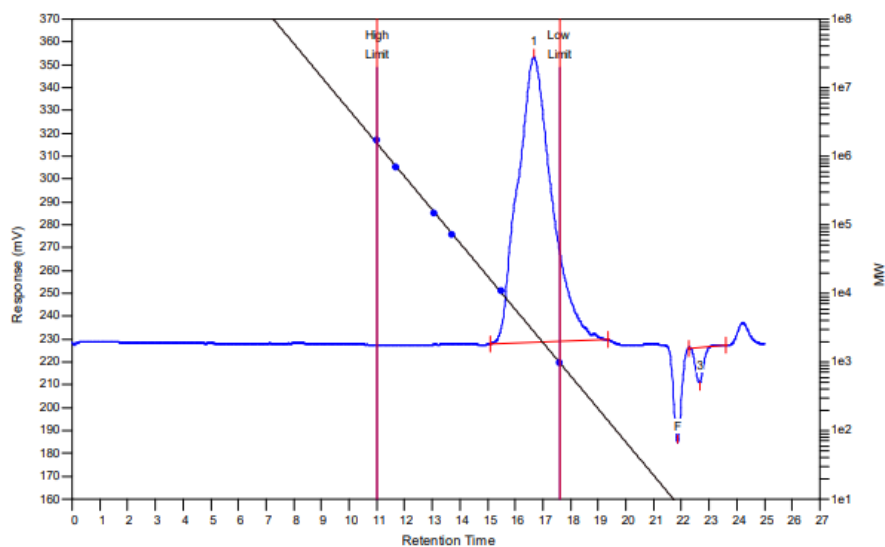


Fig. 21:GPC of PMYR in batch at 10°C

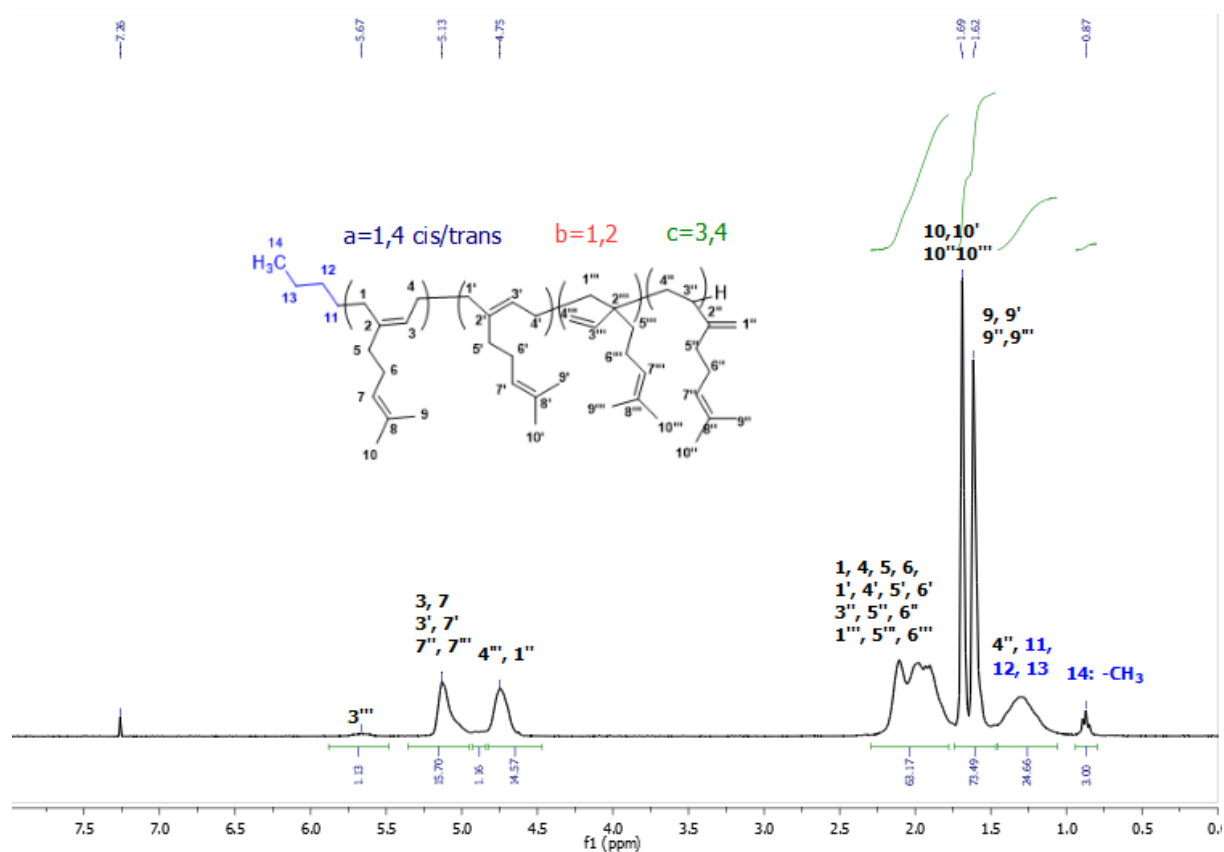


Fig. 22:1H NMR (300 MHz, CDCl<sub>3</sub>) spectrum of PMYR in batch at 10°C. Microstructure calculations:  $b=1.13(1H)$ ;  $c=(14.57-1.13)/2=6.72(1H)$ ;  $a=(15.70-6.72-1.13)/2=3.92(1H)$ ;  $a=3.92/11.77=33\%$ ,  $b=1.13/11.77=10\%$ ,  $c=6.72/11.77=57\%$

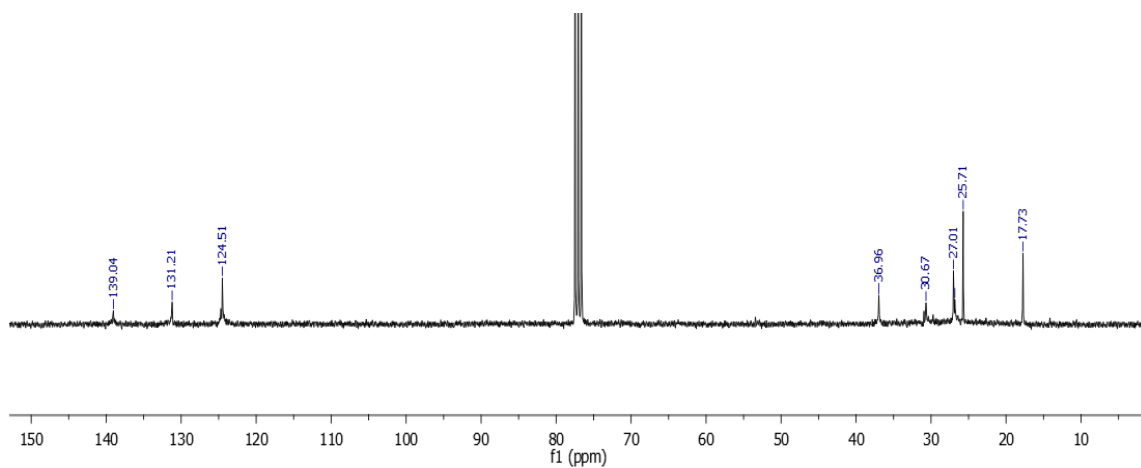


Fig. 23:  $^{13}\text{C}$  NMR (75 MHz,  $\text{CDCl}_3$ ) spectrum of PMYR in batch at  $10^\circ\text{C}$ .

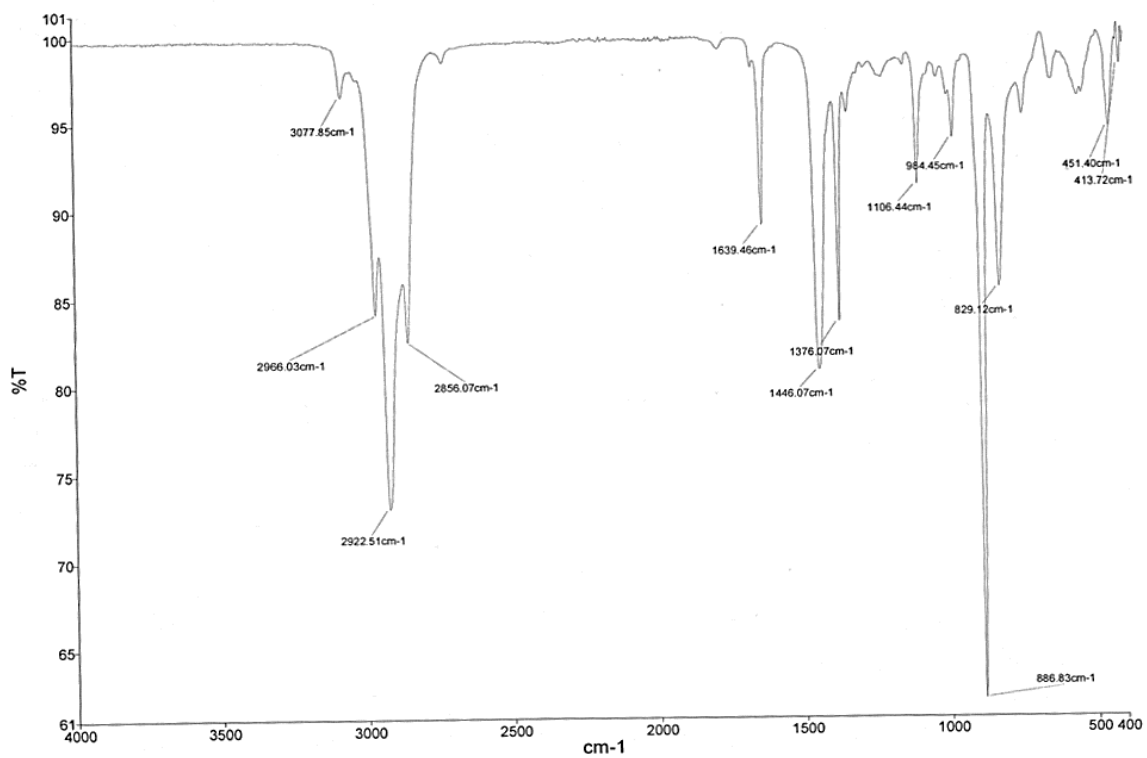
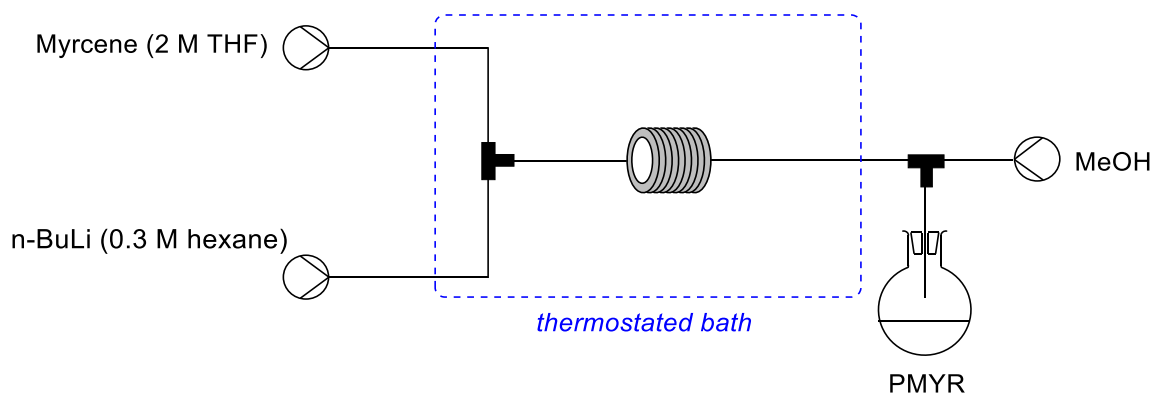


Fig. 24: Infrared spectrum of PMYR in batch at  $10^\circ\text{C}$ .

**g. Synthesis of PMYR under flow conditions**



The system is composed of a first inlet containing a solution of myrcene in THF (2 M) and a second inlet with *n*-BuLi solution (0.3 M in hexanes). The solutions are passed through a T-shape micromixer (stainless steel, 500  $\mu\text{m}$  of internal diameter (ID)). The resulting mixture is passed through a microreactor (stainless steel, 750  $\mu\text{m}$  ID, 1 m length). This microreactor is submerged in a 10°C water bath. The resulting solution is introduced in a second T-shape micromixer (500  $\mu\text{m}$  ID) to be quenched with methanol, flow rate 0.1 mL $\cdot$ min<sup>-1</sup>. The quenched mixture is passed through a second tube of 300 mm length and 750  $\mu\text{m}$  ID before collection in a vial containing 2 mL water. The quenched mixture is extracted with dichloromethane (3 x 10 mL), washed with water (20 mL), dried over magnesium sulfate, and concentrated under vacuum to afford a crude mixture, analyzed by mean of NMR (confirming previous literature report)

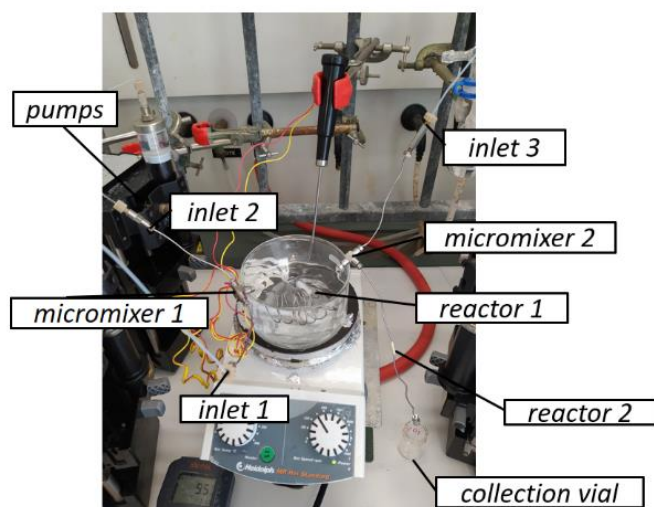


Fig. 25: Experimental setup in microflow conditions

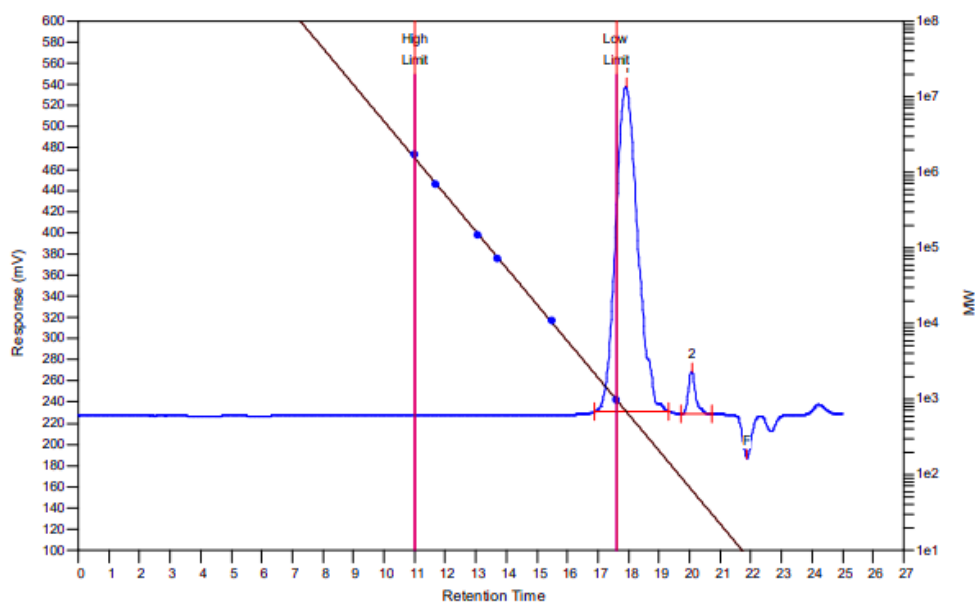
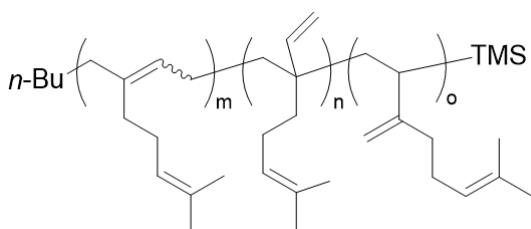
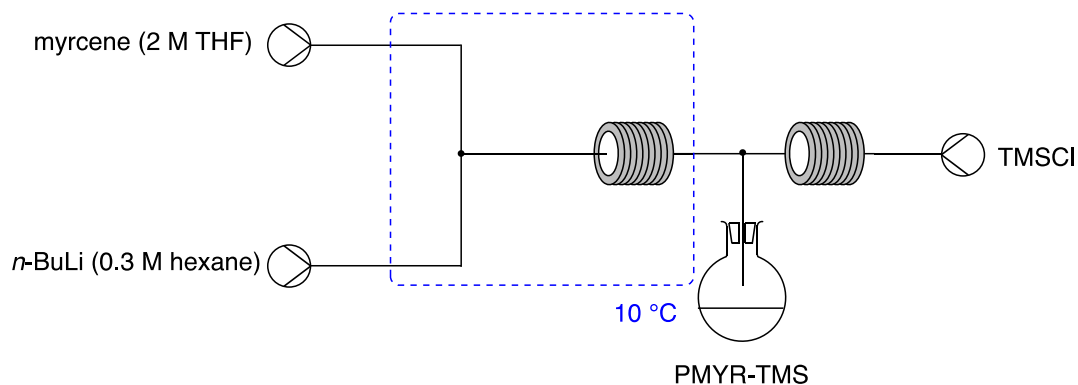


Fig. 26 : GPC of PMYR in microflow conditions, flow rate myrcene/n-BuLi/Methanol: 0.25/0.1/0.1 mL/min respectively at 10°C.

#### h. Synthesis of PMYR quenched with TMSCl under flow conditions



The system is composed of a first inlet containing a solution of myrcene in THF (2 M) and a second inlet with *n*-BuLi solution (0.3 M in hexanes). The solutions are passed through a T-Shape micromixer (stainless steel, 500  $\mu\text{m}$  of internal diameter (ID)). The resulting mixture is passed through a microreactor (stainless steel, 750  $\mu\text{m}$  ID, 3 m length). This microreactor is submerged in a 10 $^\circ\text{C}$  water bath. The resulting solution is introduced in a second T-shape micromixer (500  $\mu\text{m}$  ID) to be quenched with TMSCl, flow rate 0.1 mL/min. The quenched mixture is passed through a second tube of 300 mm length and 750  $\mu\text{m}$  ID before collection in a vial containing 2 mL of HCl (2 N). The quenched mixture is extracted with dichloromethane (3 x 10 mL), washed with water (20 mL), dried over magnesium sulfate, and concentrated under vacuum to afford a crude mixture, analyzed by mean of NMR.

**$^1\text{H}$  NMR (300 MHz,  $\text{CDCl}_3$ )**  $\delta$  (ppm)= 5.68, 5.14, 4.76, 1.70, 1.63, 0.88 (3 H), 0.04 and 0.03. (TMS).

**$^{13}\text{C}$  NMR (75 MHz,  $\text{CDCl}_3$ )**  $\delta$  (ppm) = 146.31, 139.14, 131.46, 124.72, 115.83, 113.21, 109.24, 35.03, 33.20, 32.23, 31.55, 29.86, 27.18, 26.87, 26.54, 25.85, 22.82, 22.54, 17.84, 14.27 and -0.37.



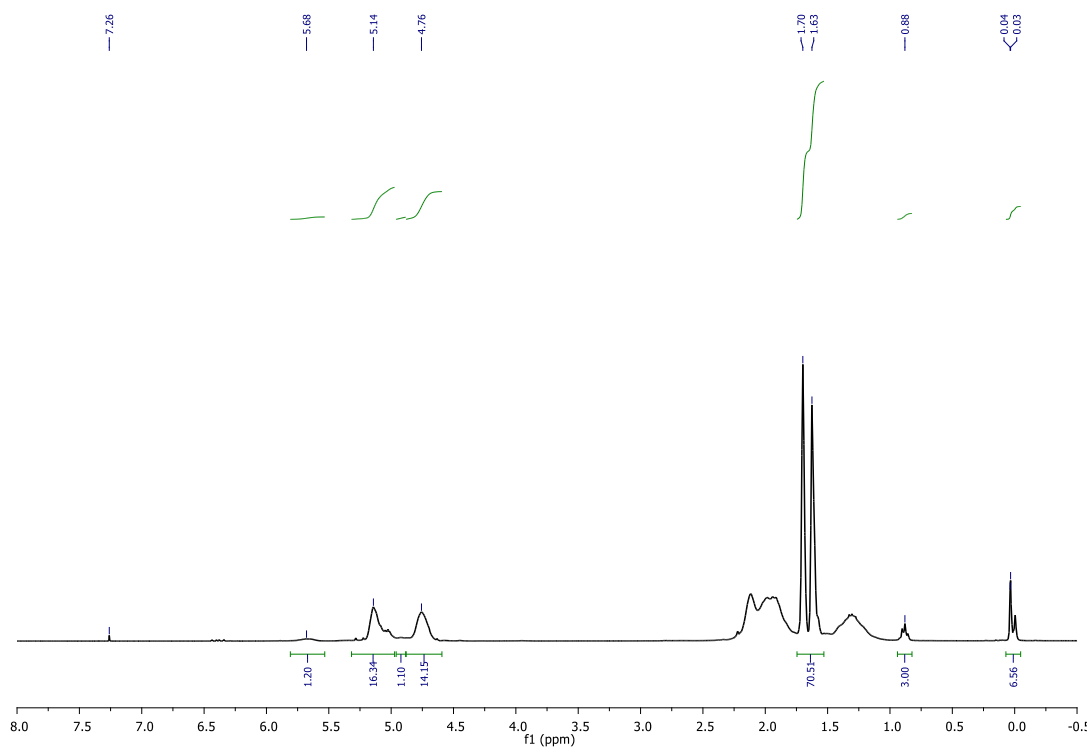


Fig. 27:  $^1\text{H}$  NMR (300 MHz,  $\text{CDCl}_3$ ) of PMYR with TMS end-group, MF: flow rate myrcene/ $n$ -BuLi/TMScI: 0.25:0.1:0.1  $\text{mL}\cdot\text{min}^{-1}$  respectively at  $10^\circ\text{C}$ . Functionalization degree:  $6,56/9 \times 100 = 73\%$ .

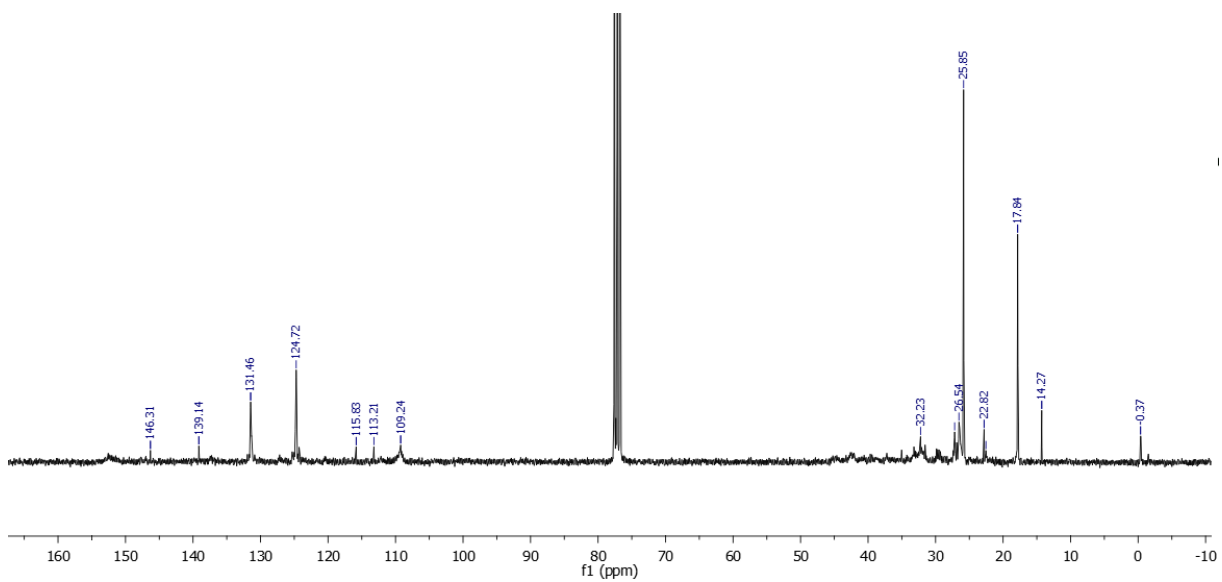


Fig. 28:  $^{13}\text{C}$  NMR (75 MHz,  $\text{CDCl}_3$ ) of PMYR with TMS end-group, MF: flow rate myrcene/ $n$ -BuLi/TMScI 0.25:0.1:0.1  $\text{mL}\cdot\text{min}^{-1}$  respectively at  $10^\circ\text{C}$ .



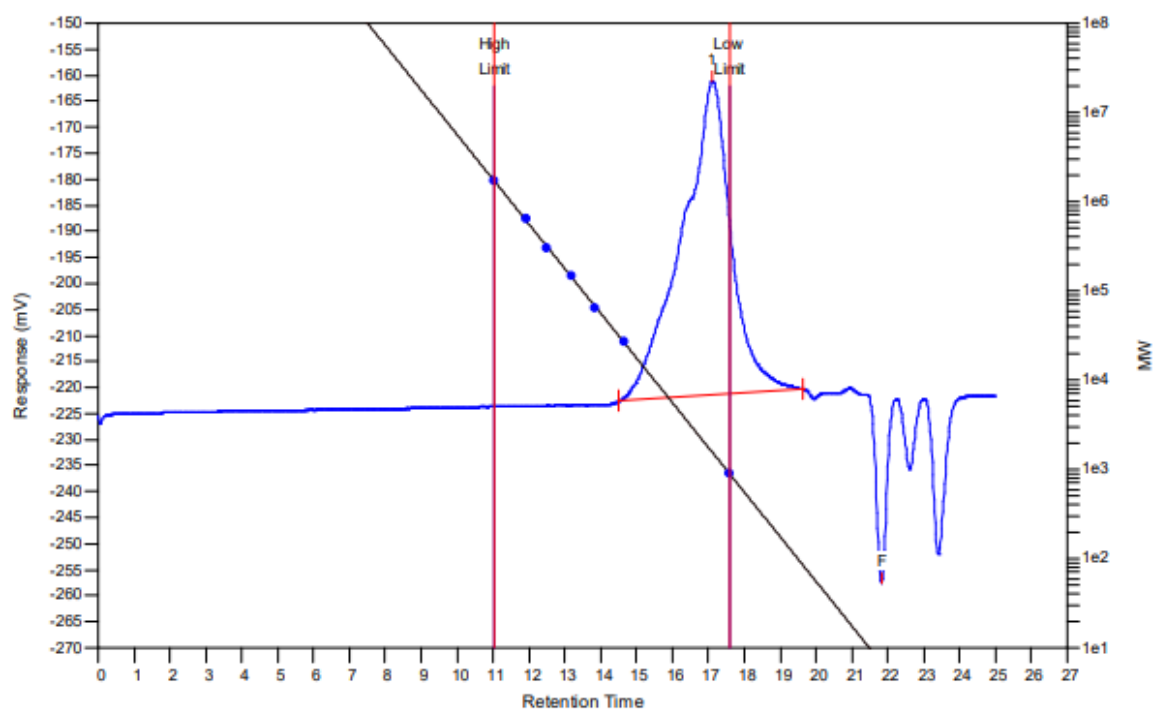


Fig. 29: GPC of PMYR ketone in batch at 10°C.

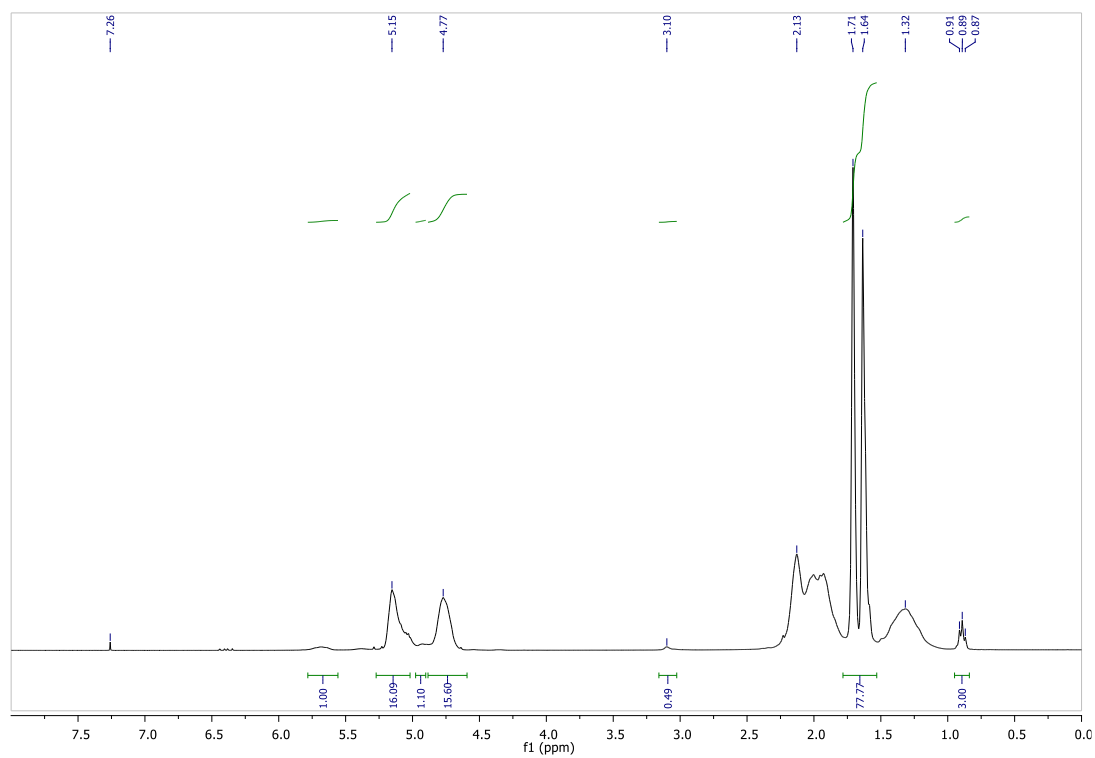


Fig.30:  $^1\text{H}$  NMR (300 MHz,  $\text{CDCl}_3$ ) of PMYR ketone in batch at 10°C.

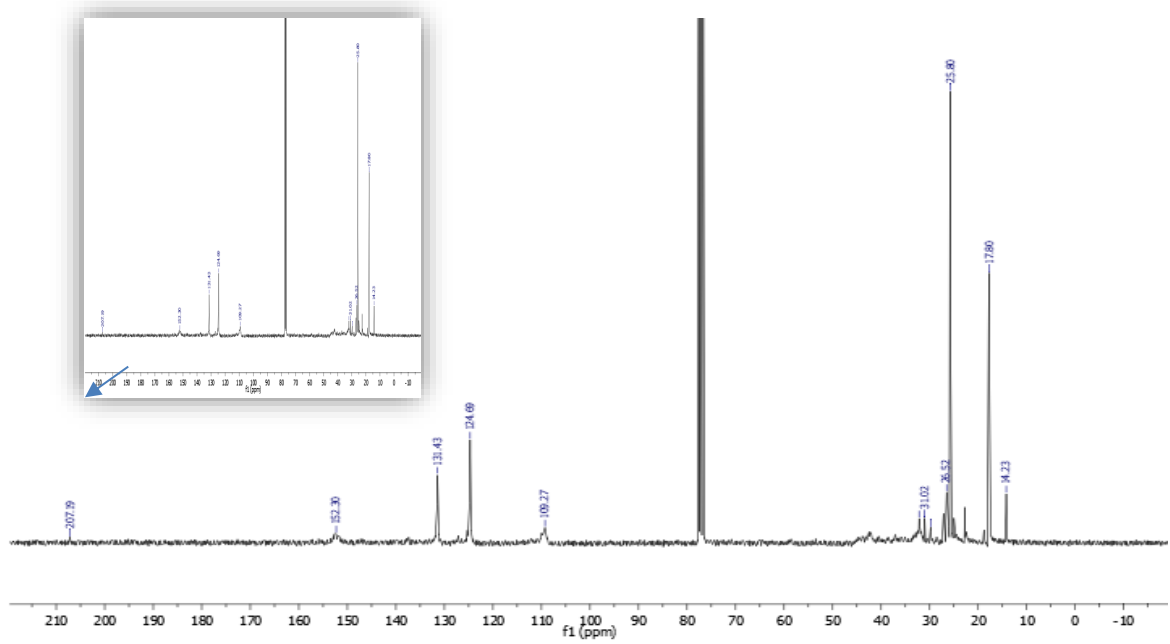


Fig. 31:  $^{13}\text{C}$  NMR (300 MHz,  $\text{CDCl}_3$ ) of PMYR ketone in batch at  $10^\circ\text{C}$ .

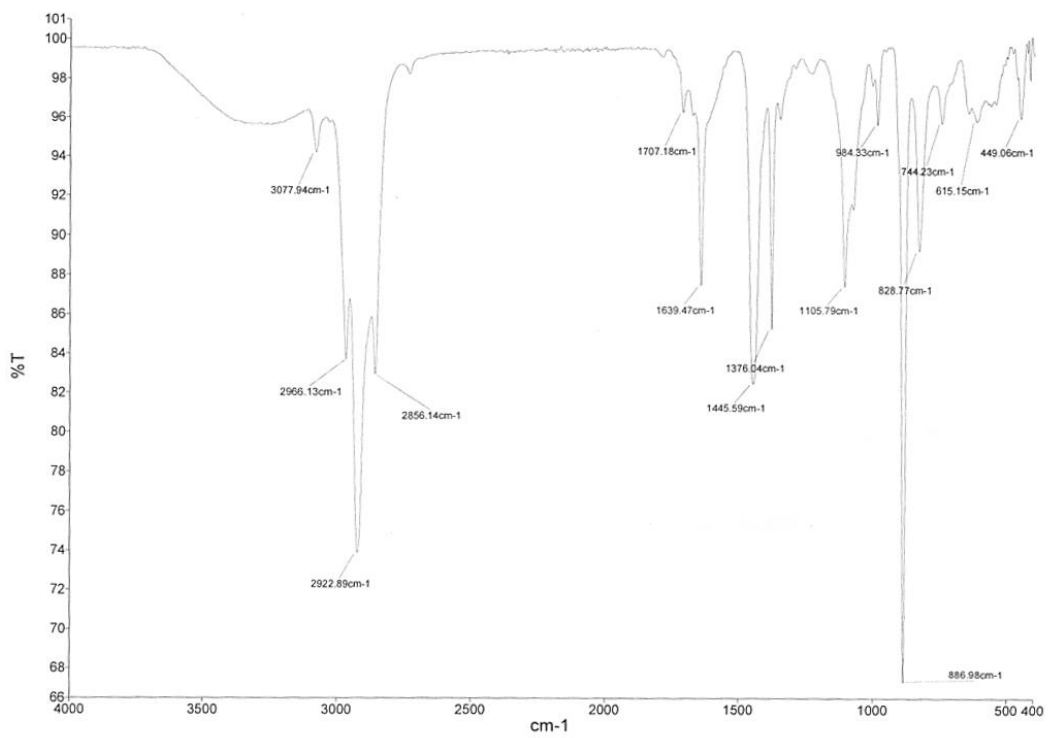
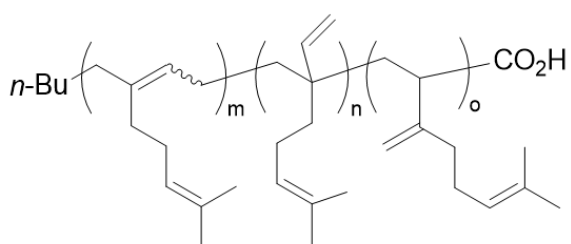
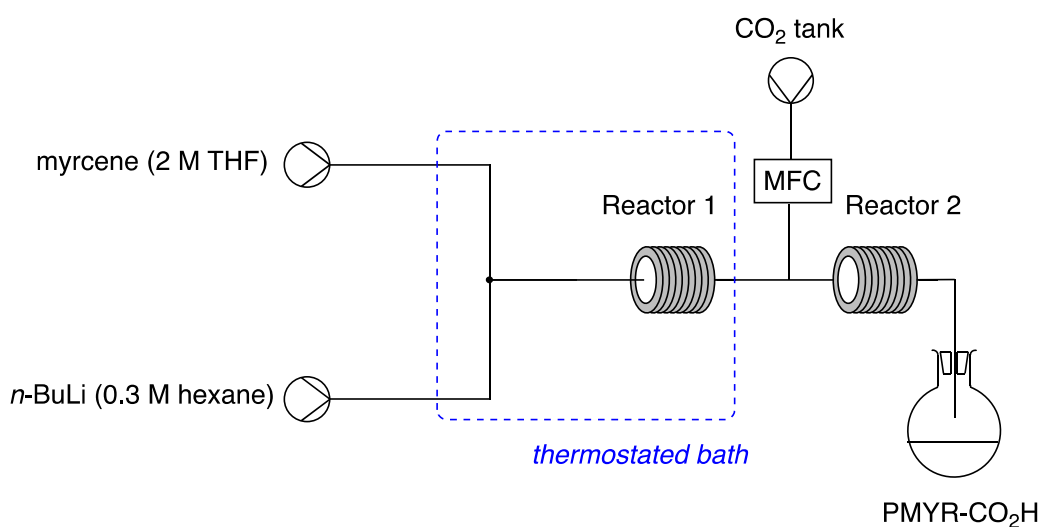


Fig. 32 : FTIR of PMYR ketone in batch (carbonyl group signal  $1707.18\text{ cm}^{-1}$ ) at  $10^\circ\text{C}$

j. **Synthesis of PMYR quenched with CO<sub>2</sub> under flow conditions**



For the functionalization of PMYR with CO<sub>2</sub> a similar system in continuous flow was used as previously mentioned. However, in the second micromixer, instead of methanol, CO<sub>2</sub> gas is introduced by connecting a gas tank to a mass flow controller (Bronkhorst High-

Tech BV). This inlet is connected to a second reactor (Reactor 2: ID = 0.75 mm, L = 30 cm) to generate the PMYR functionalized with a carboxyl group, before collection in a vial containing 2 mL of HCl 2 N. The procedure for collection, extraction and analysis of the sample was performed as above.

**<sup>1</sup>H NMR (300 MHz, CDCl<sub>3</sub>)** δ (ppm)= 5.61, 5.12, 4.74, 3.06, 1.68, 1.60 and 0.86 (3 H).

**<sup>13</sup>C NMR (75 MHz, CDCl<sub>3</sub>)** δ (ppm) = 178.48, 177.89, 152.44, 150.01, 149.19, 146.86, 146.20, 139.10, 131.34, 124.68, 115.76, 113.08, 109.29, 108.67, 36.16, 34.99, 32.19, 31.53, 27.22, 27.11, 26.84, 26.50, 26.43, 25.78, 22.78 and 17.77.

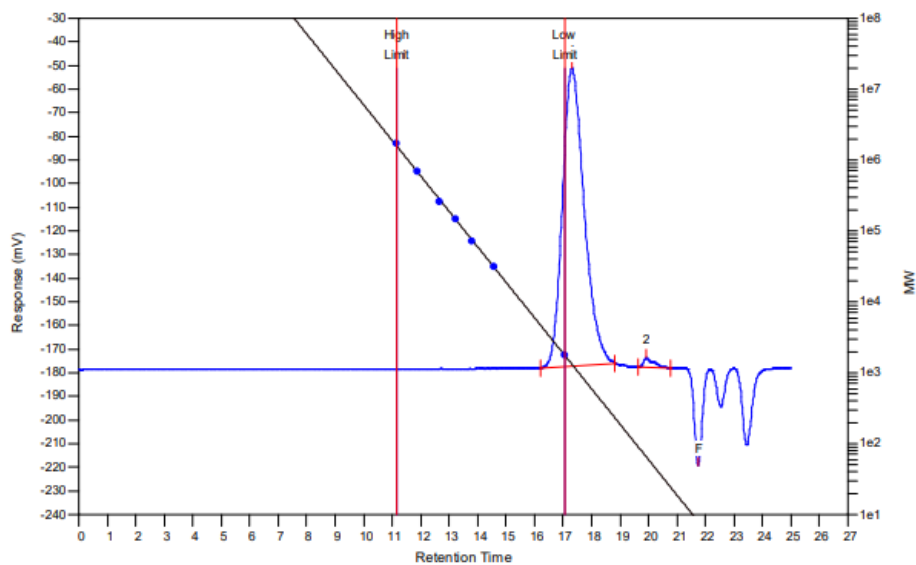


Fig. 33: GPC of PMYR end-group acid, MF conditions: flow rate myrcene/*n*-BuLi/ $\text{CO}_2$  0.25:0.1:1.36 mL.min<sup>-1</sup> respectively at 10°C.

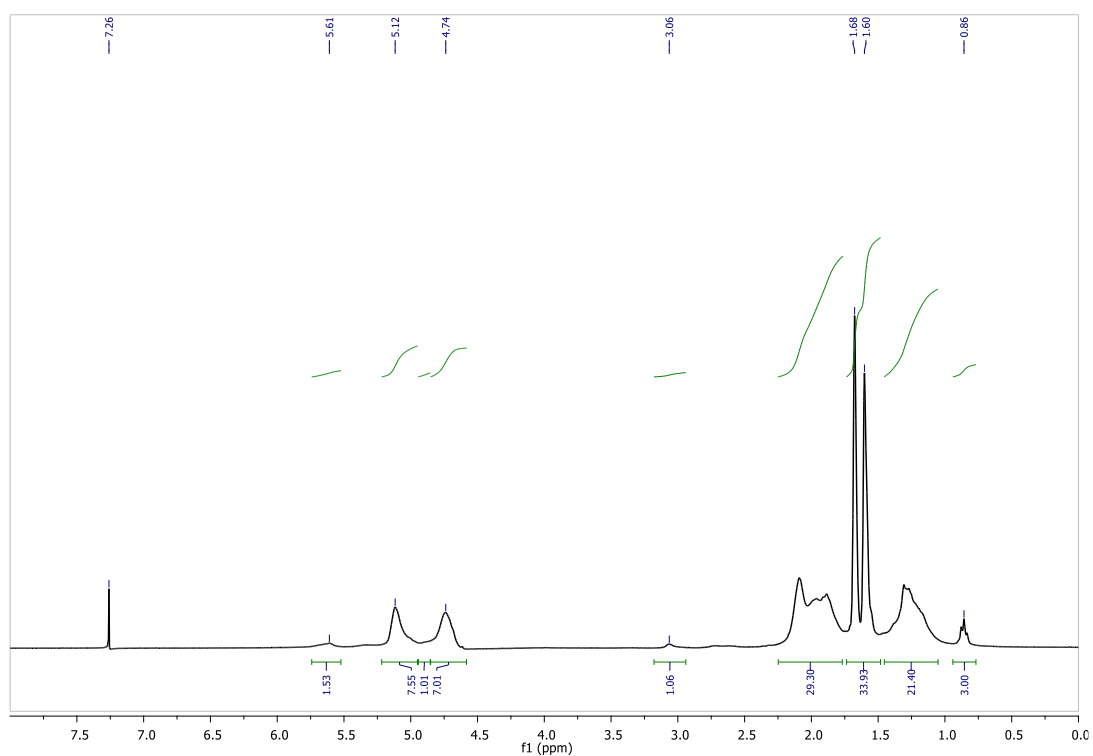


Fig. 34: <sup>1</sup>H NMR of PMYR end-group acid, MF conditions: flow rate myrcene/*n*-BuLi/ $\text{CO}_2$  0.25:0.1:1.36 mL.min<sup>-1</sup> respectively, at 10°C. Functionalization degree: 95%.

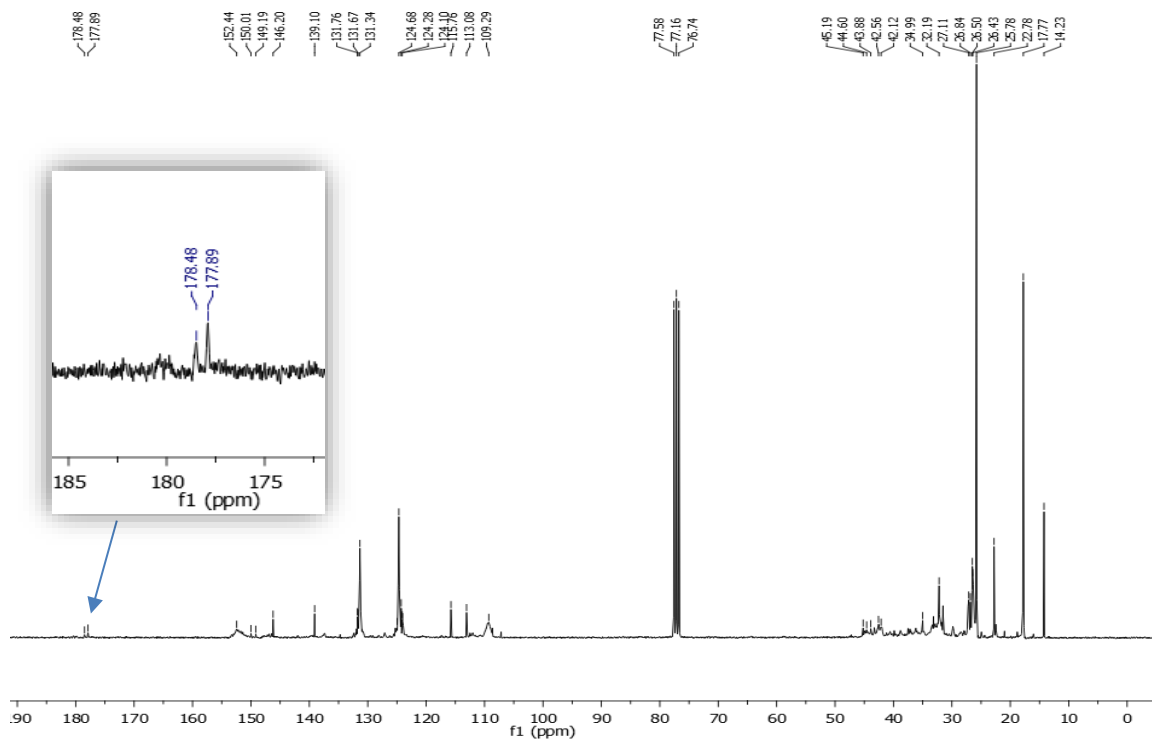


Fig. 35:  $^{13}\text{C}$  NMR of PMYR end-group acid, MF conditions: flow rate myrcene/n-BuLi/ $\text{CO}_2$  0.25:0.1:1.36 mL.min $^{-1}$  respectively at  $10^\circ\text{C}$ .

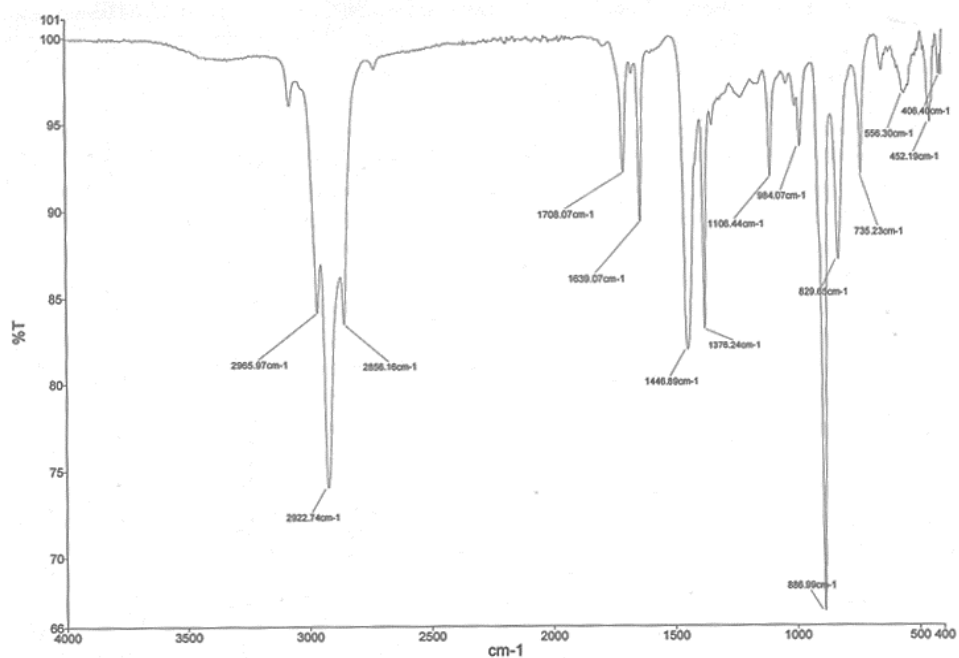
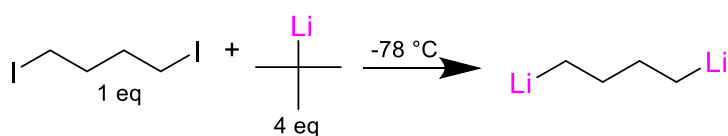


Fig. 36: FT IR of PMYR end-group acid (carbonyl group signal  $1708.07\text{ cm}^{-1}$ ). MF conditions: flow rate myrcene/n-BuLi/ $\text{CO}_2$  0.25:0.1:1.36 mL.min $^{-1}$  respectively at  $10^\circ\text{C}$ .

k. **Synthesis of 1,4-dilithiobutane**



**Procedure:**

The procedure used for this reaction has already been described by Negishi *et al.*<sup>4</sup>

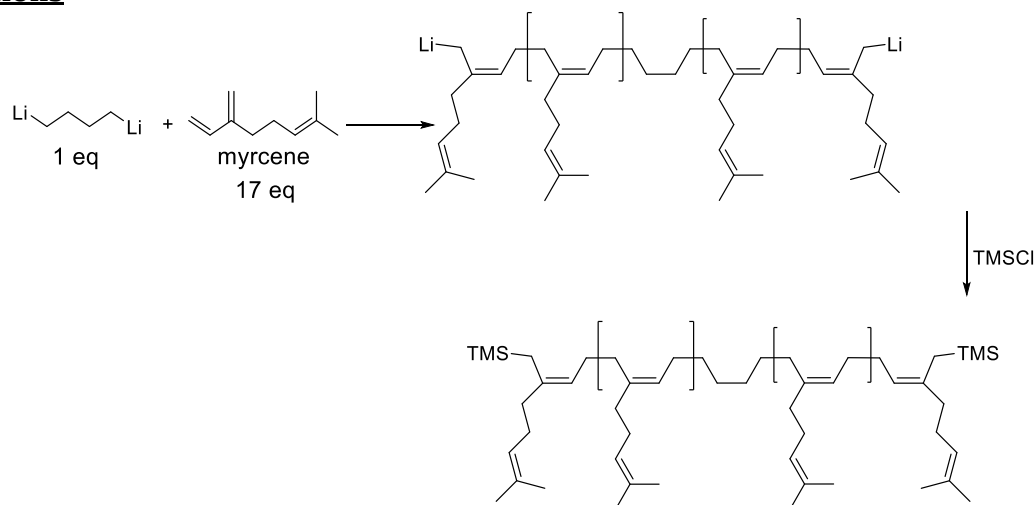
Et<sub>2</sub>O (3 mL) and 3.68 mmol of *tert*-BuLi (1.7 M in hexanes, 2.2 mL) are added at -78 °C in a 25 mL round-bottom flask. After 10 min, 1.04 mmol (0.13 mL) of diiodobutane are added dropwise. The reaction is mixed at 400 rpm during 30 min à -78°C then it is left to rest during 1 h at 20 °C to remove the *tert*-butyllithium remaining in the reaction medium. The product obtained is titrated before use (same procedure as before).

---

<sup>4</sup> Eiichi Negishi, Douglas R. Swanson, and Christophe J. Rousset, "Clean and Convenient Procedure for Converting Primary Alkyl Iodides and .Alpha.,.Omega.-Diiodoalkanes into the Corresponding Alkyl lithium Derivatives by Treatment with Tert-Butyllithium," *The Journal of Organic Chemistry* 55, no. 19 (September 1990): 5406–9, <https://doi.org/10.1021/jo00306a022>.



## **I. Synthesis of telechelic PMYR with TMS end-functionalization under batch conditions**



### **Procedure:**

Under an inert atmosphere, 2.7 mL of THF and 1.4 mL (8.1 mmol) of myrcene are added at 0 °C. The solution is left 10 min under stirring. 3 mL (0.48 mmol) of 1,4 dilithiobutane/Et<sub>2</sub>O 0.16 M is added at 0 °C. The reaction is left during 1 h at 10°C under stirring. The reaction medium turns from transparent to deep yellow color. At 0 °C, 1.44 mmol (0.18 mL) of TMSCl are added and left react overnight in constant agitation at room temperature (the reaction medium turns to white transparent). At 0 °C, 2 mL of HCl (2M) are added to quench the reaction. The product is extracted with DCM. The crude product is dried with MgSO<sub>4</sub>, filtered and the volatiles are removed *in vacuo*.

**<sup>1</sup>H NMR (300 MHz, CDCl<sub>3</sub>)** δ (ppm)= 5.66-5.63, 5.13, 4.75-4.69, 1.69, 1.62 and 0.03-0.02 (TMS)

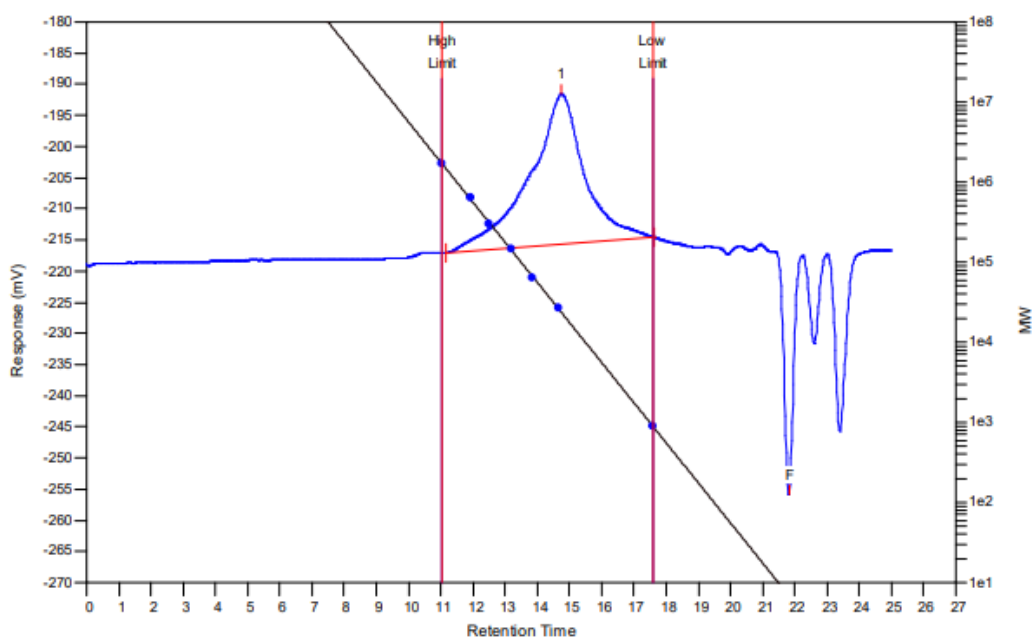


Fig. 37: GPC of Telechelic PMYR with TMS end-functionalization under batch conditions.

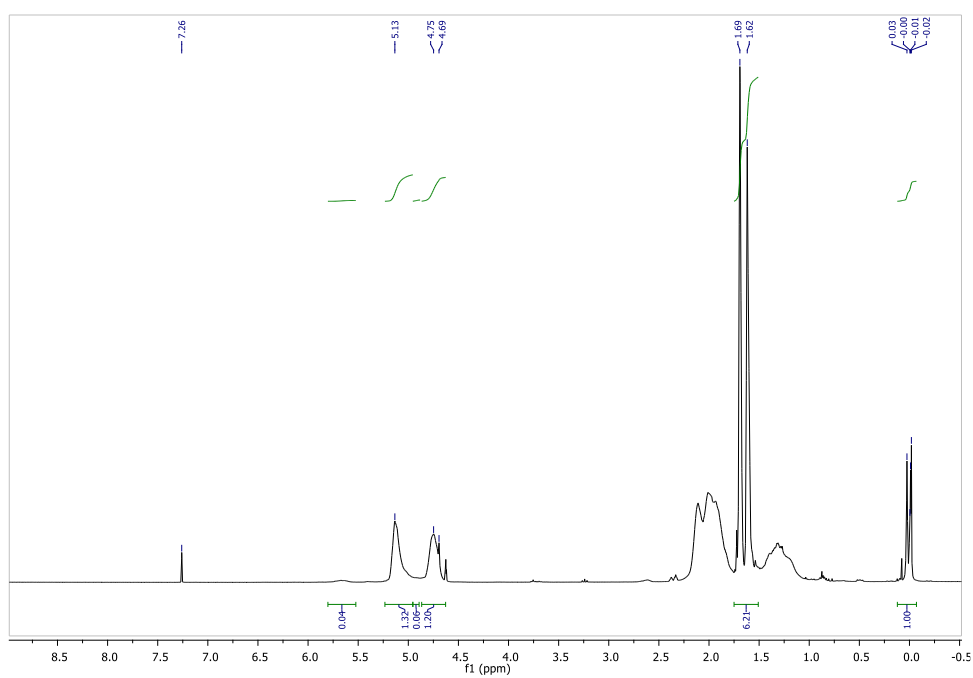
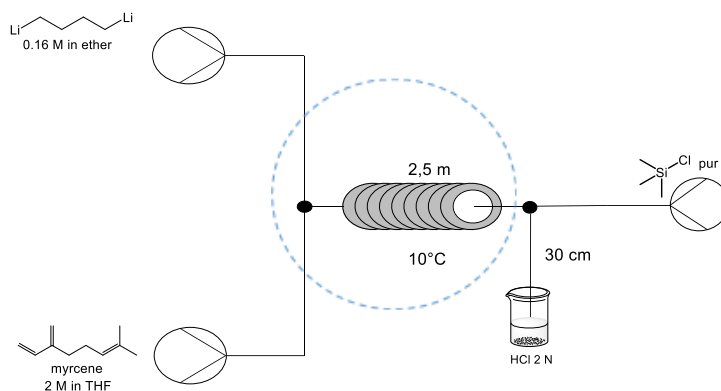


Fig.38:<sup>1</sup>H NMR of Telechelic PMYR with TMS end-functionalization under batch conditions

**m. Synthesis of telechelic PMYR with TMS end-functionalization under microflow conditions**



The system is composed of a first inlet containing a solution of myrcene in THF (2 M, 0.25 mL.min<sup>-1</sup>) and a second inlet with 1,4 dilithiobutane solution (0.16 M in Et<sub>2</sub>O, 0.20 mL.min<sup>-1</sup>). The solutions are passed through a T-shape micromixer (stainless steel, 500 μm of internal diameter (ID)). The resulting mixture is passed through a microreactor (stainless steel, 750 μm ID, 2.5 m length). This microreactor is placed in a 10 °C water bath. The resulting solution is introduced in a second T-shape micromixer (500 μm ID) to react with TMSCl at a flow rate = 0.20 mL.min<sup>-1</sup>. The resulting mixture is passed through a second tube of 300 mm length and 750 μm ID before collection in a vial containing 2 mL of HCl (2 N). The quenched mixture is extracted with dichloromethane (3 x 10 mL), washed with water (20 mL), dried over magnesium sulfate, and concentrated under vacuum to afford a crude mixture, analyzed by NMR.

**<sup>1</sup>H NMR (300 MHz, CDCl<sub>3</sub>) δ (ppm)= 5.66-5.63, 5.13, 4.74, 1.68, 1.61 and -0.02-0.02 (TMS)**

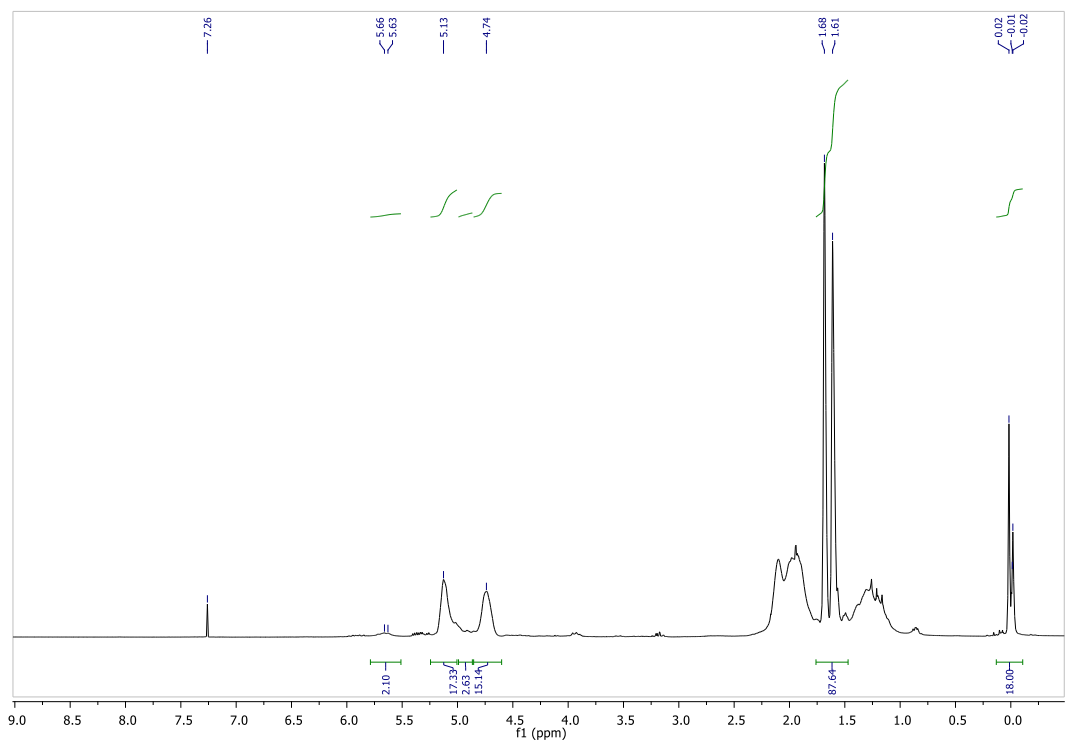


Fig. 39: <sup>1</sup>H NMR of Telechelic PMYR with TMS end-functionalization under microflow conditions

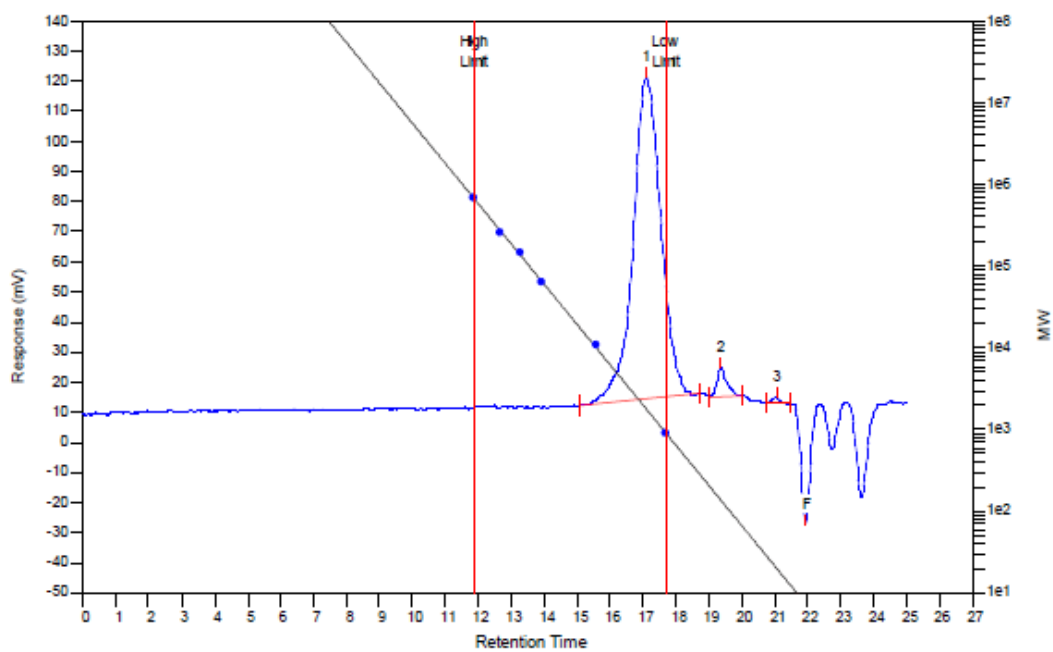
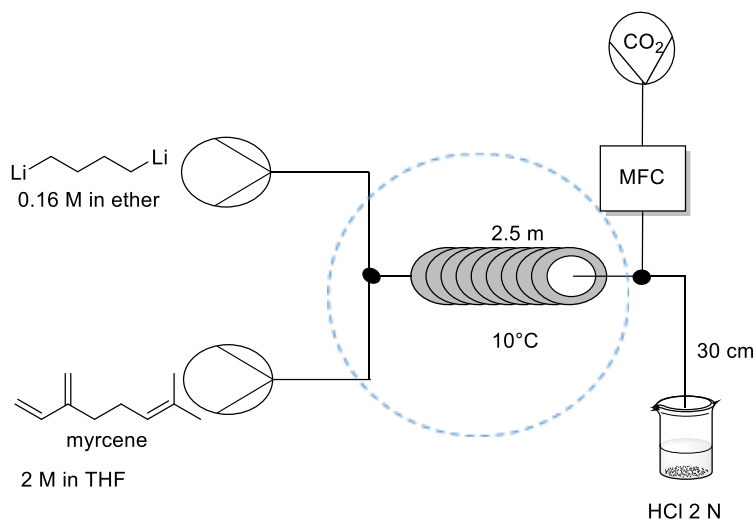


Fig.40: GPC of Telechelic PMYR with TMS end-functionalization under microflow conditions.

**n. Synthesis of telechelic PMYR with CO<sub>2</sub>H end-functionalization under flow conditions**



The system is composed of a first inlet containing a solution of myrcene in THF (2 M) and a second inlet with 1,4-dilithiumbutane solution (0.16 M in Et<sub>2</sub>O). The solutions are passed through a W-Shape micromixer (stainless steel, 500 μm of internal diameter (ID)). The resulting mixture is passed through a microreactor (stainless steel, 750 μm ID, 2.5 m length). This microreactor is placed in a 10° C water bath. The resulting solution is introduced in a second T-shape micromixer (500 μm ID), in this micromixer, CO<sub>2</sub> gas is introduced by connecting a gas tank to a mass flow controller (Bronkhorst High-Tech BV). This inlet is connected to a second reactor (Reactor 2: ID = 0.75 mm, L = 30 cm) to generate the telechelic PMYR functionalized with a carboxyl group, before collection in a vial containing 2 mL of HCl 2 N. The procedure for collection, extraction and analysis of the sample was performed as above.

**<sup>1</sup>H NMR (300 MHz, CDCl<sub>3</sub>) δ (ppm)= 5.65-5.61, 5.12, 4.74, 3.08, 1.68, 1.61.**

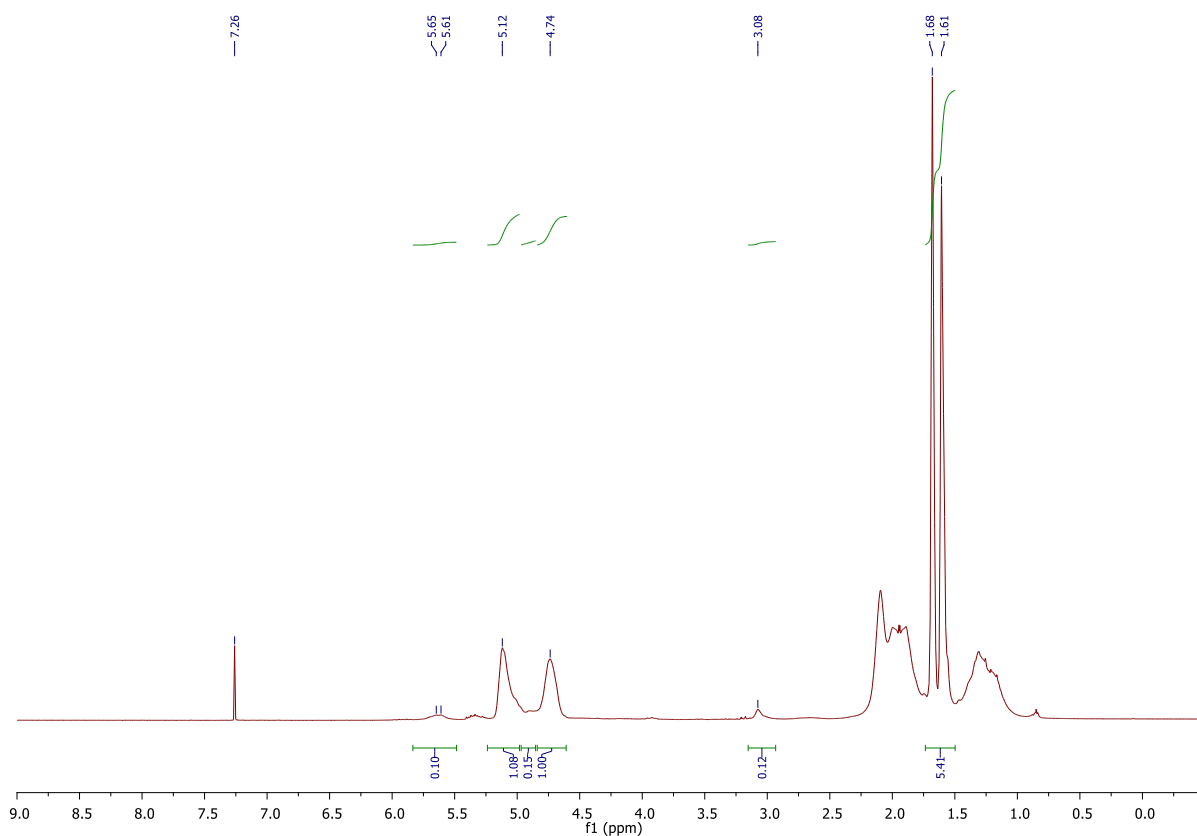


Fig. 41:  $^1\text{H}$  NMR Telechelic PMYR with  $\text{CO}_2\text{H}$  end-functionalization under flow conditions.

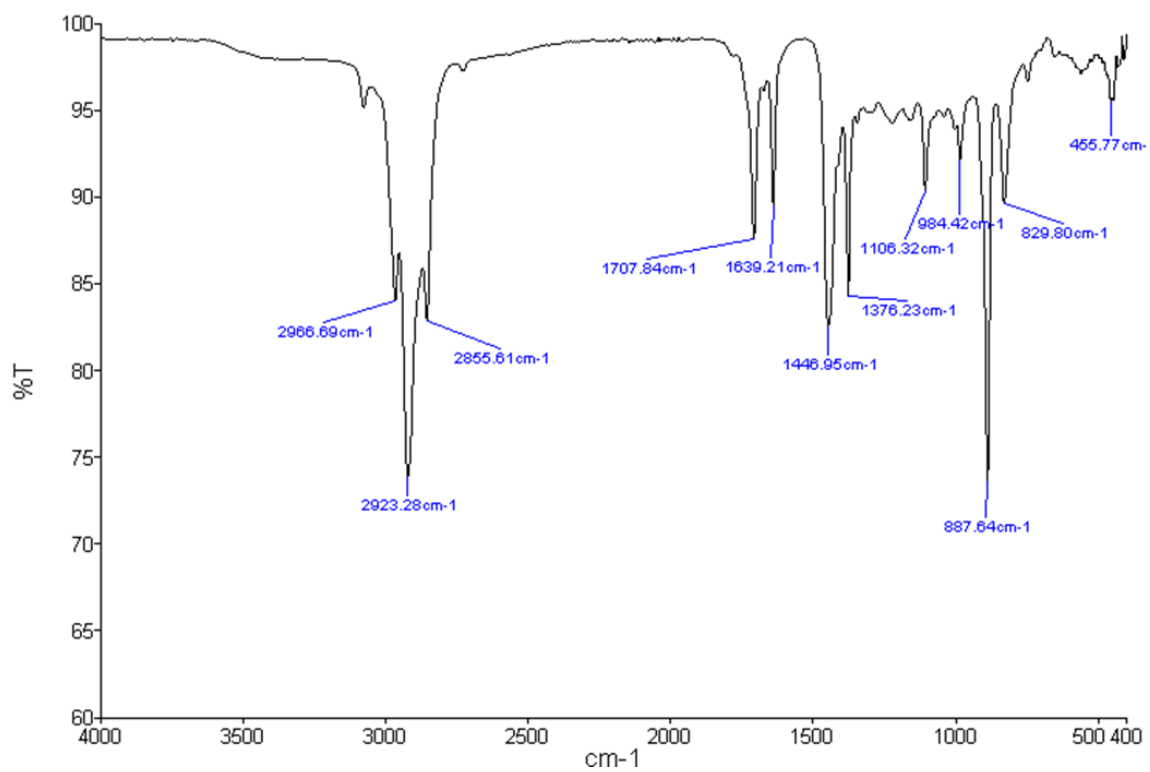
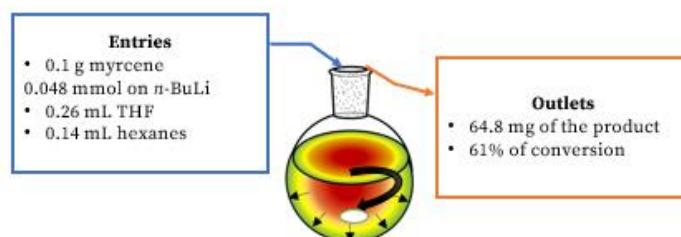


Fig. 42: FT IR spectrum of polymyrcene with  $\text{CO}_2\text{H}$  endings.  $\text{CO}_2\text{H}$  signal at  $1707\text{ cm}^{-1}$

**o. Mass balance in polymerization reaction (batch)**

In order to know if the inlet is equal to the outlet, a mass balance is necessary. Figure 42 shows, for example, the entries and outlets of the polymerization process on a scale of 0.1 g of myrcene.



*Fig.43: Entries and outlets in the reaction process (scale, 0.1 g of myrcene).*

It is necessary to understand that to obtain the final product, we have to do first washing, extraction, and concentration under vacuum of the substrate. Thus, we assumed that all the solvents were evaporated in this mass balance. So, 64.8 mg of the product is obtained after evaporation. By calculating, the entry is 112 mg, and by assuming a perfect process, the theoretical weight, with a conversion of 61%, we have to recover 68.4 mg of PMYR. Apparently, the difference of 4 mg is not a lot, and we are assuming no solvent in the sample, but in the actual case, the product has some solvent. Another problem is that myrcene was not totally recovered at the end, giving us no real values of conversion. This proves that, we do not have a perfect process. There are some events that can occur as side reactions, *i.e.*, degradation of *n*-BuLi, evaporation of myrcene or even of the dimers.

**p. Volatility of myrcene**

Myrcene is a highly volatile substance, boiling point, bp= 166 °C. During the study of the polymerization of myrcene, the volatility of myrcene was considered to determine how it could affect the process.

As a first approach, the study was performed by evaporating myrcene at room temperature.

The experiment was carried out using two round-bottomed flasks, one with 2087.3 mg of DCM/myrcene solution and the other one with 1542.2 mg of pure myrcene as a control. The mixture DCM/myrcene was prepared, because myrcene is soluble in dichloromethane and it was the solvent used in the polymer extraction.

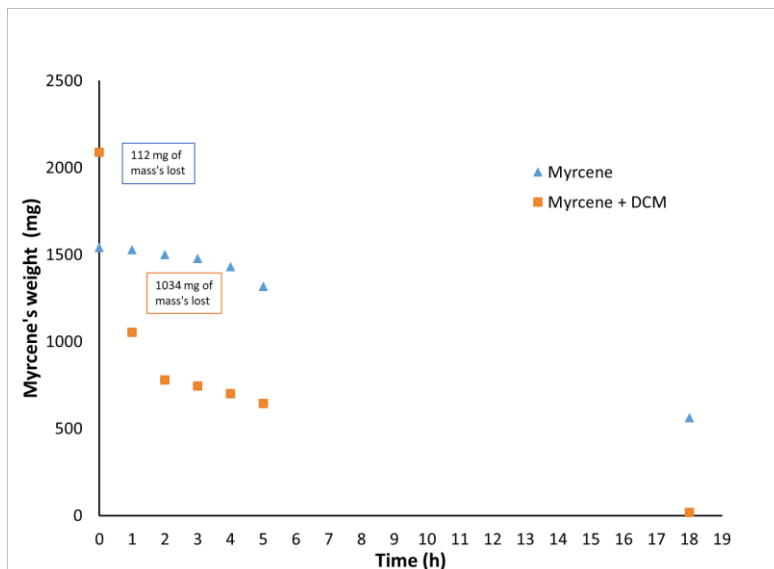
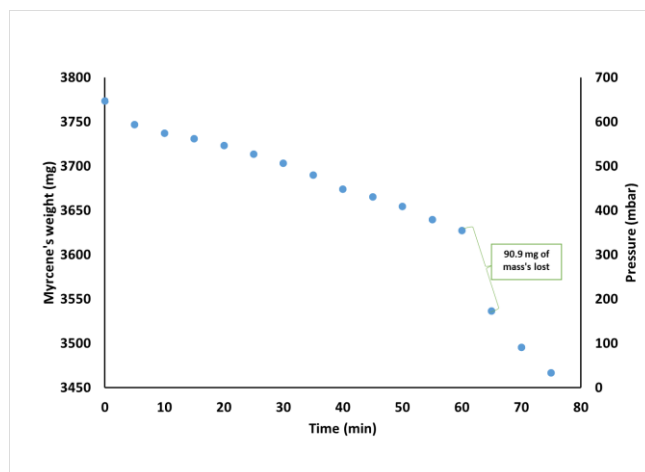


Fig. 44: Study of the evaporation of myrcene at room temperature.

Figure 43 shows that the evaporation of pure myrcene (blue triangles) and the mixture of DCM/Myrcene (orange squares) after 18 h. At 1 h, 112 mg of pure myrcene were evaporated. In the same conditions, 1034 mg of myrcene/DCM were evaporated in 1 h, and gradually, the mixture lost weight. This study shows that myrcene's evaporation is possible at room temperature and atmospheric pressure.

As the evaporation of the sample is usually performed under different pressures, near to 0 mbar), we also decided to try at reduced pressure. As in the previous experiment, the sample was weighed at the beginning of the test and every 5 minutes. Figure 44 shows that at 5 min, 26.8 mg were evaporated and 146.4 mg in 1 h.





*Fig. 45: Myrcene evaporation under different pressures.*

These experiments show that myrcene can quickly evaporate at room temperature and at reduced pressure. This factor directly affects the conversion values and the material balance.